

Finite element design of concrete structures


G.A. Rombach

Copyrighted Material

Finite element design of concrete structures

Practical problems and their solutions

G. A. Rombach

 Thomas Telford

Copyrighted Material

This One



Z9FP-SBA-Y76U

Published by Thomas Telford Publishing, Thomas Telford Ltd, 1 Heron Quay, London E14 4JD.
URL: <http://www.thomastelford.com>

Distributors for Thomas Telford books are

USA: ASCE Press, 1801 Alexander Bell Drive, Reston, VA 20191-4400

Japan: Maruzen Co. Ltd, Book Department, 3-10 Nihonbashi 2-chome, Chuo-ku, Tokyo 103

Australia: DA Books and Journals, 648 Whitehorse Road, Mitcham 3132, Victoria

First published 2004

Also available from Thomas Telford Books

Manual of Numerical Methods in Concrete, 2nd edition. M. Y. H. Bangash. ISBN 0 7277 2946 2

Finite Element Analysis in Geotechnical Engineering. D. M. Potts and L. Zdravković. ISBN 0 7277 2783 4

Structural Detailing in Concrete, 2nd edition. M. Y. H. Bangash. ISBN 0 7277 3034 7

A catalogue record for this book is available from the British Library

ISBN: 0 7277 3274 9

© Author and Thomas Telford Limited 2004

All rights, including translation, reserved. Except as permitted by the Copyright, Designs and Patents Act 1988, no part of this publication may be reproduced, stored in a retrieval system or transmitted in any form or by any means, electronic, mechanical, photocopying or otherwise, without the prior written permission of the Publishing Director, Thomas Telford Publishing, Thomas Telford Ltd, 1 Heron Quay, London E14 4JD.

This book is published on the understanding that the author is solely responsible for the statements made and opinions expressed in it and that its publication does not necessarily imply that such statements and/or opinions are or reflect the views or opinions of the publishers. While every effort has been made to ensure that the statements made and the opinions expressed in this publication provide a safe and accurate guide, no liability or responsibility can be accepted in this respect by the author or publishers.

Typeset by Academic + Technical, Bristol

Printed and bound in Great Britain by MPG Books, Bodmin, Cornwall

Contents

Foreword	vii
Notations	ix
Chapter 1 General	1
1.1 Introduction to the Finite Element Method, 6	
1.2 General problems of numerical analysis of concrete structures, 8	
1.2.1 Program errors, 9	
1.2.2 Model errors, 9	
Chapter 2 Truss and beam structures	14
2.1 Corners in frame structures – rigid regions, 15	
2.1.1 Portal frame bridge, 15	
2.1.2 Transverse design of a hollow box girder bridge, 20	
2.2 Beams with variable depth – inclined haunches, 25	
2.3 Beams with halving joints and openings, 30	
2.4 Elastic supports – elastic bedding, 38	
2.4.1 Elastic bedded foundation beam, 38	
2.4.2 Influence of the nonlinear material behaviour of concrete, 44	
2.4.3 Pile foundation – foundation of a bridge column, 47	
2.5 Shear walls with large openings, 58	
2.6 Bracing of high-rise buildings, 65	
2.6.1 Equivalent cross-section of the trusses, 69	
2.6.2 Location of the beam elements, 70	
2.6.3 Coupling of nodes, 71	
2.6.4 Example – comparison of the various models, 74	
2.6.5 Checking for stability – stability parameter, 80	

- 2.7 Design of hollow box girder bridges, 85
- 2.8 Truss system – design of T-beam bridges, 89
 - 2.8.1 Design of a rectangular solid slab, 89
 - 2.8.2 Double T-beam bridge, 95
 - 2.8.3 T-beam bridge with several longitudinal girders, 108
- 2.9 Dimensioning of reinforced beams, 112
 - 2.9.1 Design for bending and normal forces, 112
 - 2.9.2 Design for shear and torsion, 115

Chapter 3 Shear walls and deep beams 117

- 3.1 Estimation of stress resultants of a single-span deep beam, 119
- 3.2 Modelling the support condition, 124
 - 3.2.1 The influence of support settlements, 126
 - 3.2.2 Modelling of flexible supports with springs, 127
 - 3.2.3 Modelling of the columns with beam elements, 131
 - 3.2.4 Horizontal restraint, 136
- 3.3 Dimensioning of deep beams, 137
- 3.4 Strut-and-tie models, 144
- 3.5 Singularities, 147

Chapter 4 Slabs 150

- 4.1 General, 150
- 4.2 Material parameters – Poisson's ratio, 157
- 4.3 Support conditions for slabs, 160
- 4.4 One-way slab, 162
- 4.5 Slabs which can lift from the supports, 175
- 4.6 Discontinuous line support, 177
- 4.7 Concrete joist floors, 181
- 4.8 Flat slabs, 184
 - 4.8.1 Pin support of one node, 191
 - 4.8.2 Pin support of all nodes, 194
 - 4.8.3 Fully restraint of all nodes, 194
 - 4.8.4 Elastic bedded elements, 197
 - 4.8.5 Coupling of nodes above the column, 198
 - 4.8.6 Comparison of the various models, 199
 - 4.8.7 Results of the investigations, 199
 - 4.8.8 Slab – edge column connection, 202
- 4.9 Foundation slabs, 206
 - 4.9.1 Footings, 206
 - 4.9.2 Strip foundations, 210

4.10	Skewed slabs, 213	
4.11	Singularities, 215	
4.11.1	Opening with re-entrant corners, 217	
4.11.2	Re-entrant corners ($\alpha \geq 90^\circ$), 218	
4.11.3	Concentrated loads, 218	
4.12	Discretization – generation of the element mesh, 222	
4.12.1	Location of the restraint nodes, 222	
4.12.2	Size of the elements, 225	
4.13	Dimensioning of spatial structures, 228	
4.13.1	Model of Stiglat, 229	
4.13.2	Model of Baumann, 231	
4.13.3	Model of Eurocode 2, 234	
4.13.4	Comparison of the different models, 234	
4.14	Comparison with analytical methods and tables, 235	
4.14.1	Partial restraint method of Pieper and Martens, 237	
Chapter 5	Shell structures	244
5.1	Mesh generation, 244	
5.1.1	Collapse of the Sleipner Platform, 245	
5.1.2	Patch loads on shells, 250	
5.2	Continuous slab beam girder systems – T-beams, 255	
5.2.1	Models for T-beams, 256	
5.2.2	Comparison calculations with the different models, 260	
5.2.3	Flow of forces in the anchorage region of tendons, 267	
5.3	Composite structures, 270	
5.4	Singularities, 271	
References		273
Index		277

Foreword

Over the last few years electronic data processing has changed the work of engineers throughout all fields of construction. This is particularly true for design of structures where, nowadays, it is unimaginable that it can be done without the help of computer software. Even simple structures like, for example, simply supported reinforced concrete beams under uniform loading, are designed using the help now available from computers. One must admire this. In many cases, these computer calculations are faster, less costly and thus more profitable than manual calculations.

The developments of the last year or so have been to use yet more complex numerical models, as can be seen from the various contributions to conferences on the subject. It seems that today, it is only a question of computer capacity, the size of the element mesh, and the modelling of the nonlinear material behaviour, in order to model an arbitrary complex reinforced structure with almost unlimited accuracy. But then, there is a great danger that one only believes in the results from the computer, and the engineer loses his feelings for the real behaviour of the structure. Thus, in this book, the author faces up to the blind belief in computer results. One should not have a totally blind confidence, but rather a useful scepticism of the output of the computer calculations, regarding the numerical model used and hence the results achieved.

With the increasing complexity of a numerical model, it becomes more likely that important details are overlooked, due to the flood of information produced by the computer. The collapse of the so-called Sleipner Platform (see Chapter 1), resulting from an erroneous Finite Element calculation, impressively demonstrates this danger.

A complex numerical calculation should not be used to compensate for any lack of knowledge of the structural behaviour of a structure. An

engineer should be able to simplify any real structure into a well-defined, known, understandable, and designable equivalent structural system. Unimportant details are neglected. It should always be kept in mind that even very complex structures such as the Chapel of St Peter's Church in Rome or the Temples in Luxor, had been built without the help of computers and even without any knowledge of mechanics.

This book has been written for both the practical structural engineer and for students, who are using computer software for designing of concrete structures. The problems of Finite Element calculations are illustrated, not just by theoretical systems, but also by relating to real structures, mostly those on which the author has actually worked. They concern systems from all fields of engineering. Furthermore, this book should help those people who develop software for structural design to understand the difference between theory and the daily problems of designing reinforced concrete structures.

This book would not have been written without the help and support of friends and colleagues in practice and research. I am much indebted to Peter Whiting LLB (Hons), BSc. FICE for reviewing of the manuscript and his support of my work.

Guenter Axel Rombach
Hamburg, 2004

Notations

In general the symbols of Eurocode 2 are used. These are listed below together with additional abbreviations used in this book.

1 Latin upper-case letter

A	Accidental action; cross-sectional area
A_c	Cross-sectional area of concrete
A_p	Area of a prestressing tendon or tendons
A_s	Cross-sectional area of reinforcement
$A_{s,min}$	Minimum cross-sectional area of reinforcement
$A_{s,prov}$	Area steel provided
$A_{s,req}$	Area steel required
A_{sw}	Cross-sectional area of shear reinforcement
C	Symbol for grade of normal concrete
C_m	Wrapping torsional stiffness
E	Effect of action (member force)
E_c	Tangent modulus of elasticity of normal weight concrete
F	Force; action
F_d	Design value of action
FE	Finite Elements
G_k	Characteristic permanent action
H	Horizontal force
I	Second moment of area
L	Length
M	Bending moment
M_{Ed}	Design value of the applied internal bending moment
N	Axial force
N_{Ed}	Design value of the applied axial force (tension or compression)

P	Prestressing force
P_0	Initial force at the active end of the tendon immediately after stressing
P_{mt}	Mean value of the prestressing force at time t , at any point distance x along the member
Q_k	Characteristic variable action
R	Resistance
R_d	Nominal value of resistance
S	Internal forces and moments
S	First moment of area
S_m	Centre of torsion of a cross-section
S_s	Centre of gravity of a cross-section
SLS	Serviceability limit state
T	Torsional moment
ULS	Ultimate limit state
V	Shear force

2 Latin lower-case letters

a	Distance; geometrical data
Δa	Deviation of geometrical data
a_1	Shift of moment curve
b	Overall width of a cross-section, or actual flange width in a T- or L-beam
b_{sup}	Width of the support
b_w	Width of web on T, I, L beams
c	Concrete cover
d	Diameter; depth
d	Effective depth of a cross-section
e	Eccentricity
f	Strength (of a material)
h	Height
h	Overall depth of a cross-section
i	Radius of gyration
l	Length; span
l_b	Anchorage length
l_{col}	Height of a column
l_{eff}	Effective span of beams and slabs
l_n	Clear distance from the faces of the supports
m	Moment per unit length; mass
n	Number of vertical continuous members
r	Radius
x	

s	Distance; spacing of stirrups
p	Mean transverse pressure over the anchorage length
t	Time being considered; thickness
u	Perimeter of concrete cross-section having area A_c
v	Shear force per unit length
v	Coefficient relating the average design compressive stress in struts to the design value of the concrete compressive strength (f_{cd})
v	Angle of inclination of a structure, assumed in assessing effects of imperfections
x	Neutral axis depth
z	Lever arm of internal forces

3 Greek letters

α	Angle; ratio
β	Angle; ratio; coefficient
γ	Partial safety factor
δ	Increment
ζ	Reduction factor; distribution coefficient
ε	Strain
θ	Angle; rotation
λ	Slenderness ratio
μ	Coefficient of friction between tendons and their ducts
μ	Moment coefficient
ν	Poisson's ratio
ν	Strength reduction factor for concrete cracked in shear
ν	Longitudinal force coefficient for an element
ξ	Ratio of bond strength of prestressing and reinforcing steel
ρ	Over-dry density of concrete in kg/m^3
ρ	Reinforcement ratio
σ	Normal stress
σ_c	Compressive stress of concrete
σ_s	Tensile stresses in reinforcement
τ	Torsional shear stress
\varnothing	Diameter of a reinforcing bar or of a prestressing duct
$\varphi(t, t_0)$	Creep coefficient, defining creep between times t and t_0 , related to elastic deformation at 28 days
Ψ	Factors defining representative values of variable actions Ψ_0 for combination values Ψ_1 for frequent values Ψ_2 for quasi-permanent values

4	Subscripts
c	Concrete; compression; creep
b	Bond
d	Design
e	Eccentricity
eff	Effective
f	Flange
fat	Fatigue
fav	Favourable
freq	Frequent
g	Permanent action
h	Depth of a cross-section
i	Indices; notional
inf	Inferior; lower
j	Indices
k	Characteristic
l	Low; lower
m	Mean; material; bending
max	Maximum
min	Minimum
nom	Nominal
p	Prestressing force
perm	Permanent
pl	Plastic
q	Variable action
rep	Representative
s	Reinforcing steel; shrinkage
sup	Superior; upper
t	Torsion; time being considered; tension
unf	unfavourable
w	Web
y	Yield

1

General

Numerical calculations based on the Finite Element Method are becoming a standard tool in the design of structures. Furthermore, the lower cost of hardware and increased performance of more user-friendly software often displace manual calculations. This applies not only to complicated 3-dimensional structures, like slabs, shear walls and shells of complicated shape, but also to normal beams. It can be economical – as it is much faster – to design a simple supported reinforced concrete beam under uniform loading by using a computer. However, one saves time only when the necessary checking of the numerical results are omitted.

A few years ago large computers were needed and only experts and big consulting offices used this method. Nowadays, a whole building can be handled by a simple PC. Graphical input makes it easy to generate three-dimensional Finite Element meshes with several thousands of nodes. Computer programs can design concrete, steel or wooden structures, which have linear or nonlinear material behaviour, under static or dynamic loading. There no longer seems to be any limitations. Nonetheless, this development has led to an increasing number of cases where the Finite Element Method has been misused.

As daily experience shows, results from computer calculations are often trusted with blind faith. Users assume that expensive computer software must be free from any error. A graphical pre-processor and a user-friendly input of systems and loadings may suggest a high technical competence and reliability of the computer program. Nevertheless, as experience in practice shows, this confidence can only be justified to a very limited degree. Almost no software is free from errors. Therefore, a critical distrust is appropriate, as program errors may also occur in software which has been in use for a long time and which may not have been found to date.

It should always be kept in mind that the Finite Element Method is only a numerical tool based on numerous assumptions and simplifications. This must be considered when using a software for design of structures. Otherwise, the result of the numerical calculations can be totally wrong. For explanation purposes, the following is a very simple example: a plate element only provides a numerical model of a real slab. It is assumed to have a linear strain distribution over its depth under pure bending. There are no stresses at the midplane. With such a plate element, one will never be able to estimate the normal forces of a simple supported rectangular slab due to temperature changes or shrinkage, even if the supports are fully restraint in horizontal directions.

The modelling, the discretization, of real reinforced concrete structures is the focal point of this book. The fundamental aspects are illustrated by practical examples of concrete structures. This book does not look into the fundamental basis of the Finite Element Method, as numerous publications are already available (see, for example, references [1–3]). The so-called state of the art of the Finite Element techniques will not be discussed as there seems to be a great gap between the ongoing research and the day-to-day problems that a structural engineer has to face. An engineer has neither the time to make highly sophisticated numerical models nor the experimental data to verify his analysis. He is not even interested in the 'correct' results. His goal is simply to estimate the required amount of reinforcement and its accurate arrangement (the 'dimensioning' of a structure), in order to build a safe and economical structure. The calculation of the member and internal forces and moments is only a required step to reach this goal.

The examples shown in this book are calculated using standard software, used in day-to-day practice, and not with one of the advanced general-purpose Finite Element packages such as ABAQUS, ADINA or ANSYS which offer a great variety of different elements and material models. Hence, the reader can easily verify the given examples using his or her own software. A further reason for the strong relation to practical design is that a user of a software package is not usually familiar with its theoretical background. He cannot modify it. It does not help him if he knows that, for example, a reduced integrated 3-noded shell element may give better results than a full integrated 6-noded isoparametric element. He is just using the 'black box'. The user, however, is supposed to have sufficient knowledge to see and solve the problems, which may occur in a Finite Element analysis. This is where this book is intended to provide help.

It is surprising that, in structural engineering, the use of Finite Elements causes numerous problems, especially as this numerical method was first used by structural engineers. The world's first electronic programmable calculator was built by the *structural* engineer Konrad Zuse in May 1941. He was tired of repeating calculation procedures when designing structures. Zuse also developed the first algorithmic programming language, 'Plankalkuel'. In other fields of engineering, like, for example, the automobile or aircraft industry, the numerical FE-analysis of highly complex problems, such as the crash behaviour of a car, the optimization of aerodynamics, or the processes in the engine, have become a day-to-day practice. The reasons for this discrepancy is that these sorts of costly and complicated computer calculations are only economical for mass products. In contrast, a building is usually a unique structure, whose costs depend on several factors, not only the cost of its building material. The numerical modelling of the complex behaviour of the composite material 'reinforced concrete' causes far greater problems than the elasto-plastic bilinear behaviour of metals.

This book focuses on the numerical analysis of structures made of reinforced or prestressed concrete. Finite Element calculations of concrete structures have the following different and exceptional features in comparison with other materials:

- Reinforced or prestressed concrete is a composite inhomogeneous material with a very complex nonlinear material behaviour, thus an 'exact' model is far too costly for daily structural design. Therefore, the calculations of the member forces are mostly based on a linear elastic material model. Stiffness reductions, as a result of crack formations or the 'yielding' of concrete in regions with high compressive stresses, are ignored. The extent of this very large simplification should be justified for each calculation.
- The required material parameters, like, for example, elastic modulus E_c , concrete compressive strength f_c , Poisson's ratio ν , show a large scatter in comparison with other construction materials. Furthermore, they are often time-dependant. The actual quality of construction (workmanship, weather conditions, curing) is not known during the design stage, however, this can influence the material parameters.
- Concrete material is often used for massive members where, for example, the Bernoulli hypothesis of a linear strain distribution over the depth of the cross-section does not apply. Therefore, standard beam and plate elements should not be used for the design of the so-called discontinuity regions.

- Plane shell structures, like, for example, slabs and shear walls, are often made of reinforced concrete. For such members an elastic design is not sufficient. The cracking of the concrete has to be considered in the arrangement of the reinforcement of a deep beam. The pin supports of flat slabs may cause singularity problems.
- The actual detailing arrangement of the reinforcement in a member is very important for the behaviour of a structure, and not just for the calculation of the forces and the amount of reinforcement required.
- There are numerous parts of a concrete structure, where a full, detailed calculation of its load bearing and deformation characteristics cannot be economically justified (such as for the frame corners or corbels).
- Most concrete construction components are unique, for which a major computer calculation is generally not economical.
- Concrete members can be produced with arbitrary shapes and cross-sections.
- The construction process, as well as the time-dependant behaviour of concrete, can be of considerable significance.
- For some load cases, like, for example, restraints or torsional moments, the forces are reduced by cracking and do not need to be considered in the calculations.

The uncritical or erroneous use of Finite Element software can lead to serious damage as the collapse of the Sleipner A platform (Fig. 1.1) has impressively demonstrated [4, 5]. This so-called Condeep-Platform had a total height of 110 m. The four towers rested on 24 cylindrical cells, each having a diameter of 24 m. On 23 August, 1991, the concrete platform collapsed completely during its lowering and sank down to the seabed. The actual financial damage was estimated at about US\$250 million. The cause of the total collapse was found in serious inaccuracies in the global Finite Element analysis of the structure and faulty reinforcement arrangement in the connection area of the cell walls. The element mesh used for the calculations was too coarse to determine the actual forces in the members. This disaster raises a critical question, whether nowadays this sort of accident could still be allowed to happen. The essential causes of this case of damage and the consequences of the numerical analysis are discussed in detail in Chapter 5.

This accident significantly demonstrates an essential problem in complex numerical calculations: the insufficient control of the results due to the large amount of data output. The more complex the numerical

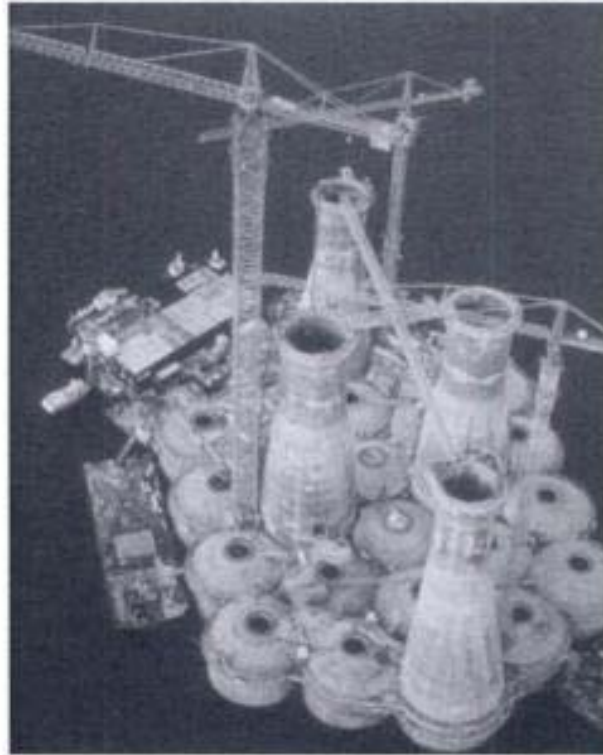


Fig. 1.1 Sleipner A platform (photo NC)

models are, the more difficult it becomes to recognize the areas of possible mistakes and inaccuracies.

In this respect, it is the author's opinion that the modelling of a structure as a whole, by the help of shell elements, for example, multi-storey buildings or bridges, is rarely meaningful; although this approach is often encouraged by the software companies. A structural engineer must always be able to understand the behaviour of any complex structure and to idealize it so that the flow of forces can easily be understood and calculated. Complex Finite Element calculations can then be used to lower any excessive safety margin of simple models and produce a far more economical structure. However, complex Finite Element models must never be used to replace either the design engineer or any of his missing expertise. Costly, sophisticated analysis does not always lead to more realistic results. Furthermore, the amount of a Finite Element analysis should be considered with respect to the degree of accuracy that is actually necessary. The results of any calculation can only be as accurate as the underlying assumption of its numerical model. One should always keep in mind that there can always be considerable variation in the actual loading of a structure and in the properties of its materials.

1.1 Introduction to the Finite Element Method

This very short introduction gives a brief precis of the basics of the Finite Element Method. Further and more detailed information can be found in numerous publications, e.g. [1–3].

In using the Finite Element Method, a complex structure is subdivided into a finite number of individual components called ‘elements’ (discretization), whose behaviour – the relation between their nodal displacements (static analysis) and their nodal reactions – can be specified by a limited number of parameters and analytical functions, the so-called shape or form functions (see Fig. 1.2). All displacements, strains and stresses within an element, as well as the resulting nodal forces, can be calculated by means of the shape functions and their derivatives respectively. The individual elements are only interconnected by their nodes. The solution of the complete system follows from the assembly of all of these elements. The stiffnesses of all the elements $[K]^e$ are added to arrive at a global stiffness matrix $[K]$, from which the unknown nodal displacements $\{u\}$ can be calculated.

$$[K] \cdot \{u\} = \{F\}$$

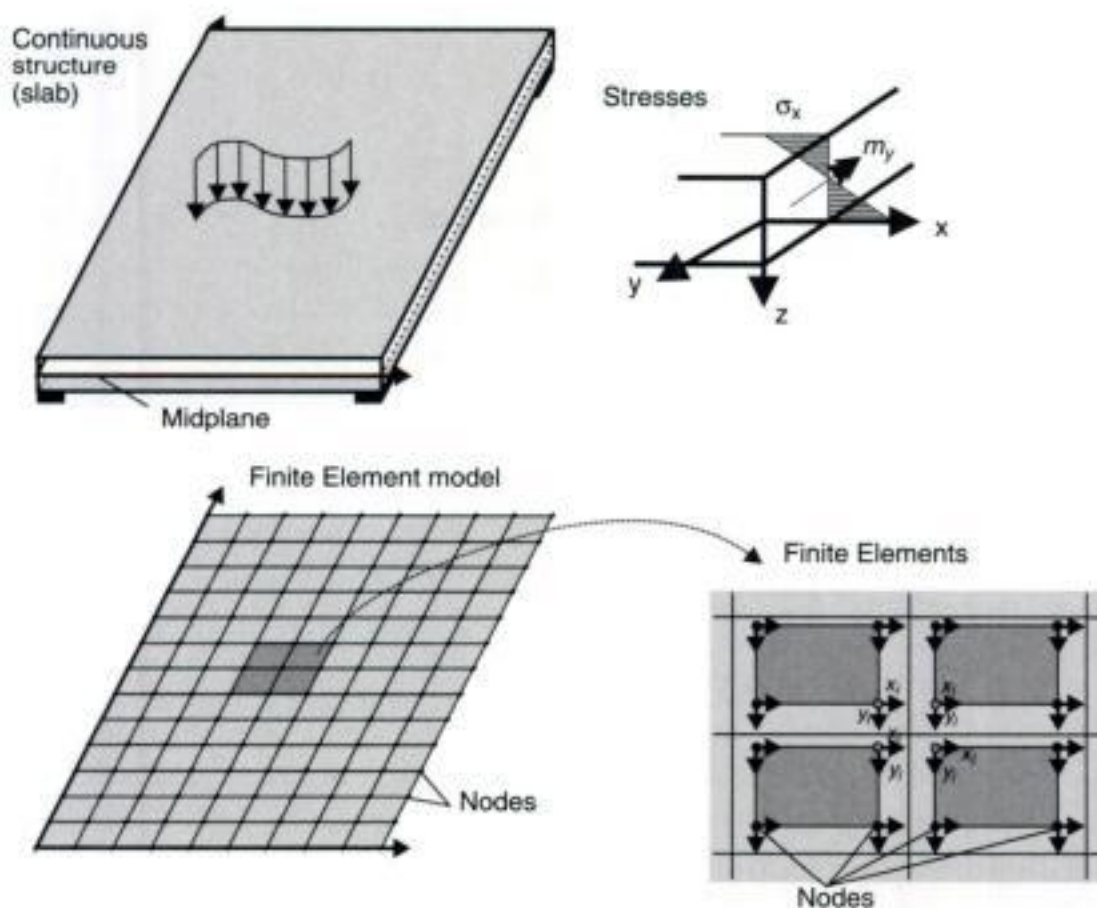


Fig. 1.2 Numerical analysis of a continuous structure (slab)

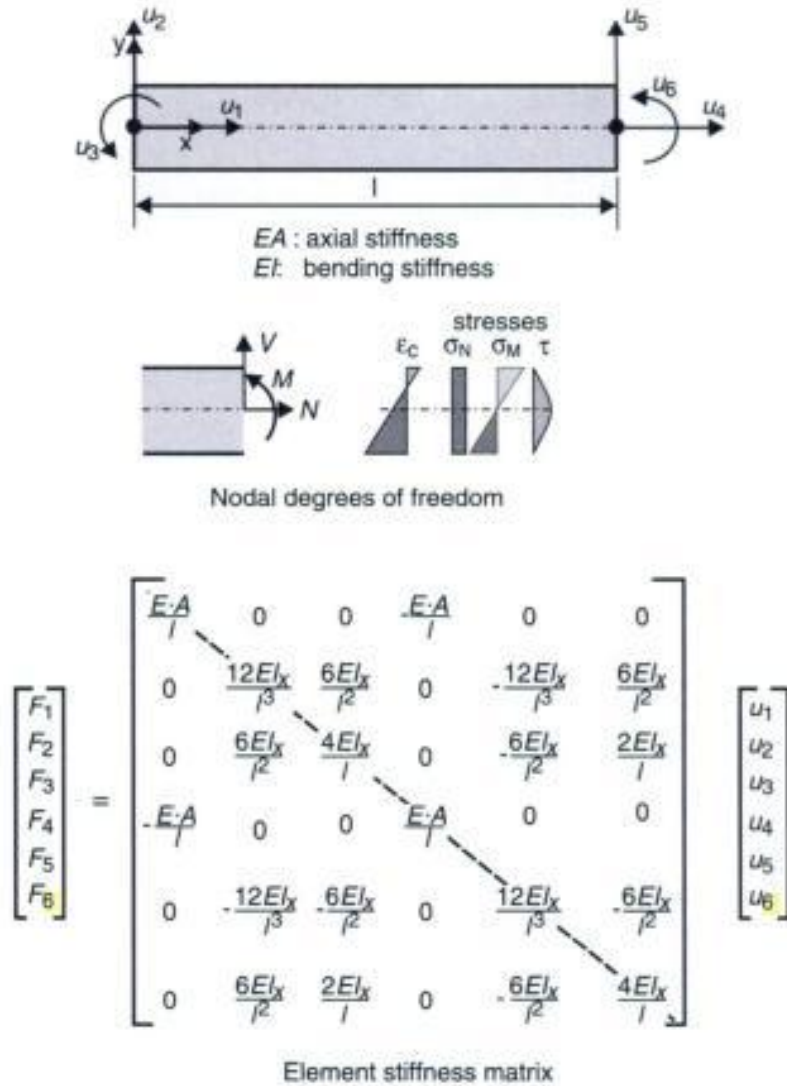


Fig. 1.3 2-noded plane truss element (without torsion)

where:

- $[K]$ is the global stiffness matrix $[K] = \Sigma[K]^e$;
- $\{u\}$ is the vector of nodal displacements;
- $\{F\}$ is the vector of nodal forces (loading).

The main task is to find form functions which can approximate the behaviour of a special structural element and satisfy the compatibility condition. For simple elements like the 2-noded truss element shown above (Fig. 1.3), the relation between the nodal forces $\{F\}^e$ and the nodal displacements of each element $\{u\}^e$ can be found by means of equilibrium conditions.

For more complex elements, like, for example, plate or shell elements, virtual work or virtual displacement principles are used.

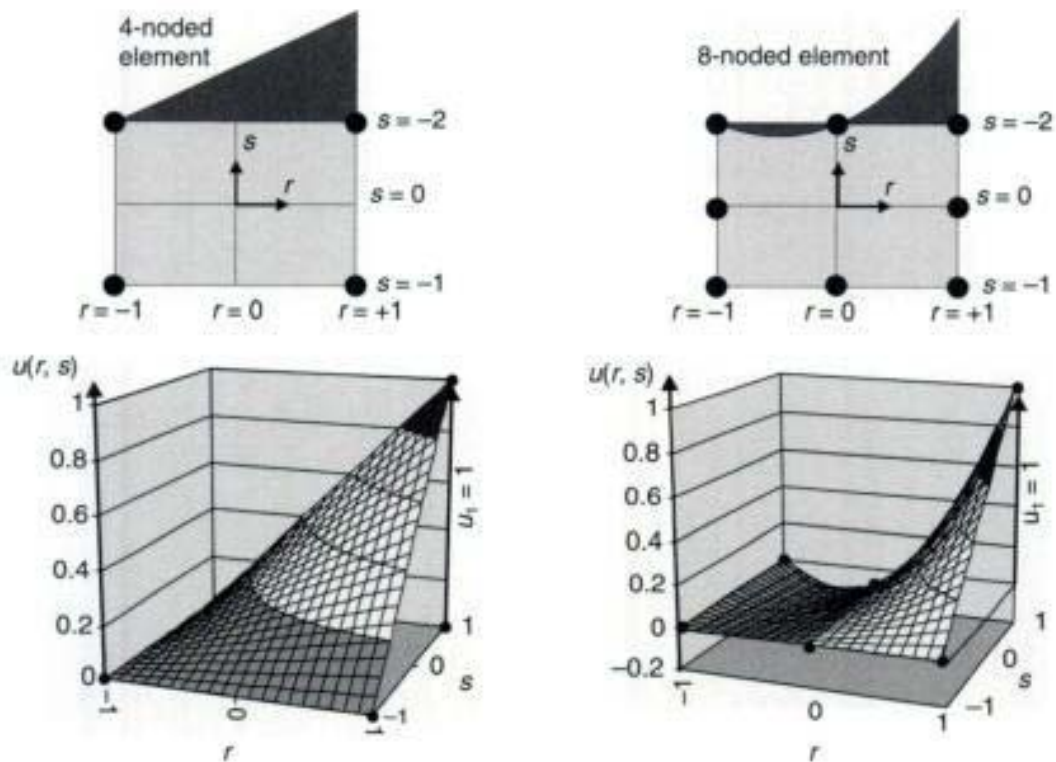


Fig. 1.4 Displacements within a 4-noded and 8-noded element for $u_1 = 1$

Figure 1.4 shows the displacements within a 4-noded and an 8-noded isoparametric element for a unit deflection of $u_1 = 1$ at node no. 1. It can clearly be seen that both elements have different displacements and thus different strains, even if the nodal values are equal.

The basics of the Finite Element technique set out above therefore give the following important conclusions:

- A Finite Element model is based on nodal forces and nodal displacements (static analysis).
- All values, like, for example, displacements, strains or stresses within an element, are calculated by means of shape functions.
- The nodal forces are calculated by shape functions and not by equilibrium conditions.

1.2 General problems of numerical analysis of concrete structures

The following is a summary of the significant problems in numerical analysis of reinforced concrete structures. A detailed discussion can be found in the chapters that follow.

1.2.1 Program errors

One should always keep in mind that computer software, in general, is not error free. The more complex the software is the sooner it becomes difficult for the software engineer to examine all of the possible eventualities in advance. This problem can be made worse for the user by the issue of updates to a previously error-free software, which then suddenly produces incorrect results. This problem can only be met by use of independent checking calculations.

Next the computer has a limited accuracy, e.g.:

$$2^{45} - 0.8 - 2^{45} = -0.8008 \quad \neq -0.8000$$

$$2^{50} - 0.8 - 2^{50} = 0.0 \quad \neq -0.8000$$

1.2.2 Model errors

The majority of errors come from the modelling, i.e. making an idealization of a real structure (Fig. 1.7).

1.2.2.1 Model material

The calculation of the action effects (internal forces and moments) is usually based on a linear elastic material behaviour, although it is well known that concrete is a highly nonlinear material. The Eurocode EC2, Part 1 [6] allows for nonlinear or plastic analysis, but, in design practice, such complex analysis is very seldom justified, due to the large amount of work needed. Furthermore, the combination of the results from various load cases is then no longer possible, which increases the workload substantially. Therefore, the design is usually based on a linear-elastic material behaviour with limited redistribution of member forces. The accuracy of such simplified analysis is generally sufficient. In addition to slender columns or thin shell structures, there are other structures where the nonlinear behaviour may be significant. This will be further discussed in Chapters 2 and 3.

1.2.2.2 Loading

A Finite Element model (FEM) is based on nodal forces and nodal displacements (Fig. 1.5). This is still valid when an arbitrary load arrangement is possible. In this case, the software calculates the equivalent nodal forces. Depending on the size of the elements this may lead to a considerable extension of the actual area under load.

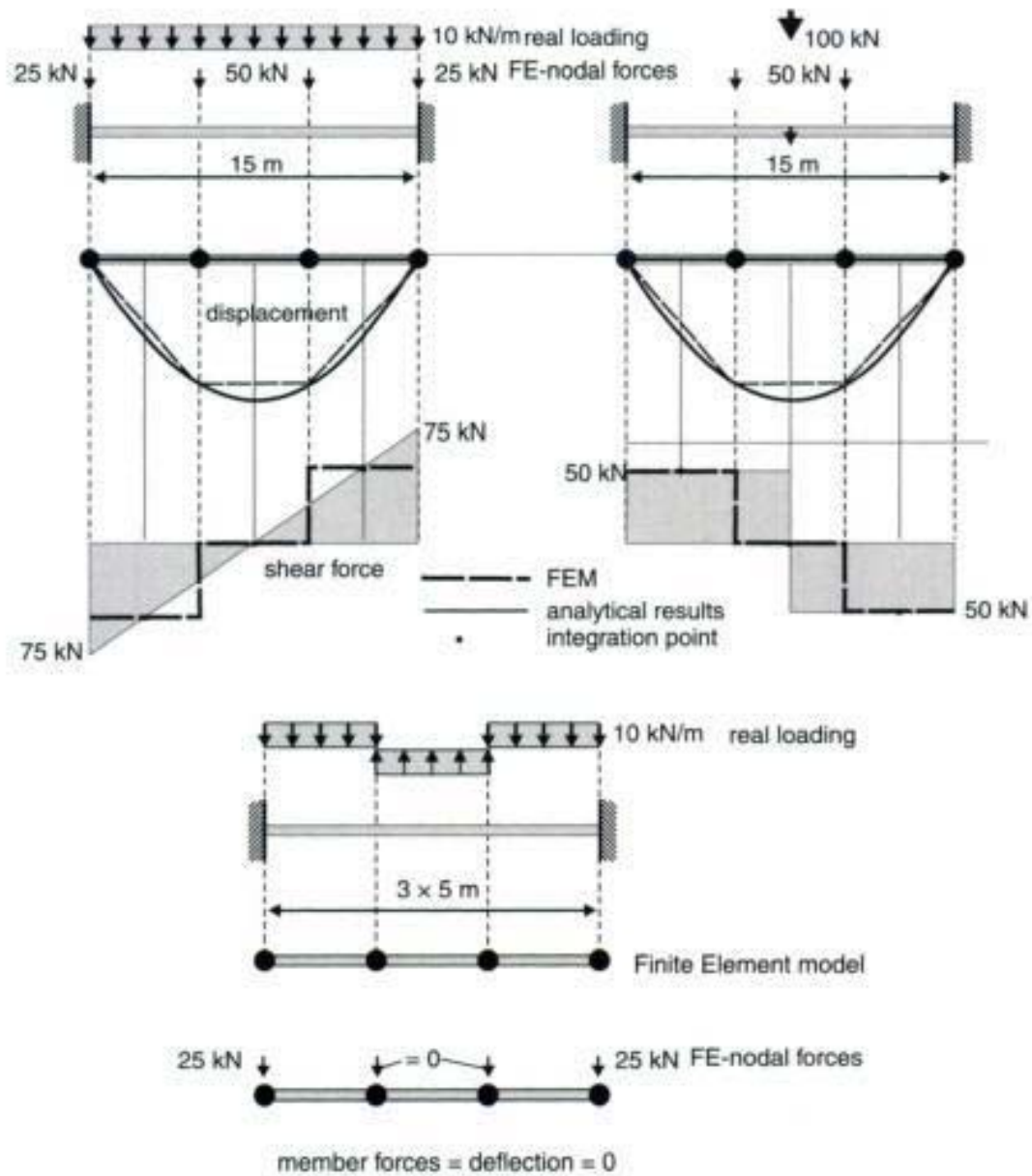


Fig. 1.5 Difference between FE-nodal loading and real loading

This is important, for example, in the calculation of slabs under concentrated loads, e.g., wheel loads on bridges.

Furthermore, loads on fully restraint nodes are mostly neglected in the design and hence in the results. The total support force is only the sum of the loads on the unrestrained nodes. This has to be considered, when support forces from the Finite Element analysis are used for loading of other members. Loads on columns and walls, which may be fully restrained in the numerical model, are neglected by some software programs.

The nodal forces result from the chosen element with respect to its shape functions and not from 'engineering' experience. Figure 1.6

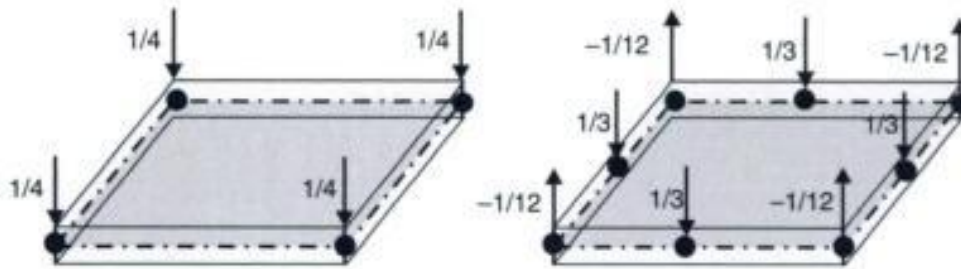


Fig. 1.6 Nodal forces for a 4-noded and 8-noded isoparametric plate element under constant vertical loading

shows the nodal forces for a 4-noded and an 8-noded plate element under a constant vertical loading. For the 4-noded element the load is distributed equally to the nodes, whereas the 8-noded element shows uplifting forces at the edge nodes.

1.2.2.3 Determination of the required reinforcement

Nowadays the estimation of the reinforcement required and its detailed arrangement in truss and plate structures, is not a problem. However, this is not the case for deep beams and shell structures. Here, a software

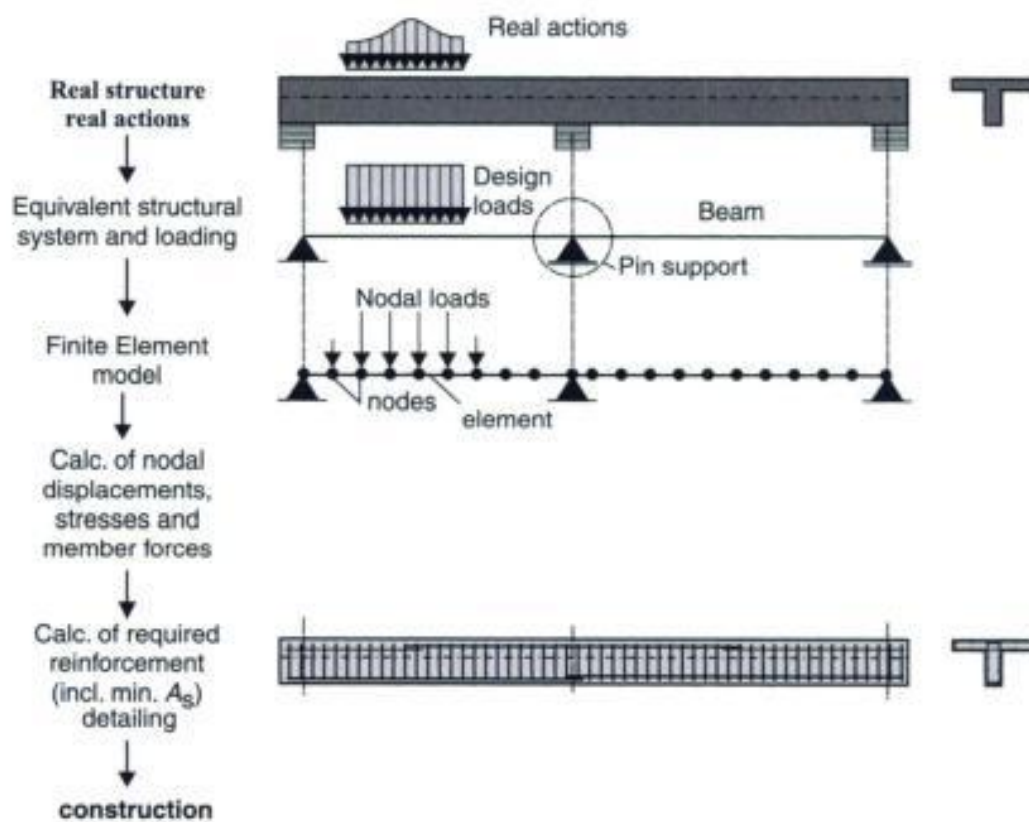


Fig. 1.7 Numerical analysis of a real structure

program in general is not able to make the best detailing of the reinforcement, as it is based on an element-wise analysis. Force redistribution, due to the cracking of the concrete, is not considered in a linear-elastic analysis. In general, a Finite Element model with shell elements will not be able to distinguish between a member in bending and one in compression, whereas their design must be different. Thus, the model can lead to incorrect results. The same is true for designs under shear forces.

1.2.2.4 Discretization

The numerical modelling of a real structure, the 'discretization' (subdividing a structure into a finite number of different elements), is where most of the errors are made. Here, among other matters, special note should be made on the following:

Size of elements: Some years ago the number of elements was limited due to the capabilities of both hardware and software, whereas nowadays a sufficient fine discretization of a whole building can easily be done without any major difficulties. Furthermore, an element mesh can be produced very quickly by graphical pre-processors. Nevertheless, even automatic mesh generation should not be used in an uncaring or uncritical manner; engineering knowledge is still required. An inadequate modelling of apparently irrelevant details, like, for example, small cantilever slabs of a bigger plate (section 4.12.2) or openings in a flat slab near columns, can lead to faulty calculations and an unsafe design. A sufficiently fine element mesh should be used in regions of high deformation or stress gradients.

Element form functions, incompatible elements: In general the user of a software program has no information of the numerical algorithms and the form functions for the elements which the software is based on. Nevertheless, he should have a basic knowledge to know at least the principal difference between a beam, a plate and a shell element in order to understand that the various element types cannot be simply joined together, even if this is possible.

Support: The numerical modelling of the supports of shell structures should be carried out with great care, as this is where fundamental mistakes can be made. This aspect of a design will be explained for a deep beam in Chapter 3, and for a flat slab in Chapter 4.

Singularities: Singularities, or infinite stresses and internal forces, occur in slabs or shear walls under high concentrated point loads. It should be

kept in mind that this problem only occurs in a numerical model caused by simplifications and assumptions of the element's behaviour. A real structure does not show any infinite internal forces. In regions of high compression, the concrete may 'yield'. Tensile stresses may cause the formation of cracks. The high forces shown by a Finite Element analysis in singularity regions, do not happen in a real structure, and thus need not be considered in the design. Nevertheless, the user should know about these problems and how the results of the numerical analysis (e.g. bending moments and shear forces) should be interpreted.

Kinematic systems: In general, a software program gives out warnings or stops the analysis when the structure becomes kinematic. In these cases, the system of equations has no unique solution. There is no unique solution for the nodal displacements. These warnings can, however, be easily overlooked due to the great quantities of data produced, which can only be checked by graphical control. If the distribution of forces is reasonable, these mistakes will not be noticed, and the structure will be designed for actions and erroneous member forces of a kinematic system.

2

Truss and beam structures

The internal forces and moments in trusses and beams can be determined by means of the Finite Element Method as well as by load transfer methods. Either method produces the same model problems when considering actual structures.

Truss systems are not only used for analysing beams and columns. Nowadays, they are also used as an equivalent system for the structural analysis of flat shell structures, like shear walls (see section 2.5) or T-beam bridges (see section 2.8). The main reason for this simplification of spatial shell structures by simple beams is that the amount of calculation needed for beam or truss systems is considerably less than that for a three-dimensional shell design. This is especially true for the calculation of the reinforcement requirements.

This chapter starts off by examining various detailed problems related to the correct modelling of so-called 'discontinuity regions'. These regions are those where the essential assumption of truss elements, the Bernoulli hypothesis which states that the section remains approximately plane before and after loading, is not valid. Examples considered are those of beam column intersections, frame corners, beams with abrupt or smooth change of cross-sections or openings, halving joints and inclined haunches.

Even if the action effects in these discontinuity regions cannot be calculated accurately, it is important to model the different stiffnesses of a structure. The main differences in the various modelling used for frame corners are shown in an example of a frame bridge with shallow foundations and the transverse design of a hollow box girder bridge. The modelling of a foundation slab bedded on ground (section 2.4.1) and a bridge column supported on piles (section 2.4.3) will also be discussed.

Following the discussion of these detailed problems, we look at the design of whole structures. The calculation of coupled concrete shear walls with large openings, which are used as bracing elements in high-rise buildings, is shown in section 2.5. Then the modelling of a complex bracing system of a high-rise building consisting of cores of different shape and shear walls is discussed, followed by the analysis of a hollow box girder and a T-beam bridge by means of a grillage (plane grid) system. This chapter ends by looking at some problems in the calculation of reinforcement requirements in beams.

2.1 Corners in frame structures – rigid regions

Beam column intersections are regions for which the assumption that a section remains approximately plane before and after loading (the Bernoulli hypothesis) does not apply. This is where a truss analysis can only provide an approximate value for the member forces.

In design calculations, 'exact' values are often not needed. In general, the purpose of the structural analysis of a frame is not to calculate the maximum member forces at the beam column junction of the centre-lines, but rather at the inner face of the corner for bending or at a distance of $1.0d$ for shear (d = effective depth of a cross-section). However, the exact modelling of the stiffness of the frame corner is important, as these can have a large effect on both the internal forces and the deformation of a member or structure.

In a real structure the frame corners generally behave like a stiff diaphragm. Therefore, in these areas the nodes of the truss model cannot move independently from each other (see Fig. 2.1). The simplest way of taking this condition into account is through a stiff coupling of the corner nodes. An alternative is to introduce an additional stiff inclined truss element. However, this may cause numerical problems because of the great stiffness differences of the system.

The following two examples will show the influence of the numerical modelling of beam column intersections. The first one is a portal frame bridge with shallow foundations, which is widely used for road underpasses. The second example deals with the transverse design of a hollow box girder bridge.

2.1.1 Portal frame bridge

When modelling a truss system, the nodes must be in sections which are relevant to the design. Most computer programs determine the member

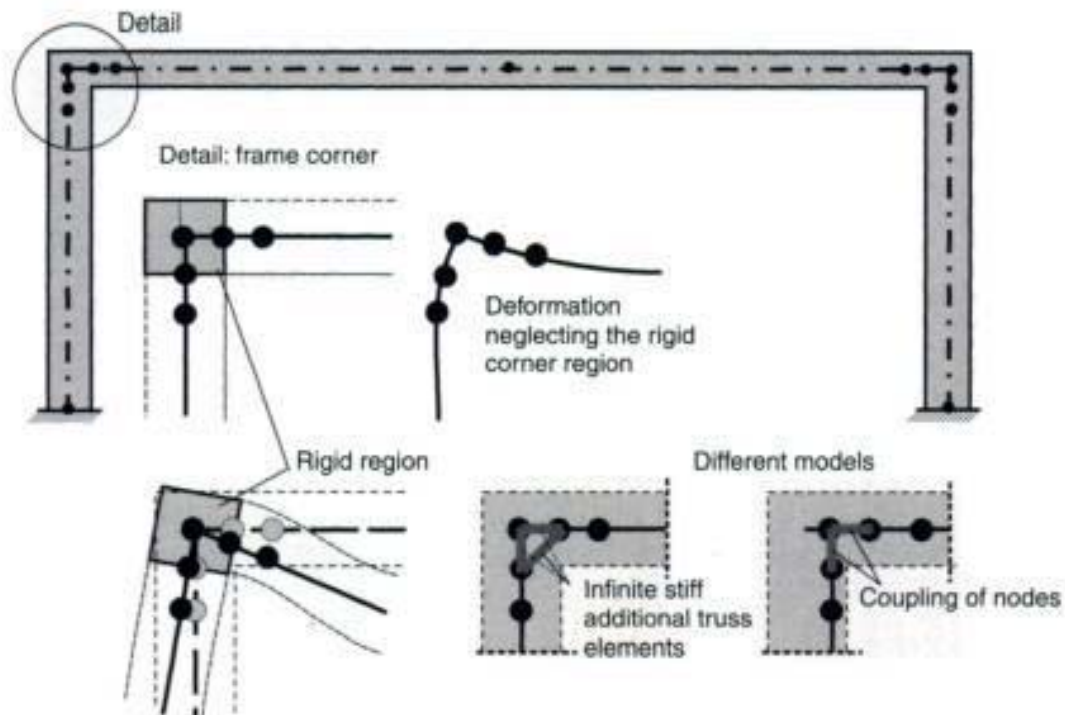


Fig. 2.1 Frame structure

forces and the reinforcement requirements only for the nodes at the beginning and the end of the element or at the integration points.

The relevant sections for design are:

- At a distance of $0.2 d_{\text{Beam}}$ from the inner face of the corner and at the inner face of the corner in the design procedure for bending moments;
- At a distance of $1.0 d_{\text{Beam}}$ from the inner face of the corner in the design procedure for shear forces;
- At the midspan of the top beam for calculation of greatest bending moments and the maximum deflection.

There are various loadings to be considered in the design of portal frame bridges. This means a considerable amount of work for the manual calculation of the member forces. In addition to the dead and live loads acting on and adjacent to the frame, various earth pressure distributions have to be considered. In general, the structure should be designed for the following load cases:

- dead load;
- active earth pressure;
- increased active earth pressure on both walls;
- asymmetric earth pressure: increased active earth pressure on one wall and active earth pressure on the other;
- live load on the backfill (left/right);



Fig. 2.2 Portal frame bridge

- loading due to the traffic on the frame horizontal member;
- traction and braking forces of the traffic;
- loading due to temperature, for example (for concrete bridge in Germany, see EC1)

$$\Delta T_{M,neg} = T_{e,min} - T_0 = -27K - T_0$$

$$\Delta T_{M,pos} = T_{e,max} - T_0 = +37K - T_0$$

- differential temperature of the horizontal member $\Delta T_{M,pos} = +15K$ and $\Delta T_{M,neg} = -8K$ (for concrete bridges in Germany).

Furthermore, it must be remembered that due to the short length of the foundation beam at the inner face of the frame (see Fig. 2.3) member forces, as calculated by the computer program, cannot be used for the purpose of the design. This is without doubt a discontinuity region to which the Bernoulli hypothesis does not apply. Nevertheless the entire foundation should be modelled, since not only the member forces of the structure but also the soil pressure distribution and the settlements must be determined.

The truss elements will be located at the centreline of the beam and columns (Fig. 2.3). But in this case, the cross-section of the corner region will not be modelled correctly. However, the additional dead load can be neglected in general. The elastic bedding of the foundations

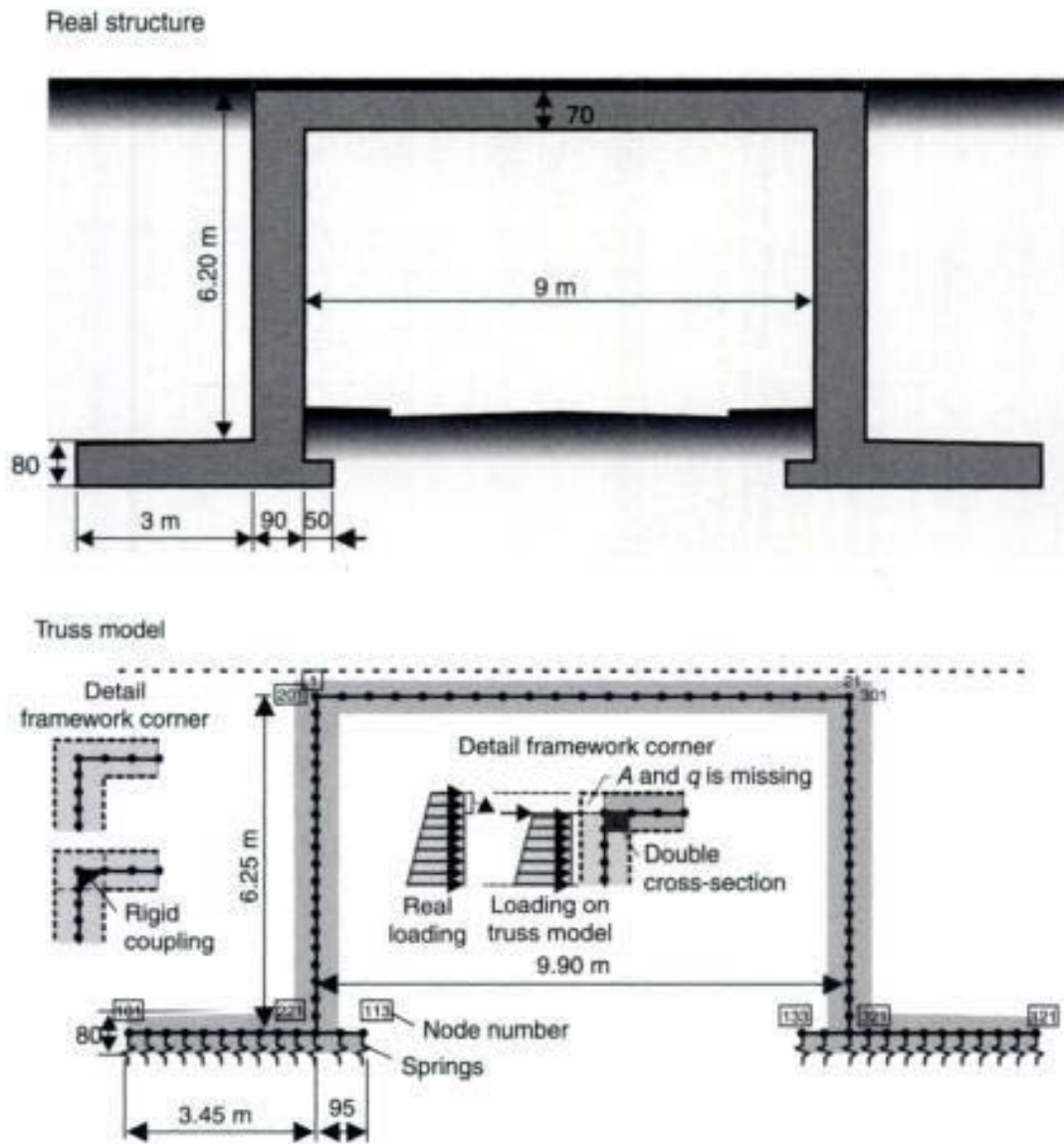


Fig. 2.3 Portal frame bridge – numerical model

can be modelled with individual springs or with special boundary elements. In this example, the bedding modulus is taken to be $k_s = 10 \text{ MN/m}^2$.

The walls are loaded by a trapezoidal earth pressure distribution. It should be kept in mind that the height of the truss model is smaller than the height of the real structure (i.e. the height of the column is 6.25 m, whereas the height of the real structure is $6.20 + 0.80 = 7.0 \text{ m}$, see detail Fig. 2.3). Therefore, additional horizontal loads must be applied on the corner nodes. The same applies to the vertical loads on the horizontal member.

Figure 2.4 shows the calculated bending moments, the shear forces, and the displacement of the structure. These were calculated both with

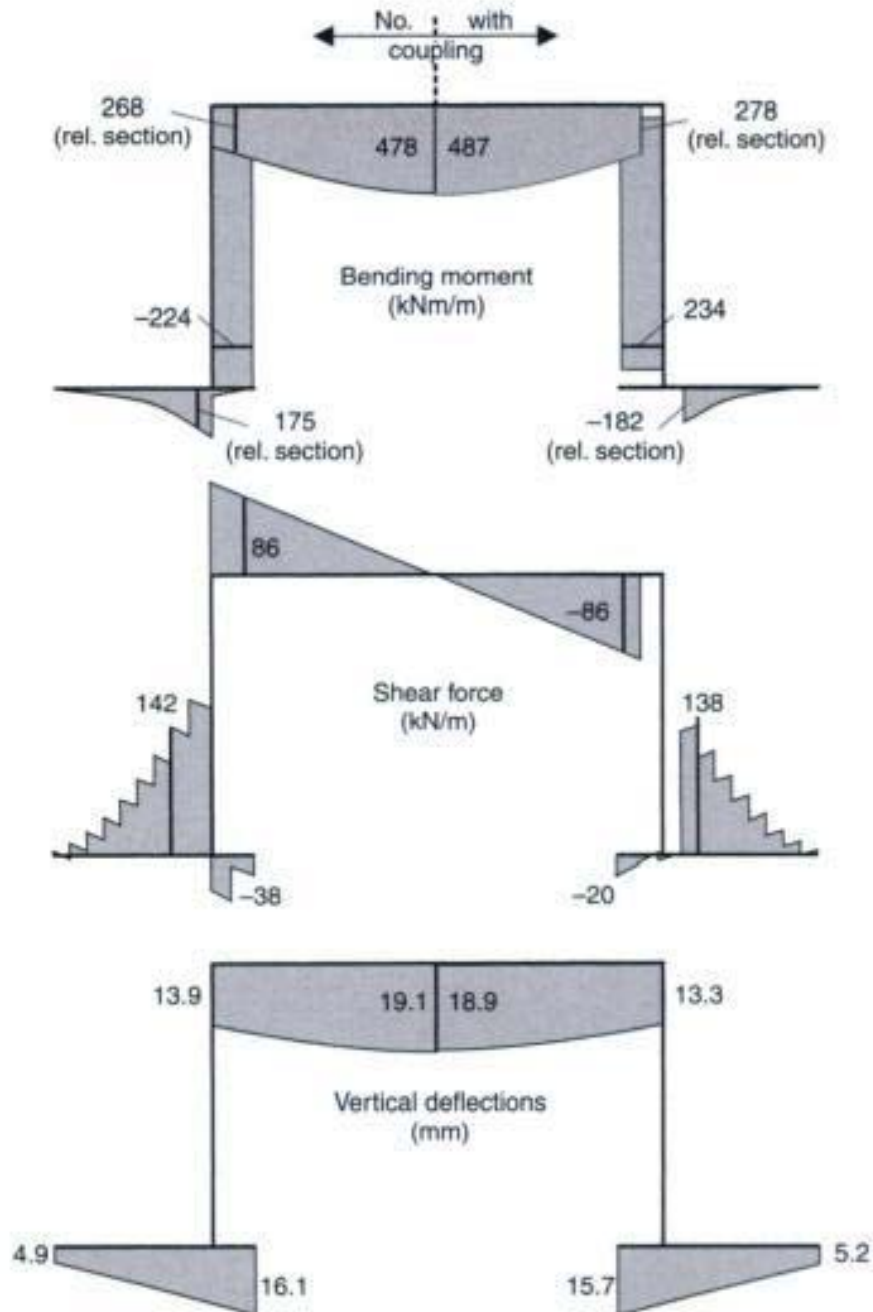


Fig. 2.4 Shear forces, bending moments and deflections with and without coupling of the corner nodes for the load case 'dead load'

and without coupling of the corner nodes. The system shown is under dead load only.

With this system, as expected, the influence of the node coupling is very small (see Fig. 2.4). This further applies to the relevant design forces from an unfavourable combination of relevant actions. The differences are estimated at less than 3% for the bending moment in the critical sections and approximately 6% for the vertical displacement at midspan.

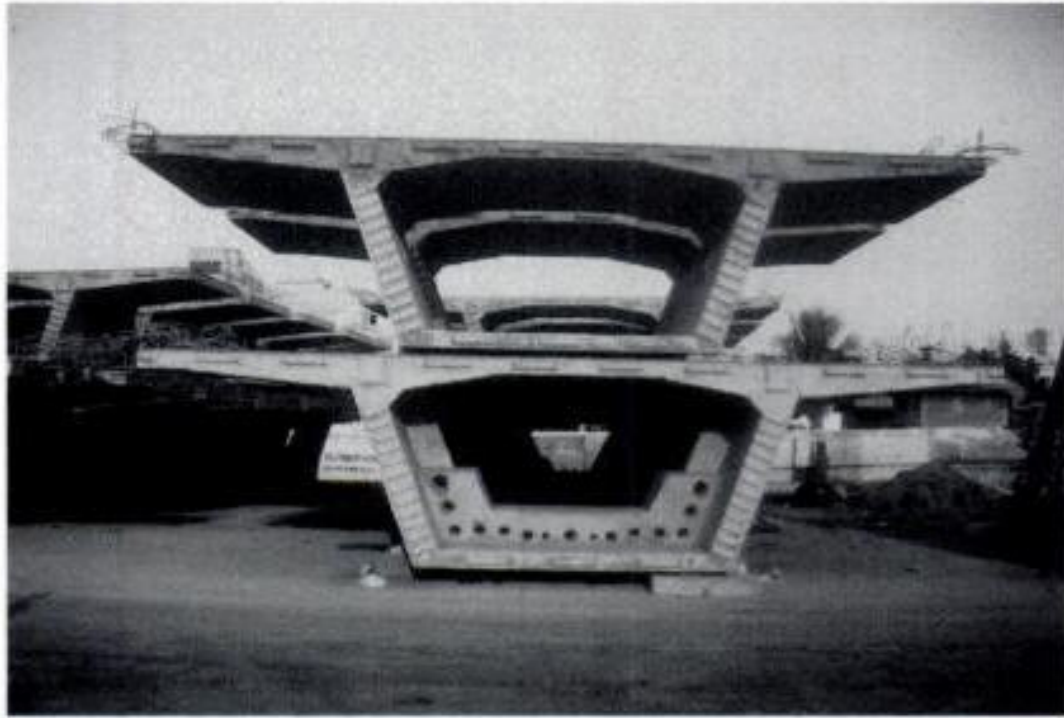


Fig. 2.5 Standard and deviator segment, Second Stage Expressway, Bangkok [12]

2.1.2 Transverse design of a hollow box girder bridge

Figure 2.5 shows a cross-section of a hollow box girder bridge. In this particular case, the segments are the standard cross-section of what is currently one of the longest segmental hollow box girder bridges in the world, the Second Stage Expressway System in Bangkok, Thailand [12] (Fig. 2.6).



Fig. 2.6 'Standard' span, Second Stage Expressway, Bangkok [12]

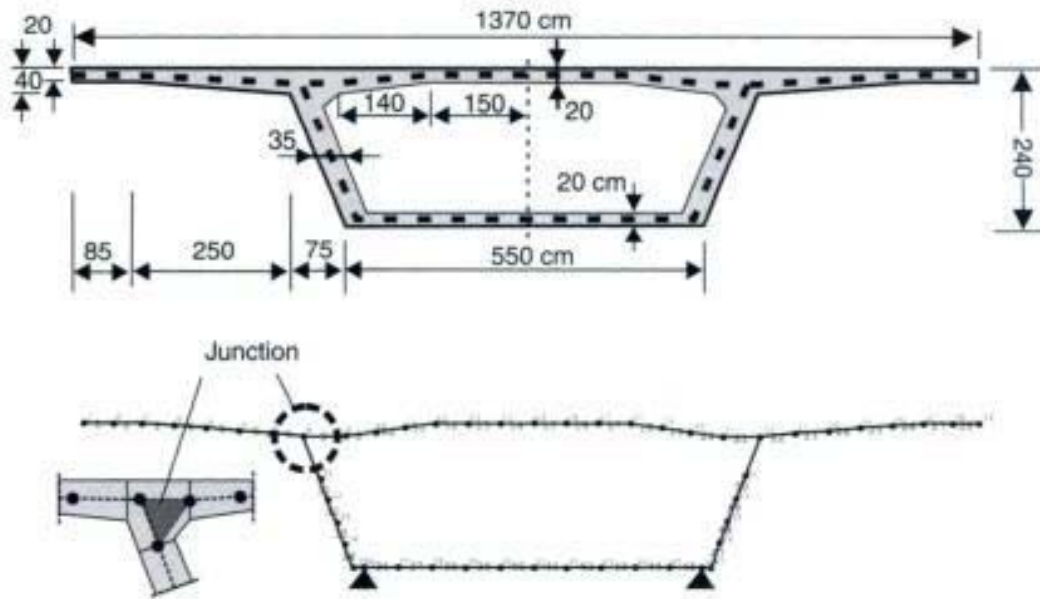


Fig. 2.7 Cross-section and resulting truss model of a hollow box girder bridge (standard segment, Second Stage Expressway, Bangkok)

The design of a bridge is usually done separately for the transverse and longitudinal directions. In the following example, we are looking at only the transverse behaviour. To do this, a '1 m' wide section is taken of the bridge and modelled by truss elements. The variable depth of the beams and the inclination of the axis of gravity are taken into account (see Fig. 2.7). There are pin supports under the webs, which are fully restrained in the vertical direction. The system is also a frame structure. Of further interest is the modelling of the corners, the junction between the webs and the deck slab.

The behaviour of the structure will be examined under two different theoretical unit loadings, a linear loading of $q = 10 \text{ kN/m}$ at (a) the outer edge of the cantilever slab and (b) at midspan of the top slab.

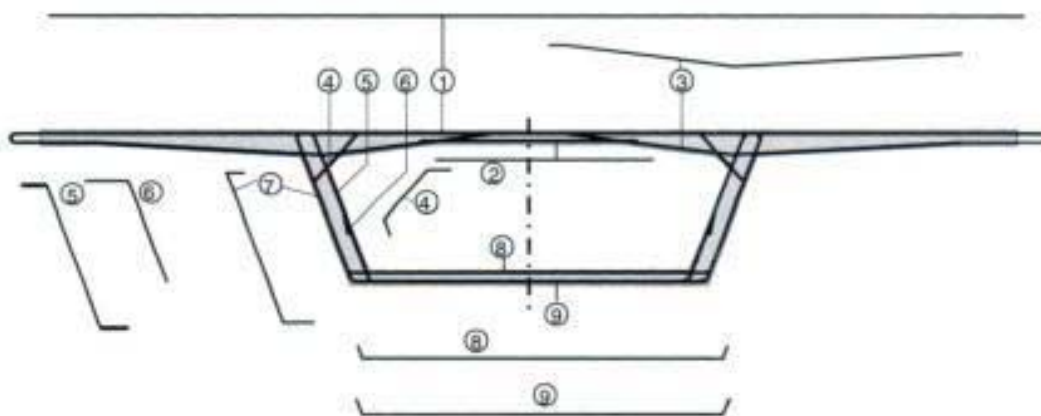


Fig. 2.8 Reinforcement layout

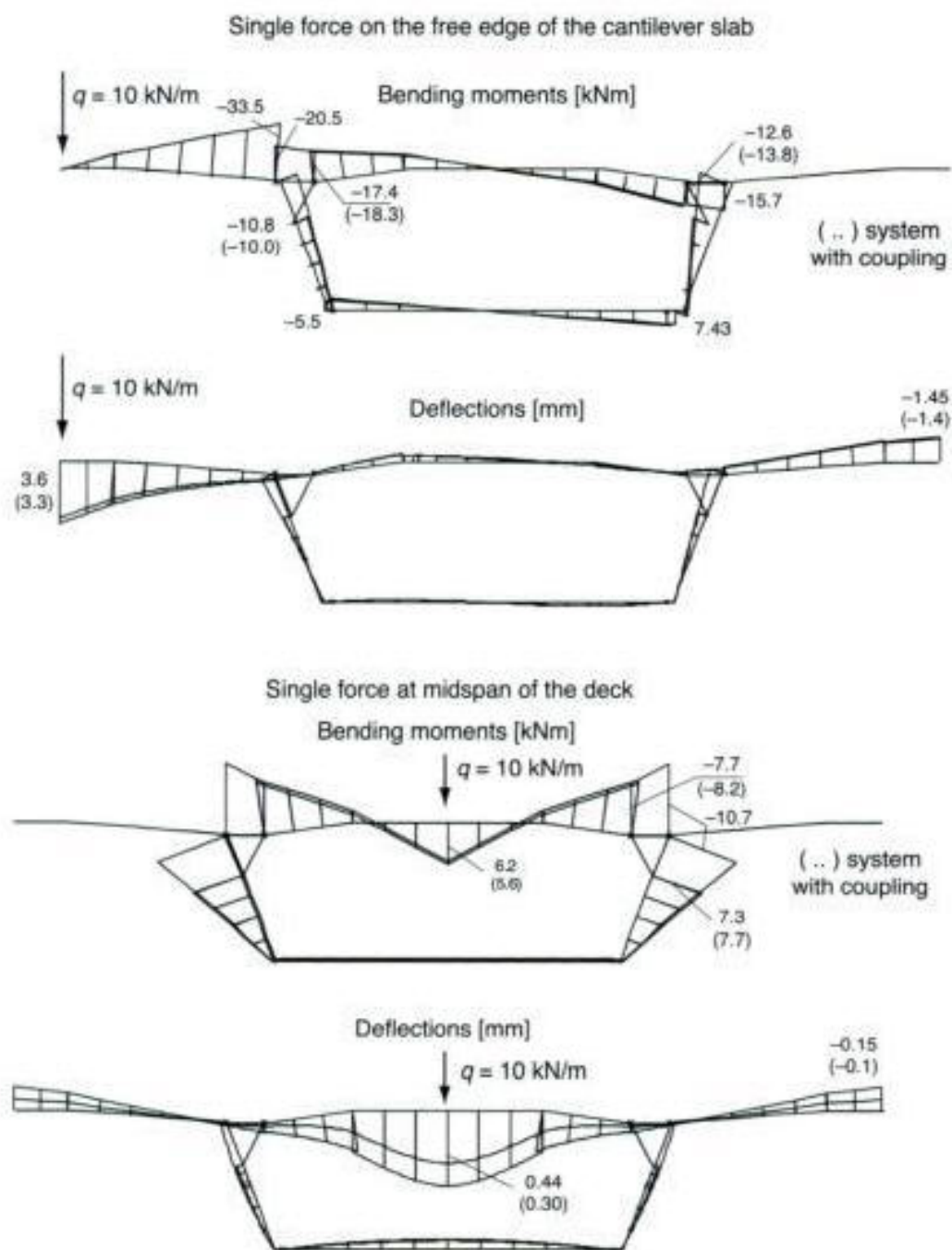


Fig. 2.9 Bending moment distribution and deflections due to a single force at the free edge of the cantilever slab (top) and at midspan of the deck (bottom)

For the load on the cantilever slab, the bending moments and the displacements are only slightly influenced (by 5%) by the modelling of the corners (with/without coupling) (see Fig. 2.9). For the line load acting at midspan of the top slab, the coupling of the corners causes the bending moments and the deflection at midspan to vary by approximately 10% and 50%, respectively. The latter value definitely cannot be neglected. The difference between the moment



Fig. 2.10 Finite Element mesh

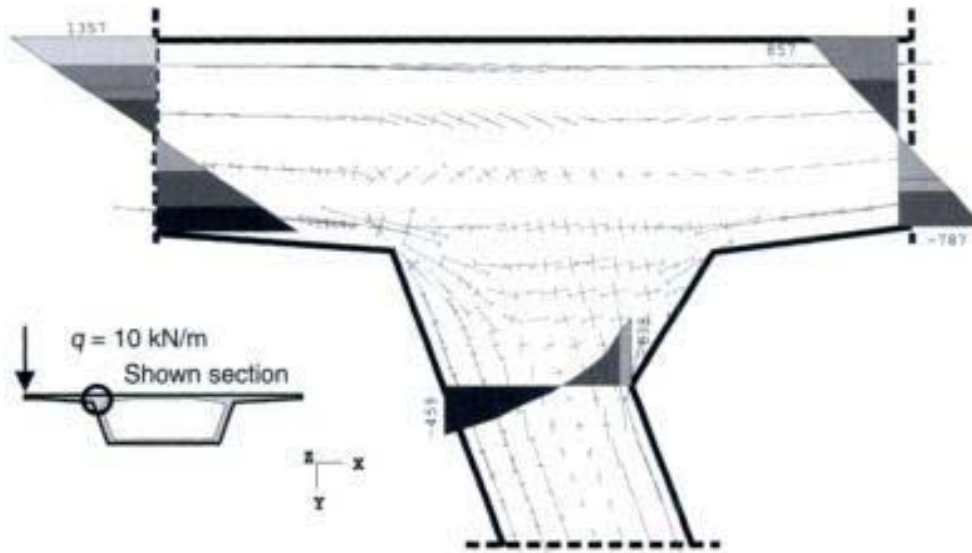


Fig. 2.11 Main membrane forces and distribution of the horizontal resp. vertical membrane force n_x (flange) and n_y (web) over the section depth; loading: $q = 10 \text{ kN/m}$ at the cantilever slab

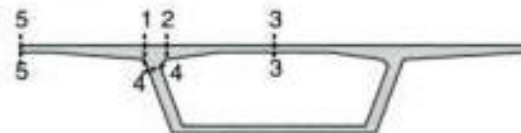
and displacement shows that the coupling of the corner nodes mainly reduces the span width. The increased restraint of the top slab does not have a significant effect on the member forces. The bending moment M_f of a fully restraint single span beam under concentrated load at midspan is proportional to the span length to the power of 1, ($M_f = F_v l/8$), whereas the deflection at midspan f is proportional to the span width to the power of 3 ($f = F_v l^3/[192 \cdot E \cdot I]$). However, it must be pointed out here that the influence of the node coupling depends largely on the geometry of the system. The width of the webs of segmental hollow box girder bridges with external prestressing is very small in relation to in-situ constructions with internal prestressing tendons. The latter usually has a web thickness of more than 50 cm due to the space required for the tendons and the couplers. Here the influence of the coupling of the corner nodes on the shear forces and moments can be much larger.

With shell models (diaphragms) the behaviour of the 'elastic' structure can be analysed more precisely. This will be shown in Chapter 3.

However, the results of such calculations are presented here in order to show the stress distribution in corner regions.

Figure 2.11 shows the membrane forces in a corner region for a load of 10 kN/m at the free edge of the cantilever beam (element mesh see Fig. 2.10). One recognizes a very complex force distribution, which certainly cannot be modelled by beam or truss elements based on the linear strain theory (the Bernoulli hypothesis). Outside this

Table 2.1 Bending moments and displacements in the relevant sections



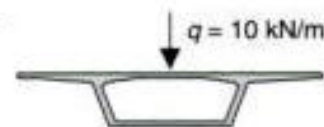
Bending moments [kNm]	Section 1-1	Section 2-2	Section 3-3	Section 4-4
Load case 1: $q = 10$ kN/m at the free edge of the cantilever slab				
Truss model without coupling	-33.5	-17.4	≈ 0	-10.8
Truss model with coupling	-33.5	-18.3	≈ 0	-10.0
Shell analysis	-33.4	-18.3	≈ 0	-11.4

Load case 2: $q = 10$ kN/m at midspan of the deck				
Truss model without coupling	0	-7.7	6.2	7.3
Truss model with coupling	0	-8.2	5.6	7.7
Shell analysis	0	-7.7	5.3	8.0

Displacements [mm]	Section 3-3	Section 5-5
Load case 1: $q = 10$ kN/m at the free edge of the cantilever slab		
Truss model without coupling	≈ 0	3.6
Truss model with coupling	≈ 0	3.3
Shell analysis	≈ 0	3.7



Load case 2: $q = 10$ kN/m at midspan of the deck		
Truss model without coupling	0.44	-0.15
Truss model with coupling	0.30	-0.10
Shell analysis	0.36	-0.17



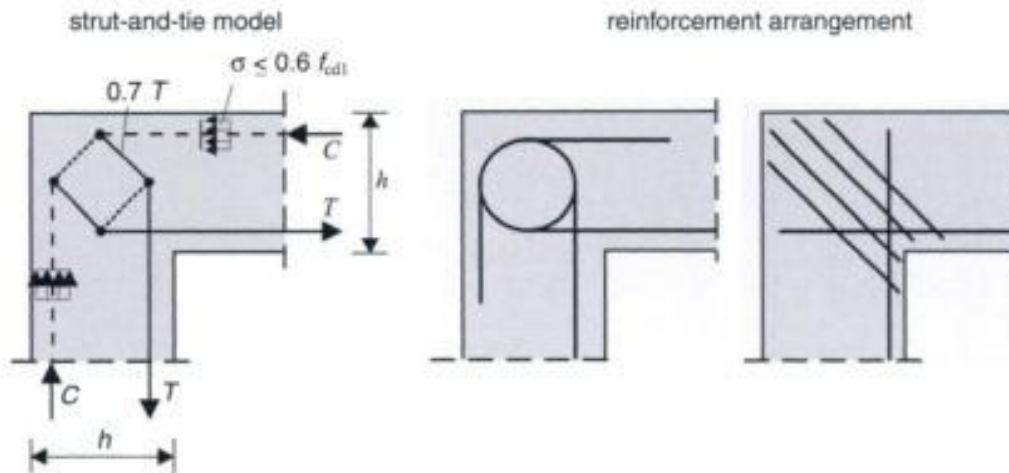


Fig. 2.12 Frame corner with high opening bending moment; strut-and-tie model and resulting arrangement of reinforcement (acc. [13])

discontinuity region, the strains and stresses are linear over the depth of the section. The discontinuity region extend up to a distance $\approx h$ from the continuity.

In Table 2.1 the bending moments and the displacements in the relevant sections of the structure are compared with each other for both load cases. Good agreement can be seen in the bending moments. However, there are relatively big differences in the midspan displacements.

Besides the structural analysis, good detailing of the reinforcement in corner regions is very important with respect to both the load bearing capacity and the serviceability of the structure (see Figs 2.8 and 2.12). Many experimental investigations were made and several theoretical design models have been evaluated to design such sections.

2.2 Beams with variable depth – inclined haunches

The depth of a beam may be increased to optimize the reinforcement arrangement at the intermediate supports (greater lever arm) and to reduce the midspan bending moment (Figs 2.13 and 2.14).

For frame structures with inclined haunches, the variable depth and the inclination of the axis of gravity should be modelled in addition to the coupling of the corner nodes. Furthermore, the inclined haunches should be discretized by a sufficient number of elements. The cross-section is usually assumed to be constant within a finite element.

As will be shown later, the inclination of the axis of gravity generally only has a small influence on the action effects, where the system is not horizontally restrained. Nevertheless, this inclination should not be

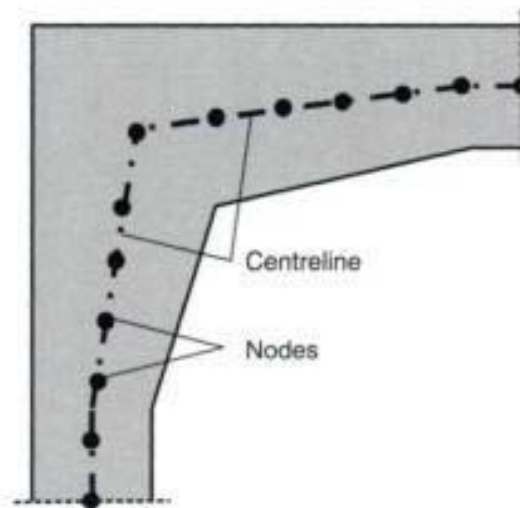


Fig. 2.13 Frame corner with inclined haunch

neglected, as it is very important with respect to the design for shear (Fig. 2.15a–c). A straight beam axis with constant depth of elements will cause mistakes as the slope of the compression strut with respect to the tension chord is neglected. Therefore, the resulting change in the design shear resistance V_{Rd} is not considered (see Fig. 2.15c).

$$V_{Rd} = V_{Rd,s} + V_{ccd} + V_{td} \quad (\text{EC2.1, eq. 6.1}) \quad (2.1)$$

where:

$V_{Rd,s}$ is the design value of the shear force which can be sustained by the yielding shear reinforcement

V_{ccd} is the design value of the shear component of the force in the compression area, in the case of an inclined compression chord

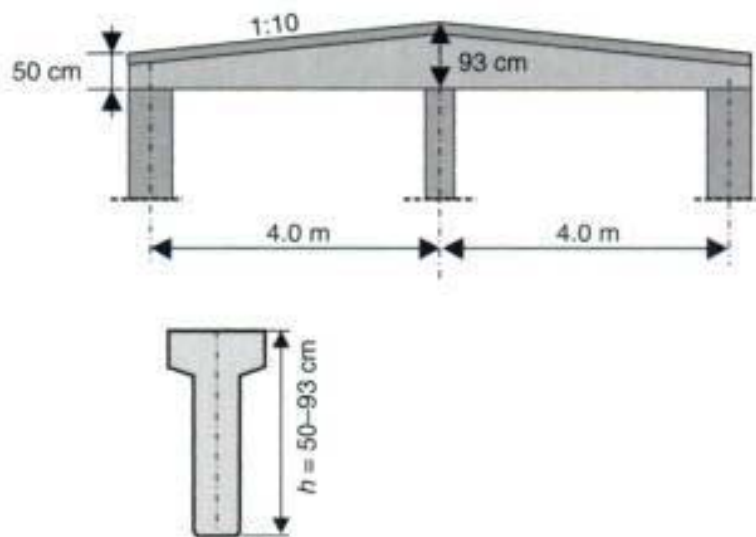


Fig. 2.14 Haunched T-beam girder of an industrial building

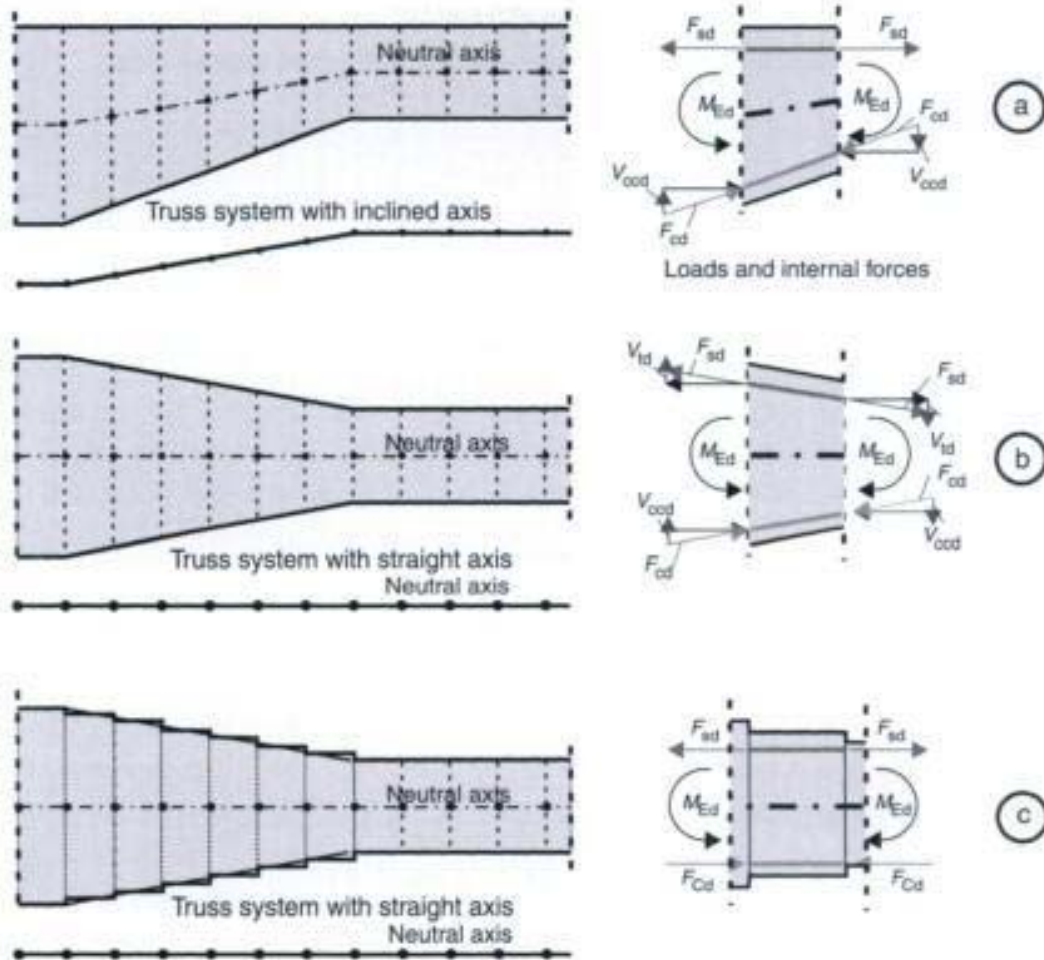


Fig. 2.15 Various models for an inclined haunched beam and resulting internal forces and moments

V_{td} is the design value of the shear component of the force in the tensile reinforcement, in the case of an inclined tensile chord.

The support conditions have to be checked, when the inclination of the axis of gravity is considered in the FE model. For a straight single span girder under uniformly distributed loads a horizontal restraint does not change the member forces and moments. This is not true for inclined truss elements with horizontal restraining supports. The strutted frame system is modelled in the following example. Figure 2.16 shows the member forces and deflections for a fully restraint single span beam of variable depth (inner span of a bridge). The span length is 50 m. In order to show the influence of the variable depth of cross-section, a relatively large depth of $h = 4.0$ m has been chosen at the supports, whereas in midspan the depth is only $h = 1.0$ m. Two different support conditions are considered:

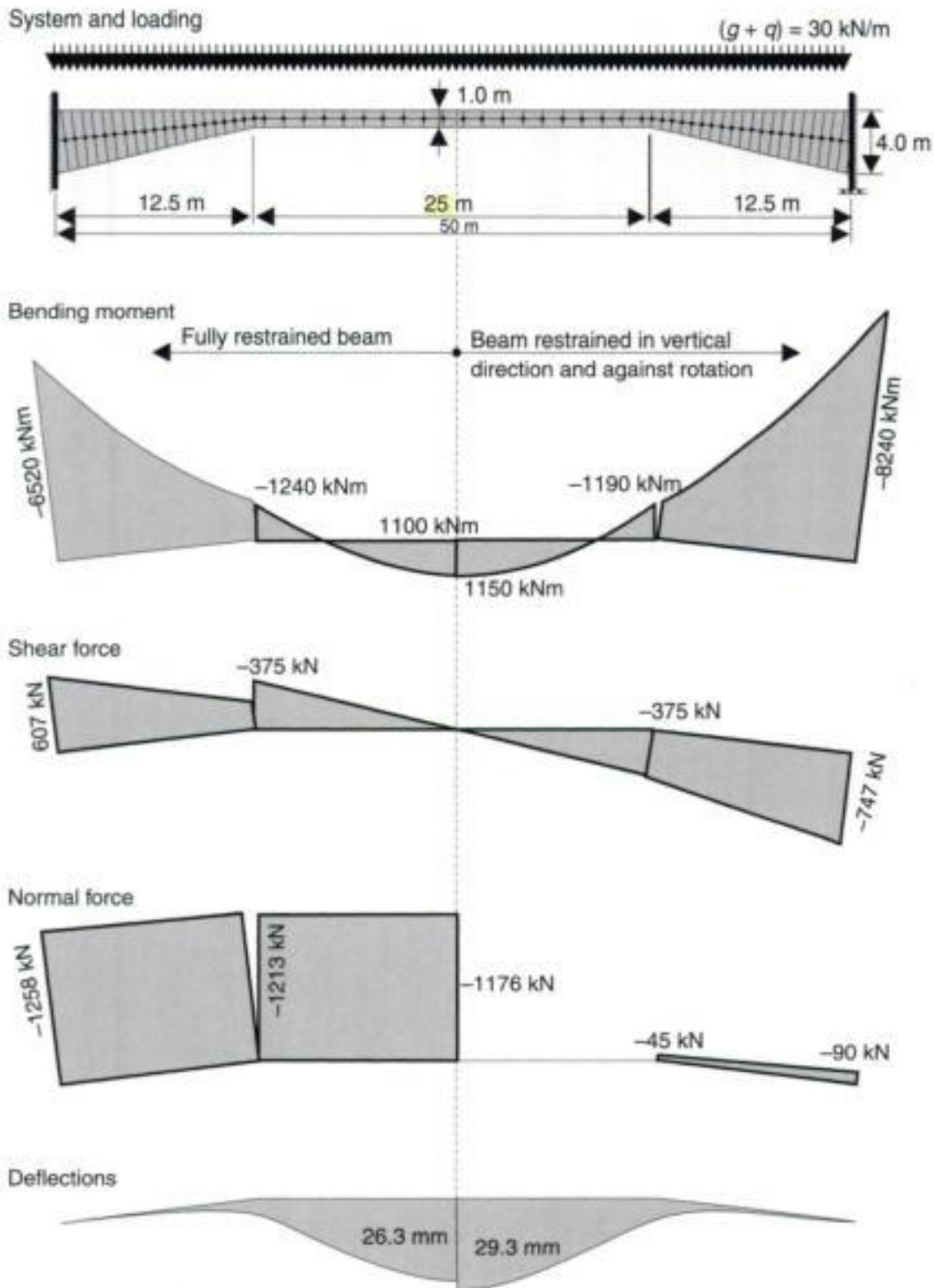


Fig. 2.16 Member forces and displacements of a single span haunched beam for fully and partial restraint support conditions

- Model a: fully restrained supports;
- Model b: no restraint in horizontal direction.

As can be seen from the distribution of the member forces, a strutted frame system results if both supports are fully restrained. This causes

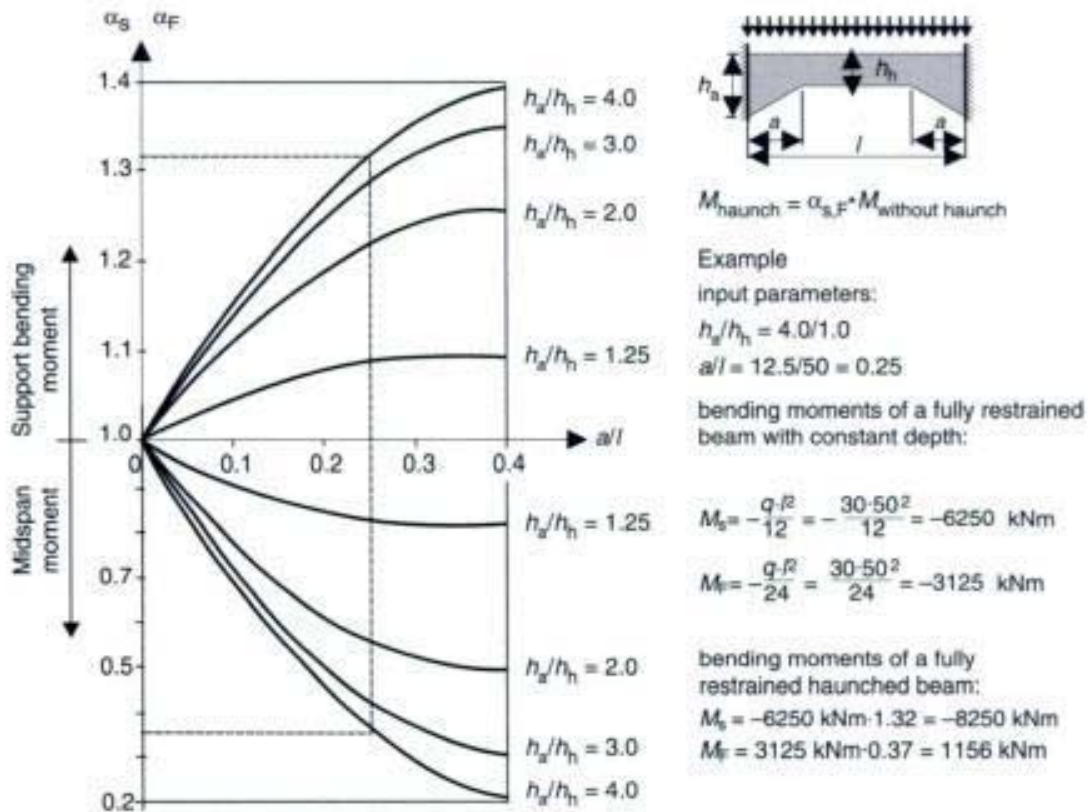


Fig. 2.17 Factors for the calculation of the support and midspan bending moment of a haunched fully restrained beam (linear increase of depth)

high normal forces, even for the slender beam in the example. In Model b, the support bending moment for the fully restrained system are reduced by 26%, the shear forces by 19%, and the displacement at midspan by approximately 10% with respect to Model a.

It should be noted that normal forces are always per definition in the direction of the beam axis and shear forces are perpendicular to it. That is why the shear force at the support is different in the two models.

The manual calculation of the internal forces of a beam with variable depth can be made with the help of Fig. 2.17. The diagram shows the relationship of the bending moment of a beam with constant depth to the one of linearly increasing depth, depending on the length of the inclined haunch and the depth of the beam h_a/h_h . For the previous system the following bending moments are calculated manually:

- support bending moment $M_s = -8250 \text{ kNm}$;
- midspan bending moment $M_F = 1156 \text{ kNm}$.

Table 2.2 lists the member forces at the supports and midspan for the various models. The results of a shell analysis are also given for comparison.

Table 2.2 Comparison of the member forces and displacements

	Analytical analysis (Fig. 2.17)	Truss analysis straight axis	Truss analysis inclined axis beam fully restrained	Truss analysis inclined axis beam not restrained in horizontal direction	Shell analysis system fully restrained at the supports	Shell analysis system not restrained in horizontal direction at the supports	
				Support			
N	0	0	-1258	-90	-1051	0	kN
V	750	750	607	747	750	750	kN
M	-8250	-8225	-6520	-8240	-6372	-8181	kNm
				Midspan			
N	0	0	-1176	0	-1150	0	kN
V	0	0	0	0	0	0	kN
M	1156	1150	1100	1150	1150	1195	kNm
				Displacement in midspan			
w	29.2	29.2	26.3	29.3	26.7	29.1	mm

The internal forces and the displacements of the truss model are confirmed by the shell model. There is also good agreement with the manually calculated results. As can be seen from Fig. 2.16, the horizontal restraint of the beam has a great influence on the internal forces.

To summarize: if the system is not restrained in horizontal direction and if there are no normal forces, the inclination of the axis of the truss elements can be neglected with regard to the member forces. However, for a shear design, the elements should be given a variable depth.

2.3 Beams with halving joints and openings

The Bernoulli hypothesis does not apply in beam-beam and beam-column intersections – regions of sudden change of cross-section or openings ('discontinuity regions' see Figs 2.18 and 2.19). Therefore, one cannot analyse these areas precisely by using a truss system with finite elements, which are based on a linear strain distribution over the depth of the cross-section. Nevertheless, the different stiffness values should be modelled, as the internal forces of a statically indeterminate system depend on it.

The location of the beam axis changes suddenly at a halving joint. This can easily be modelled by coupling the nodes in the joint similar to a frame corner. In the region of openings, two separate beams for

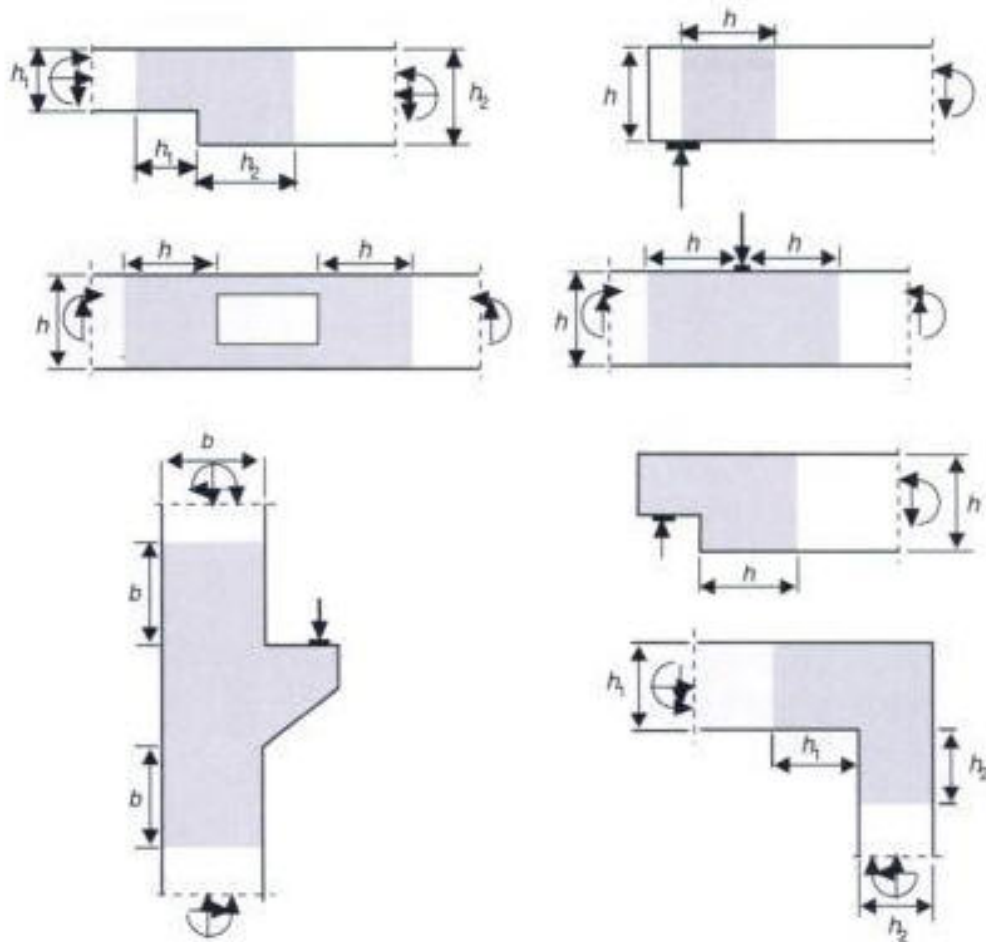


Fig. 2.18 Discontinuity regions in truss structures

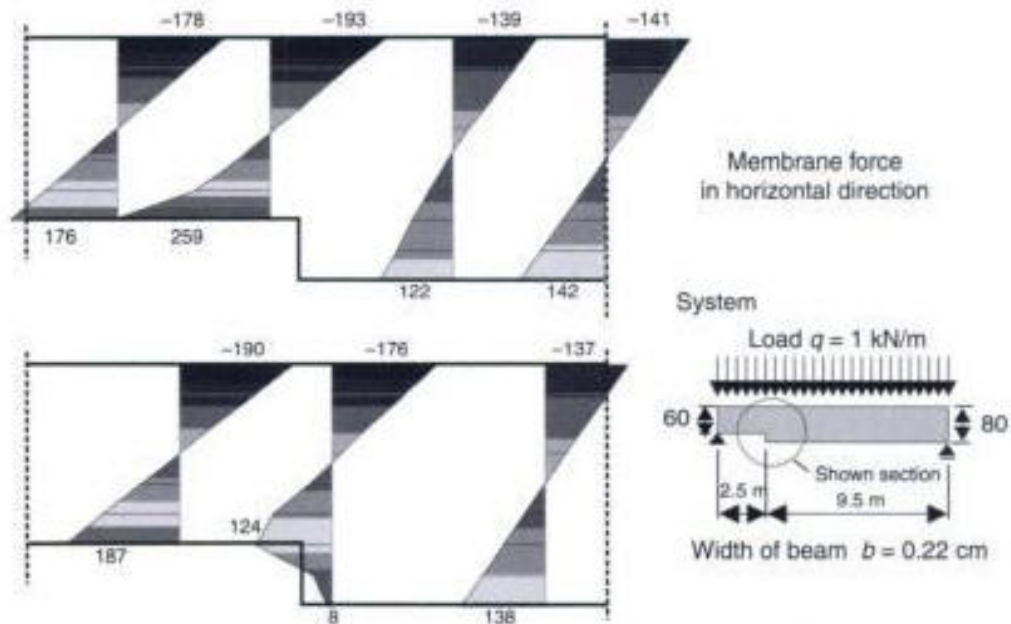


Fig. 2.19 Horizontal membrane forces (= normal stress \times width of beam) in the region of a halving joint (shell analysis)

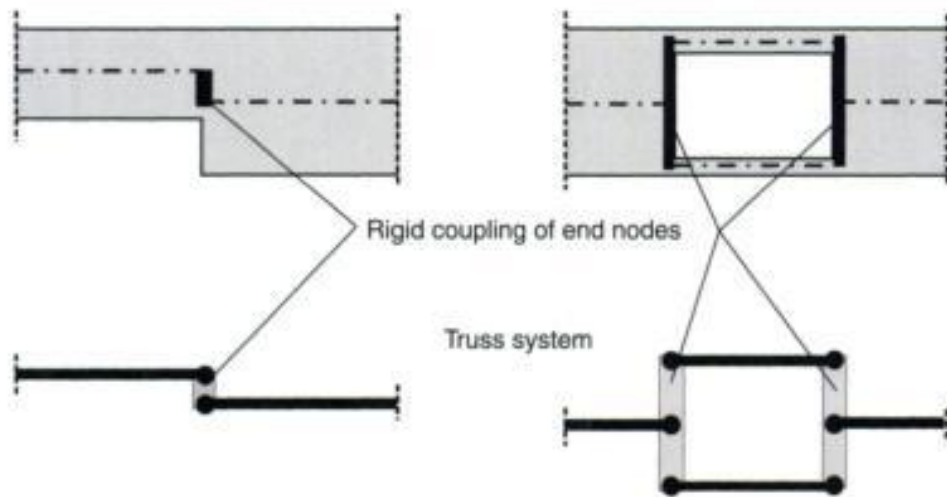


Fig. 2.20 Halving joint and opening in a beam

the compression and the tension chords should be used (Fig. 2.20). The normal and bending stiffness of these elements should be fixed taking account of possible cracking in the tension zone and the resulting reduction of stiffness.

In the following the bending moment distribution of a single span beam ($l = 12.5 \text{ m}$) under a uniformly distributed load with an opening at midspan will be examined. This beam has been used as a girder for an existing industrial building. The results of the two different beam models and a shell model will be shown.

Only one half of the structure is shown, as the system and its loading is symmetric about the midspan. The following three systems have been analysed (Fig. 2.21):

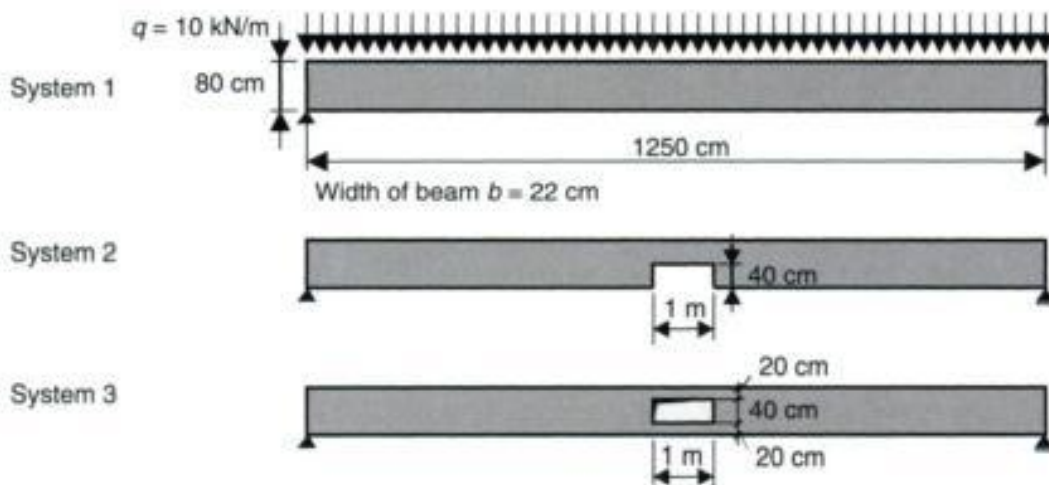


Fig. 2.21 Different beams

- System 1: beam without opening.
- System 2: beam with an opening ($1.0 \times 0.4 \text{ m}$) at midspan at the lower side of the cross-section.
- System 3: beam with an opening ($1.0 \times 0.4 \text{ m}$) at midspan on the centreline of the cross-section.

Figure 2.22 shows the bending moment distribution of the various models, both with and without considering such openings.

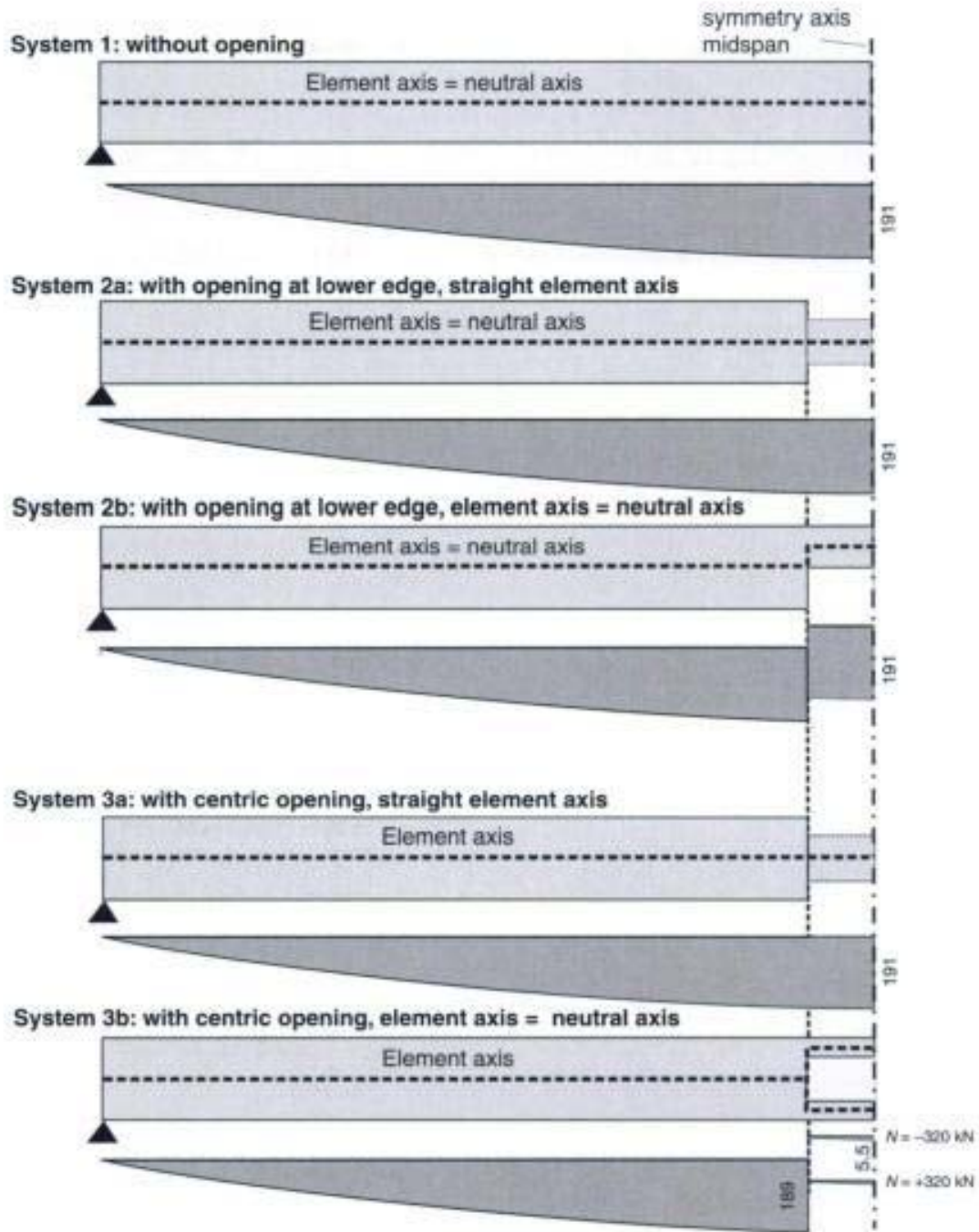


Fig. 2.22 System and bending moments

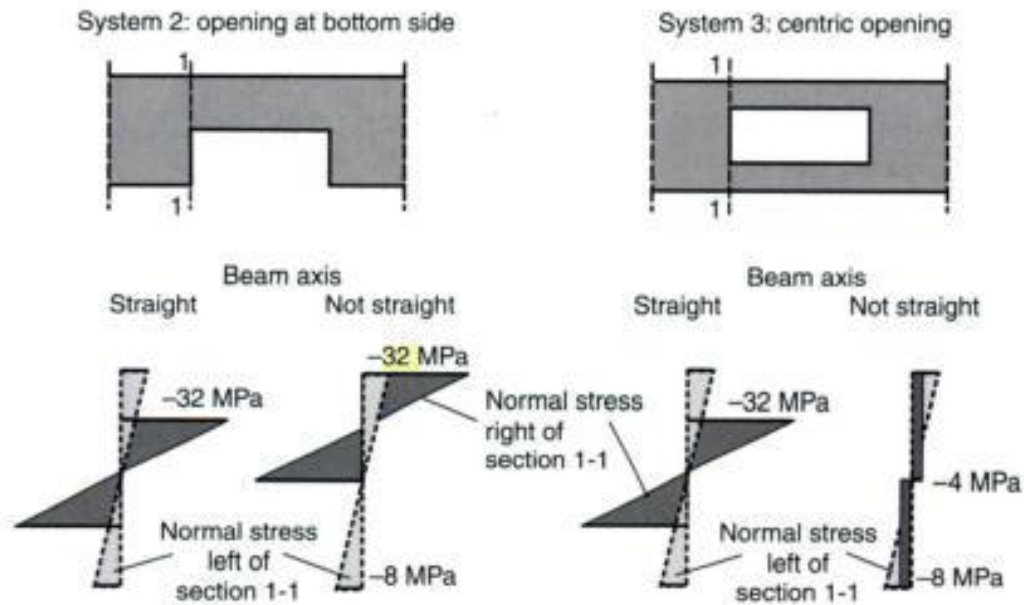


Fig. 2.23 Stress distribution near the edge of the opening – beam system

There is no change in the bending moment distribution of System 2, as there are no normal forces acting on the beam. Therefore, the bending moment distribution does not depend on the opening with respect to the model. Nevertheless, a sudden change in strain can be observed near the opening (see Fig. 2.23), which has a small influence on the deformation of the given structural system. Due to the assumption of the numerical analysis (elastic material behaviour, Bernoulli hypothesis) the strain in the concrete section is equal to:




$$\varepsilon_c = \frac{\sigma_c}{E_c} = \pm \frac{M}{E_c \cdot I} \cdot h/2$$

where:

- M is the bending moment at the face of the opening;
- h is the overall depth of the cross-section left or right of the face of the opening;
- I is the second moment of area left or right of the face of the opening.

In the case of a centric opening, the bending moment of the unweakened cross-section is divided into a compression and a tension force. This different behaviour has to be modelled by two separate beams. No normal forces are calculated when this opening is neglected and the beam axis is kept straight. This means that the stiffness is not modelled correctly, resulting in a doubling of the midspan displacement (Table 2.3).

Table 2.3 Deflection of the beam at midspan (in mm)

System	Beam axis	Truss model	Shell model
System 1 – no opening 	straight	10.7	10.0
System 2 – opening at lower side 	(a) straight (b) jump	27.6 27.8	27.4 27.4
System 3 – centric opening 	(a) straight (b) jump	19.6 10.9	10.3 10.3

For comparison purposes, the internal forces and the deformations of the beam are calculated by a shell model. Figure 2.26 shows the membrane forces and the distribution over the depth of the beam in various sections. In most sections a linear strain distribution can be seen. Here the Bernoulli hypothesis is valid. Large differences are only seen in the vicinity of the opening (see Fig. 2.24). Thus, a beam system, which is based on a linear strain distribution, will always lead to incorrect results to a greater or lesser extent.

Design of the discontinuity regions can be done by strut-and-tie models (Fig. 2.25). The results of a linear elastic shell model can be used to evaluate the load paths.

It must be noted that strut-and-tie models are only valid for the ultimate limit state design. A fully cracked structure is assumed. Therefore, these models cannot give any information with regard to the serviceability of the structure (cracking). However, it can be useful to reduce the permissible stresses in the reinforcement in order to reduce the crack width.

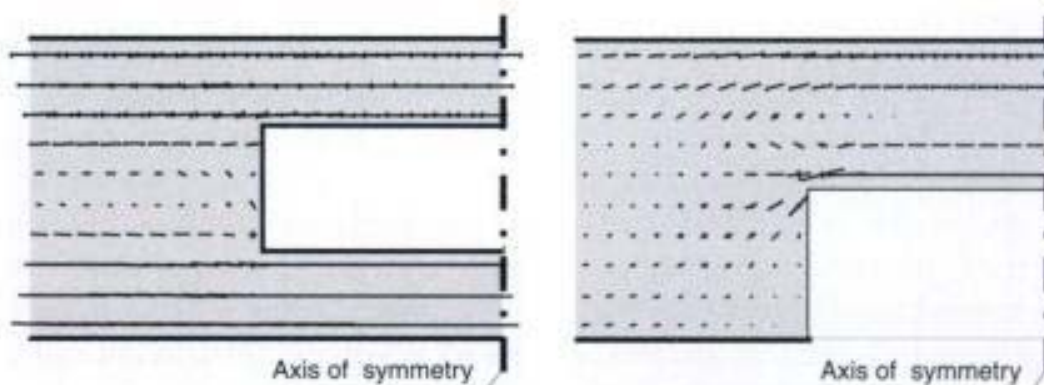


Fig. 2.24 Membrane forces in the vicinity of the opening

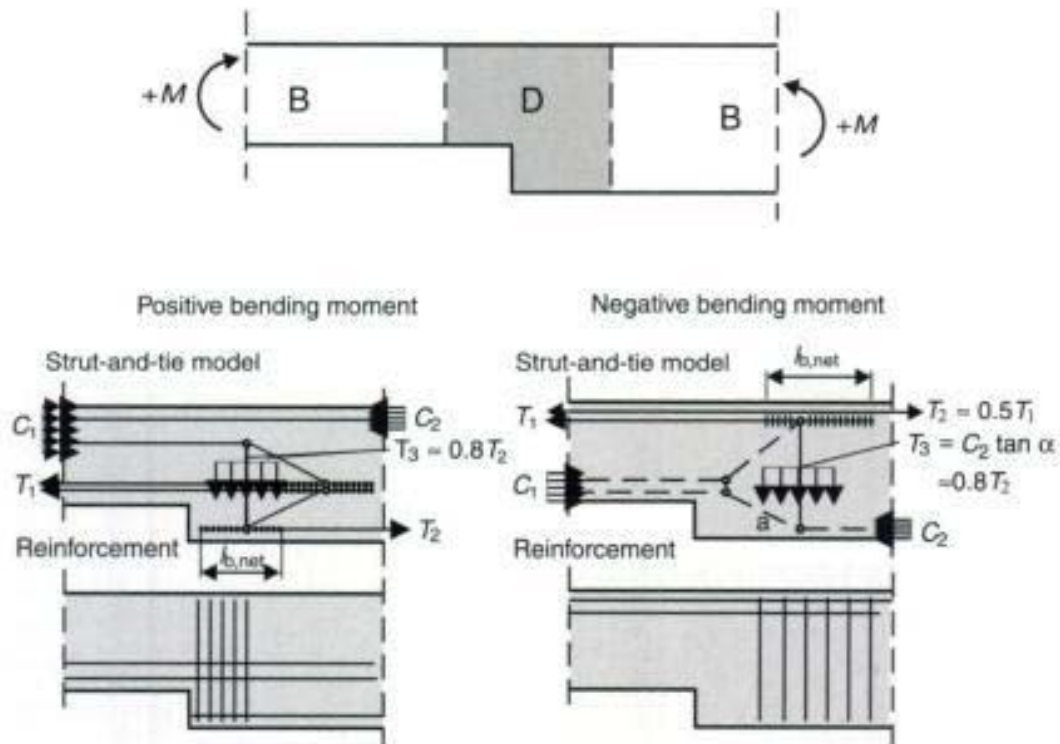


Fig. 2.25 Strut-and-tie model for a halving joint

It should be noted, that the shear force in the opening will be carried mainly by the compression member. This has to be considered in the design of the opening region.

The influence of the different FE-models on the member forces in cases where there is an opening was not significant in the above example. But this only results from it being considered as a statically determinable system with a fully elastic behaviour being assumed. One of the main questions is the stiffness of the fully tensioned chord in the tension zone of the opening. Due to cracking of concrete the stiffness is significantly reduced with regard to the elastic value.

This problem is clearly demonstrated in the following example for a fully restrained 2-span beam under uniformly distributed loads (Fig. 2.28). The beam has an opening of 20×50 cm close to the intermediate support. Three different models for the opening region are used. In the first system the opening is neglected, whereas in the second, the tension and compression chord in the opening is modelled by two separate beams which are rigid coupled with the centre nodes of the undisturbed beam. In the third system hinge couplings (no bending moments) are used to take account of the lack of bending stiffness in a fully tensioned member.

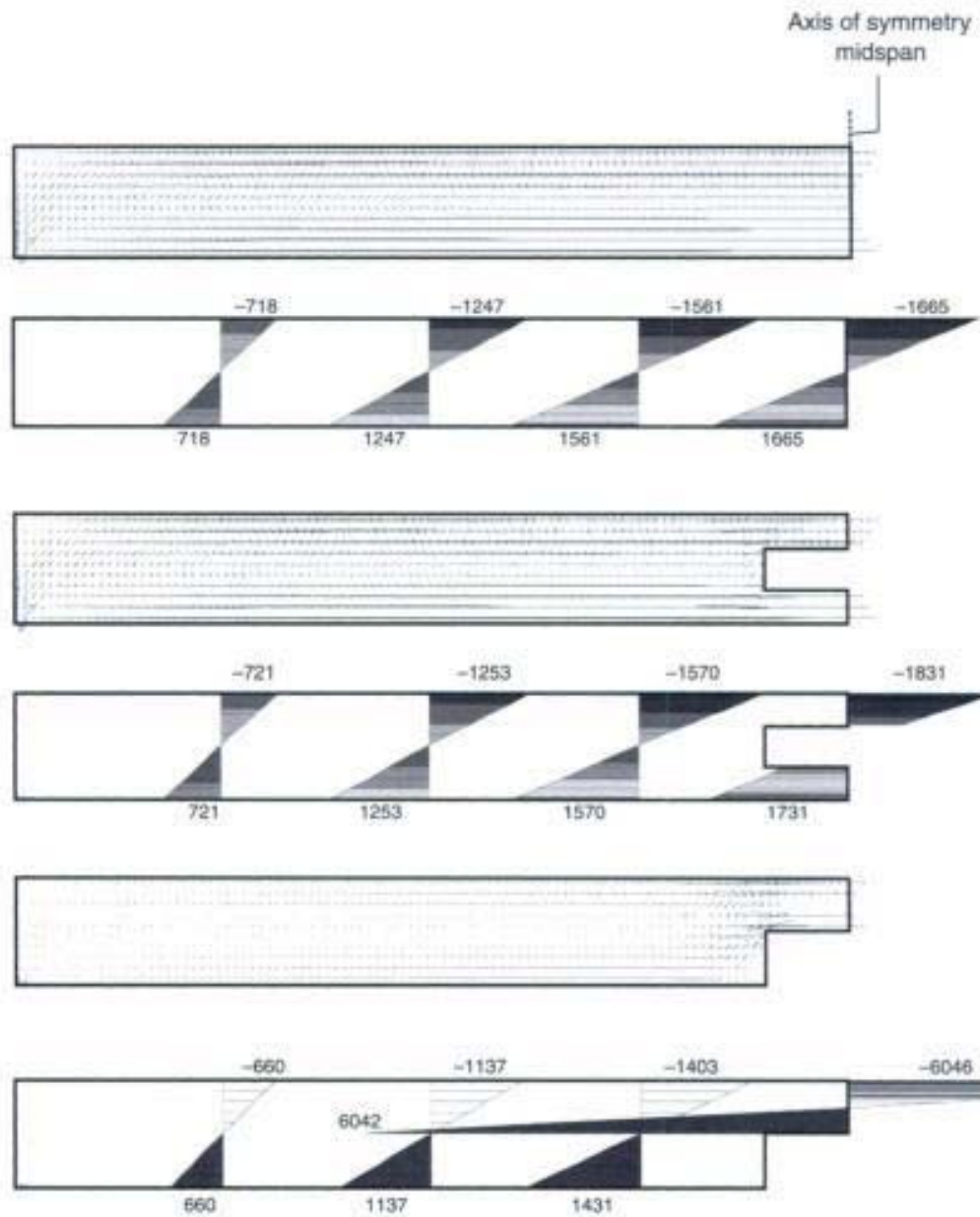


Fig. 2.26 Main membrane forces in various sections (System and loading see Fig. 2.21)

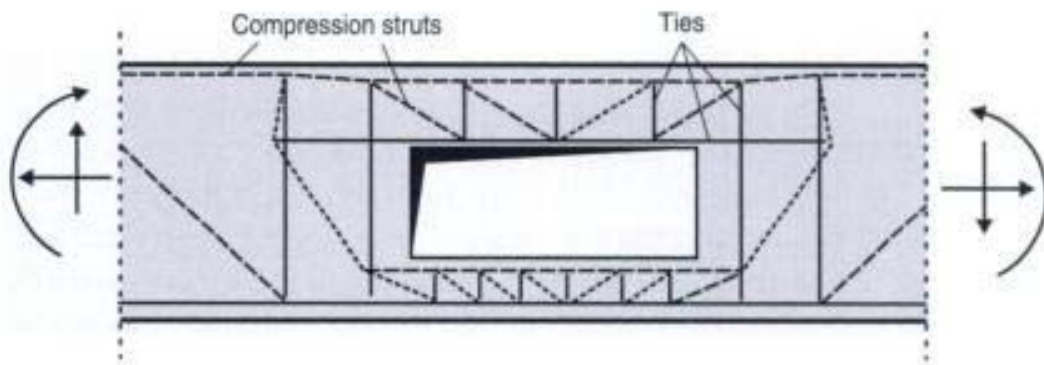


Fig. 2.27 Strut-and-tie model for a beam with an opening ([34], Fig. 4.3.7)

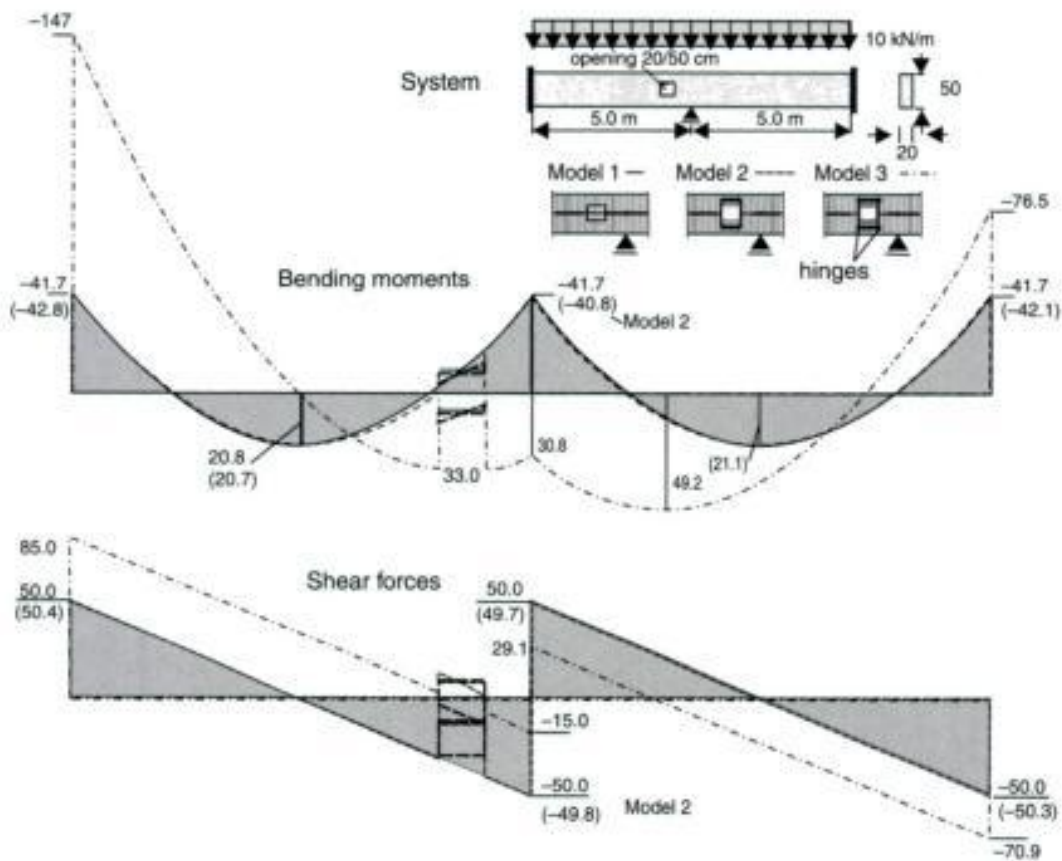


Fig. 2.28 Member forces of a 2-span beam for three different models used for the opening

There are only very small differences for Models 1 and 2 (Fig. 2.28), although Model 3 results in totally different member forces. The left span tends to become a cantilever beam. The bending moments over the intermediate support become positive. Parametric studies have to be conducted to find the most relevant distribution of member forces for this system.

It should be pointed out, however, that Model 3 is an extreme case: just to demonstrate the importance of the correct manner of modelling the stiffness in the region of the opening.

2.4 Elastic supports – elastic bedding

2.4.1 Elastic bedded foundation beam

There are a lot of structures where the supports are not fully or partly restrained and where the deformation of the supports cannot be neglected. For example, in the design of shallow foundations, the soil settlement, the interaction between the structure and the ground,

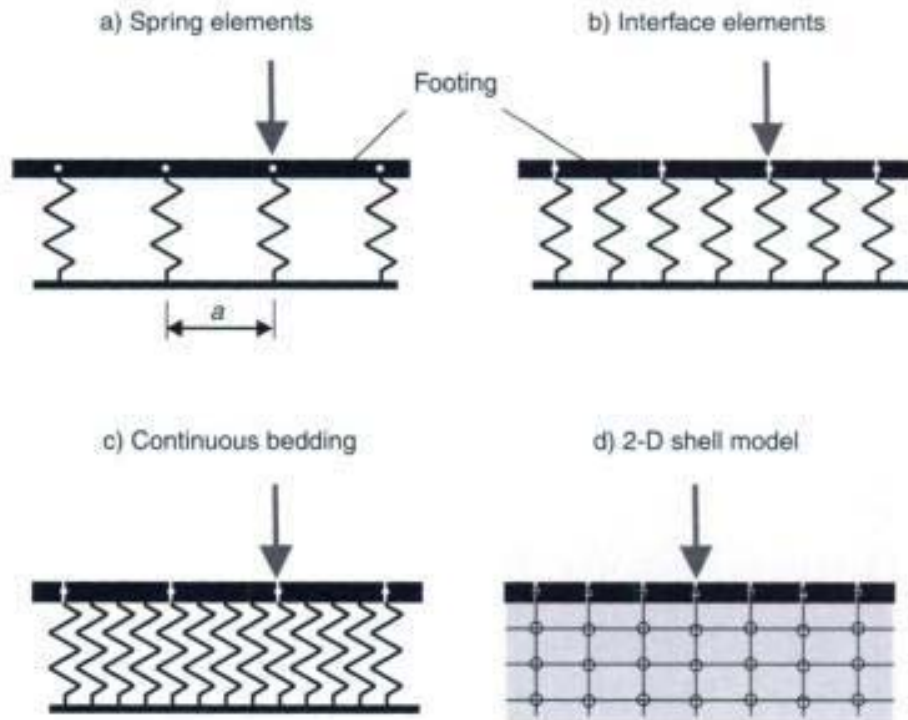


Fig. 2.29 Various models for elastic support.

must be considered. Also the deformation of the support for structures on elastomeric bearings must not be neglected either. An elastic support can be modelled by (Fig. 2.29):

- (a) individual spring elements;
- (b) special interface elements;
- (c) continuous elastic supported elements;
- (d) plane or three-dimensional shell or volume elements.

The friction between the foundation and the ground can be modelled by horizontal springs. Linear as well as nonlinear spring characteristics can be used. A nonlinear analysis is required if certain load arrangements show tension stresses in the ground, which cannot occur in reality due to uplifting of the foundation beam.

The results of the model (a–c) are identical if the lengths or the spacings of the elements is sufficiently small. In practice, the advantage of using special interface elements instead of individual springs is that the normal stiffness does not depend on the length of the element for a given soil modulus. For individual springs, the stiffness depends on the spacing of the elements (Fig. 2.29a). Continuous bedded elements are used in elastic supported foundation slabs, where the effects of the bedding can be directly introduced into the element stiffness matrices (see section 4.9).

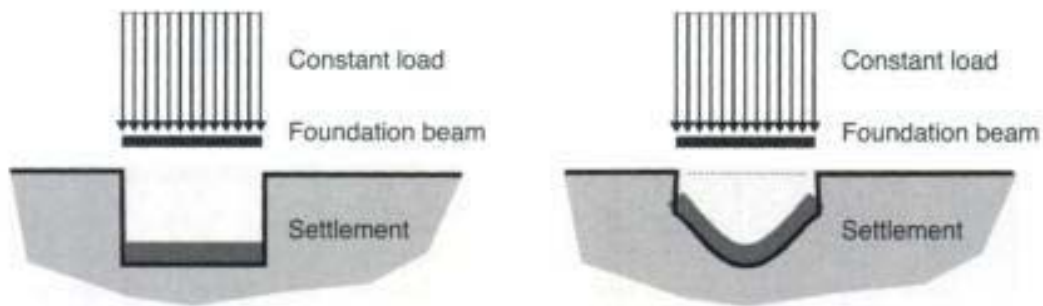


Fig. 2.30 Deformation of soil and structure – foundation modulus and constraint modulus method

All of the above mentioned methods, except the continuum model (d), are based on a linear relationship between the local force and the local deformation of the soil (stiffness modulus method). This method does not consider the shear stiffness of the soil. Therefore, in general, the displacements and associated reactions of the soil and the structure are not compatible (Fig. 2.30). The error caused by this simplification can often be neglected in practice. However, when designing a shallow foundation, one has to keep in mind that a uniformly distributed load on an elastic bedded beam or slab does not result in any member forces (see Fig. 2.30). In such a case, it is recommended that studies with two- or three-dimensional continuum models are made (e.g. constrained modulus method). But this usually requires a much greater amount of work. Please note that the considerable uncertainties of the soil behaviour cannot be overcome by using more refined numerical models.

When using distinct spring elements, the reaction of the ground is introduced into the structures by single forces. Even at the free end of a foundation beam, a force is estimated, which results in a shear force at the free end of the beam (Fig. 2.31). Therefore, the calculated shear forces are only correct in the middle of each beam element. However, for design purposes the distribution of the internal forces can be smoothed out.

The discretization, the number of elements per length have a considerable influence on the member forces. This aspect will therefore be discussed in greater detail. As an example, an elastic supported beam with rectangular cross-section ($b/h = 1.0/0.8$ m) and a length of 5.0 m is analysed under a uniformly distributed load and a single load at midspan.

First, a very coarse element mesh is used, having only two beam and three spring elements (Fig. 2.31). The spring stiffness is calculated for a

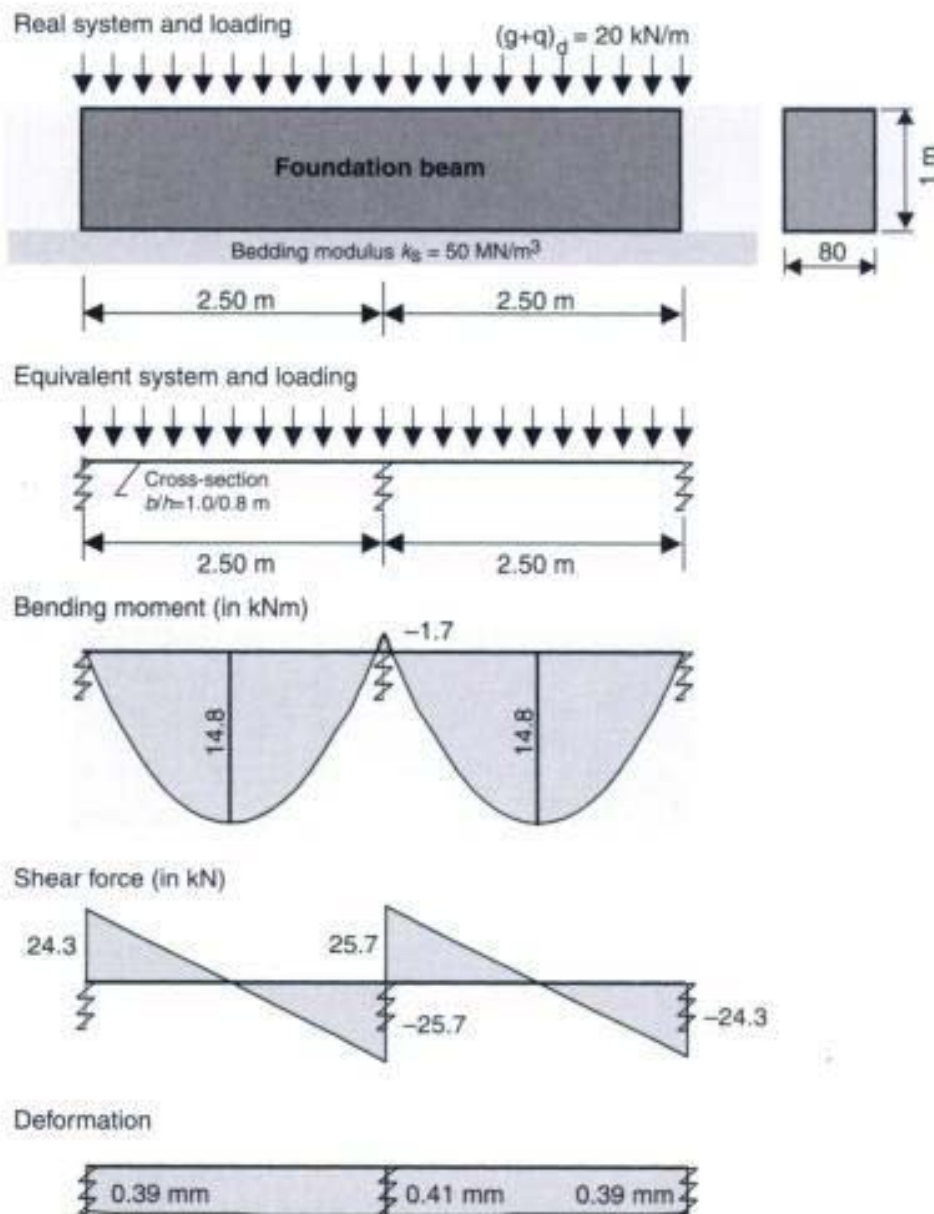


Fig. 2.31 Beam supported on three elastic springs under uniformly distributed load

constant influence width of $2.50 \text{ m}/2 = 1.25 \text{ m}$ for the outer springs and 2.50 m for the inner springs. As demonstrated in Fig. 2.31, even for a system under a uniformly distributed load, significant bending moments and shear forces are estimated. As mentioned previously, due to the assumption of the elastic modulus method, no bending moments and shear forces should be estimated under such loads. In principle, the calculated member forces correspond to a 2-span continuous beam. With a refined element mesh, the results are more reasonable (see Fig. 2.32a). Here the member forces and the displacement in midspan are plotted versus the number of truss and spring elements.

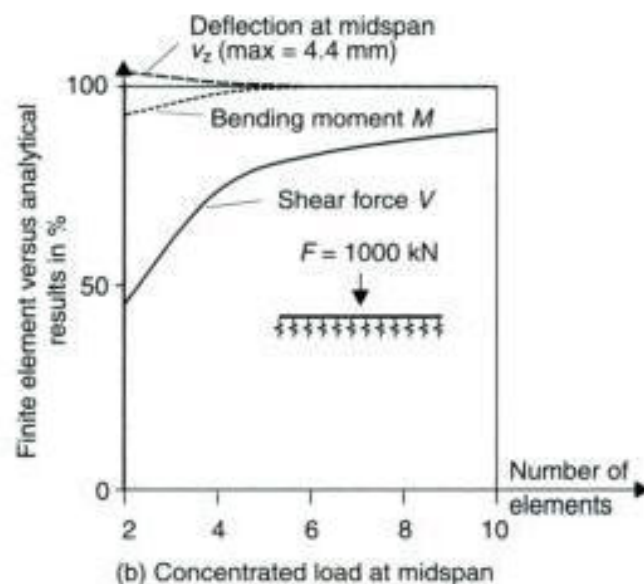
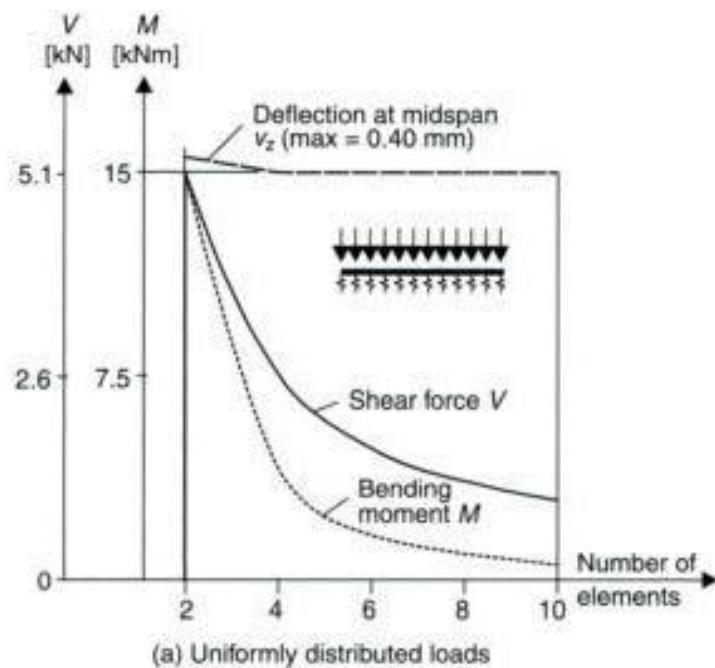
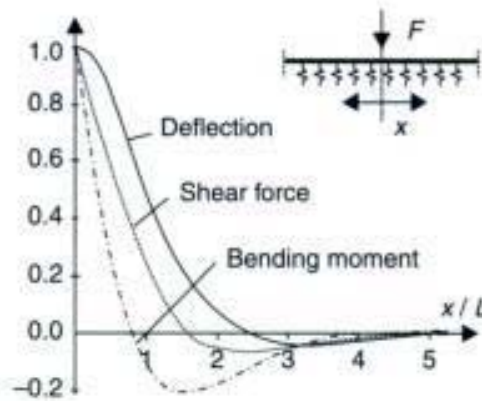


Fig. 2.32 Midspan deflection, shear forces and bending moments of an elastic supported beam with increasing number of spring and beam elements

At first one would suppose that more elements are required for a beam with a concentrated load than for one under a continuous load. This is not the case as the parametric study in Fig. 2.32b shows. Here the member forces are plotted for two to ten elements versus the analytical values (see Fig. 2.33). With regard to the bending moment and displacement at midspan, six elements are sufficient. For the shear forces, a more refined element mesh is required. The midspan deflection for both load cases is not very sensitive to the number of the elements.



Deformation $y(x)$:

$$E_c \cdot I_c \cdot y(x) = \frac{F \cdot L^3}{8} \cdot e^{-x/L} \cdot [\cos(x/L) + \sin(x/L)]$$

Bending moment:

$$M(x) = -E_c \cdot I_c \cdot y''(x) = \frac{F \cdot L}{4} \cdot e^{-x/L} \cdot [\cos(x/L) - \sin(x/L)]$$

Shear force:

$$V(x) = -E_c \cdot I_c \cdot y'''(x) = -0.5 \cdot F \cdot e^{-x/L} \cdot \cos(x/L)$$

Fig. 2.33 Deformations and member forces of an infinite elastic bedded foundation beam under concentrated load

As the previous calculations have shown, the length of beam elements with respect to the distance of the springs is limited by the following requirements:

- The deformation of the structure and the resulting soil reactions must be modelled with a sufficient degree of accuracy. The element length is limited by the shape of the structural deflection curve and the form functions of the used truss and interface elements. If the foundation has a small bending stiffness, as in the example above, the deflection curve can be described by using only a few elements.

It is generally recommended that the length of a beam element Δl depends on the so-called 'characteristic length' L . The following calculation provides the characteristic length for the above mentioned example.

$$L = \sqrt[4]{\frac{4 \cdot E_c \cdot I_c}{k_s \cdot b}} = \sqrt[4]{\frac{4 \cdot 32000 \cdot 0.8^3 / 12}{50 \cdot 1.0}} = 3.23 \text{ m}$$

where:

EI is the bending stiffness of the foundation beam;

- b is the width of the beam;
- k_s is the bedding modulus of the soil.

This recommendation is based on the deflection curve of an infinite foundation beam. The displacement of such a structure under a single load is zero at a distance of $x/L = \frac{3}{4}\pi, \frac{7}{4}\pi, \frac{11}{4}\pi$, etc. The length of the element should be chosen to describe this deformation pattern with a sufficient accuracy depending on the form functions used (see Fig. 2.33). In the case of a linear function, the length of the beam elements Δl should not be greater than approximately $\frac{1}{4}L$. For elements with quadratic and cubic functions, fewer elements are required.

- *The distribution of the member forces must be modelled with a sufficient degree of accuracy.* The correlation between the element length and the shear force distribution results from the element type used in the numerical analysis. In case of no internal element loads, they are based on an assumption of a linear shear force distribution within each individual element. Refinement of the element mesh results in a more accurate description of the actual maximum shear force under the concentrated load.

Elastic bedded beams have large maximum bending moments under concentrated loads. These high values are usually not relevant for the design, as point loads do not exist in reality. All forces act on a distinct load area. A load distribution with an angle of 45° can be assumed up to the centreline of the beam or slab. In the example, this would result in a load area of greater than 0.80 m. This would reduce the maximum bending moment by a factor of 0.8. The loaded area has to be modelled by at least two elements to describe the shear force distribution with a sufficient degree of accuracy.

In the case of a linear elastic analysis based on the bedding modulus method, one has to remember that tension forces cannot actually occur in the ground due to uplifting of the foundation beam. The bedding of the beam has to be neglected in those regions where the numerical calculation shows any uplifting of the foundation beam. In such a case, load superposition is not permissible, and this will significantly increase the amount of calculation effort.

2.4.2 Influence of the nonlinear material behaviour of concrete

In the examples mentioned above, a linear elastic material behaviour has been assumed for the foundation beam and the ground. Not only

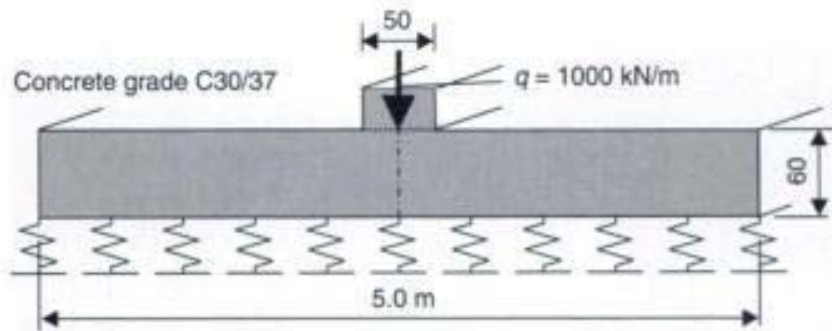


Fig. 2.34 Elastic bedded foundation beam

the complex deformation characteristics of the soil, but also the change of stiffness of a concrete beam due to cracking may have a significant influence on the member forces and deflections, as will be shown in the following example.

A strip foundation having a thickness of $h = 60 \text{ cm}$ and a transverse width of $b = 5.0 \text{ m}$ is analysed (Fig. 2.34). The calculations are carried out for a strip of 1 m width in the longitudinal direction. The system is loaded in the middle by a wall. The geometry of the foundation beam and the bedding modulus have been chosen, so that for a central load of $q = 1000 \text{ kN/m}$ a reasonable amount of reinforcement and a realistic maximum settlement is calculated.

The member forces, the settlements and the required reinforcement are shown in Fig. 2.35 for both the linear elastic as well as the nonlinear material behaviour of the reinforced concrete beam. For the nonlinear calculations, the amount of reinforcement has been fixed by the results of the linear analysis. A linear elastic analysis results in a maximum bending moment under the wall of $m = 520 \text{ kNm/m}$ and a maximum displacement of $w = 4.7 \text{ mm}$. However, the maximum bending moment is reduced by 20 to 25% and settlements are increased by 32%, when a nonlinear behaviour of the reinforced concrete beam and its resulting stiffness reduction in the region of the maximum bending moments are considered. Figure 2.36 (below) shows the results of the nonlinear analysis, both with and without taking the tension stiffening effect into account. It can be seen that neglecting the tension stiffening effect results in smaller bending moments. Therefore, this effect has to be included in the design of foundation beams and slabs.

Figure 2.36 shows the distribution of the bending moment at midspan and the settlements of the strip foundation under an increasing load. At the beginning, there is a linear relation between the load and the vertical displacements and bending moment respectively. The beam is uncracked and behaves fully elastic. At an approximate load of

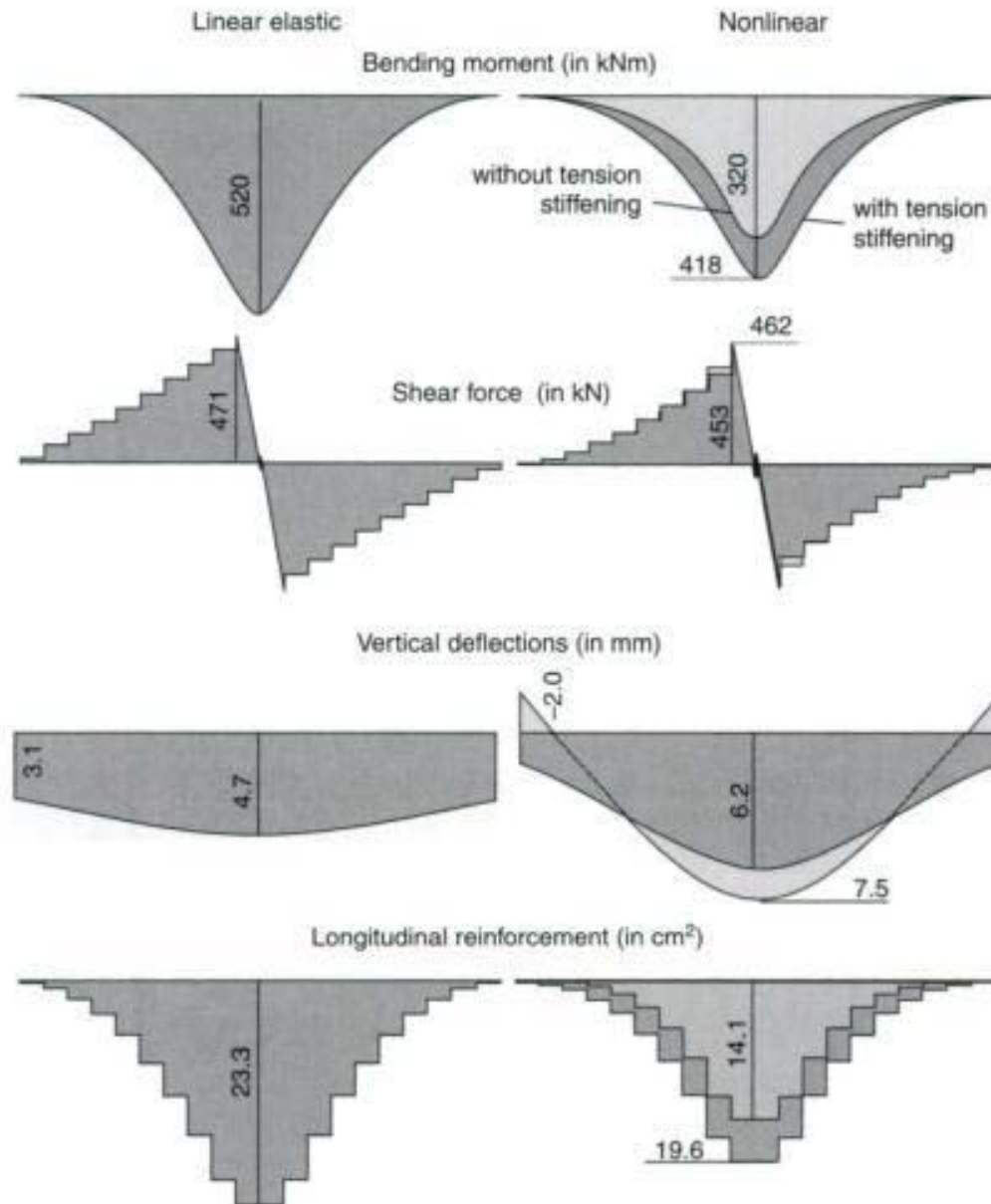


Fig. 2.35 Member forces and settlements of a foundation beam with linear elastic and nonlinear behaviour of concrete (max. load $q = 1000 \text{ kN/m}$)

$q = 1400 \text{ kN/m}$, the elastic load bearing capacity of the critical section at the midspan is reached, starting the formation of cracks. A plastic hinge develops. In this area, the bending moment can only increase slightly. Any further increase in load bearing capacity can only be possible for a load redistribution to the less stressed sections and a concentration of the soil pressure under the wall. This results in excessive increases in the settlements. It should be considered in the design that a load increase with a safety factor γ does not affect the maximum bending moments but will lead to a considerable increase in the settlements. The shear force at the relevant section near to the wall does not

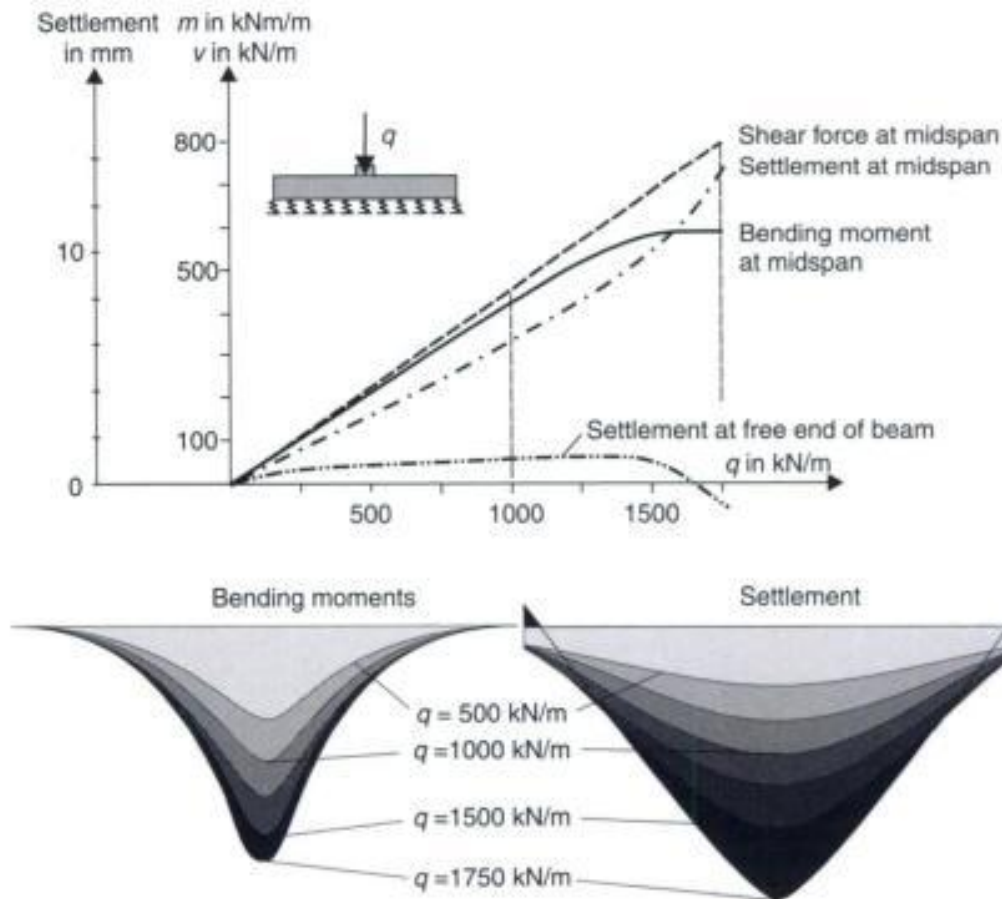


Fig. 2.36 Bending moment and settlements with increasing load (nonlinear material)

depend on the stiffness of the system, for it results from the equilibrium condition.

2.4.3 Pile foundation – foundation of a bridge column

Pile foundations are used to transfer the loads from the structure in deeper and stiffer soil layers with a greater load bearing capacity. They are required when the load bearing capacity of a shallow foundation is insufficient or if the size of the foundation slab would be uneconomical.

One must distinguish between bored and driven piles. Due to their great diameter and reinforcement, bored piles can carry normal forces and bending moments. Driven piles have small bending stiffness and can only carry vertical loads due to their slenderness.

In the following example only bored piles will be discussed, as the vertical normal forces in driven piles can easily be estimated from the equilibrium conditions (see Fig. 2.42).

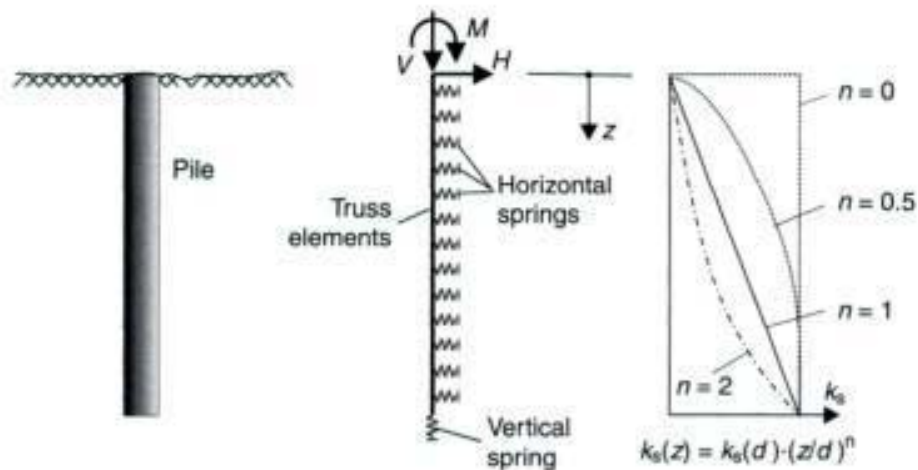


Fig. 2.37 Bored pile – numerical model and distribution of bedding modulus k_s for a horizontal force at the pile head

Rigid piles can be modelled by linear-elastic supported truss elements. The bedding modulus k_s and the stiffness of the horizontal springs may vary along the length of the pile and its circumference. According to Timm [17], the distribution of k_s along the length of the pile respectively the exponent n should be chosen as follows (see Fig. 2.37):

- $n = 0$ for cohesive soil under small to medium loads;
- $n = 0.5$ for medium cohesive soil and non-cohesive soil above the ground water level;
- $n = 1.0$ for non-cohesive soil below the ground water level or under greater loads;
- $n = 1.5$ to 2.0 for loose non-cohesive soil under very high loads.

If there are no results available from actual pile tests, the bedding modulus k_s may be estimated by the following expression:

$$k_s = E_s/d$$

where:

- k_s is the bedding modulus;
- E_s is the stiffness modulus of the ground;
- d is the diameter of the pile $d \leq 1.0$ m.

The stiffness modulus for non-cohesive soils varies between $E_s = 100$ to 200 MN/m^2 for gravel and $E_s = 10$ to 100 MN/m^2 for sand. The elastic horizontal support in the upper region of the pile should only be included in the design if it can always be guaranteed during the whole lifetime of the foundation.

The problem of determination of the relevant soil properties will not be discussed further here. It should only be noted that, in every

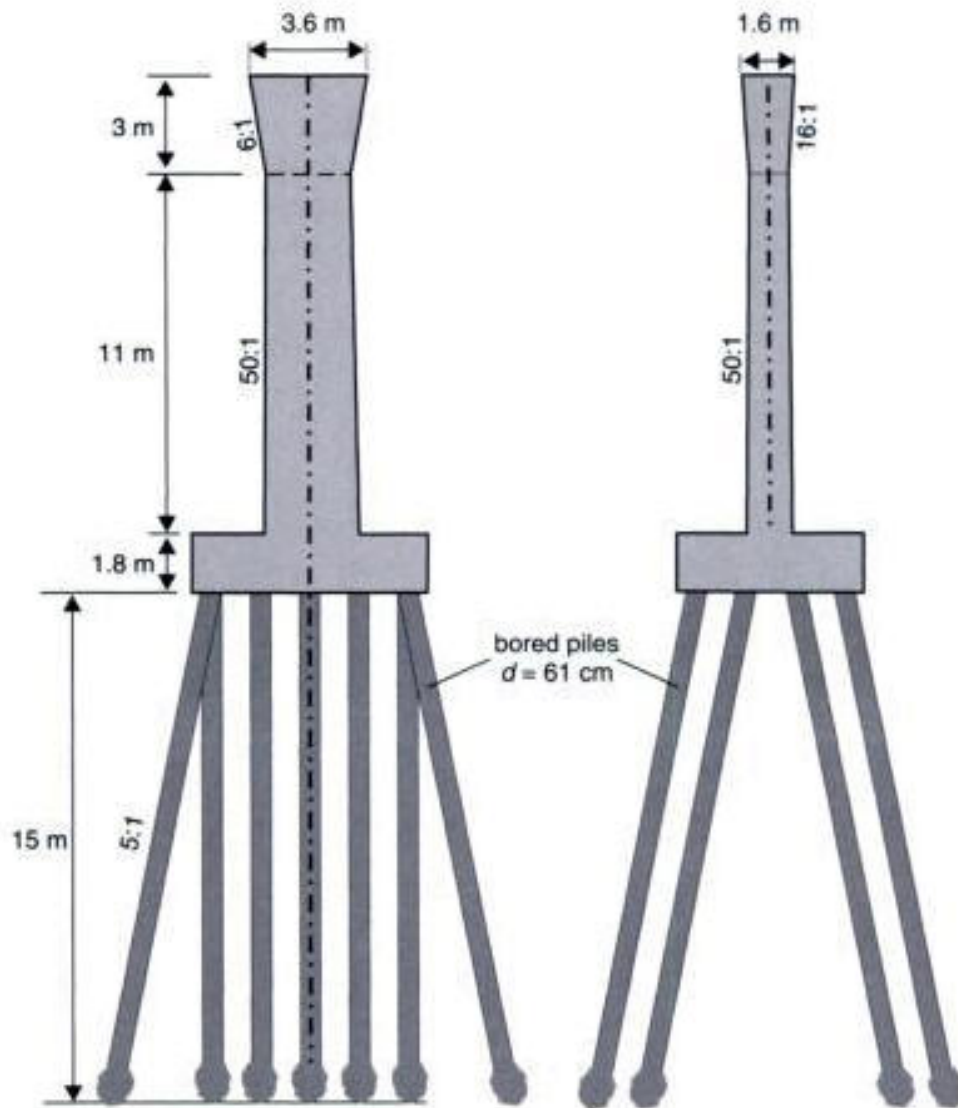


Fig. 2.38 Pile foundation of a bridge column (Schornbachtalbrücke [21])

design, the distribution of the member forces and the displacements are considerably influenced by the behaviour of the soil.

The modelling problems will be further considered for a bridge column on a pile foundation (Schornbachtalbrücke [21], bridge under construction, see Figs 2.39–2.41). Figure 2.38 shows the dimensions of the structure. The bridge column is founded on 14 reinforced piles, each having a diameter of $d = 61$ cm. In order to simplify the numerical model the pile inclination and the enlarged footing are neglected.

2.4.3.1 Loading

Only a horizontal braking force of $H = 870$ kN, acting at the top of the bridge column in the horizontal (y -) direction, is considered. This



Fig. 2.39 Bridge during construction

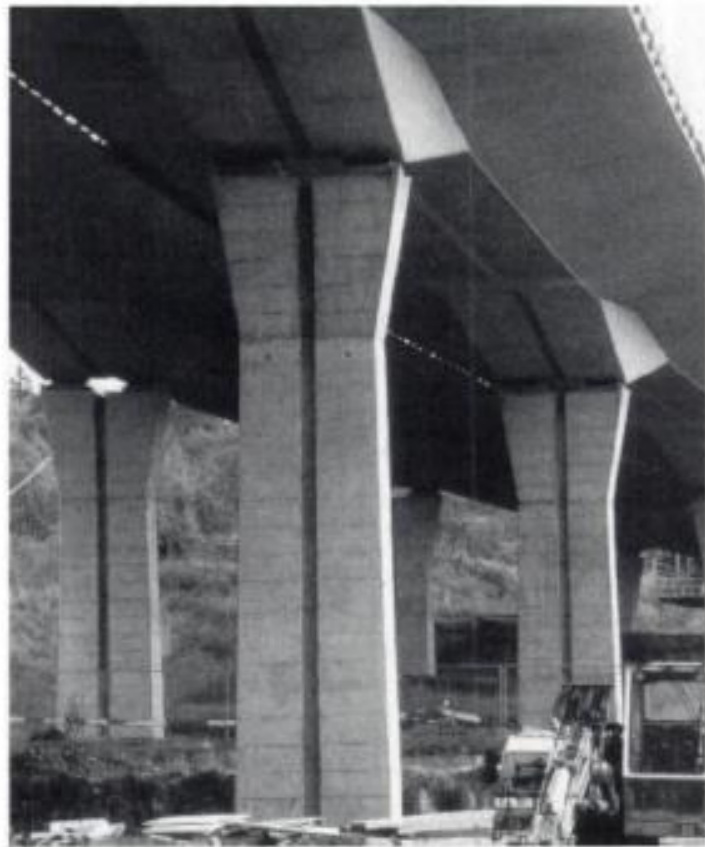


Fig. 2.40 Bridge column



Fig. 2.41 Pile boring rig

results in a bending moment at the bottom of the pile cap of:

$$M = 870 \text{ kN} \cdot 15.8 \text{ m} = 13\,750 \text{ kNm}$$

2.4.3.2 Manual analysis

The normal forces in the different piles can be calculated from equilibrium conditions if one neglects the deformation of the structure (rigid pile cap). This results in normal pile forces of $F_2 = \pm 585 \text{ kN}$ for the outer row and $F_2 = \pm 195 \text{ kN}$ for the inner row (Fig. 2.42). No bending moments are estimated in this approach.

2.4.3.3 Truss system

The piles are modelled with truss elements that are supported horizontally by spring elements (see Fig. 2.44). A linear distribution of the bedding modulus along the length of the pile with $k_s = 0 \text{ MN/m}^2$ at the head and $k_s = 100 \text{ MN/m}^2$ at the pile toe is assumed. The interaction between the piles and the friction between the piles and the ground is neglected. The vertical settlement of the pile toe is modelled

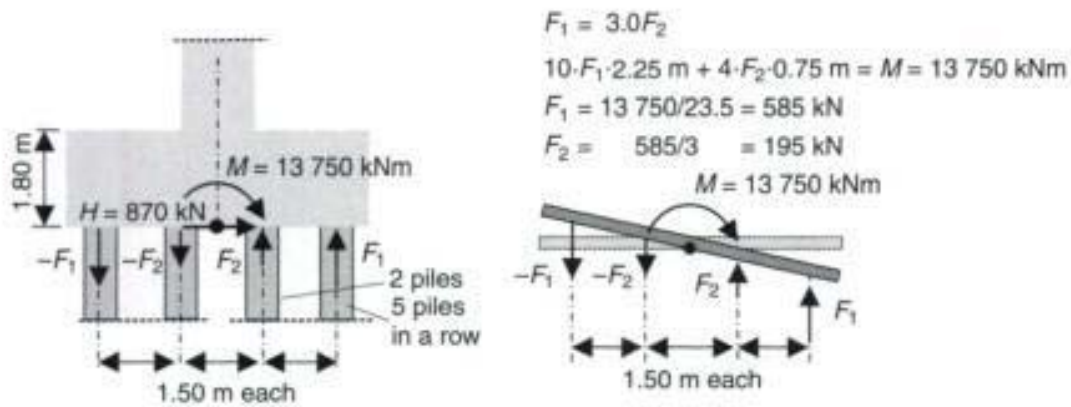


Fig. 2.42 Manual calculation of the pile forces

by linear-elastic springs. For simplicity, a constant cross-section of the column is used in the following, for, in this example, only the pile foundation is of interest.

The pile cap cannot be modelled by truss elements, as this is a typical discontinuity region (see Fig. 2.43). Therefore the nodes of the pile's heads are fixed to the end node of the column base. The pile cap is, therefore, modelled as an infinite stiff body. The disadvantage of this model is that the member forces of the pile cap are not calculated. Further investigations are required if the bending deformations of the pile cap cannot be neglected.

2.4.3.4 Variation of the vertical spring stiffness

The stiffness of the vertical spring at the pile toe can only be estimated by tests. The codes provide rough, approximate values only (Fig. 2.45). As the stiffness of the vertical support of a pile may show a great scatter in practice, the results of a parametric study will be discussed in the following example. The stiffness of the vertical spring varies from $C = 400 \text{ MN/m}$ to infinity (full vertical restraint).

As can be seen in Fig. 2.46, the stiffness of the vertical spring has a great influence on the bending moments in the piles. A fixed vertical support reduces the greatest bending moment by a factor of 2 compared

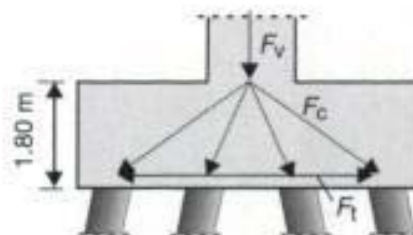


Fig. 2.43 Flow of forces in a pile cap

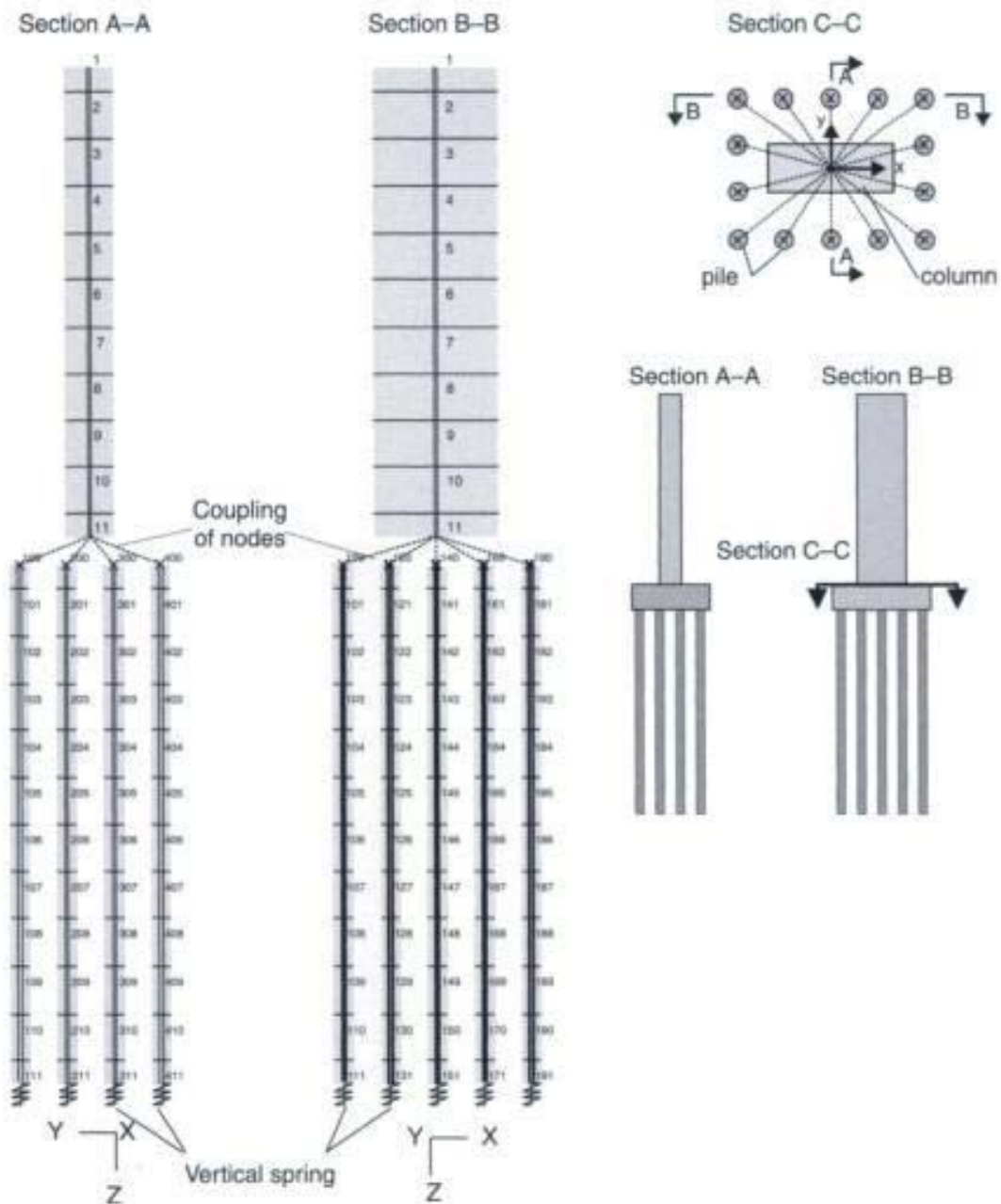


Fig. 2.44 Truss model

with that from an elastic support with $C = 400 \text{ MN/m}$. The main reason for this big difference is the rotation of the pile cap. The greater the inclination of the infinite stiff pile cap due to settlements of the piles the greater is the rotation of the pile heads and the resulting bending moments.

When comparing the bending moment distributions, one has to remember that a pile usually has a uniform reinforcement arrangement around its circumference. Therefore, the (+/-) sign of the bending moments does not matter.

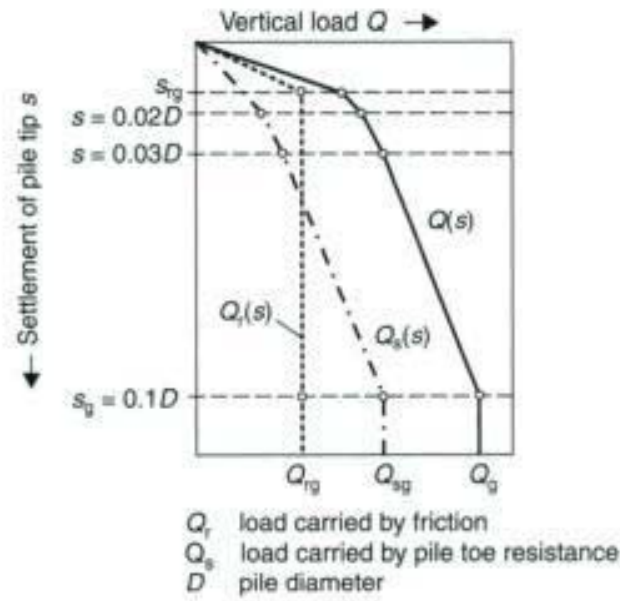


Fig. 2.45 Load-settlement curves acc. DIN 4014 ([18], Fig. 3)

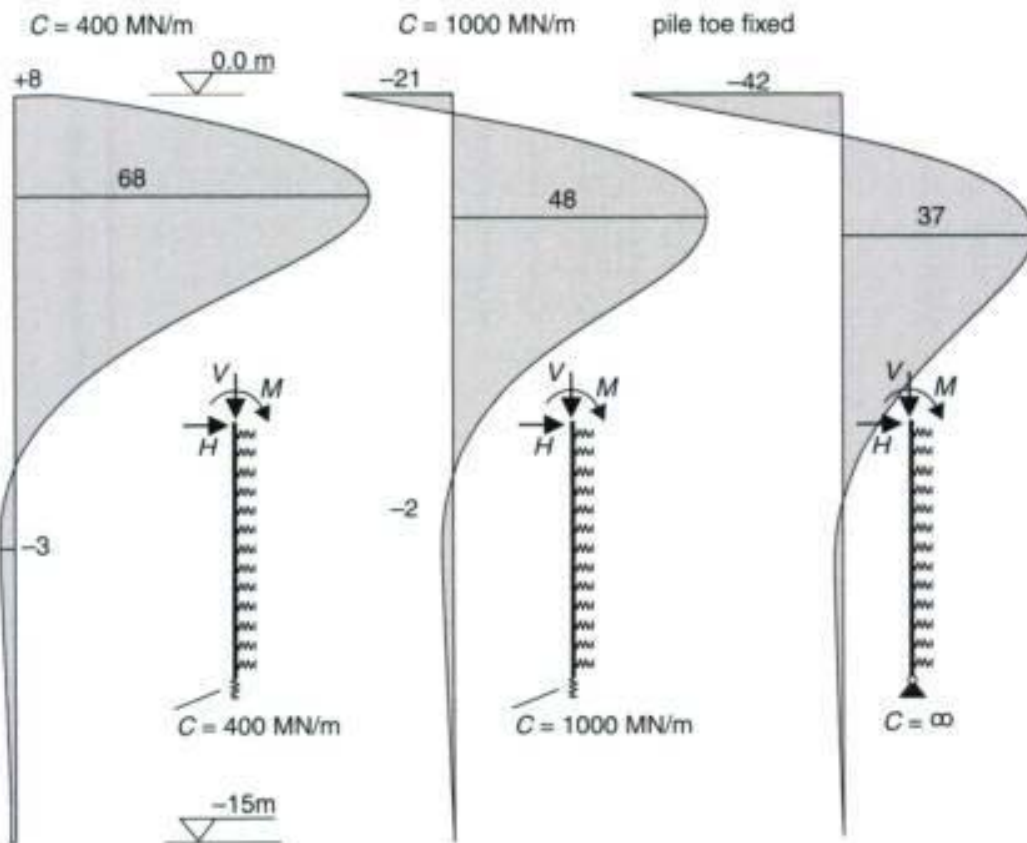


Fig. 2.46 Bending moment distribution in the pile (load: $H_y = 870 \text{ kN}$ at column head)

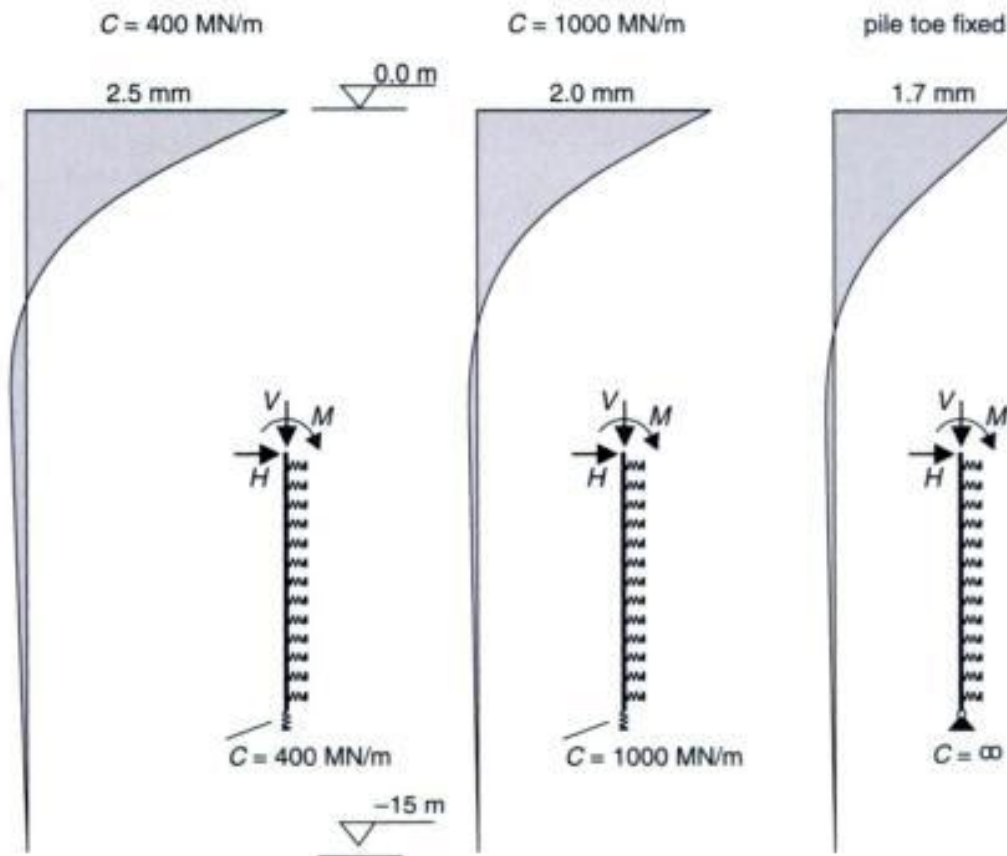


Fig. 2.47 Horizontal deformation of the pile (load: $H_y = 870 \text{ kN}$ at column head)

The distribution of the normal forces is not shown in this example, as it is only slightly influenced by the stiffness of the vertical spring. The normal forces in the piles can easily be calculated manually from the bending moment at the base of the bridge column (Fig. 2.42).

The main difference between a manual and a numerical analysis is that in the latter, bending moments and normal forces are estimated. Bending moments may cause a high increase of the pile reinforcement due to the small lever arm of the internal forces.

In this example, the displacement and rotation of the pile cap does not significantly increase the member forces of the column. The horizontal deformation of the column head is less than 18 mm ($C = 400 \text{ MN/m}$) or 8 mm (fully restrained) assuming an elastic material behaviour.

2.4.3.5 Horizontal restraint of the pile cap

In the analysis above, it was assumed that the pile cap can move horizontally without any reacting forces of the ground. In reality this

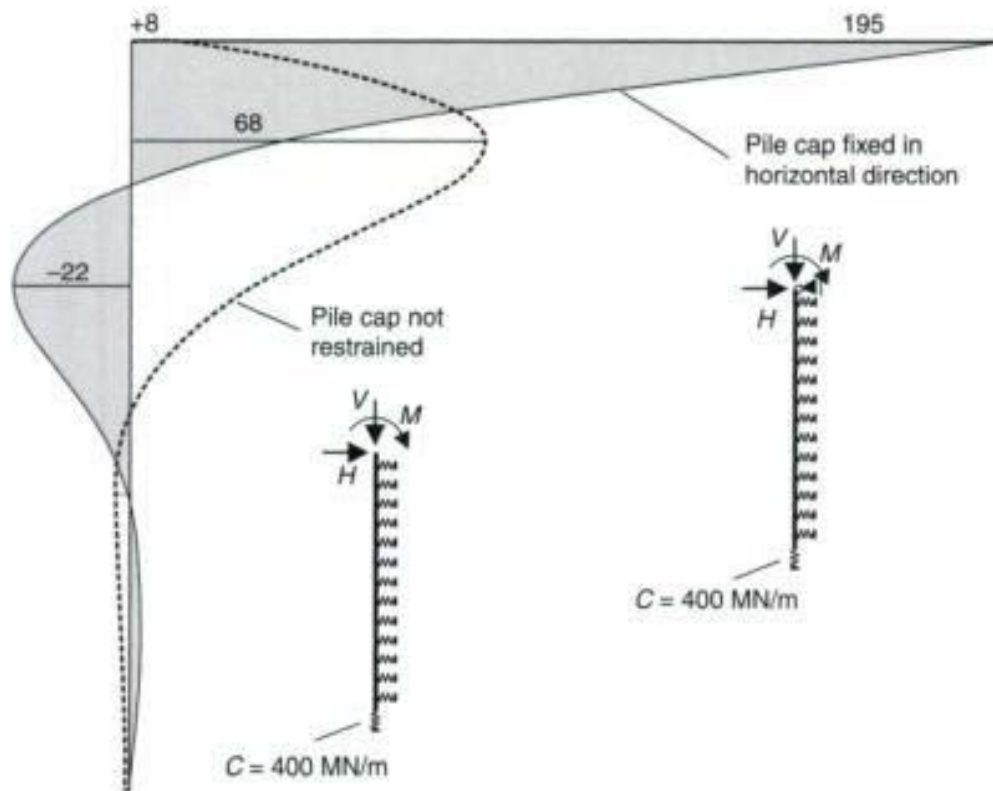


Fig. 2.48 Bending moment distribution in the pile respectively with/without horizontally fixed pile cap (load: $H_y = 870 \text{ kN}$ at column head)

displacement is partly restrained due to the friction between the pile cap and the ground, and the horizontal passive earth pressure. A horizontal restraint of the pile cap has a large influence on the bending moments of the piles (see Fig. 2.48). The bending moment at the pile head increases from $M = 8 \text{ kNm}$ (no restraint) to $M = 195 \text{ kNm}$ ($C = 400 \text{ MN/m}$).

Please note that long-term settlements of the soil underneath the pile cap may reduce the vertical and horizontal bedding of the pile cap.

2.4.3.6 Inclined piles

If the inclination of the outer row of piles is considered in the numerical model as in reality (Fig. 2.38), the maximum bending moments are estimated at the pile heads (Fig. 2.49). Again there are large differences in bending moments between those of fully restrained and elastically supported pile toes.

To summarize, the vertical restraint, the elastic bedding of the piles and their distribution along its length, and any horizontal restraint of the pile cap have significant influences on the member forces in the structural system. All these parameters depend on the soil

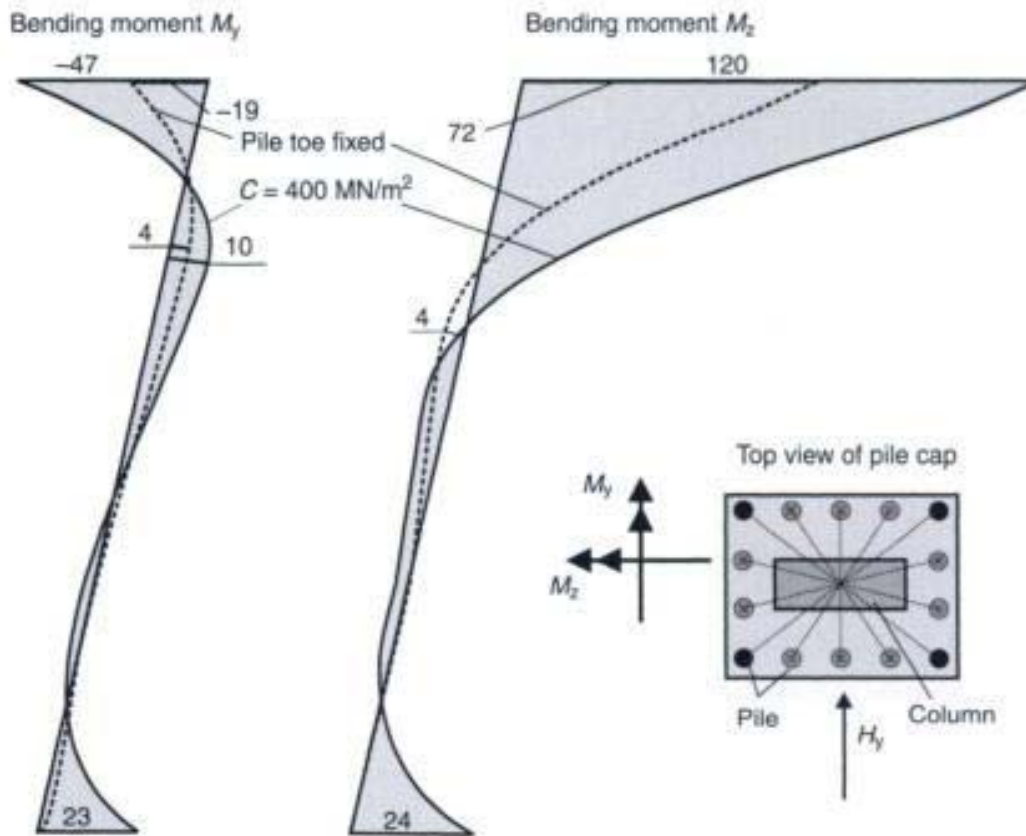


Fig. 2.49 Bending moment distribution in the edge piles (load: $H_y = 870 \text{ kN}$ at column head)

characteristics, which in reality can vary within a great range. Therefore, parametric studies may be required to estimate the correct relevant design forces.

As the restraint of the column due to the foundation shows less scatter, it may be useful to estimate the required design forces of the column by a separate model (i.e. a truss which is partially restrained at its lower end). The resulting forces can then be used as loads for the foundation.

A linear increase of the bedding modulus over the length of the piles has been assumed in the example given above. In general, the restraint of the soil against horizontal deformation is not proportional to the ground reactions. Therefore, such nonlinear behaviour has to be considered in the case of large horizontal loads.

During all calculations, one must check that the calculated soil pressure is not positive (tension) or greater than the permissible one.

In the case of large bending moments, a nonlinear design of the piles (including the reduction of stiffness due to cracking) can result in a significant reduction of the maximum member forces. But it is doubtful

whether such a refined model is more accurate than a linear elastic one, as the basic input parameter – the soil stiffness – can show a great scatter in reality.

2.5 Shear walls with large openings

Shear walls are used in high-rise buildings as bracing elements (Fig. 2.50). Modelling of such a structure is a difficult task. At first, one may think of it as a two-dimensional model with shell elements (diaphragm). However, these calculations are generally too time-consuming for practical purposes. Furthermore, the estimation of the reinforcement requirements is difficult (see Chapter 3). With a truss model one can only approximate the behaviour of a shear wall with large openings due to the considerable width of the structural elements and the non-uniform strain distribution in most parts of the structure. Nevertheless, due to its simplicity, it is interesting to use this model. In such a case one has to model the stiffness of the structure correctly.

In a frame model, the structural system is modelled by straight truss elements which are located at the centreline of the cross-section of the individual members. Modifications are required for massive structural parts, like the columns as shown in Fig. 2.51. In addition, it should be noted that truss models are only valid for slender shear walls (beam system). Further investigations may be required for areas near the supports at the base of the structure.

The member forces of the horizontal beams and vertical 'columns' are required for the design of the structure. In this case, one must consider the deformation behaviour of the whole structure. The different parts of the structure are modelled by straight truss elements. Special attention has to be given to the joints between the horizontal beams and the vertical 'columns'. The horizontal beams are restrained at the inner face of the vertical 'columns' and not at their centreline. If this is not considered, the span length would be much too large, and the calculated stiffness of the structure would be smaller than in reality. There are various possibilities to model the real behaviour of the structure (Fig. 2.51):

- Model 1: Special truss elements. The horizontal beam is modelled by special beam elements, which have infinite stiffness at both ends.
- Model 2: Beam with variable stiffness. The horizontal beam is modelled by at least three elements: two very stiff elements at the ends and one with normal stiffness in between (see Figs 2.51a and

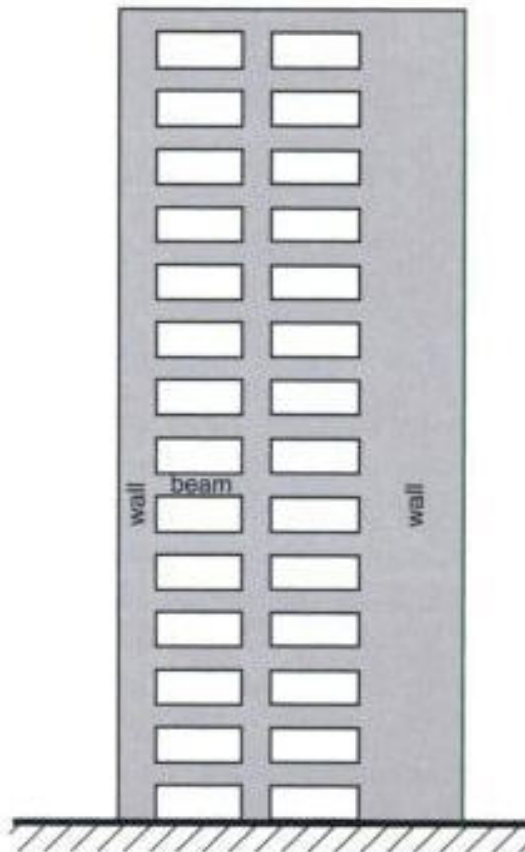


Fig. 2.50 Bracing elements of a high-rise building – frames and shear walls

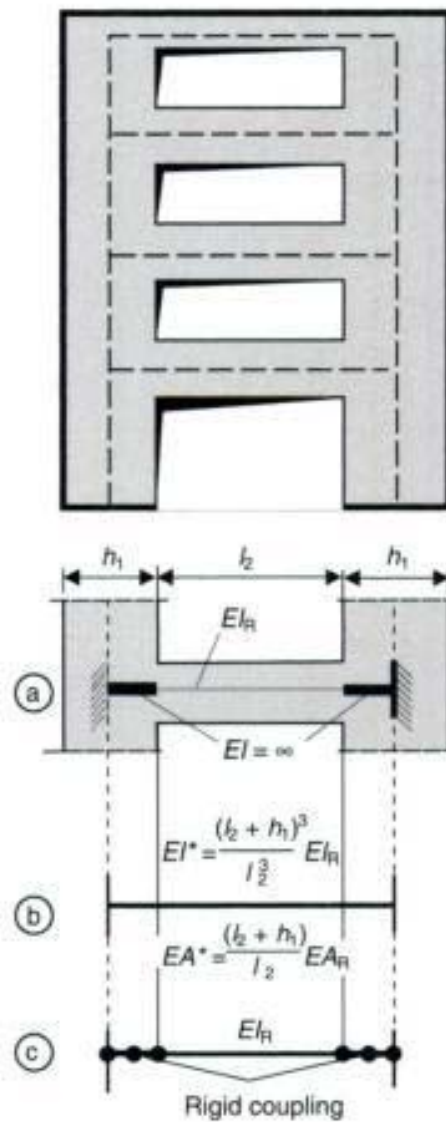


Fig. 2.51 Models for the beam/column junction of a shear wall with large openings

- 2.52). The considerable stiffness differences between the rigid and elastic elements may cause some numerical problems.
- Model 3: Modification of the stiffness. The bending and normal stiffness of a fictitious member, having a constant cross-section, is increased in order to consider the actual true behaviour of the horizontal beam in the structure. The moment of inertia of the new beam is calculated as though it has the same bending stiffness as the real beam but with a shorter span length. It must be noted that the deformation of the horizontal beam is not calculated correctly.
 - Model 4: Coupling of the nodes at the joints. The nodes in the joints are coupled together (see Fig. 2.51c). This method has been previously explained in section 2.1.

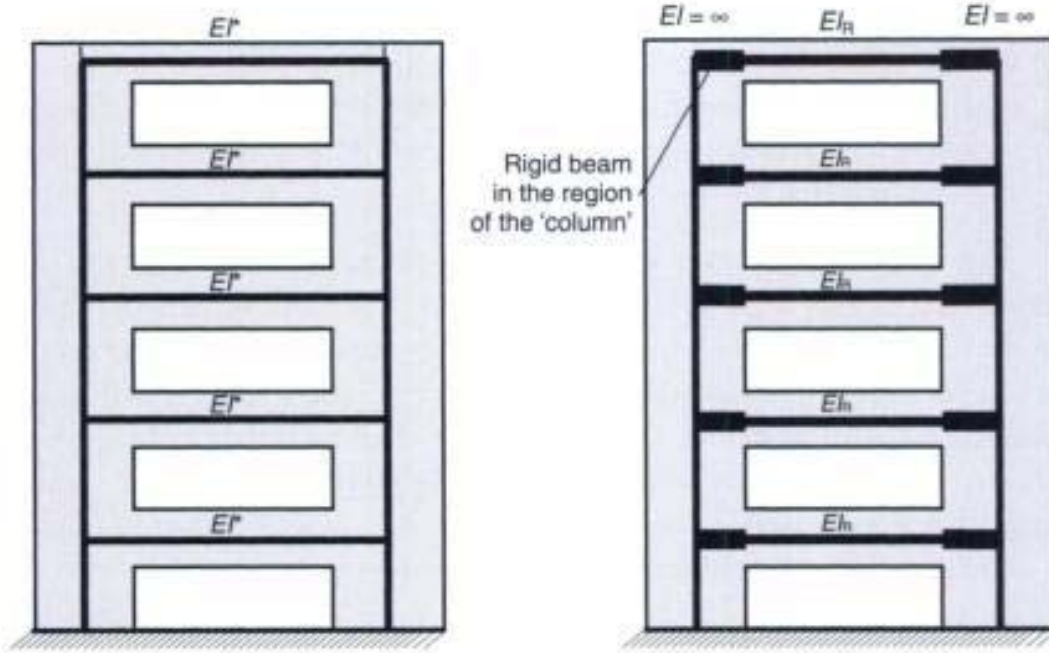


Fig. 2.52 Models for a coupled shear wall with large openings

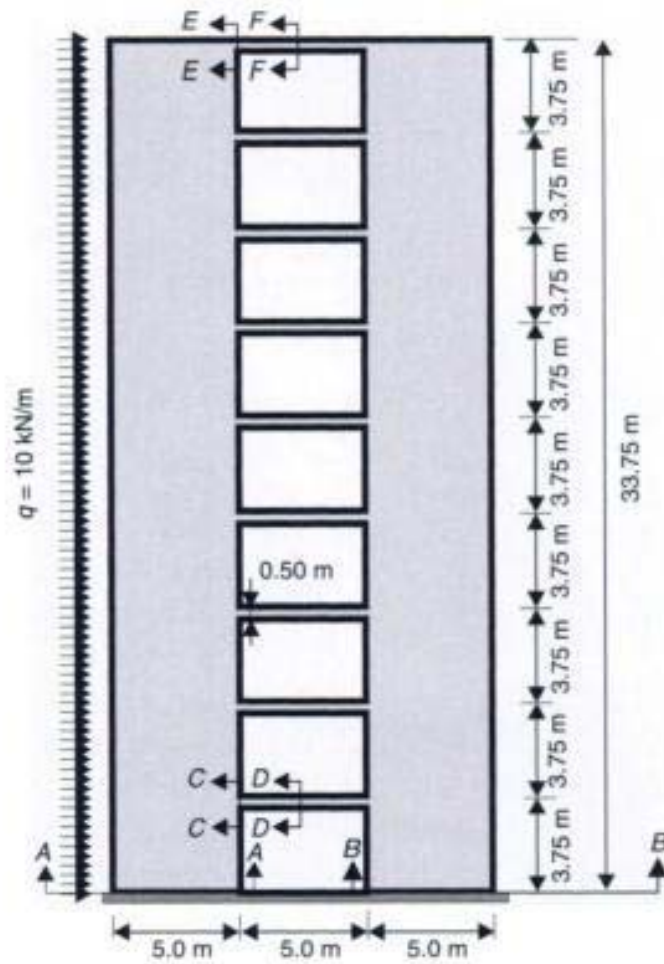


Fig. 2.53 Shear wall with large openings

Copyrighted Material

- Model 5: Two-dimensional shell model (diaphragm). Shell models will be discussed in Chapter 3. A considerable effort is needed to evaluate such a model. Furthermore, the software cannot usually estimate the reinforcement requirements. This is the reason that shell models are not widely used.

The major difference of the above-mentioned models will be examined for the system shown in Fig. 2.53. The walls have a thickness of $h = 20$ cm. They are made of concrete grade C35/45. The structure is loaded with a uniform horizontal load of $q = 10$ kN/m. The deflection pattern, which has been calculated with a shell model (diaphragm), is shown in Fig. 2.54. A large shear and bending deformation in the upper horizontal beams can be observed.

Table 2.4 lists the member forces in a few sections of the various models. Models 3 and 4 give nearly the same results. The influence of the axial stiffness EA is relatively small (i.e. 5%). As expected, the

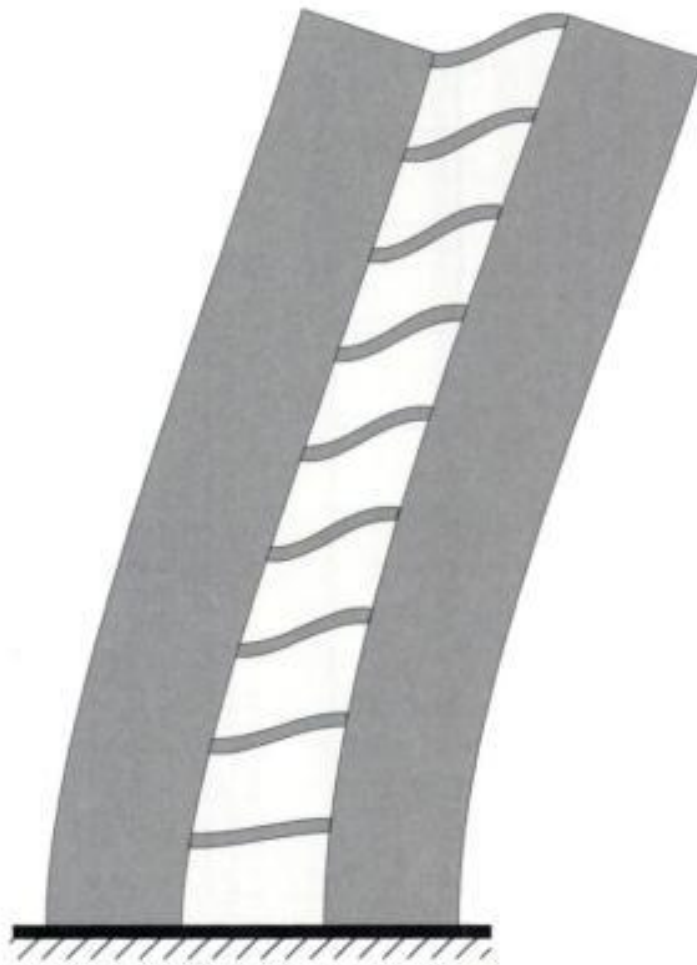


Fig. 2.54 Deformation (shell model)

Table 2.4 Member forces of a shear wall with large openings (Fig. 2.53)

Sections see Fig. 2.53		Without modifi- cations	Model 3 with modified I^* (Fig. 2.51b)	Model 3 with modified I^* , A^* (Fig. 2.51b)	Model 4 coupling of nodes (Fig. 2.51c)	Model 5 shell analysis
Section A-A	N	25.6	133.2	133.2	133.2	117.8 kN
	V	200.1	187.7	195.2	195.2	191.9 kN
	M	-2818	-2216	-2251	-2251	-2316 kNm
Section B-B	N	-25.6	-133.2	-133.2	-133.2	117.9 kN
	V	137.4	149.8	142.3	142.3	145.5 kN
	M	-2621	-2146	-2112	2112	2199 kNm
Section C-C	N	-4.4	-9.2	-5.7	-5.7	kN
	V	-1.1	-6.6	-6.6	-6.6	kN
	M	2.7	16.5	16.6	16.4	kNm
Section D-D	N	-4.4	-9.2	-5.7	-5.7	kN
	V	-1.1	-6.6	-6.6	-6.6	kN
	M	0	0	0	0	kNm
Section E-E	N	-11.5	-17.5	-10.8	-10.8	kN
	V	-3.5	-18.5	-18.5	-16.5	kN
	M	8.7	41.2	41.2	41.3	kNm
Section F-F	N	-11.5	-17.5	-10.8	-10.8	kN
	V	-3.5	-18.5	-18.5	-16.5	kN
	M	0	0	0	0	kNm
Horizontal displacement	w_x	10.7	7.3	7.3	7.3	8.0 mm

unmodified frame system results in much greater displacements, greater bending moments, and less normal forces than the ones of a two-dimensional shell system.

The resulting member forces of a shell model are provided in column 7 of Table 2.4. There is a good agreement in the results of the truss system. Therefore, the considerable work required for a shell analysis does not seem to be justified for this particular structure.

The calculations shown above are based on a linear elastic material behaviour. The maximum tensile stresses in the horizontal beam are greater than the mean tensile strength of the concrete f_{ctm} ($\max M = 41.2 \text{ kNm}$, Section E-E, $\sigma_{ct} = M/W = 41.2/8.33 = +4.9 \text{ MPa}$), resulting in cracking of the horizontal girders and a reduced restraint.

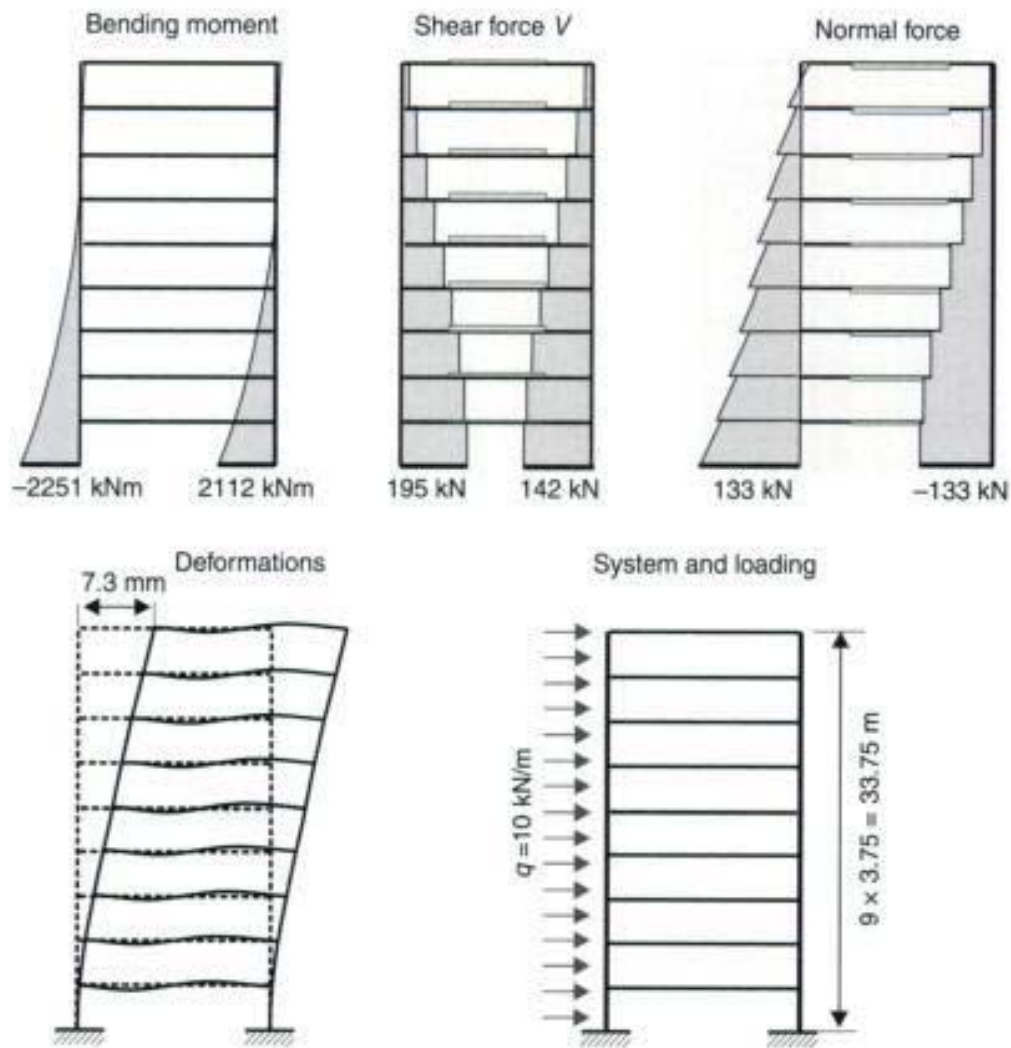


Fig. 2.55 Member forces and deformation of a shear wall with large openings, nodes at the column/beam joints coupled

This aspect must be considered in design if more precise data for the deformation of the structure is required. But for the example above, the influence of the stiffness of the horizontal beams on the member forces is small.

It should be noted here that the accuracy of a truss system in the region of the support depends on the restraint conditions (nonlinear strain distribution). If more precise information is needed, then a shell model (diaphragm) may be helpful.

In the above example, special beams are used to connect the two vertical elements ('columns') together. Considerable construction effort would be needed to build such beams. Therefore, one is interested to avoid them, where possible, and to use the existing slab only as a

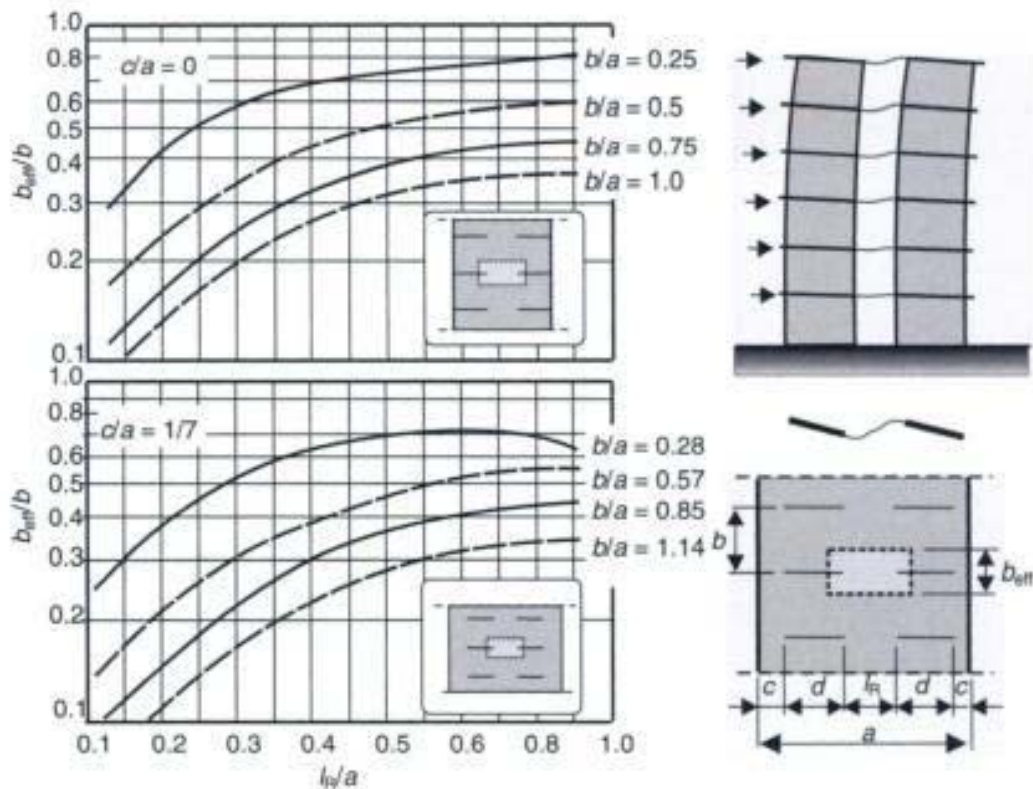


Fig. 2.56 Effective width b_{eff} of a slab [9]

coupling element. However, this results in a complicated three-dimensional shell system which requires much calculation effort. To avoid this, one may again use a truss system. First of all, the cross-section properties of the equivalent, fictitious horizontal beams are needed. The effective width b_{eff} can be taken from diagrams provided by Wrong [9] (Fig. 2.56). As great accuracy cannot be expected from such a model, the figures are only valid for simple regular systems which are rarely built in practice. If more accurate values for the stiffness of the horizontal beams are required, then it is better to use a shell model with a simplified equivalent structural system.

2.6 Bracing of high-rise buildings

The bracing elements of a building have to be designed to resist the vertical loads and more importantly the horizontal actions (e.g. wind, earthquake and their resultant effects) on a structure. Furthermore, the stability of the structure must be assured.

Nowadays, whole buildings can be modelled by three-dimensional shell elements. But this tremendous effort is not justified for ordinary

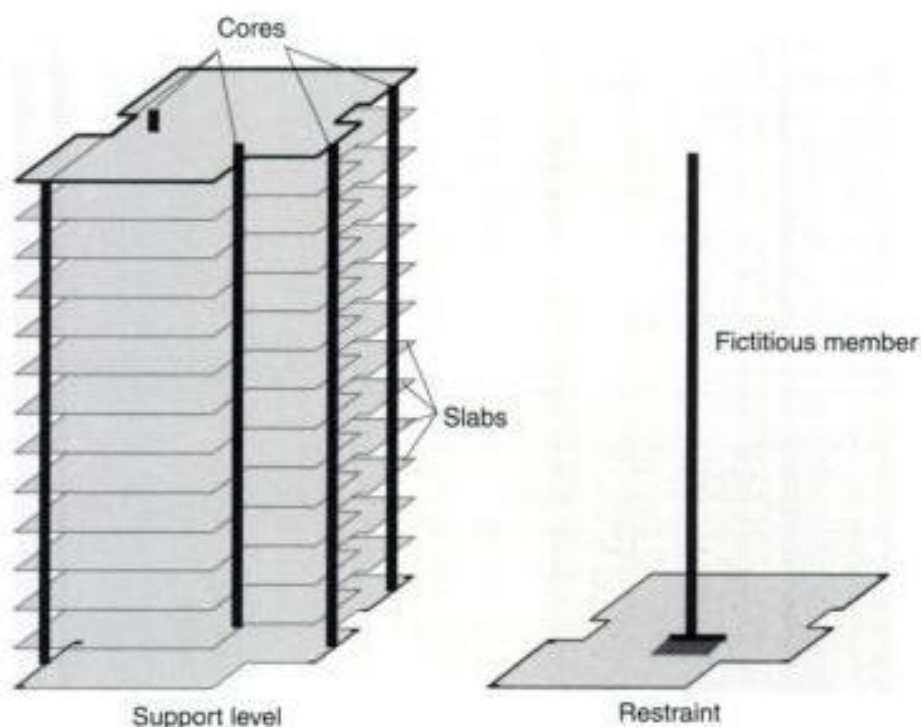


Fig. 2.57 Modelling of a bracing system – fictitious bar method

structures. A truss system, where the whole structure is reduced to just the main load bearing elements, the so-called 'cores', is sufficient for most cases in practice. In the real system the bracing elements are connected together by the slabs, which are assumed to be rigid in their midplane. Also, the bending stiffness of each slab is neglected.

Simple regular systems with a congruent deformation pattern of the bracing elements can easily be designed with the so-called method of fictitious bars (equivalent beam method) [15] (see Fig. 2.57). This simple method is often used to check numerical results, even for complex bracing systems. If there are differences between the analytical and the numerical analysis, it is always a question of which are the correct member forces. Therefore, in the following the differences between manual and numerical models are discussed.

In reality, often complicated bracing systems are built like, e.g. girders which have different cross-sections over their length or columns which are not continuous throughout the height of the building. In such cases, a manual calculation using the method of fictitious bars is not possible. A numerical analysis will then be required for a three-dimensional truss model of the bracing system.

In addition, a numerical model can be useful where nonlinear material behaviour has to be considered, or when a dynamic analysis is required (i.e. an earthquake).

Even in this day-to-day task, engineering knowledge is needed when using design software. There are several problems which may arise when using a truss model, such as:

- cross-sectional properties of the truss elements;
- location of the axis of gravity of the trusses (axis of gravity – axis of torsion);
- modelling of the behaviour of the slabs – coupling of the truss nodes.

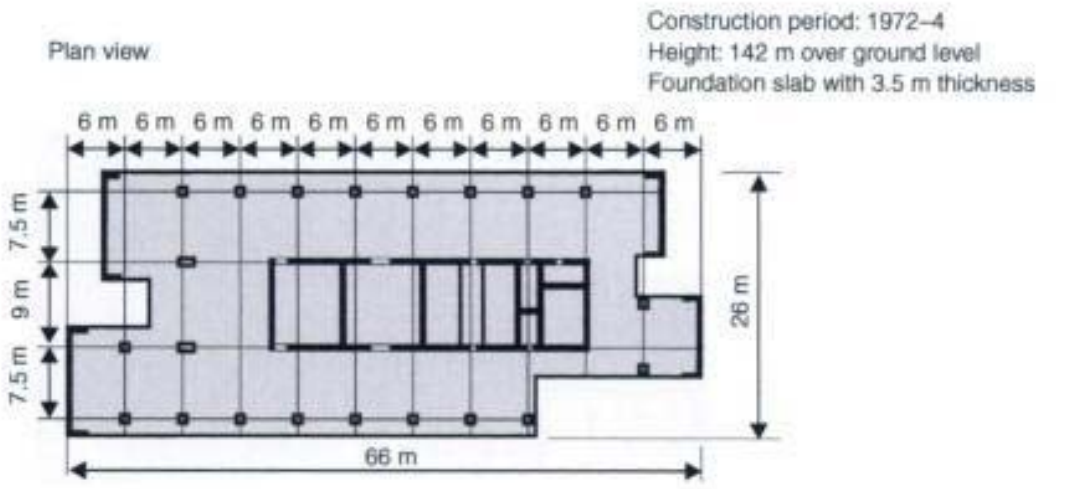
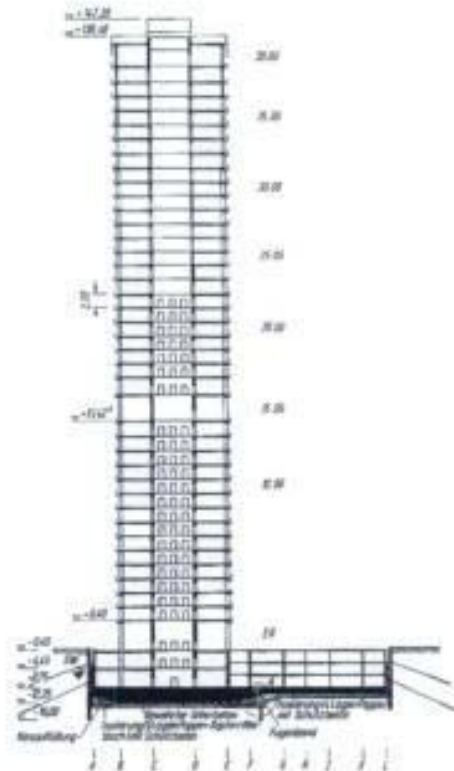
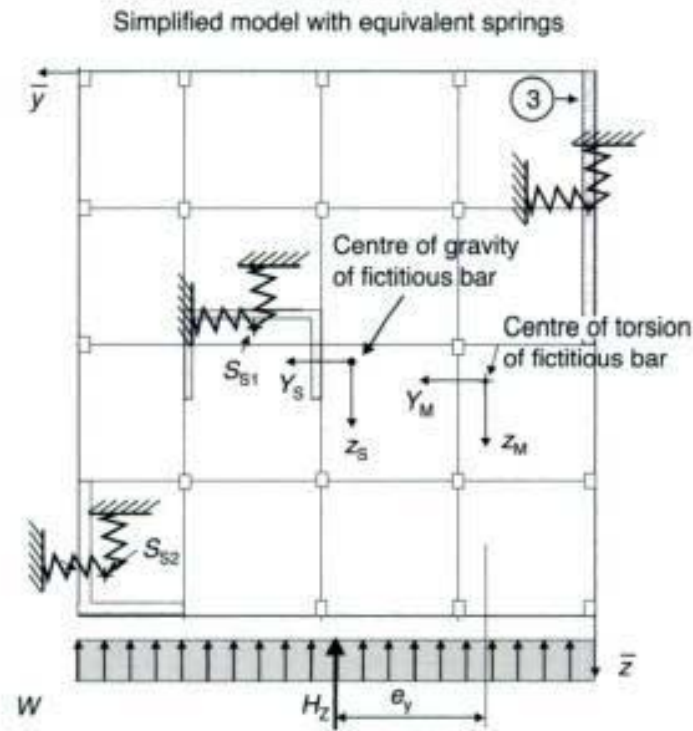
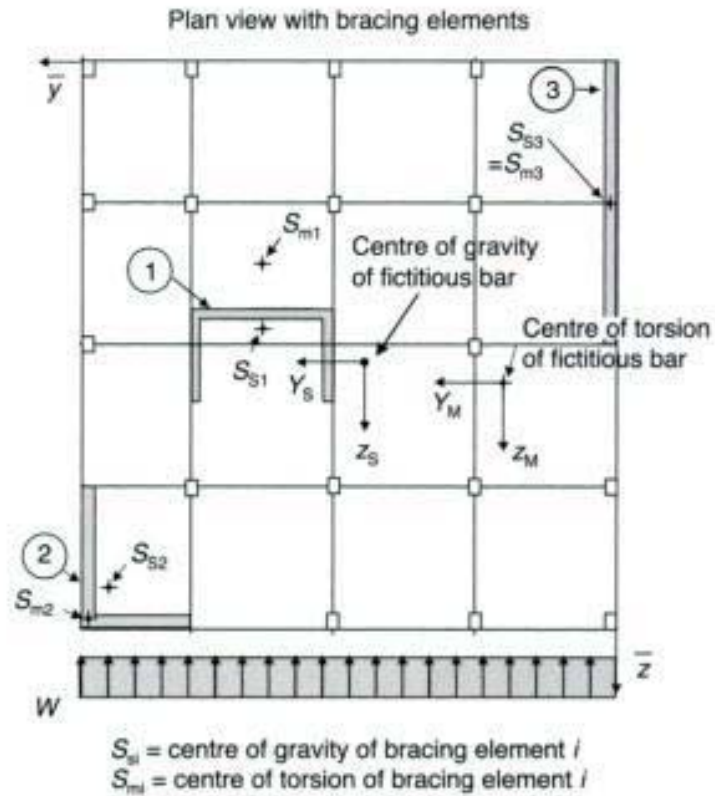


Fig. 2.58 High-rise building – bracing system (Mainzer Landstraße, Frankfurt [16])

Copyrighted Material

Method of fictitious bars



Copyrighted Material

The following items are neglected:

- moment of inertia I_{yz} of the bracing elements;
- wrapping torsional stiffness of the individual elements $G \cdot C_{M,i}$;
- St Venantsche torsion stiffness of individual elements $G \cdot I_{T,i}$;
- shear deformations.

Forces due to translation:

$$H_{y,i} = \frac{H_{y,M} \cdot E \cdot I_{z,i}}{\sum_{i=1}^n E \cdot I_{z,i}}; \quad H_{z,i} = \frac{H_{z,M} \cdot E \cdot I_{y,i}}{\sum_{i=1}^n E \cdot I_{y,i}}$$

Forces due to rotation:

$$H_{y,i} = -\frac{M_{x,M} \cdot E \cdot I_{z,i} \cdot z_{Mm,i}}{\sum_{i=1}^n E \cdot C_M}; \quad H_{z,i} = -\frac{M_{x,M} \cdot E \cdot I_{y,i} \cdot y_{Mm,i}}{\sum_{i=1}^n E \cdot C_M}$$

with:

- $H_{y,M}$; $H_{z,M}$ resultant horizontal force, related to the centre of torsion;
- $M_{x,M}$ resultant torsional moment, related to the centre of torsion.

The member forces of the individual bracing elements are estimated on a cantilever beam loaded by horizontal forces H_y and H_z . Torsional effects of the individual elements are neglected.

2.6.1 Equivalent cross-section of the trusses

The following stiffness parameters are needed for design purposes:

- normal stiffness $E \cdot A$
- bending stiffness $E \cdot I_x$ and $E \cdot I_y$
- shear stiffness $G \cdot A_{sy}$ and $G \cdot A_{sz}$
- torsional stiffness (St Venant) $G \cdot I_T$
- torsional stiffness (warping torsion) $G \cdot C_M$

For closed thin-walled sections, in which equilibrium is satisfied by a closed shear flow, these parameters can easily be calculated, e.g. by means of a computer software based on the linear-elastic behaviour of the concrete material. However, the reduction of stiffness in Stage II

(cracked concrete) has to be considered. It is well-known that the torsional stiffness of a cracked member is significantly lower than the elastic value. Therefore, the torsional stiffness GI_T may be neglected for a concrete structure in Stage II condition. Rough data are given in *Heft 240* of the German Association for Concrete Design [10], where the following values are listed:

beam uncracked (Stage I) $(G \cdot I_T)^I \cong 1/3 \cdot E_c \cdot I_T$

beam cracked (Stage II) $(G \cdot I_T)^{II} \cong 0.1 \cdot E_c \cdot I_T$

shear modulus $G = \frac{E_c}{2 \cdot (1 - \nu)} \approx 0.6 \cdot E_c$ (Poisson's ratio $\nu \approx 0.2$).

According to Eurocode 2, a structural member may be treated as uncracked if the greatest tensile stress σ_{ctd} under a certain load combination is less than the guaranteed tensile strength $f_{ct,0.05k}/\gamma_c$.

Very often the bracing elements have large openings (e.g. for the doors to the elevator shaft) which may reduce the shear and torsional stiffness significantly. For beams with open cross-sections or for hollow box girders with openings the influence of the floor slab has to be considered when calculating the stiffness parameters. An engineering judgement is required here.

Further investigations are required if the bracing elements are close to each other. In the fictitious truss model, it is assumed that the slab can only transfer normal forces and that it has no bending stiffness. This assumption is not valid if the distance between the bracing elements is small. In such a case, the cores may be modelled as one single, stiff cross-section. An alternative is to introduce a stiff coupling of the nodes. This will be explained in section 2.6.3.

2.6.2 Location of the beam elements

In a numerical model, the beam axis coincides with the axis of gravity of its cross-section. All external loads and internal forces relate to this point. Special attention should be taken for beams where the centre of gravity does not coincide with the centre of torsion. In such a case torsional moments are calculated if a load does not act at the centre of torsion. Some software programs do not consider this effect. Also, some FE-programs do not consider that the beam rotates around its axis of torsion and not around its axis of gravity (Fig. 2.59). In such a case, the axis of the beam elements should be located in the axis of torsion. Otherwise the stiffness of the global system is overestimated.

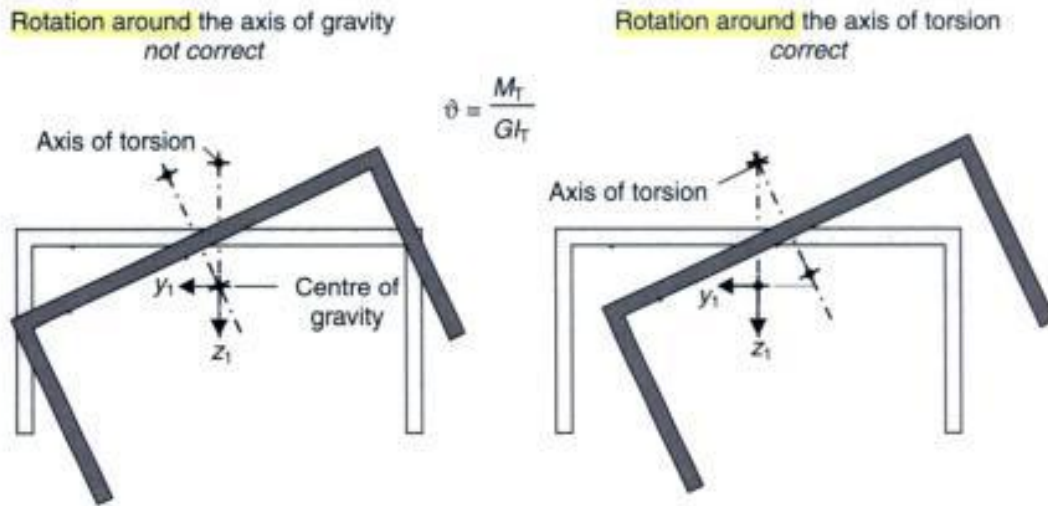


Fig. 2.59 Rotation of a beam with U-section under pure torsional moment

2.6.3 Coupling of nodes

The bracing elements are modelled by truss elements (see Fig. 2.63). The axis of the elements coincides with the axis of gravity of the real system, as explained above. It is useful to introduce extra fictitious master nodes, to which all cores at one level are coupled (Fig. 2.60). These nodes simplify the input of the external loading. It can be located at the centre of the load area. It should be noted that, in the numerical model, loads are usually only considered when the loaded node is connected to the truss system (see Fig. 2.61).

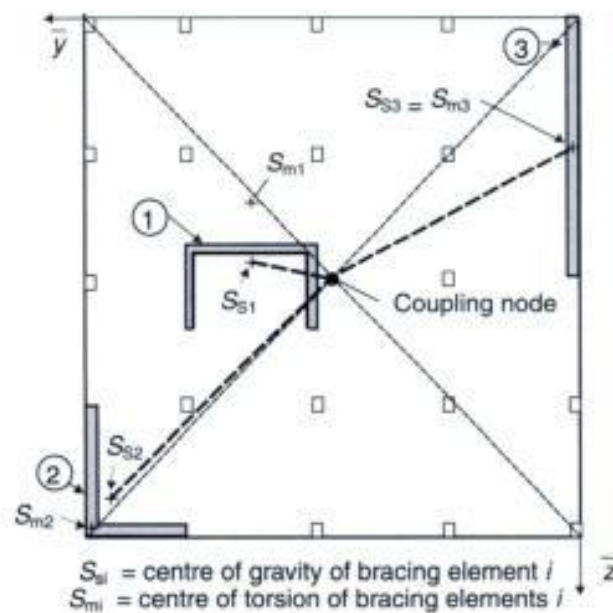


Fig. 2.60 Location of the bracing elements and master node

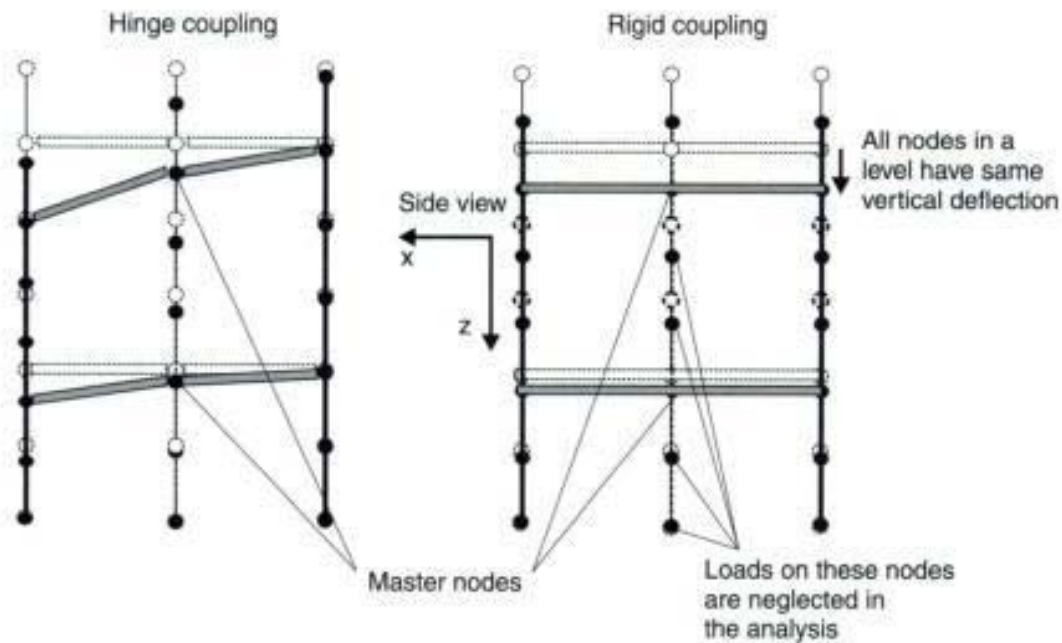


Fig. 2.61 Coupling of nodes – elevation

It is very time consuming to model a slab by using shell elements. Therefore, the behaviour of the slab is simulated by special coupling of the truss nodes. The type of coupling – hinge, full or partially restraint – depends on the real system. The deck slab in normal buildings is usually relatively thin and the distance of the bracing element and the columns is considerably larger. In such cases, one may assume that the deck slab has no bending stiffness but an infinite normal stiffness. The slab may only transfer normal forces. The bending restraint of the bracing elements due to the slab is neglected.

The following different types of coupling are used in practice (see Fig. 2.62):

1. Bending stiff slab

$$v_x = v_{x0} + \varphi_{y0} \cdot (z - z_0) - \varphi_{z0} \cdot (y - y_0)$$

$$v_y = v_{y0} + \varphi_{x0} \cdot (z - z_0) + \varphi_{z0} \cdot (x - x_0)$$

$$v_z = v_{z0} + \varphi_{x0} \cdot (y - y_0) - \varphi_{y0} \cdot (x - x_0)$$

2. No bending stiffness, where the rotation of the nodes at the same level is not identical

$$v_x = v_{x0} - \varphi_{z0} \cdot (y - y_0)$$

$$v_y = v_{y0} + \varphi_{z0} \cdot (x - x_0)$$

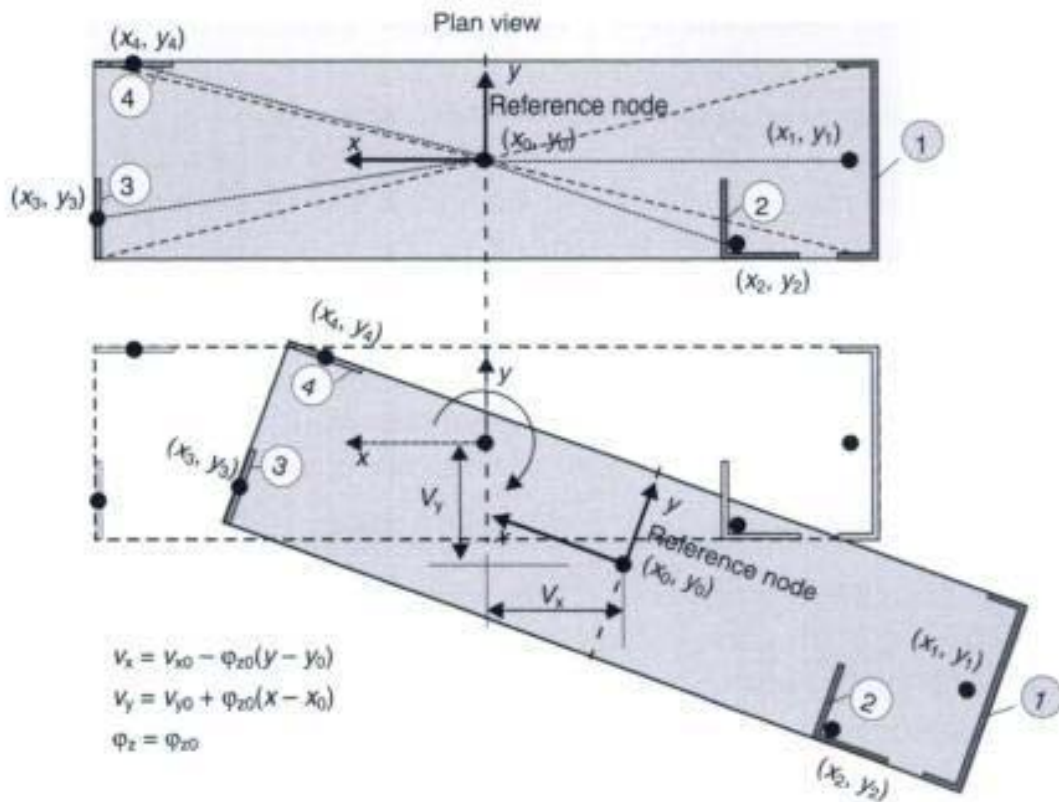


Fig. 2.62 Displacement and rotation of the bracing element in case of a stiff slab

3. No bending stiffness, where all nodes at the same level have the same rotation

$$v_x = v_{x0} - \varphi_{z0} \cdot (y - y_0)$$

$$v_y = v_{y0} + \varphi_{z0} \cdot (x - x_0)$$

$$\varphi_z = \varphi_{z0}$$

with:

v_{x0}, v_{y0}, v_{z0} is the displacement of the reference node;

$\varphi_{x0}, \varphi_{y0}, \varphi_{z0}$ is the rotation of the reference node.

Model 2 is used for comparison only. It does not reflect the real behaviour of the slab. Whether Model 1 or 3 should be used depends on the behaviour of the actual system with respect to the stiffness of the slab and the distance of the bracing elements. A stiff coupling (additional to coupling without bending stiffness: rotation $\varphi_x = \varphi_{x0}$, $\varphi_y = \varphi_{y0}$, $\varphi_z = \varphi_{z0}$) may cause restraints in the system, as can be seen from Fig. 2.61. When the deformation and the rotation of all nodes in the same level are identical, vertical loads are distributed according to the normal stiffness of an individual bracing element.

This does not reflect the actual behaviour of the structure. In reality, the loads are carried by the bracing element which is close to the load.

The actual load bearing and deformation behaviour of a slab is generally similar to a slab without bending stiffness but which is infinitely stiff in its normal plane. In such a case the rotation of all elements around the vertical axis φ_2 must be identical at one level. Therefore, Model 3 should be used.

The axis of gravity of the different truss elements is coupled together, resulting in torsional moments where the axis of torsion does not coincide with the axis of gravity (e.g. cross-section with L or U shape). In this case, torsional moments and rotations are estimated.

2.6.4 Example – comparison of the various models

The following calculation will be done for the bracing system shown in Fig. 2.63 (the height of the building is $h = 24$ m). This structure has been chosen as the member forces can be calculated by the equivalent beam (fictitious bar) method. Therefore, the manual calculated results can be used to verify the numerical models. There are four different bracing elements: two shear walls, a flanged member with L-shape, and a member with U-shape. The slabs are modelled as mentioned before, using special restraints with and without coupling of the nodal rotation φ_2 (φ_2 is the rotation around the vertical axis).

For the sake of simplicity of the further calculations, it is assumed that all bracing elements are fully restrained by the foundation slab. If the structure has a stiff box as a basement, it can be assumed that the trusses are fully restrained at ground level, thus resulting in smaller forces and displacements. An elastic foundation can be modelled by using spring elements at the base of the trusses.

The distribution of the bending moments, from the method of fictitious bars, are shown in Fig. 2.64 for a uniformly distributed horizontal load of $q = 0.442$ kN/m² (total horizontal force is $H = 106.1$ kN) in the x-direction.

The distribution of the total load between the different bracing elements is as shown in Table 2.5.

Figure 2.64 shows the bending moment distribution from manual analysis (fictitious bar method), and the values of the two different truss models. It can be seen that the coupling of the rotation around the vertical axis φ_2 has a considerable influence on the member forces. The bending moments in the bracing elements numbers 1 and 3 are more than 1.5 times larger than for the system without coupling.

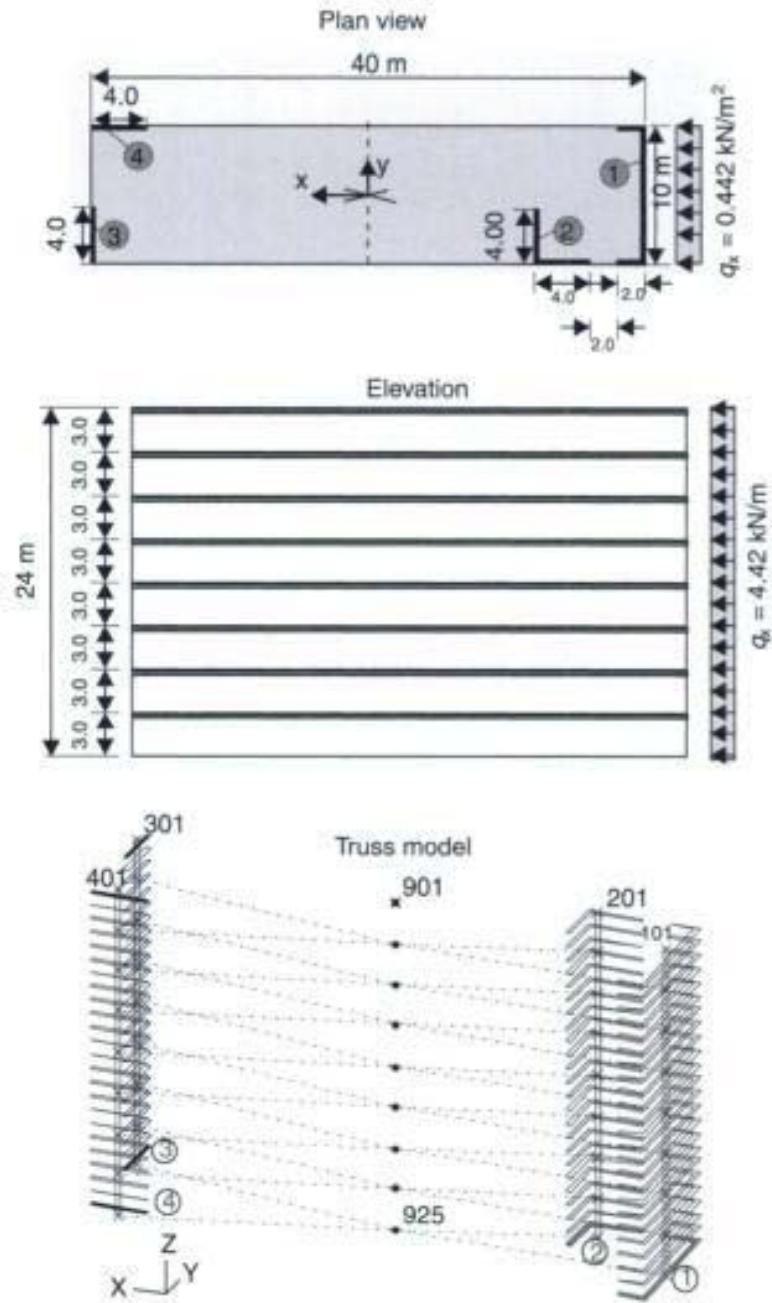


Fig. 2.63 System, loading and truss model

Table 2.5 Support reactions (horizontal force and restraint bending moment) of the bracing elements calculated with the method of fictitious bars

Element no.	1	2	3	4
Support force in x-direction (in kN)	18	60	≈ 0	28
Fixed end moment (in kNm)	-215	-725	≈ 0	-335
Load distribution (in %)	17	57	≈ 0	26

Copyrighted Material

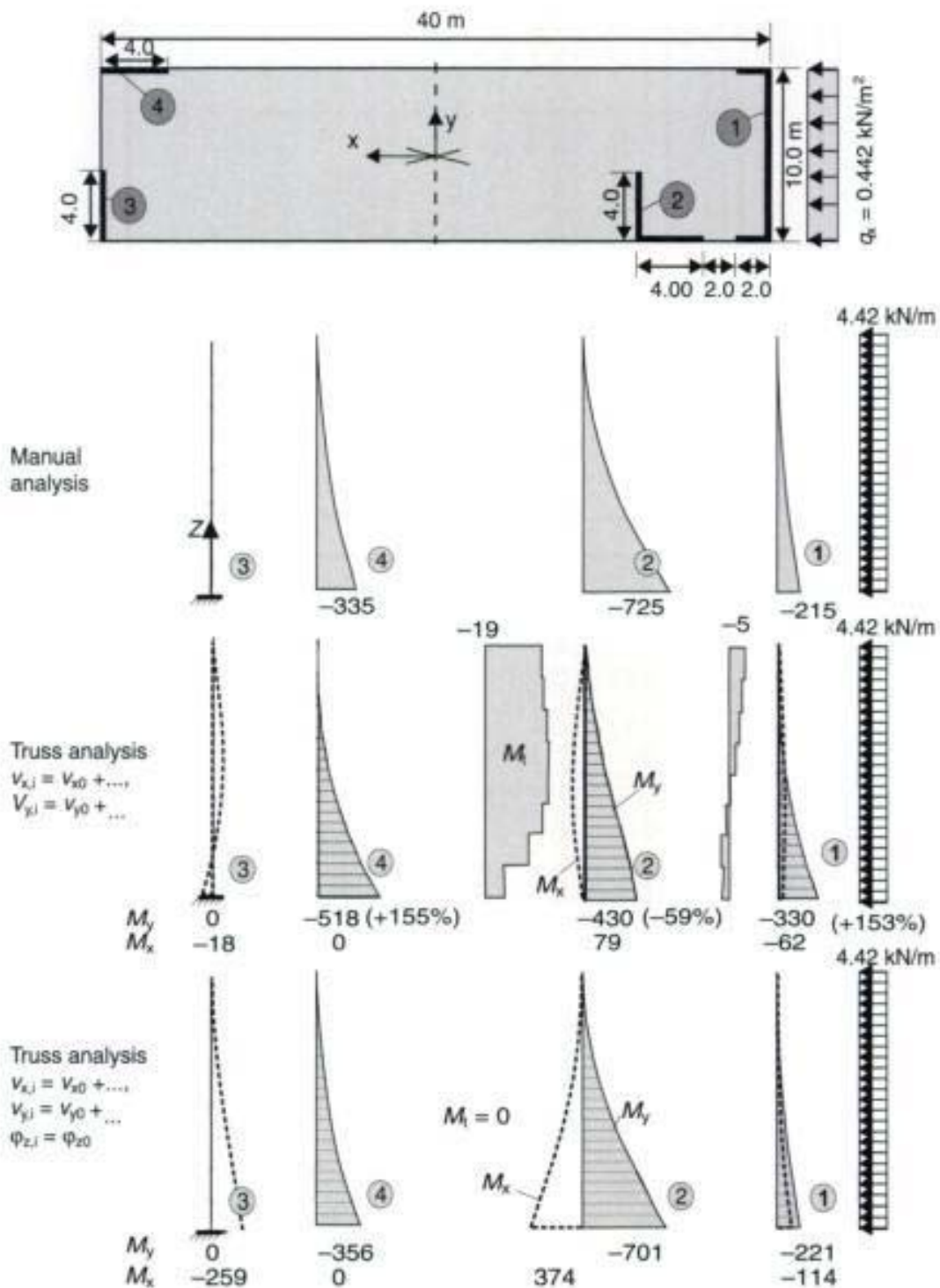


Fig. 2.64 Bending and torsional moments of the bracing elements

These large differences are caused by the torsional moments of element number 2, which results from the distance of the axis of gravity and the axis of torsion (Fig. 2.65). Without coupling the rotation around the vertical axis, the transverse bending moments, M_x , are small. In the case of coupling of the rotation φ_z the torsional

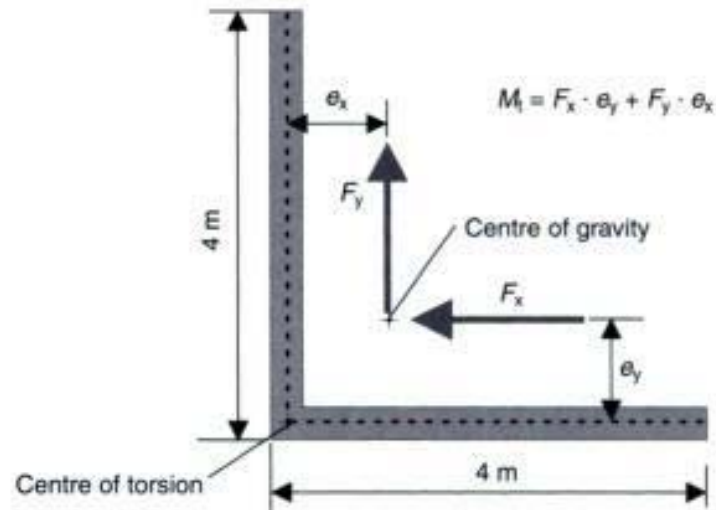


Fig. 2.65 Bracing element number 2

moments of bracing element number 2 are nearly zero. On the other hand, the transverse bending moment, M_x , increases.

The small differences between the results of the equivalent beam method and the numerical truss model are caused by different assumptions for each model. Within the equivalent beam method the bending stiffness of the bracing elements is considered, whereas the torsional stiffness of the individual members is neglected. This simplification is required in order to obtain an easy analytical solution. On the other hand, a numerical calculation will always be based on a linear-elastic material behaviour. An elastic bending *and* a torsional stiffness are used in this example (Stage I – uncracked).

The assumption of a linear-elastic material behaviour should be checked in the case of large bending and torsion loads. As already mentioned in section 2.6.1, it may be necessary to neglect the torsional stiffness GI_T if the section is cracked.

The results of a three-dimensional shell analysis are used to verify the truss models. The whole structure had been modelled with approximately 4410 shell elements (element size 1×1 m) (see Fig. 2.66). The columns are neglected.

Table 2.6 Bending moment M_y at the supports of the bracing elements (in kNm)

Element no.	1	2	3	4
Method of fictitious bars	-215	-725	0	-335
Truss analysis $v_{x,i} = v_{x0}; v_{y,i} = v_{y0}$	-330	-430	0	-518
Truss analysis $v_{x,i} = v_{x0}; v_{y,i} = v_{y0}; \varphi_{z,i} = \varphi_{z0}$	-221	-701	0	-356
Shell analysis	-267	-636	0	-334

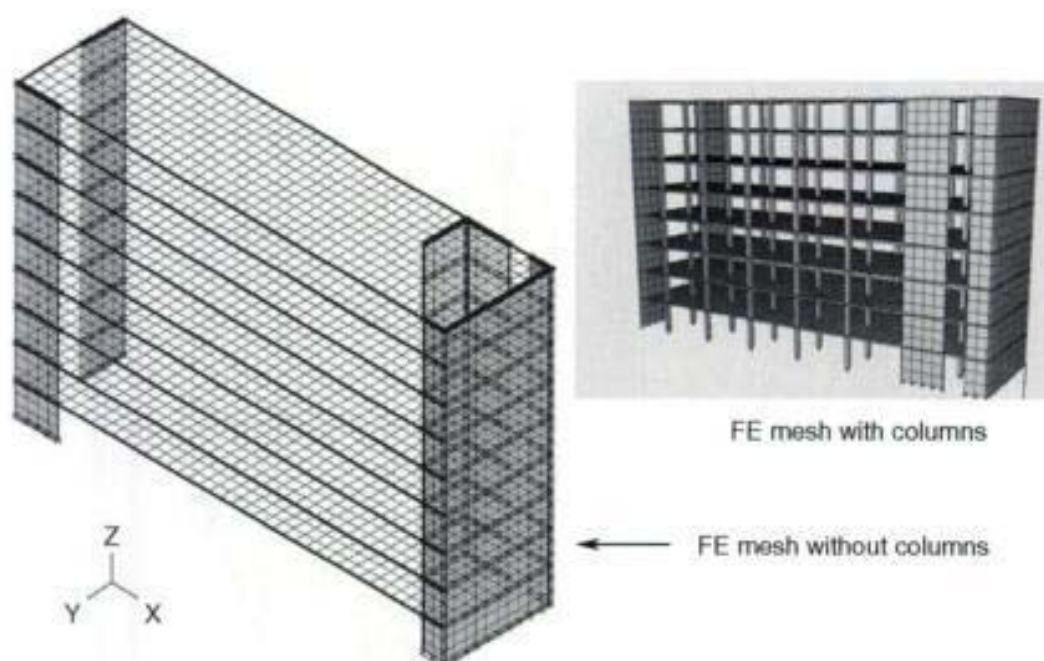


Fig. 2.66 Three-dimensional shell model

Table 2.7 summarizes the main results of the shell analysis. The load on bracing element no. 1 is increased by approximately 30%, and that of element no. 2 is reduced by approximately 13% relative to the values from the equivalent beam method. Overall, there is a relatively good agreement with the results of the simple manual model.

In Fig. 2.67, the deformation of the structure is plotted. The displacements are increased by a factor of 10 000 thus resulting in a big differential deformation of bracing elements numbers 1 and 2.

In reality, the maximum displacements are approximately 1.1 mm in the x-direction and 0.2 mm in the y-direction only (building material C35/40 concrete, linear-elastic material behaviour).

The good agreement in the results of the three different models demonstrates that a considerable effort to calculate the 'correct'

Table 2.7 Support forces of the bracing elements (shell model)

Element no.	1	2	3	4
Support force in x-direction [kN]	39	48	1	28
Support force in y-direction [kN]	7	-12	5	0
Fixed end moment M_x [kNm]	28	-2	-91	0
Fixed end moment M_y [kNm]	-267	-636	0	-334
Fixed end moment M_z [kNm]	132	2	0	1

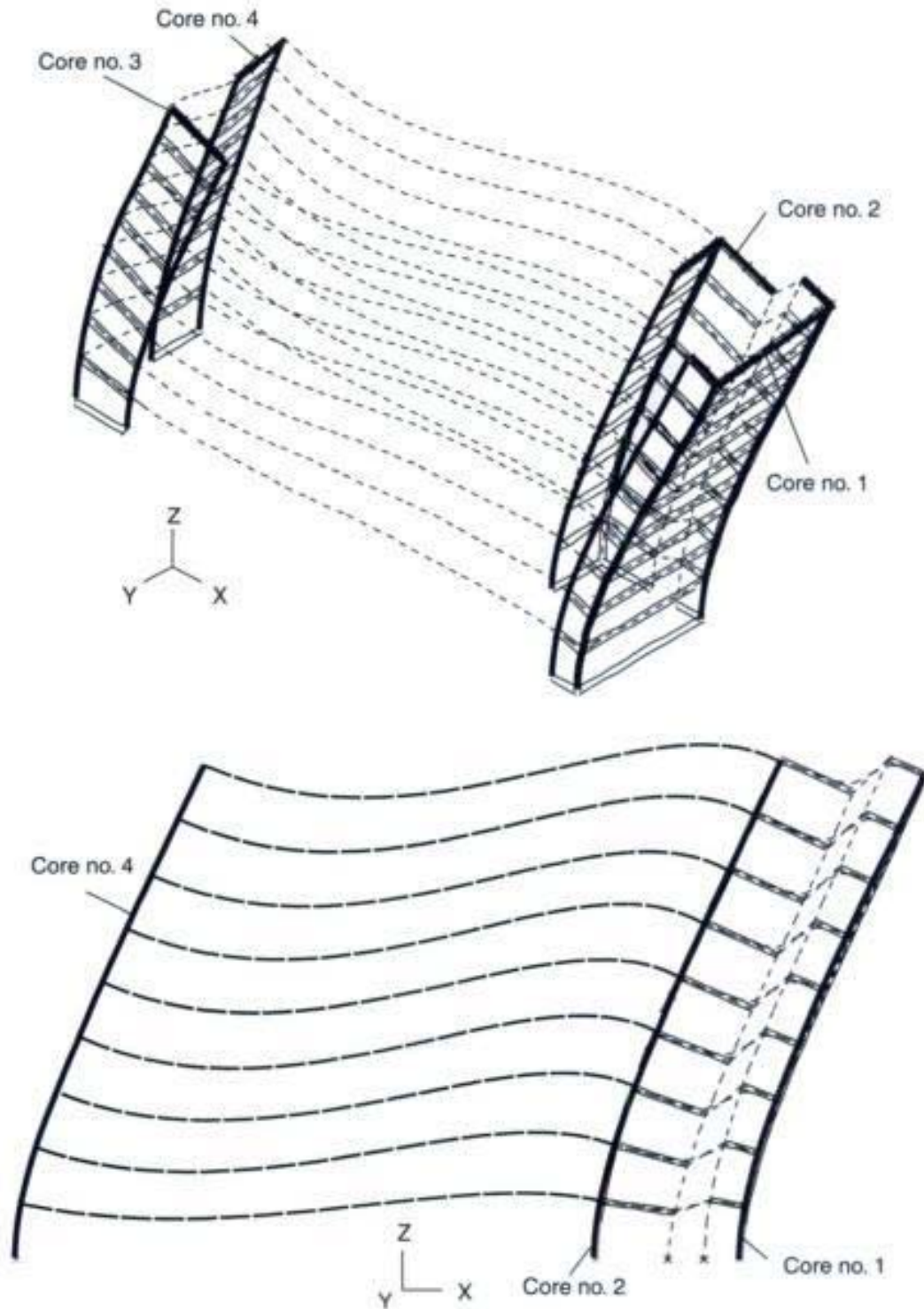


Fig. 2.67 Deformed structure (increased by a factor of 10 000) loaded in the *x*-direction

member forces, for example with a three-dimensional shell model, is generally not required. However, the computer calculation time for the three-dimensional shell model is more than 100 times larger than that for the truss model. More time is needed for the discretization,

the verification of the results, and for summarizing the main output. In addition, a computer program can generally not calculate the correct arrangement of the reinforcement bars for a shell model, as will be demonstrated in Chapter 3. One advantage of a shell model is that not only the bracing elements but also the slabs can be modelled. Thus, the deformation and load bearing behaviour of the structure is modelled with higher accuracy. However, the calculated member forces of the slabs cannot be used for the design, as the columns are neglected and the size of the plate elements is too big.

In Table 2.8 the bending and torsional moments, shear forces at the base of the columns and the deflection and rotation for a uniformly distributed load in the x-direction are listed for different numerical models.

The various analyses of the given bracing system can be summarized as follows:

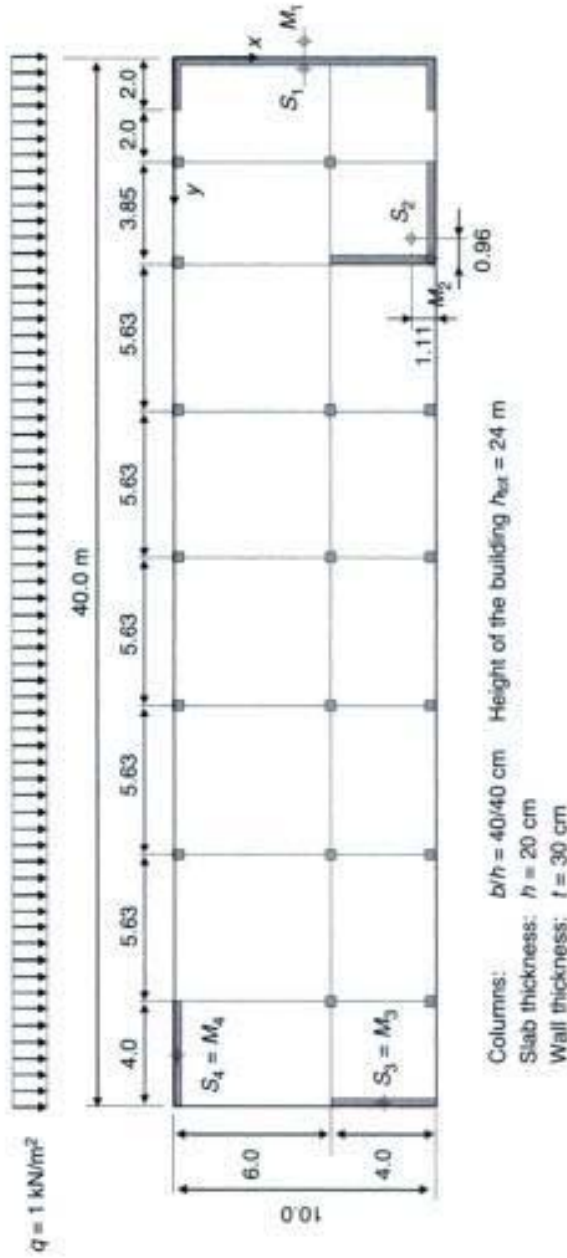
- The calculated bending moments of all truss models are greater than that of the 'real' structure (shell model no. 6).
- There is a significant difference between the member forces of the various truss models and the more realistic shell model no. 6.
- The results are very sensitive to the method of coupling. Rigid coupling with $\varphi_{2,1} = \varphi_{2,0}$ should be used.
- Wrapping torsion can be neglected with regard to the simplifications of the truss model.
- The support reactions are not very sensitive to the location of the beam axis as the global deformation behaviour dominates.

2.6.5 Checking for stability – stability parameter

In addition to the design of the structural elements of a building which can carry the relevant design loads, it is important to note whether the structure is classified as sway or non-sway. In case of a sway system, it is necessary to consider the deformation of the structure when calculating the member forces of all individual elements, including columns (second-order effect). In theory, this can easily be done with an available software. It should be noted that the amount of calculation is increased significantly in such cases, as the superimposition of the various loadings may no longer be valid. Second-order effects may be ignored if they are less than 10% of the corresponding first order effects (EC2, Part 1 [6]).

In the case of a manual analysis, the stability of the structure is checked with the so-called stability parameter α . Only if the parameter

Table 2.8 Support forces and deflections



Models

- 1 Fictitious bar method (manual analysis)
- 2 Truss model – without wrapping torsion – beam axis in centre of gravity
- 3 Truss model – with wrapping torsion – beam axis in centre of torsion
- 4 Truss model – with wrapping torsion – beam axis in centre of gravity
- 5 Shell model without columns
- 6 Shell model with columns

Core no. 1

Model	Shear force V_x in kN	Bending moment M_y in kNm	Torsional moment M_T in kNm	Deflection u_x in mm	Rotation φ_z
1 Fictitious bar method	322	-3869	230	-	-
Truss					
2 No w.t. - centre of gravity*	318/265	-4069/-4357	7/197	0.8/1.9	-0.36/-1.8
3 With w.t. - centre of torsion*	346/404	-4083/-4864	42/302	0.8/1.0	-0.34/-0.57
4 With w.t. - centre of gravity*	352/412	-4233/-5025	42/308	0.8/1.1	-0.35/-0.60
5 Shell model without columns	273	-4102	154	0.7	-0.28
6 Shell model with columns	258	-3789	67	0.6	-0.21

Core no. 2

Model	Shear force V_x in kN	Bending moment M_y in kNm	Torsional moment M_T in kNm	Deflection u_x in mm	Rotation φ_z
1 Fictitious bar method	212	-2543	-204	-	-
Truss					
2 No w.t. - centre of gravity*	182/194	-2447/-1741	3.6/-54	3.1/4.2	-0.36/1.8
3 With w.t. - centre of torsion*	140/46	-2490/-1171	3.0/-24	3.5/4.0	-0.34/1.8
4 With w.t. - centre of gravity*	134/44	-2251/-1029	3.0/-21	3.1/3.5	-0.35/1.5
5 Shell model without columns	246	-2217	5.8	2.6	-0.28
6 Shell model with columns	263	-2168	5.1	2.0	-0.21

Core no. 3

Model	Shear force V_x in kN	Bending moment M_y in kNm	Torsional moment M_T in kNm	Deflection u_x in mm	Rotation φ_z
1 Fictitious bar method	423	-5081	0	-	-
Truss					
2 No w.t. - centre of gravity*	393/433	-4967/-5382	1.8/0	15/16	-0.36/0
3 With w.t. - centre of torsion*	412/448	-4921/-5456	1.4/0	14.3/15.7	-0.34/0
4 With w.t. - centre of gravity*	412/442	-5009/-5436	1.5/0	14.6/15.8	-0.35/0
5 Shell model without columns	386	-4184	1	11.5	-0.27
6 Shell model with columns	380	-3578	0.3	8.8	-0.21

Core no. 4

Model	Shear force V_x in kN	Bending moment M_y in kNm	Torsional moment M_T in kNm	Deflection u_x in mm	Rotation φ_z
1 Fictitious bar method	2.3	-27.3	0	-	-
Truss					
2 No w.t. - centre of gravity*	6.3/7.3	-36/-40	1.8/0	14.4/15.5	-0.36/0
3 With w.t. - centre of torsion*	2.3/2.5	-27/-30	1.4/0	13.7/15.1	-0.34/0
4 with w.t. - centre of gravity*	2.3/2.5	-27/-29	1.5/0	14.0/15.1	-0.35/0
5 Shell model without columns	-4.7	0	-0.1	11	-0.26
6 Shell model with columns	-3.3	0	-0.7	8.4	-0.2

* Rigid coupling, $\varphi_{z,i} = \varphi_{z,j}$ /hinge coupling

becomes greater than the specific value given in the codes, e.g. Eurocode 2.1 [6], a more refined analysis, including second-order effects, is required. The same holds true in the case of an unsymmetric arrangement of various bracing elements.

Stability parameter α

EC 2 A 3.2:

$$\text{for } n \leq 3: \alpha = h_{\text{tot}} \sqrt{(F_v/E_{\text{cm}}I_c)} \leq 0.2 + 0.1n$$

$$\text{for } n \geq 4: \alpha = h_{\text{tot}} \sqrt{(F_v/E_{\text{cm}}I_c)} \leq 0.6$$

where:

n is the number of storeys

h_{tot} is the total height of the building above level of moment restraint

$E_{\text{cm}}I_c$ is the sum of the bending stiffness of all vertical bracing elements, which carry a load in a considered direction. In all bracing elements the maximum tensile stress should be less than $f_{\text{ctk};0.05} = 0.7 f_{\text{cm}} = 0.21 f_{\text{ck}}^{2/3}$ under the relevant serviceability loads.

I_c is the second moment of area of uncracked bracing members

F_v is the total vertical loads in the serviceability limit state ($\gamma_F = 1$)

The stability parameter α depends on the bending stiffness of the bracing system $E_c I_c$, the height of the building h and the total vertical loads F_v . F_v is the maximum load under serviceability condition, including the reduction of the live loads allowed by Eurocode 2. The elastic modulus E_c is given in the codes. Thus, only the moments of inertia I_{cy} and I_{cz} are unknown.

In the case of regular structural systems, the required cross-section parameter is the total sum of the moment of inertia of the individual bracing elements in the relevant direction. In non-regular bracing systems, the equivalent moment of inertia I_c may be estimated by a comparison of the maximum horizontal deformation of a cantilever beam with the results from the truss model loaded by an arbitrary horizontal force (Fig. 2.68).

The calculation can be based on linear-elastic material behaviour, as long as the maximum tensile stress in the concrete is less than $f_{\text{ctk};0.05}/\gamma_c$.

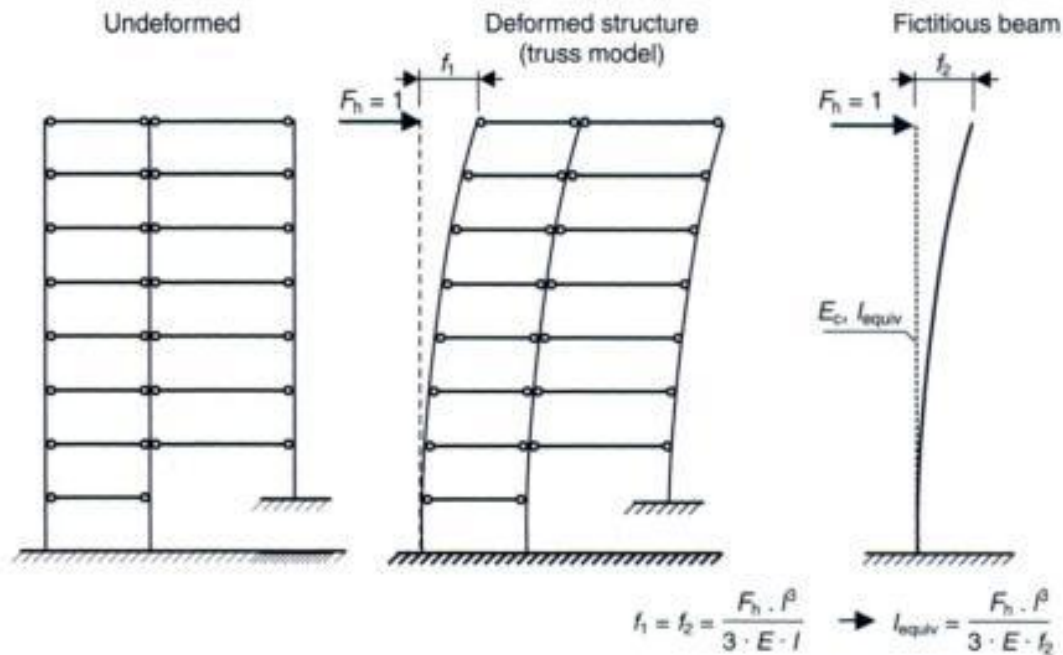


Fig. 2.68 Estimation of the equivalent moment of inertia I_{equiv} of the bracing system

2.7 Design of hollow box girder bridges

The structural analysis of a hollow box girder bridge in the transverse direction has been provided in section 2.1.2. Next, we consider its modelling in the longitudinal direction. In practice, the designs in the transverse and longitudinal directions are made separately. The bridge is modelled as an ordinary beam, having a rigid cross-section with no distortions due to either bending or shear (Fig. 2.69). This model is used to estimate the longitudinal, shear and torsion reinforcements, the relevant support forces, the stresses, and the deflections of the bridge.

The torsional moments are estimated by assuming two bearings located at one support axis. In such a case it is recommended that each bearing be considered separately in the numerical model, including the transverse spacing between them as well as their distance from the centre of gravity of the beam. This results in a three-dimensional numerical model instead of a plane grillage system. The additional work is justified in this case, as the greatest components of forces in each bearing are needed and not only the maximum total support reactions. As an alternative, the rotation around the longitudinal axis may be restrained, however this requires manual calculation of the relevant bearing forces from the vertical load and the torsional moments. A three-dimensional model is also required for the case of a superstructure which has an unsymmetric cross-section.

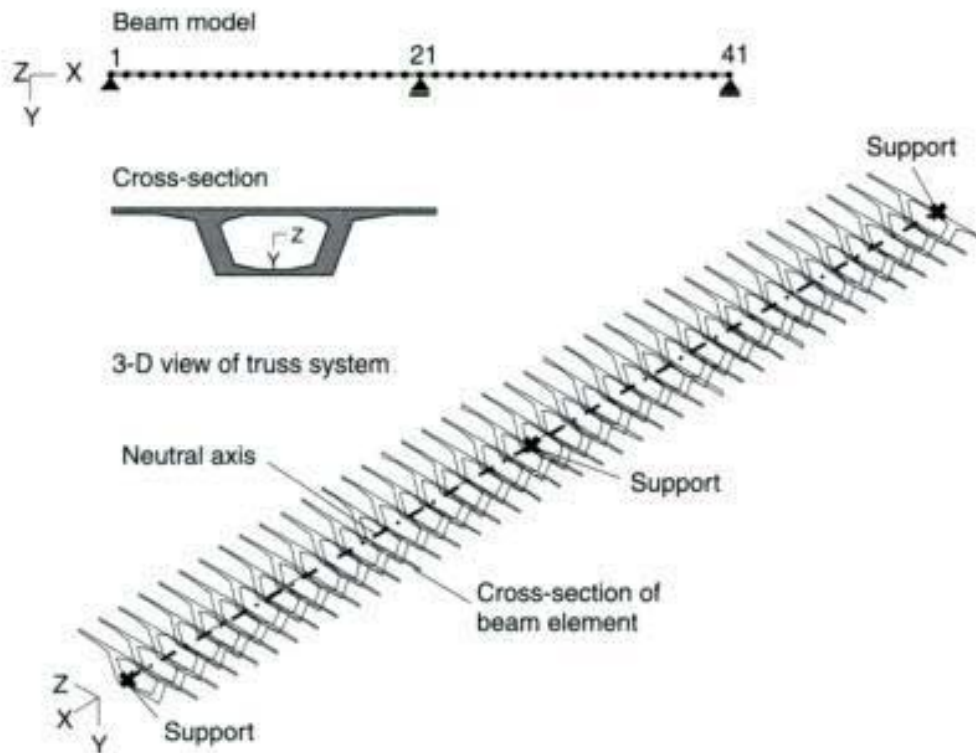


Fig. 2.69 Numerical model of a two-span hollow box girder bridge

The diaphragms at the support axis are modelled by stiff beam elements, or more efficiently, by coupling of the nodes at the support. As an alternative, torsional restraint at the supports can be considered.

Various different load cases have to be considered in the design of a bridge structure. They then have to be combined in the most unfavourable manner. The relevant positioning of the traffic loads, e.g. axle loads, can be considered in two different ways. First one can 'drive' the traffic loads by the computer over the bridge in all different lanes. This results in an enormous number of load cases and a major computational effort. In addition one has to know in advance which parts of the structure should be loaded to get the greatest member forces (see Fig. 2.70). Therefore, numerical integration of influence lines for each node and each force can be used as a reasonable alternative (Fig. 2.70).

Influence line for

- bending moment – deflection curve caused by a rotation of $\Delta\varphi = 1$;
- shear force – deflection curve caused by a deformation jump of $\Delta w = 1$.

The beam model is based on a rigid cross-section (Figs 2.71 and 2.72). Distortions caused by unsymmetrical actions have to be considered

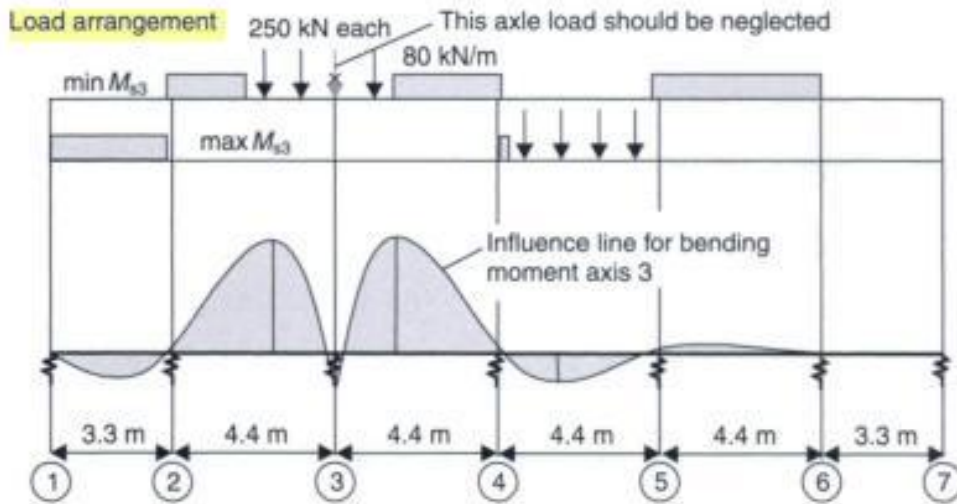


Fig. 2.70 Load arrangement by means of an influence line (train load UIC 71) max./min. bending moment at axis 3

separately by means of a frame system. This system may be supported either in the vertical direction or in the direction of the webs (see section 2.1.2). For this model the relevant member forces in the webs and in transverse direction are estimated for a longitudinal uniformly distributed load.

The displacements may be considered approximately by analysing the equivalent forces in an elastically supported frame system.

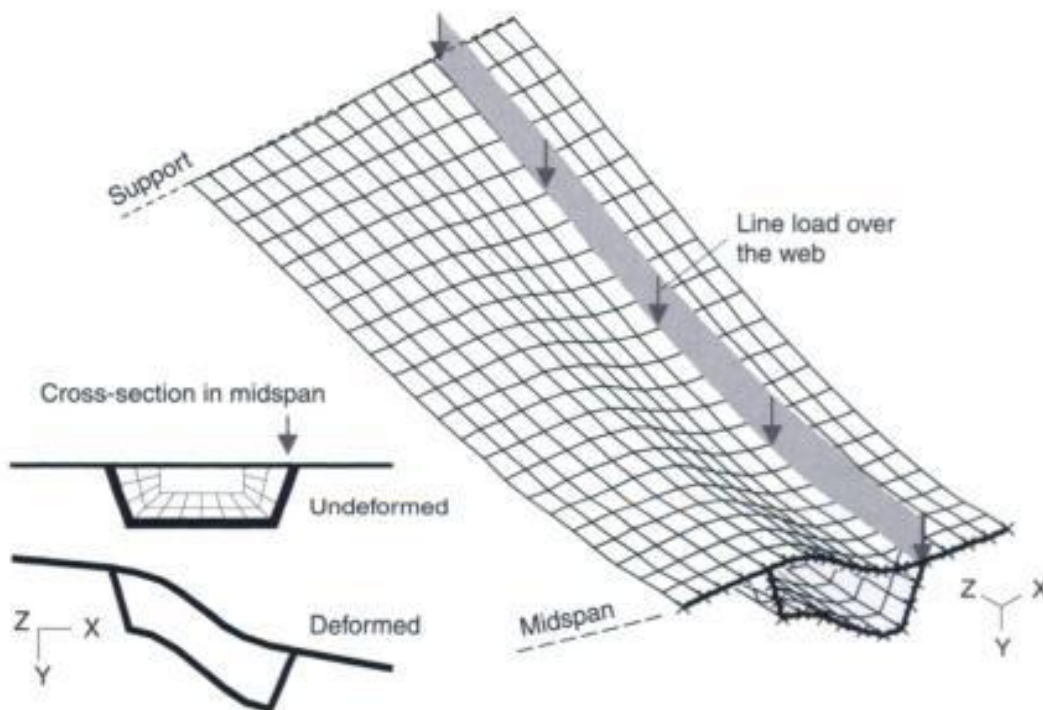


Fig. 2.71 3-D shell model of a hollow box girder bridge (only one half of the structure is shown)

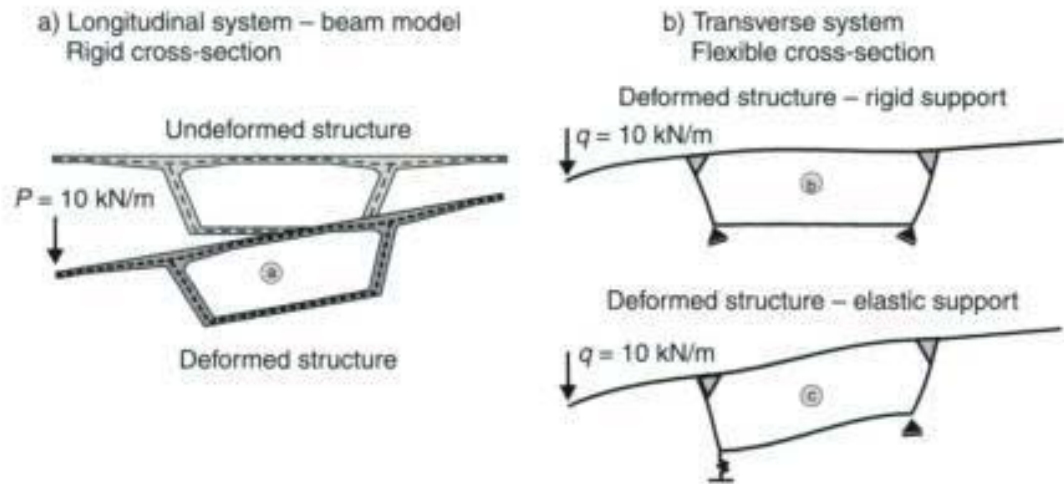


Fig. 2.72 Distortion of a hollow box girder bridge at midspan; beam model (left) and real deformations (right, bottom)

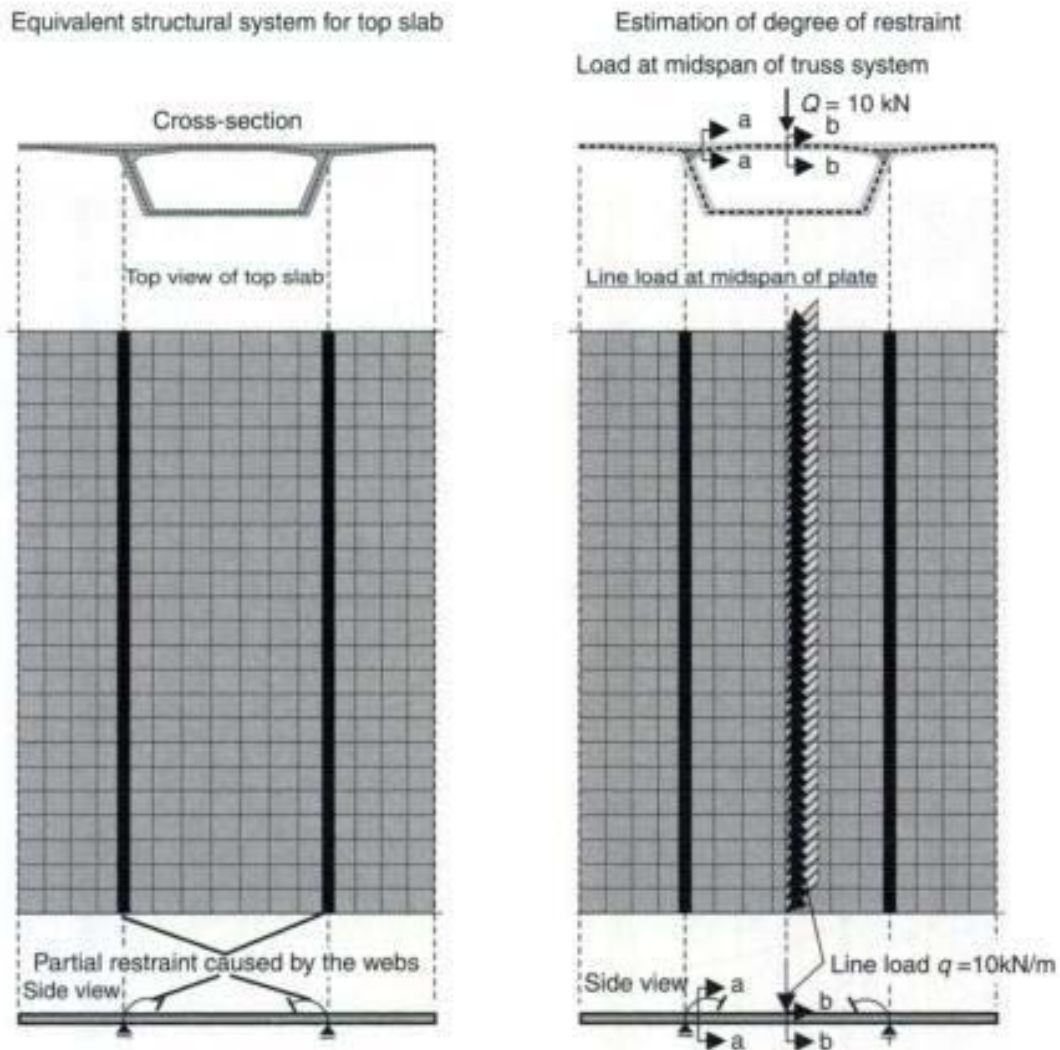


Fig. 2.73 Simplified equivalent system for a deck slab

A slab system may be used to calculate the bending moments and the shear forces caused by single forces (e.g. wheel loads) and non-symmetric loads on the top slab (see section 4.11.3). This slab is partially restrained at the webs (see Fig. 2.73). The stiffness of the equivalent bending springs can be estimated by comparison of the bending moment of a beam and a plate structure under a uniform line load. As an alternative, bending moments can be estimated from charts, such as those of Homberg (influence lines) [19,20]. Sometimes an interpolation of the values of different support conditions (fully or partially restraint at the web supports) and the location of the single loads is required. However, such an analysis may be more time-consuming than an FE analysis. Further information on plate structures is given in Chapter 4.

2.8 Truss system – design of T-beam bridges

Until recently the capabilities of personal computers and the software available were not able to compute a plate or a 3-D shell system by means of the Finite Element Method. Until then two-dimensional truss systems, e.g. grillage, were used. One of the best known examples for this idealization of a three-dimensional shell structure is the Opera House in Sydney, Australia. At the time of construction it was not possible to design the roof as a thin unstiffened shell. Therefore, a truss system was used instead of a more elegant spatial structure.

This idealization is still widely used, e.g. in prestressed T-beam bridges. For such structures the results of a 2-D plate or 3-D shell analysis (see Fig. 2.71) may be 'nice looking' but are generally of little use for a design where the resulting member forces are required rather than the accurate stresses. Also a considerable amount of computation time is needed in order to consider all the relevant load cases.

An example of a T-beam bridge is shown in Fig. 2.74. This structure has been constructed by prefabricated T-beams with an additional cast-in-situ concrete top slab. However, before we consider the modelling of real structures, we will examine the essential special features of a grillage system for a simply supported rectangular slab.

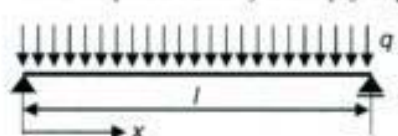
2.8.1 Design of a rectangular solid slab

The internal forces of a rectangular simply supported concrete slab can be determined from tables or by means of a spatial FE analysis. These methods can be used to check the results of a grillage system.

The solid 2-way slab is represented by a 2-D grillage system where the longitudinal and transverse beams are connected at the nodes. The loading is always perpendicular to the midplane of the system. The following example only considers uniform loading.

After the discretization of the structure, one has to determine the equivalent vertical line loads on the beams in both directions. This can be done by assuming that the displacement of the beams at the nodes, where they are connected together, should be the same (Fig. 2.75). For midspan of a simply supported beam structure under uniformly distributed loading q ($q = q_1 + q_2 = \text{total load}$) this results in:

max. displacement of a simply supported beam under uniform loading:



$$w(x) = \frac{q \cdot l^4}{24 \cdot E_c \cdot I_c} \cdot \left(\frac{x}{l} - 2 \cdot \left[\frac{x}{l} \right]^3 + \left[\frac{x}{l} \right]^4 \right)$$

<p>System A ($x/l = 0.5$) – midspan (Fig. 2.75 left)</p> $f_1 = \frac{5}{384} \cdot \frac{q_1 \cdot l_1^4}{E_c \cdot I_c}$ $f_2 = \frac{5}{384} \cdot \frac{q_2 \cdot l_2^4}{E_c \cdot I_c}$	<p>System B ($x/l = 0.1$) – near support (Fig. 2.75 right)</p> $f_1 = \frac{5}{384} \cdot \frac{q_1 \cdot l_1^4}{E_c \cdot I_c}$ $f_2(x = 0.1l_2) \approx 0.0041 \cdot \frac{q_2 \cdot l_2^4}{E_c \cdot I_c}$
-------------------------------------------------------------------------------------------------------------------------------------------------------------------------------------------------------------	------------------------------------------------------------------------------------------------------------------------------------------------------------------------------------------------------------------------------

with $E_c I_c = \text{constant}$ and $f_1 = f_2$ this results in:

$q_1 \cdot l_1^4 = q_2 \cdot l_2^4$	$q_1 \cdot l_1^4 = 0.3139 \cdot q_2 \cdot l_2^4$
-------------------------------------	--------------------------------------------------

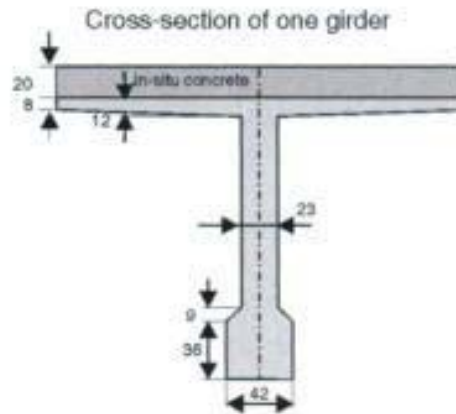
with $q = q_1 + q_2$ it follows:

$q_1 = q \cdot \frac{l_2^4}{l_1^4 + l_2^4}$	$q_1 = q \cdot \frac{l_2^4}{3.186 \cdot l_1^4 + l_2^4}$
$q_2 = q \cdot \frac{l_1^4}{l_1^4 + l_2^4}$	$q_2 = q \cdot \frac{l_1^4}{l_1^4 + 0.3139 \cdot l_2^4}$

with $l_1 = l_2$

$q_1 = q_2 = 0.5 \cdot q$	$q_1 = 0.24 \cdot q; \quad q_2 = 0.76 \cdot q$
---------------------------	------------------------------------------------

However, this load distribution only applies to one location. It follows from the deflected condition (see the right-hand side of Fig. 2.75), as well as the previous calculations that the equivalent load on the beams decreases from midspan to the supports respectively in the direction of the shorter span length. This non-uniformity is usually neglected in the analysis of a grillage system.



Cross-section of a standard span

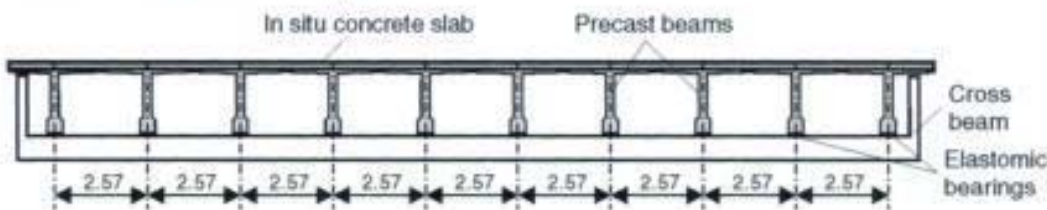


Fig. 2.74 Don Muang Tollway, Bangkok [22]

The accuracy of the calculation usually increases with the number of trusses in both directions. In the following example the influence of the number of beams on the member forces and the displacements of a simply supported rectangular slab with a aspect ratio of $l_x/l_y = 1.5$ is examined. The structure is loaded by a uniformly distributed load of $q = 10 \text{ kN/m}^2$.

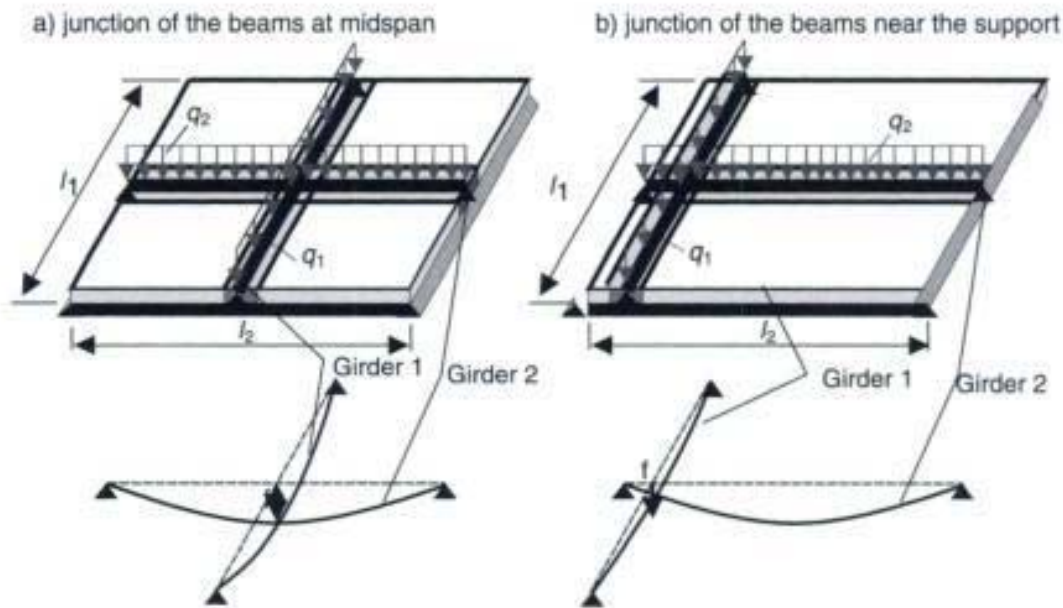


Fig. 2.75 Load distribution for a grillage system

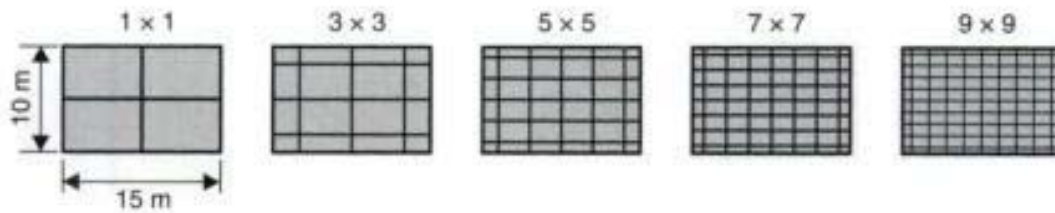


Fig. 2.76 Grillage systems used in the analysis

For the purpose of comparison, the displacement at midspan and the relevant bending moments in both directions are calculated either by tables or by a two-dimensional FEM (shell).

Czerny [11] gives the following values (concrete grade C30/35, slab thickness $h = 30$ cm):

$$m_{x_{\text{m}}} = 73.0 \text{ kNm/m}; \quad m_{y_{\text{max}}} = 28.8 \text{ kNm/m}; \quad f = 10.8 \text{ mm}.$$

Figure 2.77 shows the bending moments, the shear force and the displacements of the grillage system with three girders in each direction. As would be expected, the load is mainly transferred in the direction of the shorter span. The bending moment and shear force distribution show some jumps, which are caused by the pointwise connection of the beam elements.

The convergence of the grillage model is shown in Fig. 2.78. Here the ratio of the results of the grillage system to that of the slab are given for an increasing number of beams in both directions.

A system with one beam in both direction results in 43% ($m_{x_{\text{m}}}$) resp. 61% ($m_{y_{\text{m}}}$) greater bending moments compared to the slab. This large error can be traced back to the fact that the two-dimensional spatial load dispersion of a solid slab is not modelled. Even for this simple system at least 7×7 beams are required in order to achieve a sufficient accuracy in the member forces. Figure 2.78 shows that with more than 9×9 beams, the calculated results are lower than the correct values (factor < 1.0) which may lead to an unsafe design.

By means of a truss system the forces in members can be calculated for slabs with reduced twisting stiffness or orthotropic slabs. Slabs which have a reduced twisting stiffness can only carry the loads in two orthogonal directions. The twisting bending moment m_{xy} cannot be sustained in the edges where two simple line supports meet. Some examples of systems with reduced twisting stiffness are:

- precast concrete slabs without additional cast-in-situ concrete cover, if a joint is located closer than $0.3l$ from the corners;
- slabs having large openings in the region of the corners;
- slabs, where the corners are not restraint against uplifting.

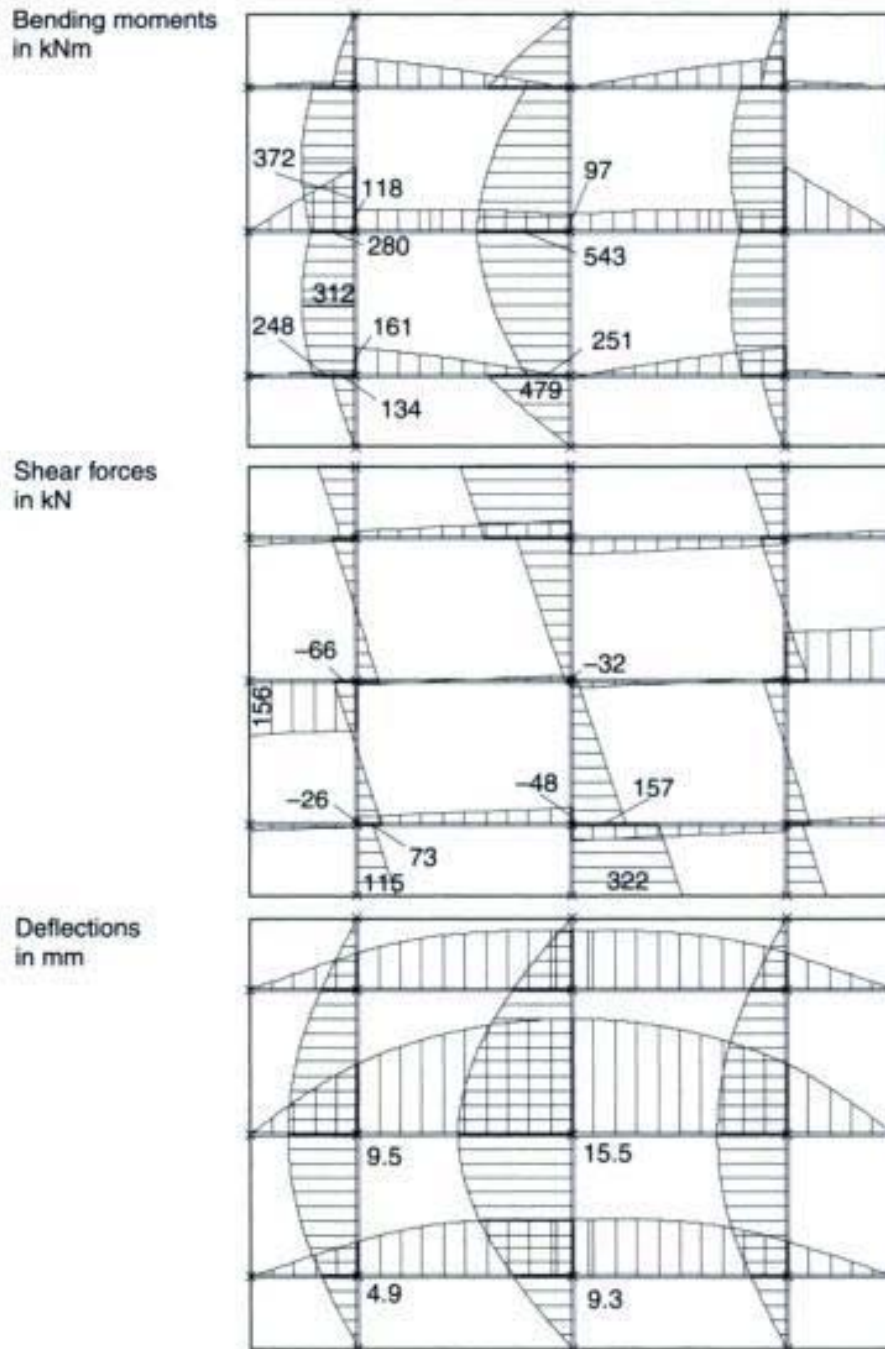


Fig. 2.77 Bending moments, shear forces and displacements of the beams (3×3 division)

The reduction of twisting stiffness in the girder model is considered by reducing the torsional stiffness of the beam elements. Figure 2.79 shows the results for the extreme value $I_T = 0$ in relation to that of the elastic value I_T for an increasing number of beams in each direction. The bending moments at midspan increase to more than 80% if the torsional stiffness is neglected. This factor is significantly higher than

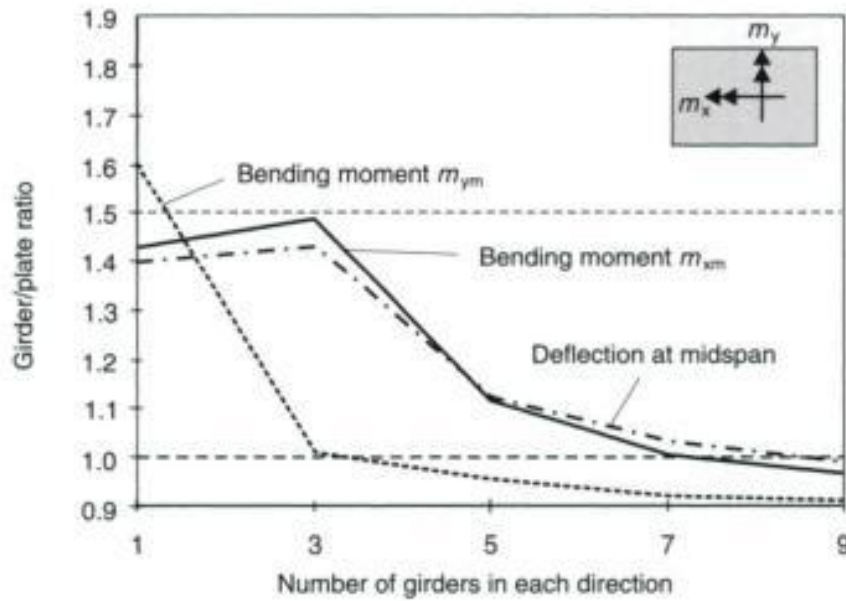


Fig. 2.78 Comparison of the results of a grillage with increasing number of beams with the plate values

the value given in *Heft 240* of the German Concrete Association [10]. According to this publication, the bending moments of an isotropic slab should be increased by only 26% (aspect ratio of the slab 1:1.5) if the real system has a reduced twisting stiffness. This big differences between the calculated values for $I_T = 0$ and that of *Heft 240* [10] can be traced back to the fact that the latter one assumes a reduction and not a complete loss of the twisting stiffness.

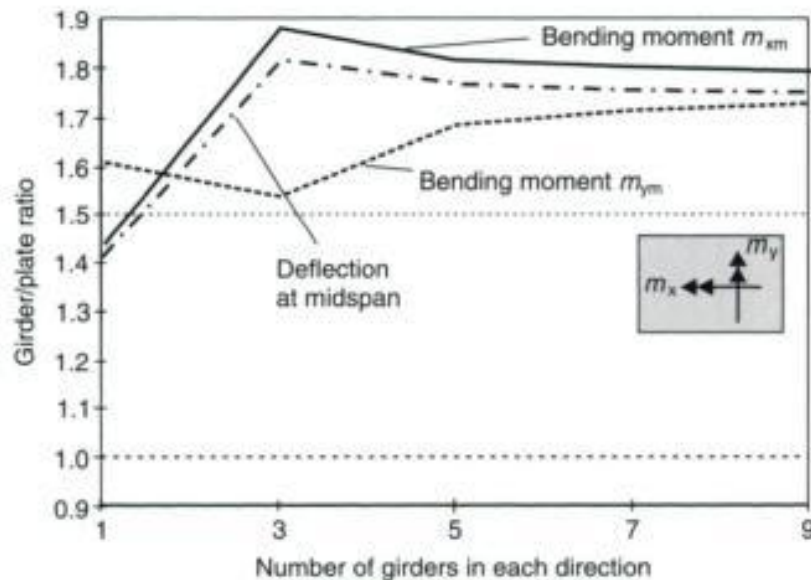


Fig. 2.79 Comparison of the bending moments and displacement at midspan with the plate values (stiffness against twisting moments) for an increasing number of beams in both directions with $I_T = 0$

2.8.2 Double T-beam bridge

Different numerical models can be used for T-beams and ribbed slabs. These will be discussed in detail in Chapter 5. In the following, only the modelling of a double T-beam by means of a grillage is shown. As mentioned earlier, truss systems are still applicable as, for example, the dimensioning of prestressed beams is much more complicated if a shell model is used. Furthermore, the computational effort for truss systems is considerably less than a folded slab analysis.

The procedure for a girder calculation is demonstrated for the double T-beam bridge shown in Figs 2.80 and 2.81. The numerical model is shown in Fig. 2.82. The longitudinal girders are represented by straight beam elements. Their axis is located in the centre of gravity of the T-cross-section. Where the longitudinal girders have an unsymmetrical cross-section, which is very often the case for the outer girders (see Fig. 2.81), the principal axis is not purely in the vertical and horizontal direction. This results in a 2-axial bending for the beam, which can only be considered by a three-dimensional numerical model. In order to avoid this additional effort, the inclination of the principal axes is generally neglected. This simplification is justified since, in most cases, the effect of the inclination of the main axis on the member forces and moments is very small. Furthermore, the shear centre is placed in the centre of gravity of the cross-section. The effective width of the flanges has to eventually be taken into account. With these simplifications, the structural analysis of the bridge by using a flat truss system (grillage) is possible.

For simplicity, a pin support in the centre of gravity of the main girders and a restraint against torsion caused by the cross beams and

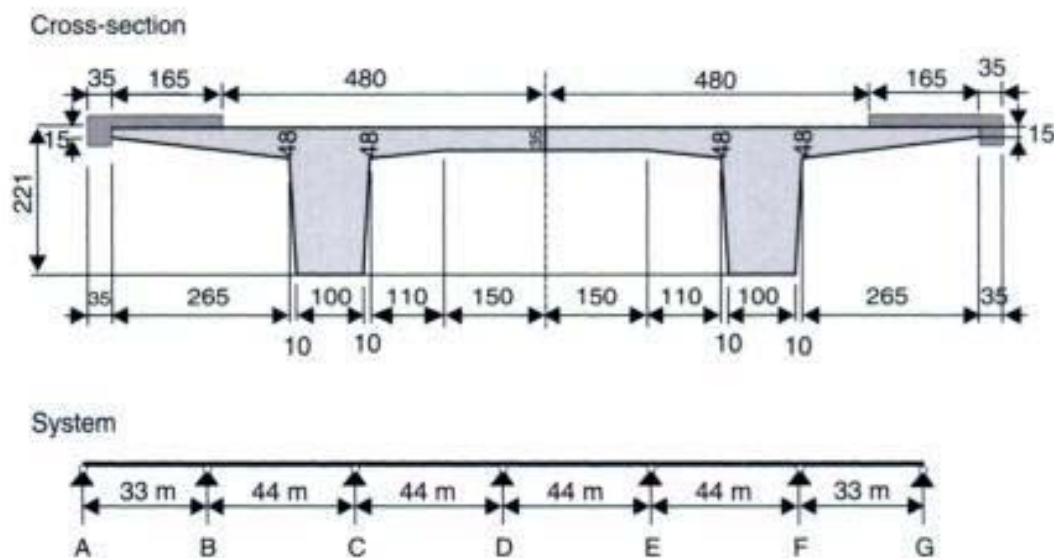


Fig. 2.80 Double T-beam bridge

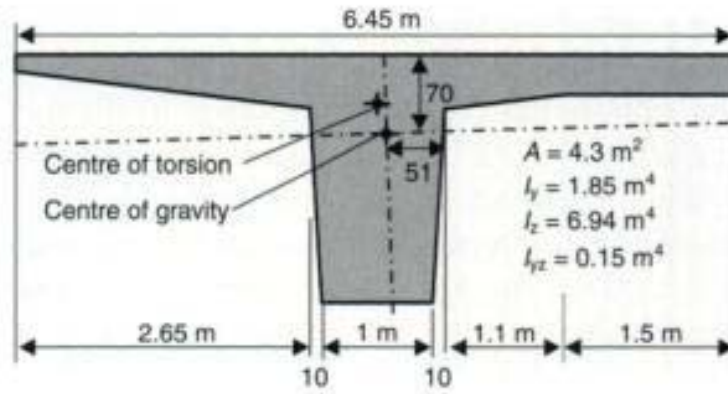


Fig. 2.81 Cross-section of one girder

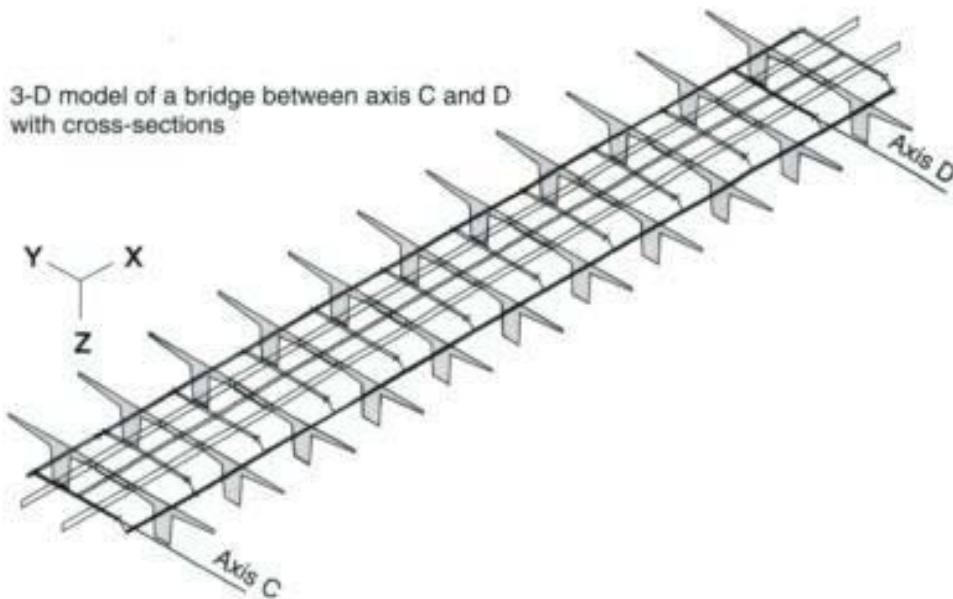
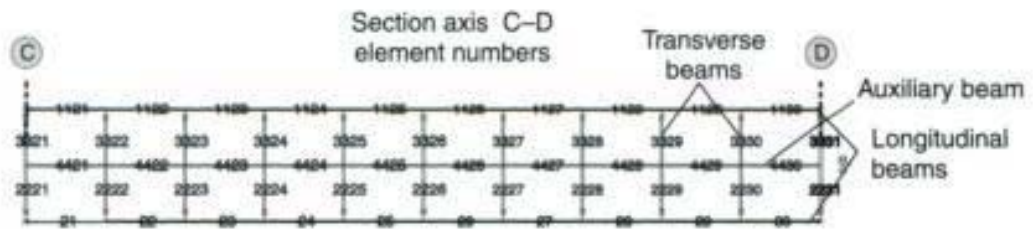
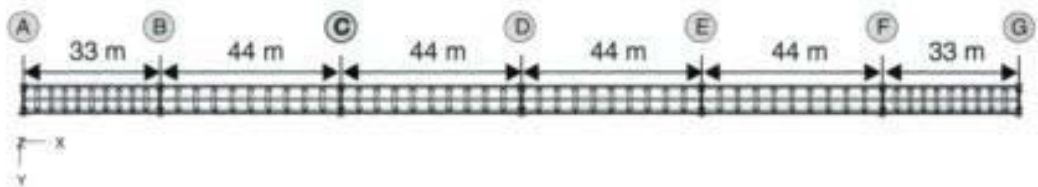


Fig. 2.82 Numerical model of a double T-beam bridge

the two separate bearings in each axis at the supports are assumed in the system shown in Fig. 2.82. Therefore, the distance between the bearings and the distance of the support level to the centre of gravity has to be considered when estimating the relevant bearing forces.

While the discretization of the longitudinal girders creates no difficulties, detailed investigations are required for correct and realistic modelling of the transverse load-bearing behaviour of the bridge. This includes the vertical location of the equivalent 'fictitious' transverse beams, their connection with the longitudinal main girders and their bending stiffness.

2.8.2.1 Location of the beams in transverse direction

The transverse girders can either be arranged in the centre of gravity (model A) or at the height of the deck (model B) (Figs 2.83 and 2.84). The main difference between these alternatives is that model B requires a three-dimensional truss model. The effect of the discretization on the member forces will be discussed in section 2.8.2.4 by a special example.

In the case of torsion, the longitudinal girders rotate around their centre of torsion, which in the case of a symmetric T-beam is located at the

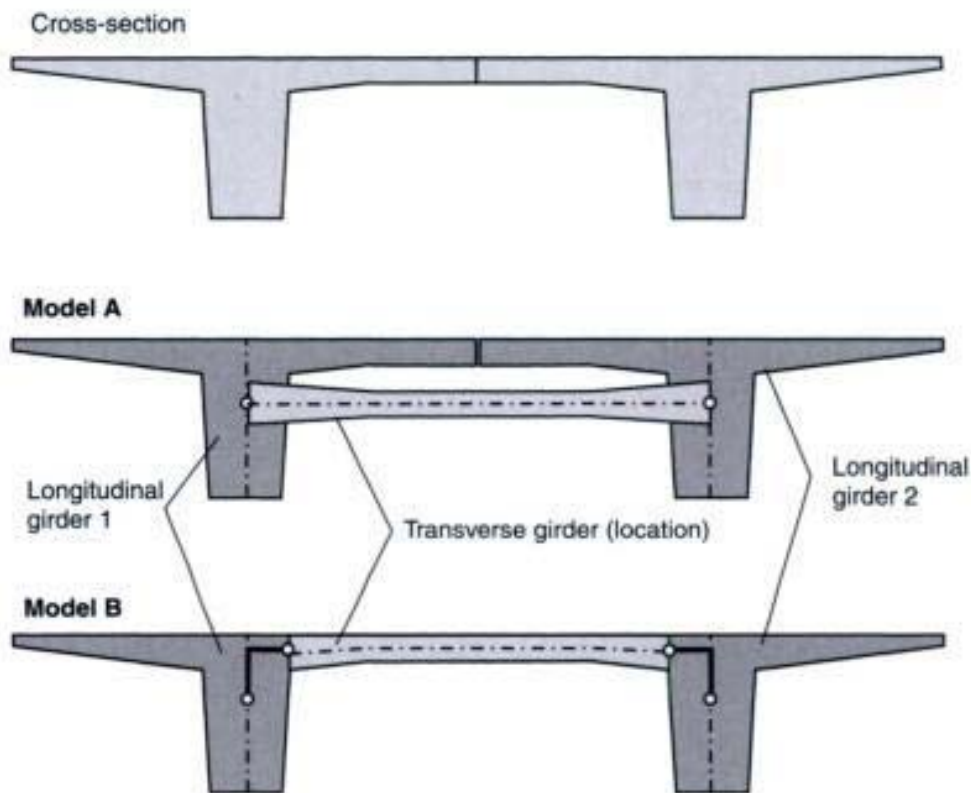
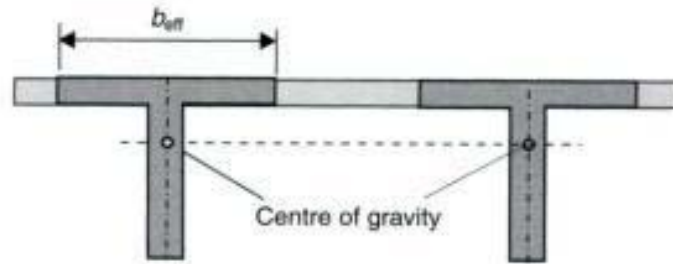


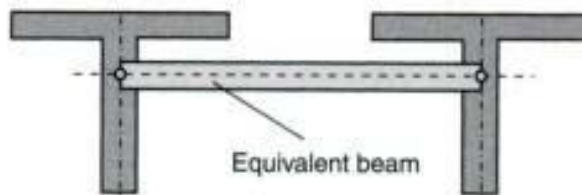
Fig. 2.83 Location of the transverse beams

Real system – cross-sections

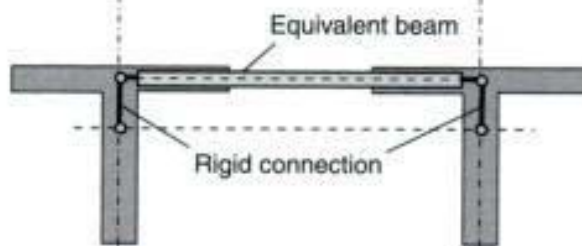


Truss system

a) Transverse beam in centre of gravity of longitudinal girder



b) Transverse beam in the centreline of the deck slab



Grillage – plan view

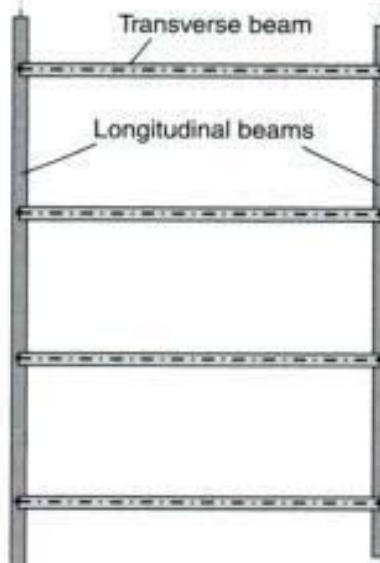


Fig. 2.84 Two different models for a double T-beam bridge

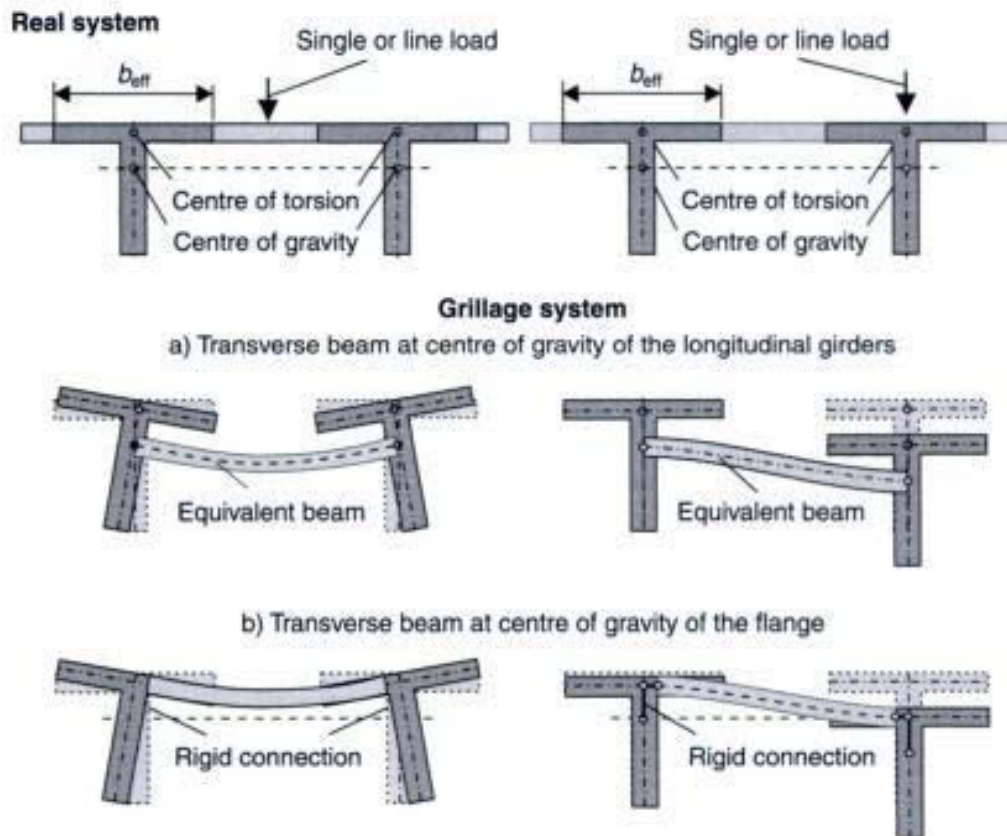


Fig. 2.85 Deformation of the longitudinal and transverse beams under constant line loading

junction of the centreline of the flange and the web. It follows from this that a load on the flanges results in tension forces in model A and compression forces in model B in the transverse beams (Fig. 2.85). However, since the torsional stiffness and thus the restraint against rotation of a T-beam is small, the difference between the two models can usually be neglected. It should be noted that in the case of model B the end forces of the transverse beams are introduced into the T-beam eccentrically which results in torsional moments in the longitudinal girder.

2.8.2.2 Number of transverse beams

The number of transverse beams, hence their distance from each other, influences the load distribution in the transverse direction of the bridge deck. Therefore, the spacing of the transverse beams should not be too great. This is of special importance in the case of concentrated loads (e.g. truck loads on a deck). A point load on a slab will always disperse in two directions, whereas a beam can only transfer the load in the direction of its axis. In such a case, it is recommended to design the bridge in the transverse direction with another system, e.g. a slab,

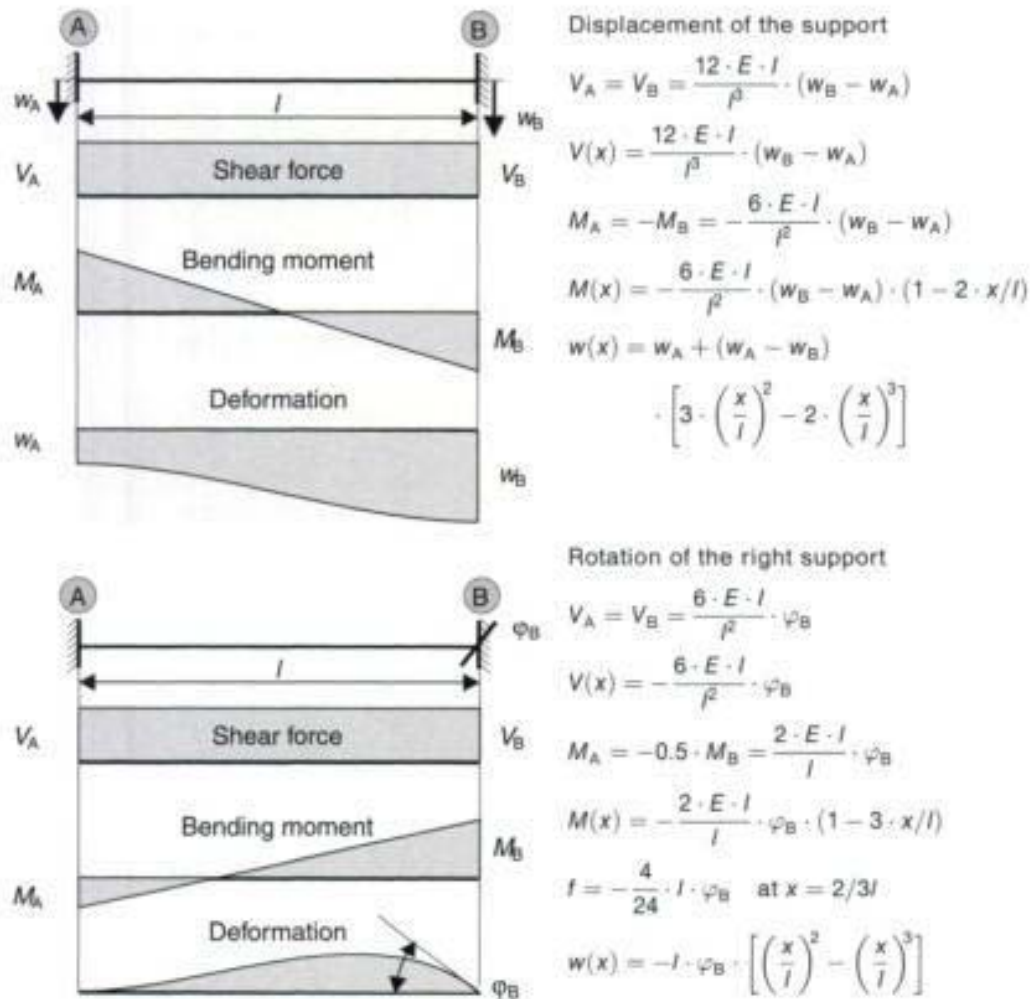


Fig. 2.86 Member forces and deflections of a fully restrained beam due to vertical displacement or rotation of one support

modelled by 2-D plate elements. This has already been explained for a hollow box girder bridge (see Fig. 2.73). Thus, to improve the load transfer in the longitudinal direction, it may be useful to add additional (fictitious) beams in the longitudinal direction.

2.8.2.3 Section properties of the transverse beams

The stiffness of the transverse beams should be the same as that of the real slab. Due to the considerable stiffness of the longitudinal girders it is assumed that the transverse beams are fully restrained by the longitudinal beams. If the transverse beam is located on the axis of gravity of the T-beams (model A), its span length is longer than in reality ($l_{\text{beam}} = l_n + b_w$) (Fig. 2.85). Therefore, the cross-section height has to be modified to get the same stiffness as the real slab.

This can be done by comparing the angle of rotation or the vertical support force of a fully restraint single span beam (Fig. 2.87). The relevant deformation case depends on the stiffness of the total system. If the longitudinal girders mainly deflect in the vertical direction under external loading, the support displacement Δw has to be used. In

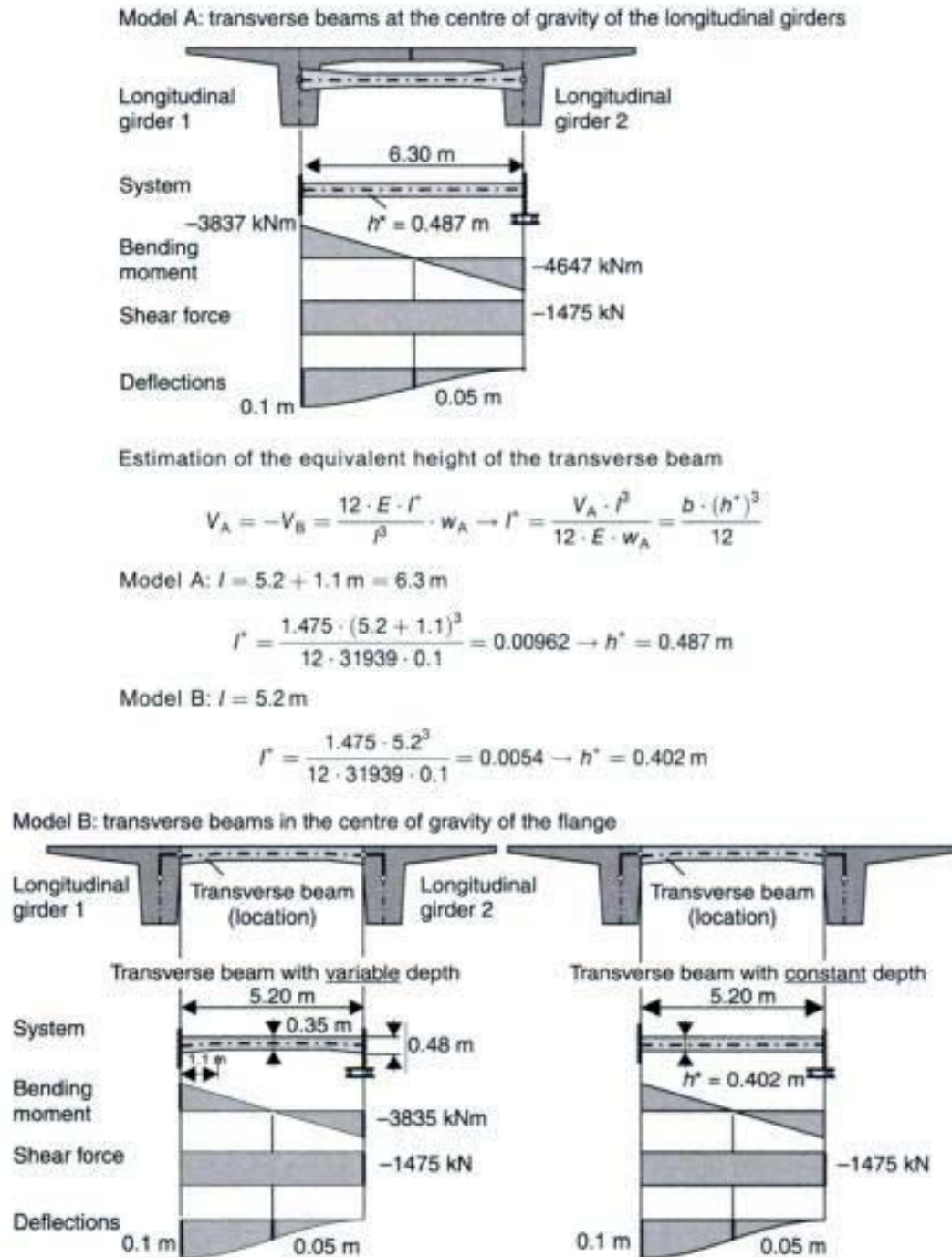


Fig. 2.87 Forces in members and displacements of the equivalent structural systems due to a displacement of the supports of $w = 0.10 \text{ m}$

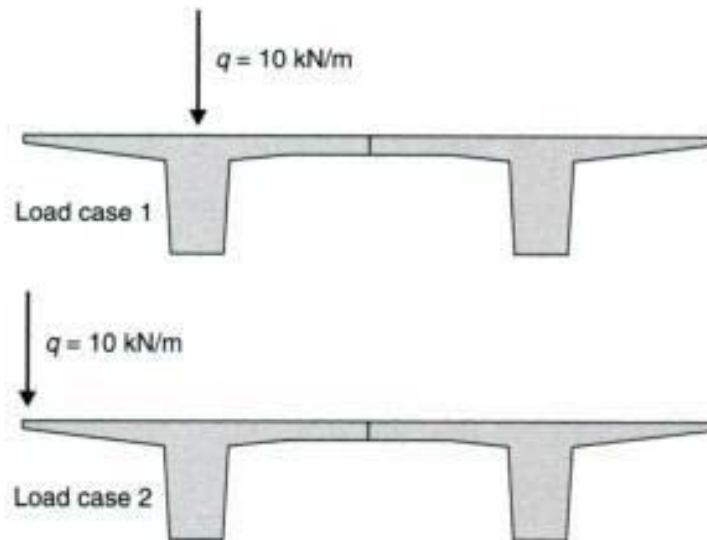


Fig. 2.88 Load cases

such a case the shear force at the support is:

$$V_A = V_B = \frac{12 \cdot E_c \cdot I}{l^3} \Delta w$$

Thus, the equivalent moment of inertia is proportional to the span length powered by a factor of 3.

If the bending behaviour of the deck slab is the dominant feature, i.e. the longitudinal girders rotate under external loading, the unit rotation of the support $\Delta\varphi$ has to apply. In this case the equivalent moment of inertia is proportional to the span length powered by a factor of 2.

$$V_A = V_B = \frac{6 \cdot E_c \cdot I}{l^2} \Delta\varphi$$

In the case of inclined haunches, as in the chosen example, the support forces due to the unit displacement $\Delta w = 1$ and the unit rotation $\Delta\varphi = 1$ may be estimated numerically by a plane truss system. As the bending moments are independent from the bending stiffness of the equivalent system (support bending moment of a fully restraint beam under uniformly distributed load $M = -ql^2/12$), model A would result in correct shear forces but with incorrect bending moments (Fig. 2.87). Therefore, in such cases the model B is recommended as the member forces in the longitudinal and transverse girders are needed for design.

2.8.2.4 Comparison of both models

Figures 2.89 and 2.90 show the member forces and deflection of the inner span of double T-beam bridge shown in Fig. 2.80 for both

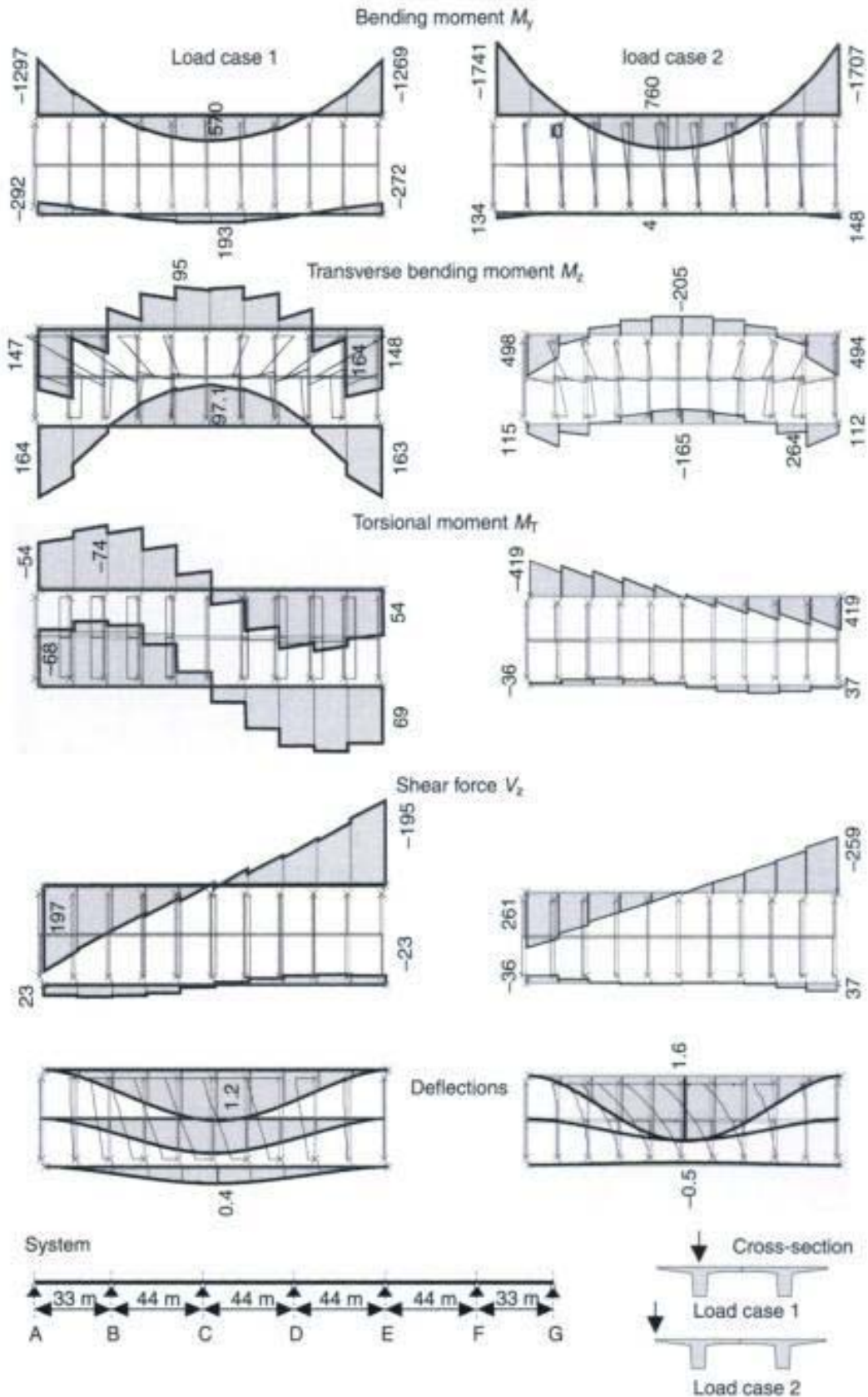


Fig. 2.89 Member forces and deflections of span C-D – three-dimensional truss system

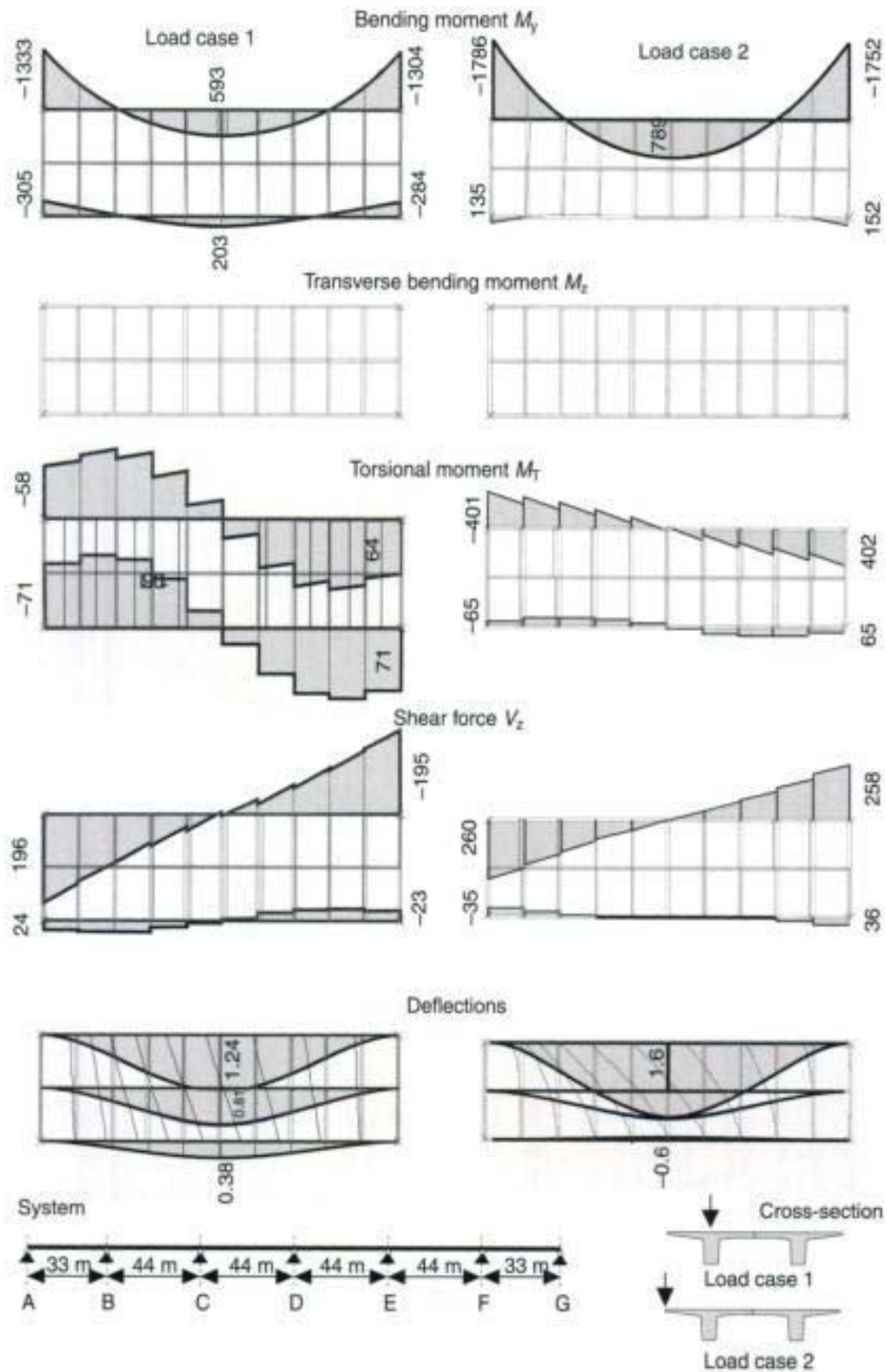


Fig. 2.90 Member forces and deflections of span C-D – two-dimensional truss system

Table 2.9 Forces in members and displacements of the relevant sections

		Load case 1		Load case 2	
		Plane	3-D System	Plane	3-D System
Support axis	bending moment M_y	-1333/-305	-1297/-292	-1786/135	-1741/134
	bending moment M_z	0/0	147/164	0/0	498/115
	torsional moment M_T	-58/-71	-54/-68	-401/-65	-419/-36
	shear force V_z	196/24	197/23	260/-35	261/-36
Mid- span	bending moment M_y	593/203	570/193	789/0	760/4
	bending moment M_z	0/0	95/97	0/0	-205/-165
	torsional moment M_T	≈ 0	≈ 0	≈ 0	≈ 0
	shear force V_z	≈ 0	≈ 0	≈ 0	≈ 0
	displacements	1.2/0.38	1.2/0.4	1.6/-0.6	1.6/-0.5

models of the transverse beams, namely a plane (grillage) and a three-dimensional truss system. Two different unit loads are considered (Fig. 2.88):

- load case 1: line load $q = 10 \text{ kN/m}$ in the centreline of longitudinal girder 1;
- load case 2: eccentric line load $q = 10 \text{ kN/m}$ (is equivalent to $q = 10 \text{ kN/m} + m_T = 33.4 \text{ kNm/m}$).

From the figures in Table 2.9 it can be seen that the results of both models are quite similar except the transverse bending moment M_z , which is from its definition equal to zero 0 in the case of a plane truss system.

The sawtooth shape of the forces in members (Figs 2.89 and 2.90) results from the local loading of the transverse beams. For dimensioning purposes, these values can be smoothed.

The different parts of the load transfer should first be analysed. This is done for the transverse beam in the middle of the span C–D. Figure 2.91 shows the member forces and the displacements of this beam.

Using the numerically determined deformation pattern of the beam, the two parts of the shear force caused by either a vertical shift or a rotation of the supports can be calculated by means of the expressions provided in Fig. 2.86. The resulting bending moment distributions are shown in Fig. 2.91. For the two load cases, the shear forces due to vertical shift and those due to rotation have similar ranges and different signs. For this system, the equivalent stiffness of the transverse beam consists of both parts of equal size.

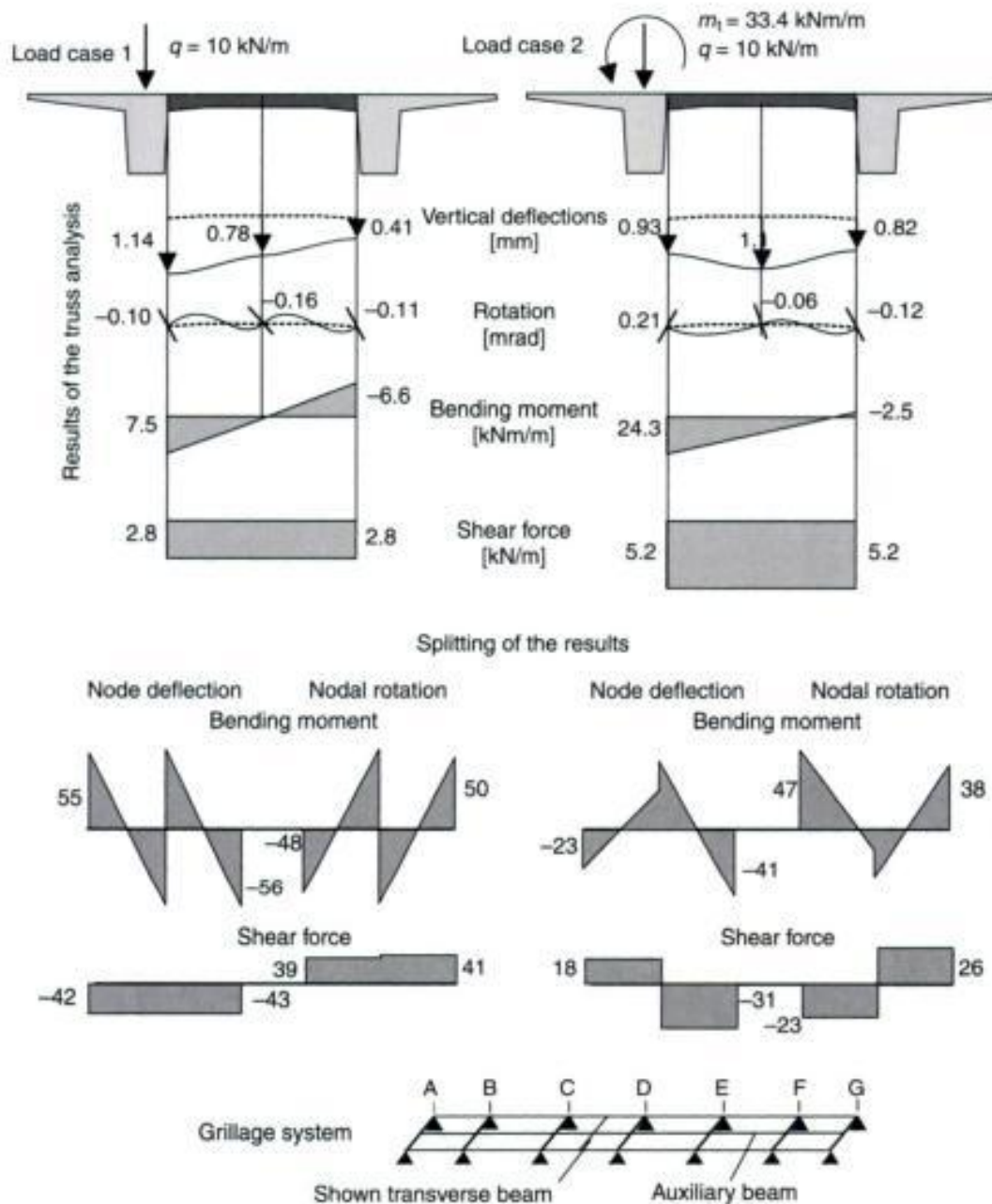


Fig. 2.91 Member forces and deflection of the transverse beam at midspan of span C–D

As noted above, the equivalent stiffness of the transverse beams depends on different parameters and cannot be determined exactly. Therefore, the influence of the stiffness of the transverse beams should be examined in more detail. For this, the sectional height is varied from $h = 0.0$ (no transverse beams) up to $h = 0.60$ m. The study of parameters is made by a plane truss system (grillage). Figure 2.92 shows the bending moments at the supports M_s and at midspan

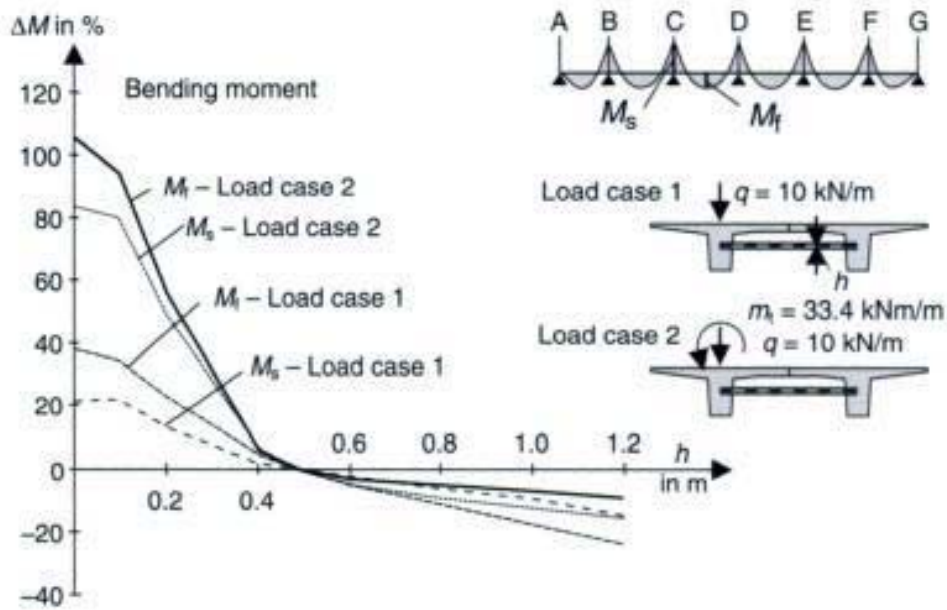


Fig. 2.92 Influence of the section depth h of the transverse beams on the bending moments of the loaded longitudinal girder

of span C–D M_f of longitudinal girder No. 1 for the different depths. In Fig. 2.93 the vertical support forces at axis C are plotted. This figure shows the significant influence of the loading. An increase in the section depth only results in minor changes in the bending moment, whereas its reduction causes a considerable increase in the forces in members of the loaded girder.

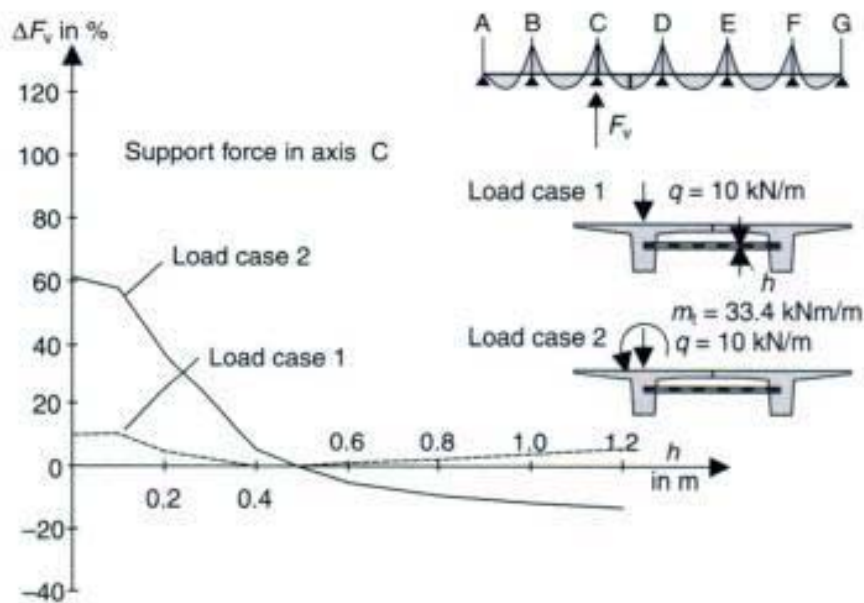


Fig. 2.93 Influence of the section depth h of the transverse beams to the support forces at axis C

2.8.3 T-beam bridge with several longitudinal girders

Eccentric loads, e.g. loads on a cantilever slab, cause a sawtooth kind of pattern for the torsional moments in the longitudinal girders (see Figs 2.89 and 2.90). This pattern results from the local restraint of the longitudinal girders by the transverse beams and vice versa. A design of the longitudinal girders for the peak torsional moments is, however, not required. This will be shown in the following example.



Cross-section of superstructure

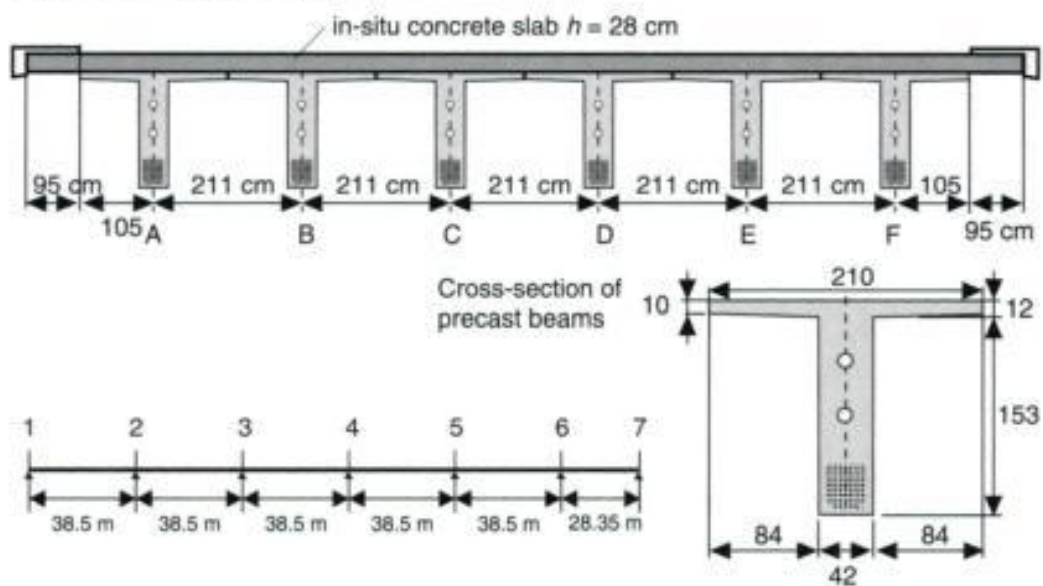


Fig. 2.94 Theodor-Heuss Bridge in Heidelberg [21]

image

not

available

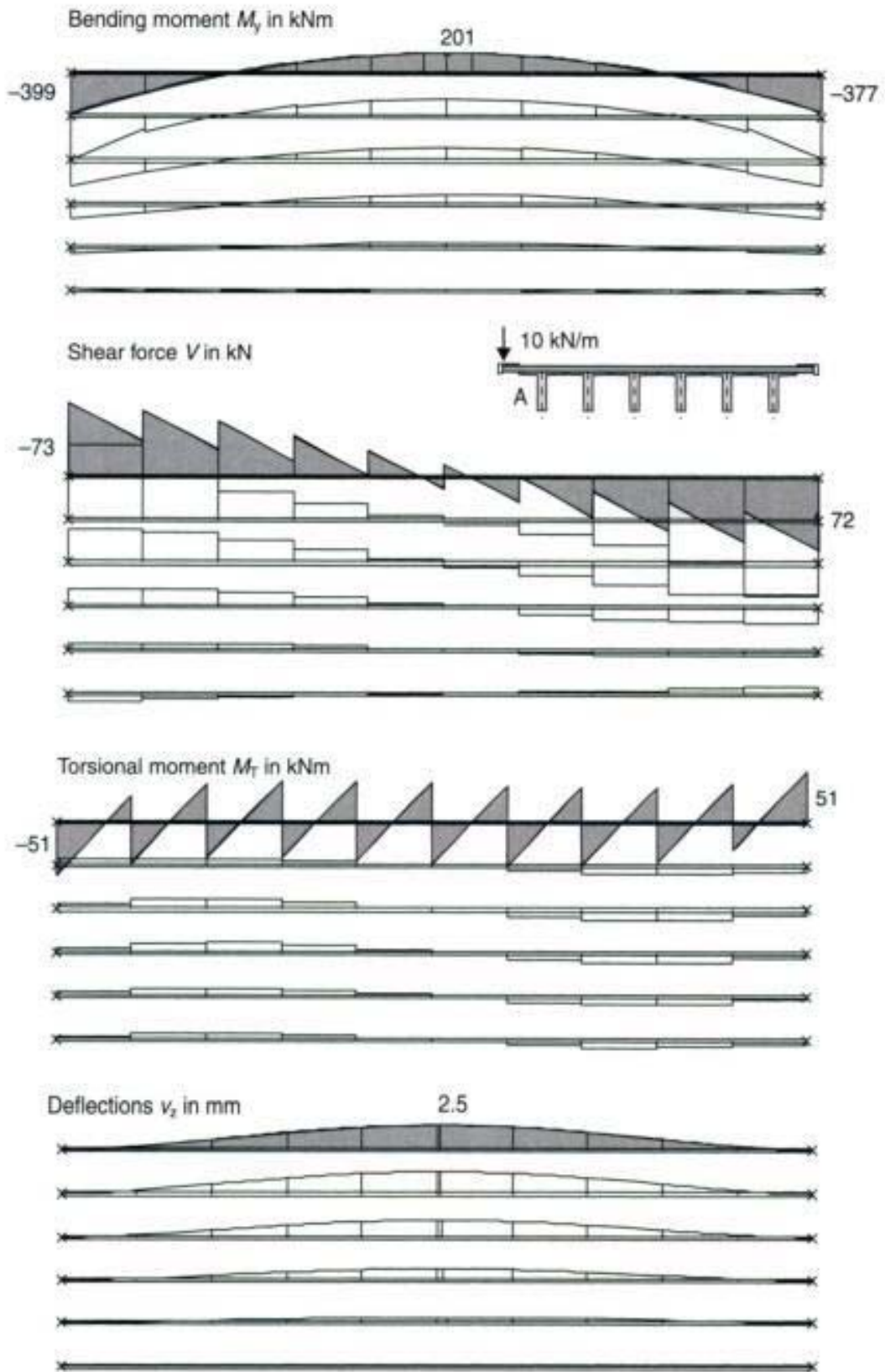


Fig. 2.96 Forces in members of the longitudinal girder between axis 3–4 due to an eccentric line load of $q = 10 \text{ kN/m}$ – 10 transverse beams per span

image
not
available

slab is nearly unstressed. Due to creep and shrinkage, load redistribution between the precast beams and the cast-in-situ slab takes place. In addition, the design in the transverse direction has to consider that the full height of the flange of the precast girders cannot be taken into account. The joint between the precast girders is not reinforced and is, therefore, not able to carry any tensile forces.

2.9 Dimensioning of reinforced beams

In the previous sections, the estimation of the member forces and deflections of truss systems have been explained in detail. However, the goal of any design is not the calculation of the action effects in the members but the dimensioning of the system for the ultimate and serviceability limit state. Therefore, it is often not necessary to model the structure with a high degree of accuracy and to consider all possible actions and effects. The actual amount of structural analysis to be carried out should be adapted to the required accuracy.

The following only refers to the ultimate limit state (ULS) design, as the design for serviceability can be very different according to the requirements of the relevant codes.

2.9.1 Design for bending and normal forces

The computation and dimensioning of an arbitrary concrete cross-section under ultimate condition has been described in detail by Quast and Busjaeger in *Heft 415* of the German Concrete Association [14]. Therefore, the following only provides some brief comments on this.

The design of a concrete cross-section requires the following items:

- Checking of the structural safety and balance between internal and external forces without exceeding the permissible stresses and strains of the materials.
- Estimation of the required reinforcement and its distribution in the beam under consideration of the ultimate and the serviceability limit state.
- Estimation of the strains and stresses.

The nonlinear behaviour of concrete and steel as building materials has to be considered in the design (Fig. 2.98). In addition, concrete is not allowed to carry any tensile forces in ultimate limit state design. The tensile strength of concrete is only used in the design of the serviceability limit state (crack width, restraint forces and displacements).

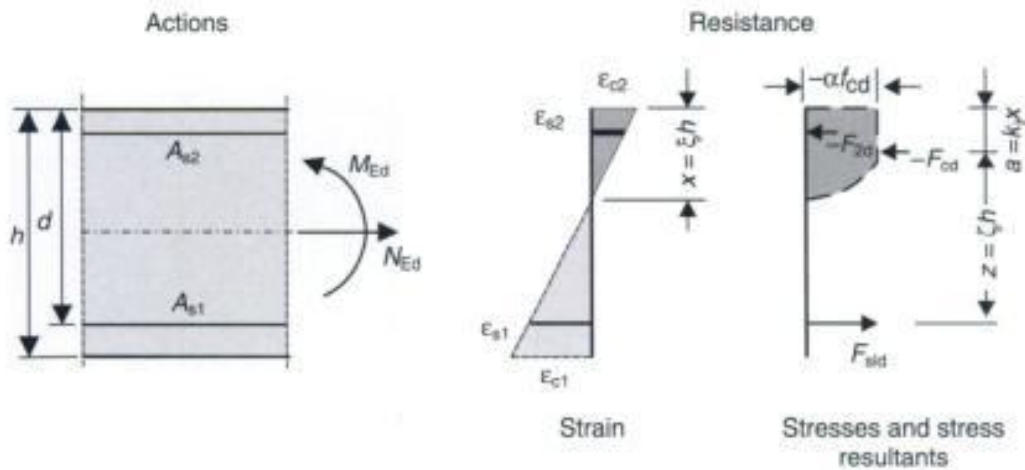


Fig. 2.98 Actions, strains and internal forces (resistance) of a reinforced concrete section

The design is based on the straight strain distribution over the depth of the cross-section in Stage I (uncracked) as well as in Stage II (cracked) (Bernoulli's hypothesis) condition.

The nonlinear material behaviour with respect to the stress–strain relation is defined in the relevant codes (see Fig. 2.99). It should always be kept in mind that these curves are only approximations of the real material behaviour for use in the design. The parabola–rectangle stress–strain relation of concrete is only a simplification of the stress distribution in the concrete compression zone, and cannot be used for other design purposes. In reality significant deviations may occur. In the design the permissible concrete strains, which are different in various codes, should be checked (Fig. 2.100).

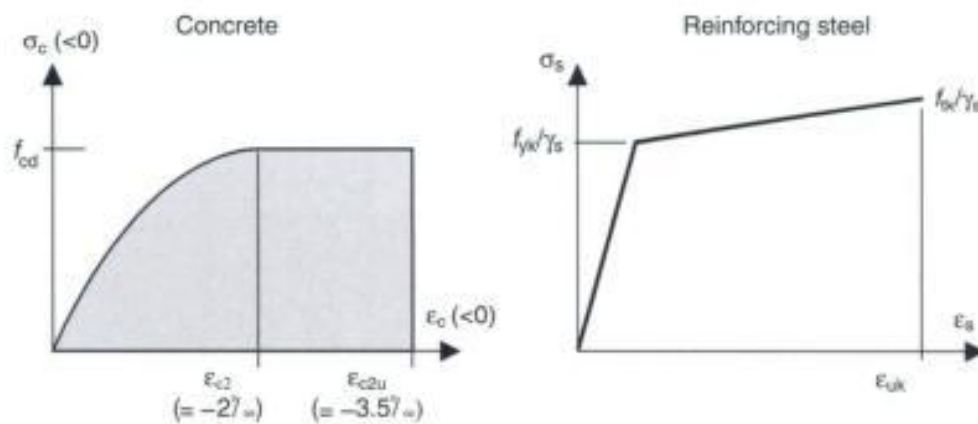


Fig. 2.99 Stress-strain relationship of concrete and steel according to EC2, Part 1 Fig. 4.2 and 4.5 [6]

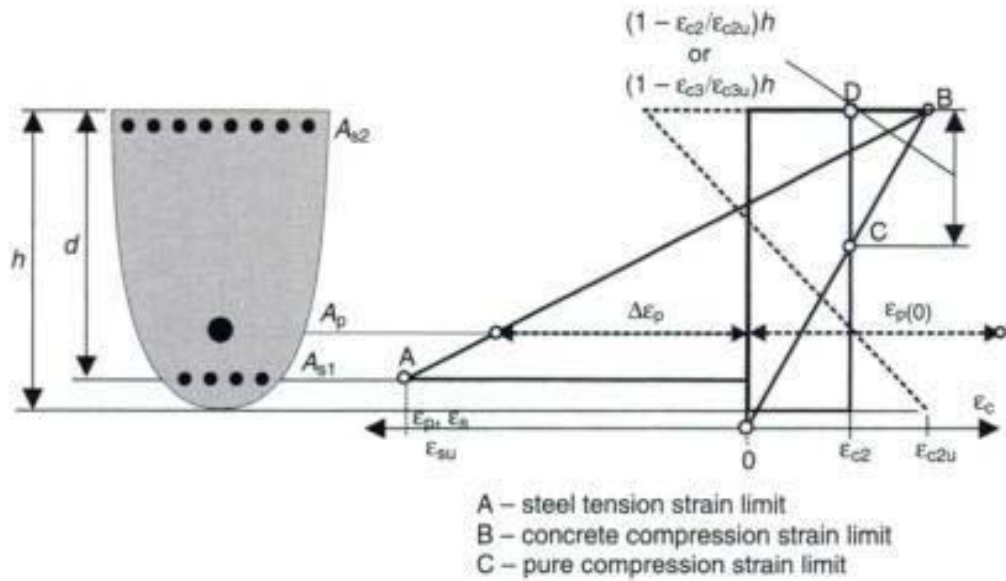


Fig. 2.100 Possible strain distributions under ultimate limit state according to EC2, Part 1, Fig. 4.11 [6]

For a more realistic estimation of the stiffness of a member, the tension stiffening effect has to be taken into account (see section 2.4.2). Otherwise the stiffness of the member in the relevant section is underestimated. The tension stiffening effect can be considered by modifying the stress strain relation of steel in Stage II, e.g. according to Fig. 2.101. From Fig. 2.101 it can be seen that the tension stiffening effect only has a significant influence on the stiffness of the member when the steel strain has not reached the point of yielding.

The dimensioning, i.e. the estimation of the required reinforcement, can only be done by iteration. This is true even for simple rectangular

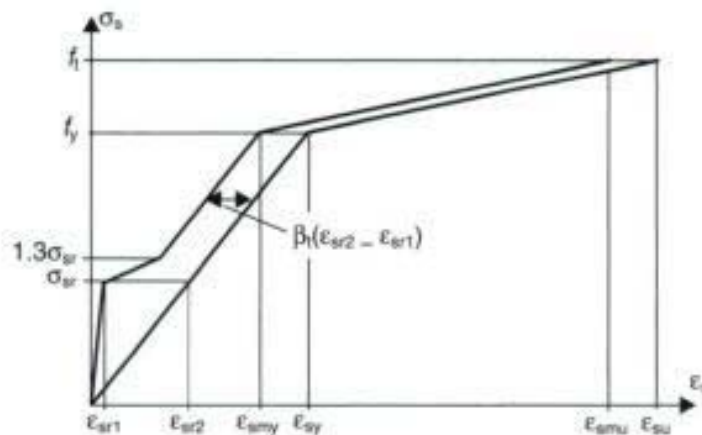


Fig. 2.101 Modified stress–strain relation of steel with regard to the tension stiffening effect (DIN 1045-1, Fig. 7 [7])

cross-sections under uniaxial bending. For cross-sections of arbitrary shapes, such dimensioning is an optimization problem. The designer must provide a reasonable distribution of the reinforcing bars in the cross-section and give some information regarding the iteration process (i.e. how the calculated reinforcement has to be increased or decreased).

In addition to the reinforcement required for the ULS, the minimum reinforcement and the 'shift rule' (horizontal displacement of the envelope line of the total tensile force) have to be considered. The latter is done by increasing the local normal force in the longitudinal tensile reinforcement by:

$$\Delta F_{sd} = V_{Ed} \cdot \frac{\cot \theta - \cot \alpha}{2}$$

where:

- θ is the inclination of compression struts;
- α is the inclination of the shear reinforcement against the horizontal axis.

2.9.2 Design for shear and torsion

The design for shear and torsion for a cracked section is based on a strut-and-tie model (Fig. 2.102). There are considerable differences between the various codes with regard to the permissible angle between the concrete compression struts and the main tension chord θ , the shear capacity due to the dowel effect, the shear friction in the cracks caused by aggregate interlock, and the permissible stresses in the compression struts. Therefore, the results of the numerical calculation should always be verified by manual analysis of some critical sections of the beam.

The shear and compressive stresses depend on the minimum width of the beam in the tensile region. For polygonal cross-sections of an arbitrary shape, the relevant section for the shear design has to be defined by the user of the computer program.

In addition the influence of point loads close to the supports, the variation of the cross-section's depth (inclined haunches), and the influence of an indirect support has to be taken into account.

In the case of torsion, a reduction in the resulting tensile force in the compression zone of the cross-section can be applied. It should be noted that torsion reinforcement is only required in the case of an equilibrium

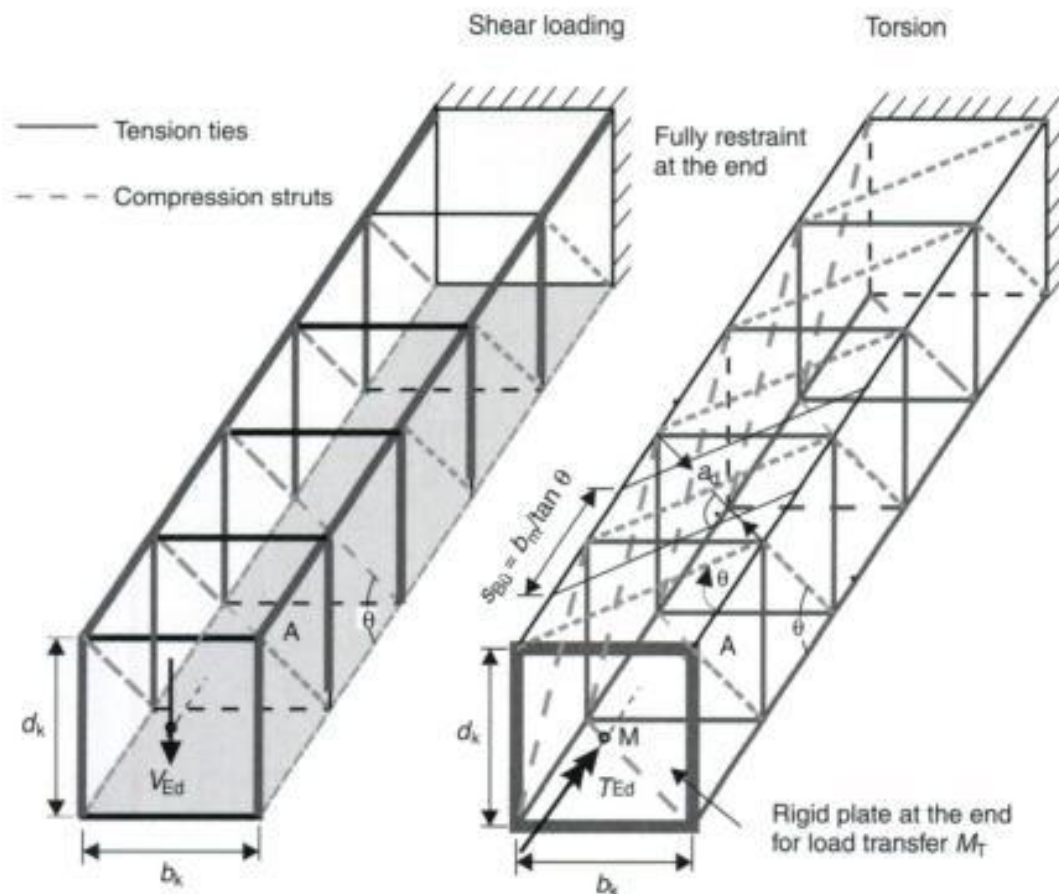


Fig. 2.102 Strut-and-tie model for shear and torsion design

torsion where the equilibrium of the structure depends on the torsional stiffness of the elements of the structure. As the torsion stiffness of a concrete member decreases significantly in case of cracking (Stage II), the minimum reinforcement is sufficient for the compatibility torsion. The calculation of the internal forces is usually based on a linear-elastic material behaviour. Therefore, a computer program will always determine an amount of torsional reinforcement. This problem can be overcome by setting the torsional stiffness of the members to very small values.

3

Shear walls and deep beams

Shear walls and deep beams are thin two-dimensional flat spatial structures, which are loaded by forces parallel to the midplane of the plate (Fig. 3.1). The stresses and strains are uniformly distributed over the thickness. However, one must make a distinction between shear walls and deep beams (Fig. 3.2). Shear walls are continuously supported plane members loaded by normal forces, where the maximum width of the cross-section is greater than four times its minimum width. If this is not the case, the member is treated as a column. Deep beams are plane spatial members, whose height is greater than half of their effective span width l_{eff} [6]. Furthermore, these beams are not continuously supported. In contrast to ordinary beams, shear walls and deep beams usually have a nonlinear strain distribution over their depth (see Fig. 3.3). Shear deformation cannot be neglected.

Copyrighted Material

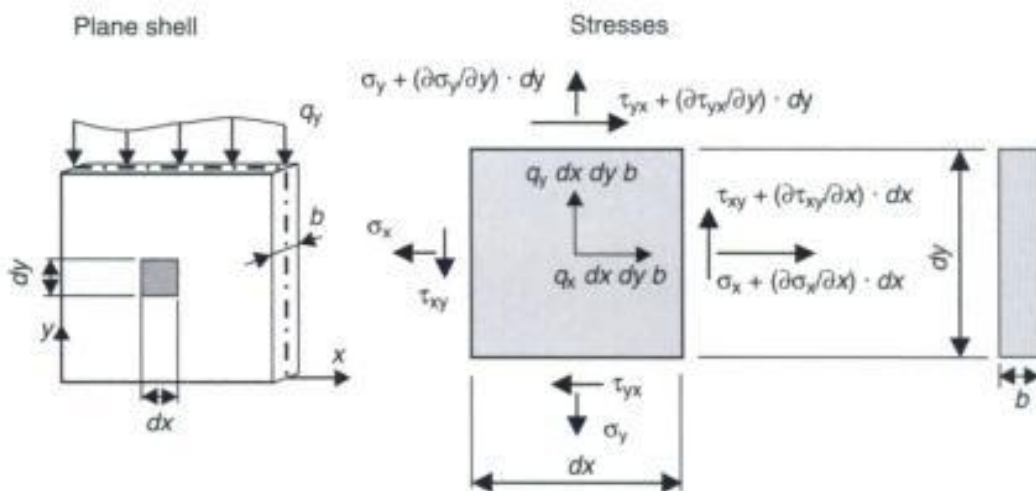


Fig. 3.1 Finite element of a shear wall and stresses considered in the model

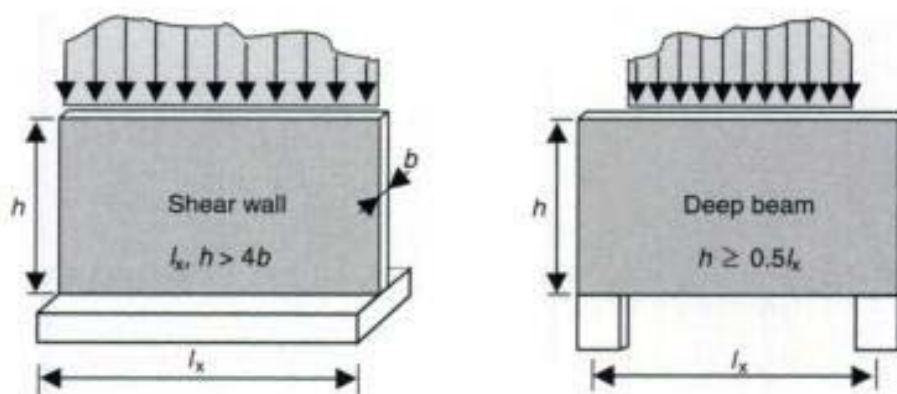


Fig. 3.2 Shear wall and deep beam

The distinction between deep and slender beams is not only necessary for the calculation of the internal forces but also for the reinforcement detailing. In ordinary beams a minimum shear reinforcement of stirrups is needed, whereas deep beams only need the minimum surface reinforcement.

This section only discusses the calculations of deep beams, as they are more often used in practice. Shear walls can be designed in the usual manner, similar to a column.

In accordance with Section 2.5.3.2 of EC2 [6], the internal forces in the ULS can be calculated by using the following methods:

- methods based on a linear elastic material behaviour;
- methods based on a linear elastic material behaviour with limited redistribution;

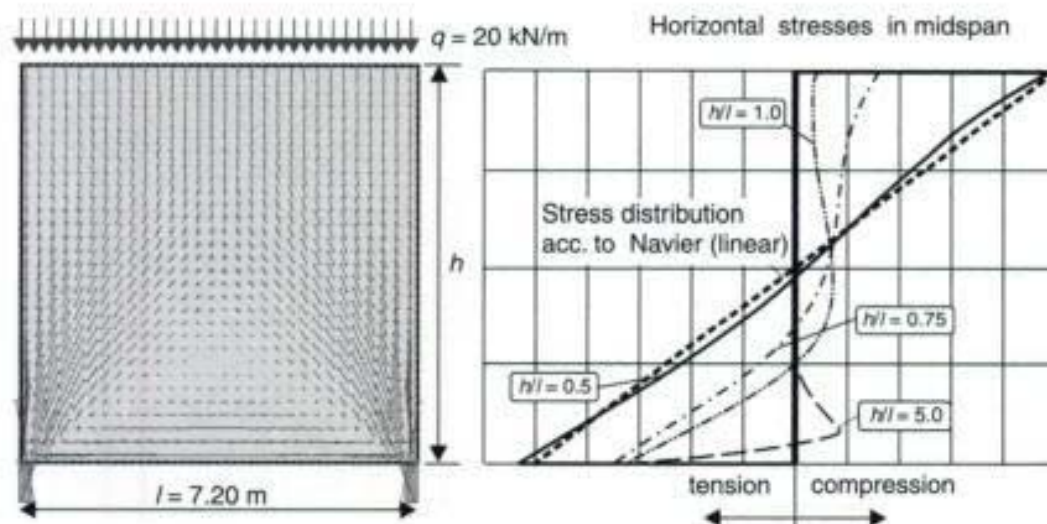


Fig. 3.3 Single span deep beam – main membrane forces (left) and horizontal stresses in midspan (right) for various heights h

- methods based on a plastic material behaviour including strut-and-tie models;
- methods based on a nonlinear material behaviour.

Of these methods, the one which uses Finite Element models based on a linear-elastic material behaviour is most commonly used in practice. Comments on the evaluation of strut-and-tie models (plastic analysis) are given at the end of this chapter.

Linear-elastic calculations can be used for both the ULS and the serviceability limit state. The effects of the redistribution of internal forces due to cracking of concrete or its 'yielding' under high pressures are neglected. Nevertheless, the nonlinear behaviour should be considered in both the design and the detailing of the reinforcement. For example, the longitudinal reinforcement of a single-span deep beam should be located at the bottom face of the member and should not be distributed according to the tensile stresses, which are estimated by a linear-elastic analysis.

The next section will provide the principles of a Finite Element calculation for deep beams by a very simple example of a single-span deep beam.

3.1 Estimation of stress resultants of a single-span deep beam

The beam in this example has a width to depth ratio of 1:1 ($l_x = l_y = 7.20$ m) (see Fig. 3.4). A uniform loading of $q = 20$ kN/m is

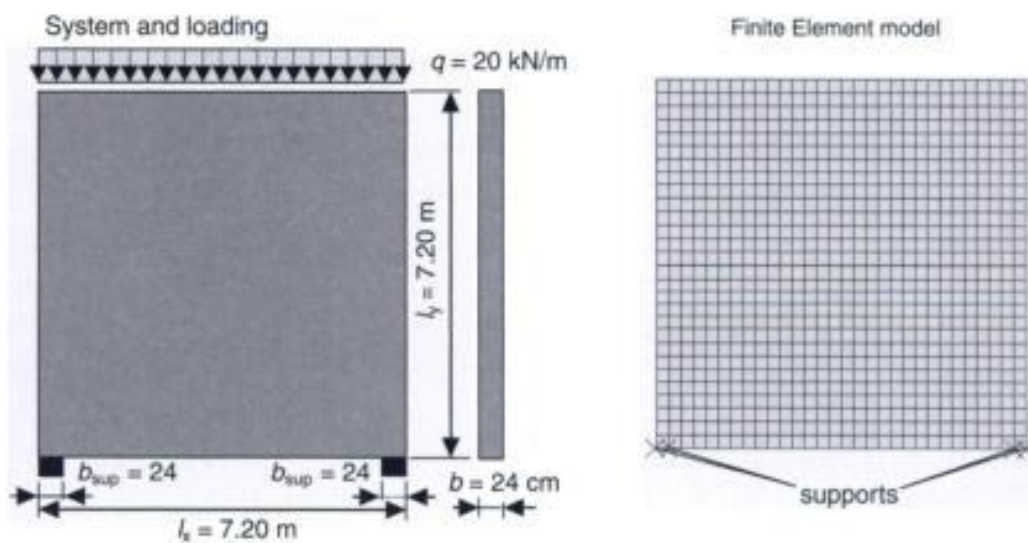


Fig. 3.4 System and Finite Element model

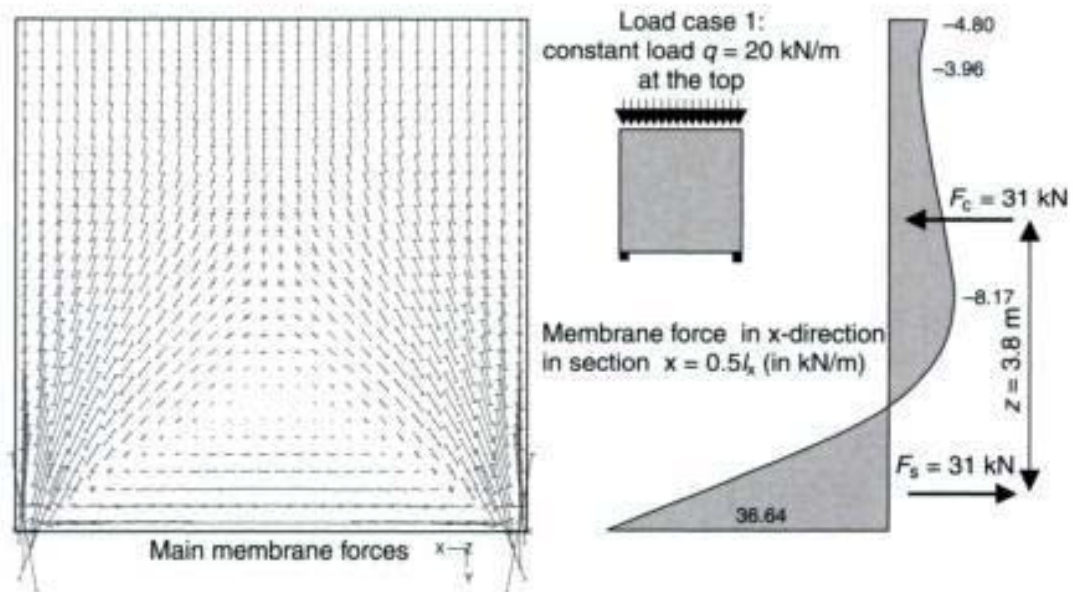


Fig. 3.5 Main membrane forces – load case 1: uniform load $q = 20 \text{ kN/m}$ on the upper edge

acting on its upper free edge. The structure is modelled by $30 \times 30 = 900$ rectangular plane elements which gives an element size of $0.24 \times 0.24 \text{ m}$.

The results of the Finite Element calculation are the node deformation v_x, v_y , the membrane forces n_x, n_y, n_{xy} and the stresses $\sigma_x, \sigma_y, \sigma_{xy}$ within the elements (see Figs 3.1 and 3.5). The membrane forces are obtained by multiplying the normal stress σ_x or σ_y by the thickness of the wall.

The objective of the design of a concrete member is to estimate its required reinforcement. For beams and slabs this can be automatically produced by a computer program. In the case of walls, a computer program is usually unable to estimate these reinforcement requirements or its correct distribution, as it is based on an element per element design. This problem will be further discussed in section 3.3. The reinforcement requirements of the single-span deep beam, therefore, should be estimated by numerical integration of the horizontal tensile forces n_x over the midspan depth. For the structure in this example (load case 1), this results in a tensile force of $F_s = 31 \text{ kN}$ (see Fig. 3.5). The lever arm of the compressive and tensile force is equal to $z = 3.80 \text{ m}$. The reinforcement requirements are obtained from dividing the tensile force F_s by the permissible stresses of steel: $A_{s, \text{req}} = F_s / \sigma_{sd}$. The stress in the reinforcement should be chosen to fulfil the crack width requirements ($\sigma_{sd} \leq f_{yd}$).

We will now compare the results of the Finite Element calculation with the widely used manual design method given in CEB [30] or *Heft 240* of the German Association of Reinforced Concrete [10]. The example considers four different load cases.

- Load case 1: uniform load $q = 20$ kN/m on the upper edge of the deep beam;
- Load case 2: uniform load $q = 20$ kN/m on the lower edge of the deep beam;
- Load case 3: concentrated load $F = 96$ kN on the upper edge of the deep beam (loaded width $t = 0.96$ m);
- Load case 4: concentrated load $F = 96$ kN on the lower edge of the deep beam (loaded width $t = 0.96$ m).

Manual design methods (beam theory)

The horizontal tensile force is estimated from the bending moments of a beam at midspan (field) $M_{Ed,F}$ and at the supports $M_{Ed,S}$ (Fig. 3.6).

Resulting tensile force in midspan:
$$F_{td,F} = M_{Ed,F} / z_F$$

Resulting tensile force over the supports of a multispans or cantilever beam:
$$F_{td,S} = M_{Ed,S} / z_S$$

where:

M_F midspan moment of a beam having the same span lengths as the deep beam

M_S moment over the supports of a beam having the same span lengths as the deep beam

z_F lever arm of the internal forces at midspan

z_S lever arm of the internal forces over the supports

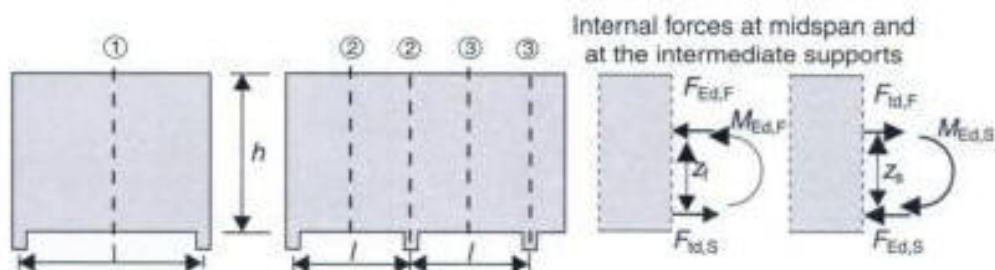


Fig. 3.6 Internal forces according to the simplified design model

The lever arm of the internal forces z_F and z_S can be estimated as follows:

1. single-span member

$$0.5 < h/l < 1.0 \quad z_F = 0.3h (3 - h/l) \quad (\text{DAfStb})$$

$$z_F = 0.2 (1+2h) \quad (\text{CEB})$$

$$h/l \geq 1.0 \quad z_F = 0.6l \quad (\text{DAfStb and CEB})$$

2. two-span member and end span of a multispan member

$$0.4 < h/l < 1.0 \quad z_F = z_S = 0.5h (1.9 - h/l) \quad (\text{DAfStb})$$

$$z_F = z_S = 0.2l (l + 1.5h) \quad (\text{CEB})$$

$$h/l \geq 1.0 \quad z_F = z_S = 0.45l \text{ resp. } 0.5l \quad (\text{CEB})$$

3. intermediate spans of a multispan member

$$0.3 < h/l < 1.0 \quad z_F = z_S = 0.5h (1.8 - h/l) \quad (\text{DAfStb})$$

$$h/l \geq 1.0 \quad z_F = z_S = 0.40l \quad (\text{DAfStb})$$

4. cantilever member

$$1.0 < h/l_k < 2.0 \quad z_F = z_S = 0.65l_k + 0.10h \quad (\text{DAfStb})$$

$$h/l \geq 2.0 \quad z_F = z_S = 0.85l_k \quad (\text{DAfStb})$$

(h = height of the deep beam; l = span of the deep beam; l_k = span of a cantilever member)

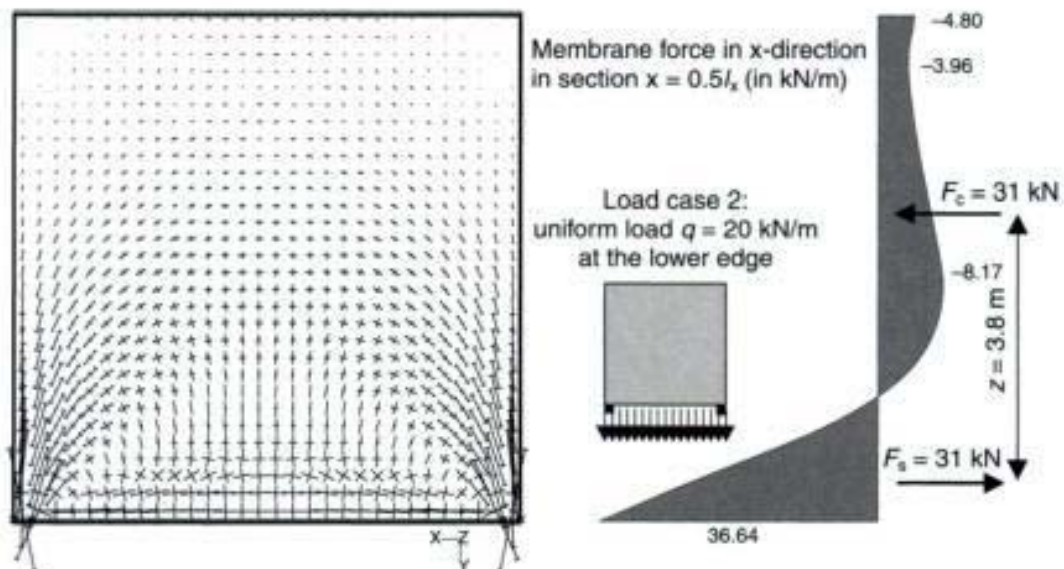


Fig. 3.7 Main membrane forces – load case 2: uniform load $q = 20 \text{ kN/m}$ on the lower edge

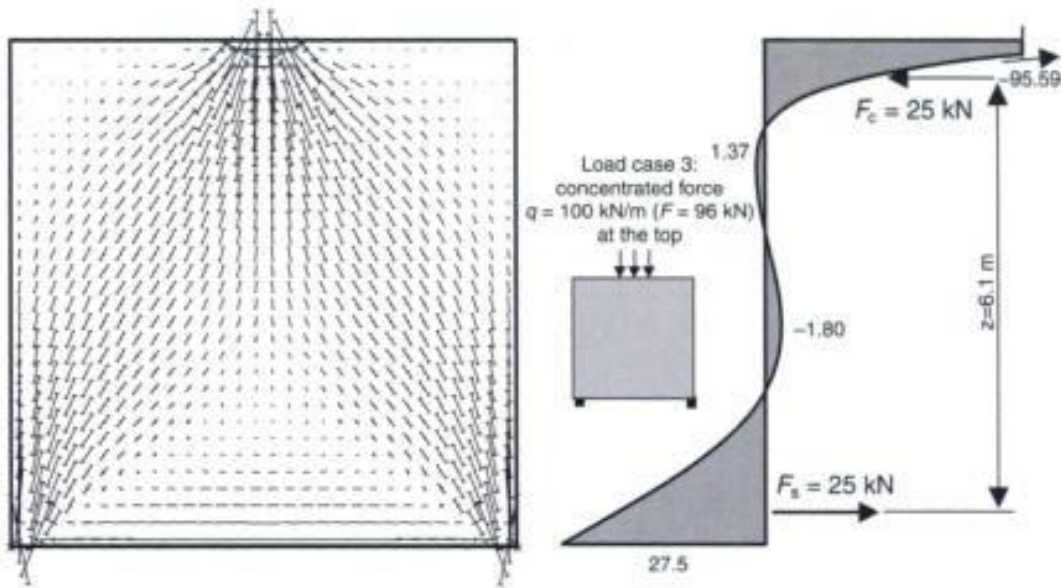


Fig. 3.8 Main membrane forces – load case 3: force $F = 96$ kN on the upper edge

The results of the Finite Element analysis are shown in Fig. 3.5 and Figs 3.7 to 3.9 for the various load cases. The resulting forces and the lever arms are obtained from numerical integration of the horizontal membrane forces at midspan.

CEB [30] and Heft 240 of the German Association of Reinforced Concrete [10] offers two different design methods (see the boxed text shown previously):

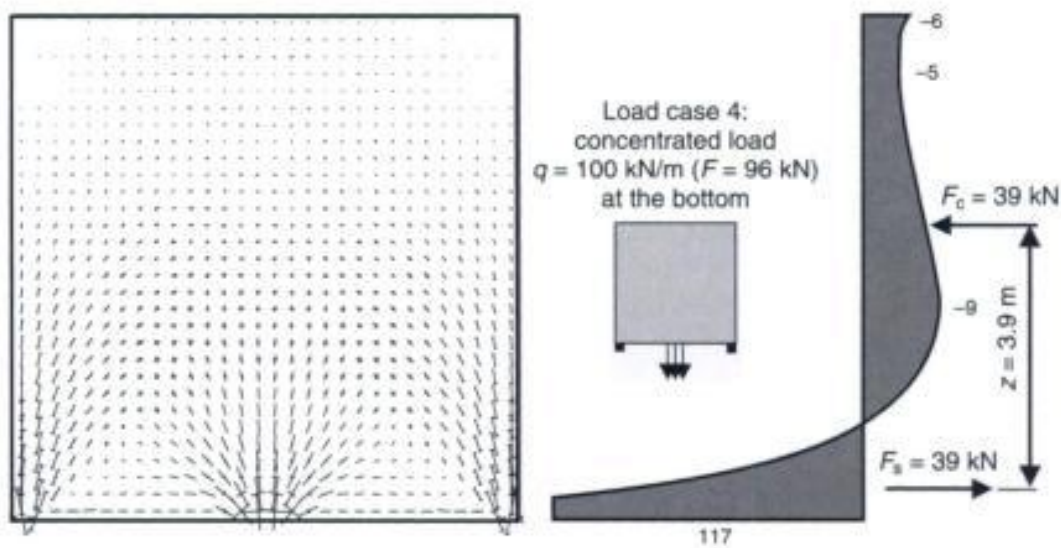


Fig. 3.9 Main membrane forces – load case 3: force $F = 96$ kN at the lower edge

Table 3.1 Resulting forces and lever arms – single-span deep beam

	Load case 1		Load case 2		Load case 3		Load case 4	
	$F_s = -F_c$ (in kN)	z (in m)	$F_s = -F_c$ (in kN)	z (in m)	$F_s = -F_c$ (in kN)	z (in m)	$F_s = -F_c$ (in kN)	z (in m)
FE-analysis	31	3.8	31	3.8	25	6.1	39	3.9
DAfStb								
beam	29	4.2	29	4.2	40	4.2	40	4.2
tables	29	–	29	–	26	–	38	–

- beam theory: the resulting tensile force of a single-span deep beam: $F_s = M_F/z_F$, with $z_F = 0.6l$ (for single-span deep beam with $h/l \geq 1.0$);
- tables based on shell theory.

Table 3.1 shows the results of the Finite Element analysis and the simplified method of DAfStb 240 [10].

A good agreement can be seen between the Finite Element results and the manual calculation, except for load case 3 (beam theory), which is mainly due to the simple single-span system. However, it will show greater differences for other structures (e.g. multispan deep beams), as shown in the following example.

The internal forces for a two-span deep beam are calculated, carrying the loads from the facade columns of an 11-storey office building, above the entrance to the underground car park (see Fig. 3.10). The concentrated loads in the columns are simplified to an equivalent uniformly distributed load ($g_{Ed}/q_{Ed} = 400/200$ kN/m). The wall is modelled by 52×15 plane shell elements (element size 0.25×0.25 m). In the first analysis, an infinitely stiff vertical support is assumed. The stiffness of the supporting columns is neglected.

Table 3.2 shows the resulting tensile forces in midspan and over the intermediate support and the support reactions. The tensile forces obtained from the manual design method (in accordance with DAfStb 240 [10]) are greater than those from the Finite Element analysis. In particular, the beam model results in much higher forces over the intermediate support (+172%). This is due to the small lever arm z_S with respect to the numerical analysis.

3.2 Modelling the support condition

In the case of statically indeterminate structures like multispan deep beams it is very important to model the support conditions as

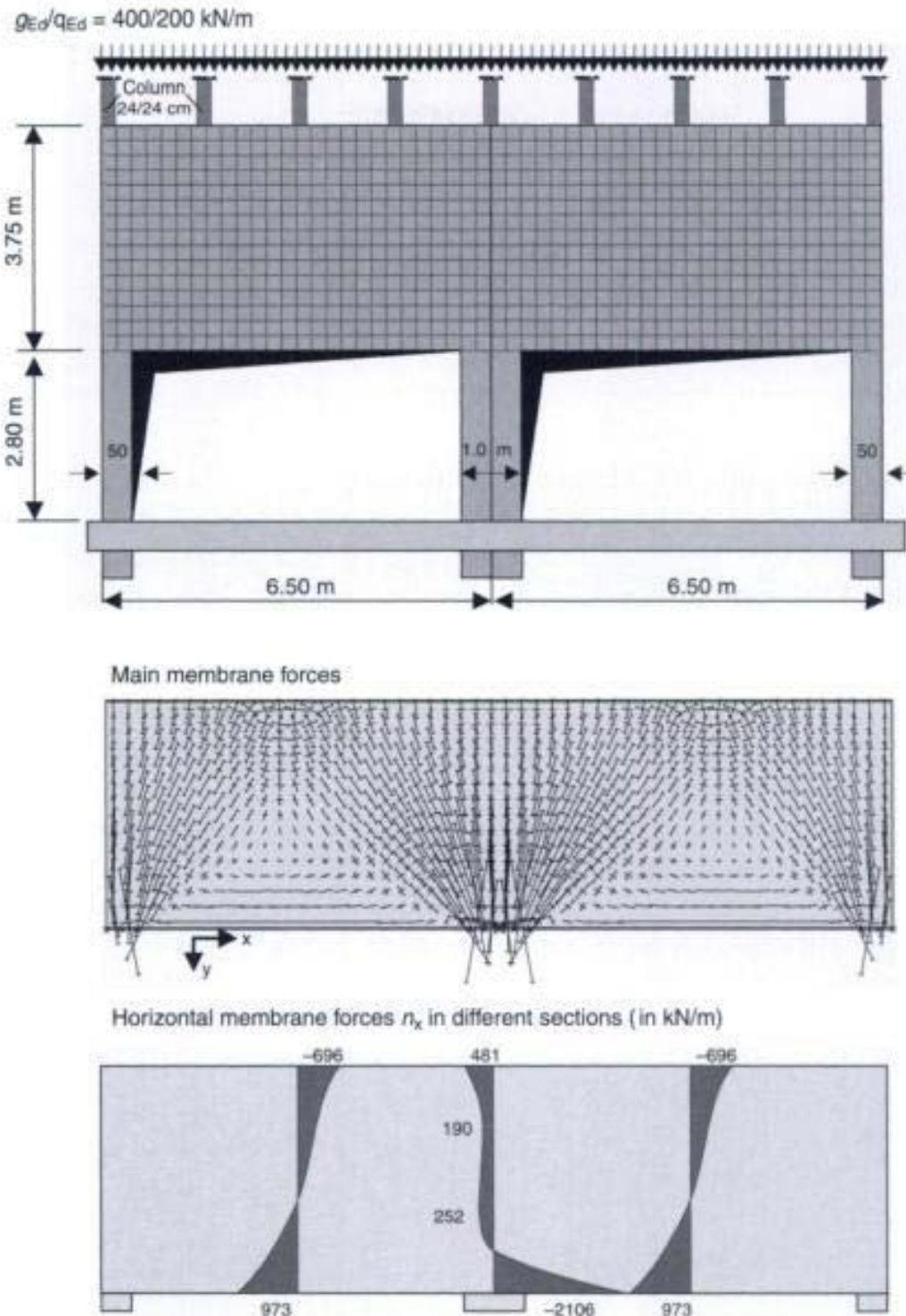


Fig. 3.10 Two-span deep beam: system, loading and membrane forces

accurately as possible. In contrast to normal beam structures, the stiffness of the supports and the resulting deflections have a considerable influence on the stresses and resulting internal forces in deep beams.

Table 3.2 Tensile forces and lever arms – double-span deep beam

	Midspan				Intermediate support				Support forces			
	$F_{s,F}$		z_F		$F_{s,S}$		z_S		A = C		B	
	kN	%	m	%	kN	%	m	%	kN	%	kN	%
FE-calculation	650	100	2.6	100	700	100	3.6	100	1692	100	4417	100
DAfStb												
beam	675	104	2.4	94	1201	172	2.4	68	1609	95	4802	109
tables	713	110	–	–	825	118	–	–	1609	95	4802	109

3.2.1 The influence of support settlements

The above mentioned double-span deep beam (see Fig. 3.10) was fully restrained in the vertical direction at the supports. In general, the stiffness of the elastic supports should not be neglected. This is particularly true in the case of deep beams supported on slender columns or walls, or where differential settlements are expected. It is a well-known fact that the internal forces and the reactions of multi-span deep beams are very sensitive to differential deflections of the supports. This will be discussed in the following example.

First, the influence of the deflection of the supports will be demonstrated for the slender ($h/l=0.6$) double-span deep beam shown in Fig. 3.10. The structure is loaded by a uniform loading of $q=600$ kN/m at the top edge. Furthermore, it is assumed that there is a settlement of the intermediate support by up to 7 mm. Figures 3.11 and 3.12 show the results of the numerical analyses of the varying amounts of settlements.

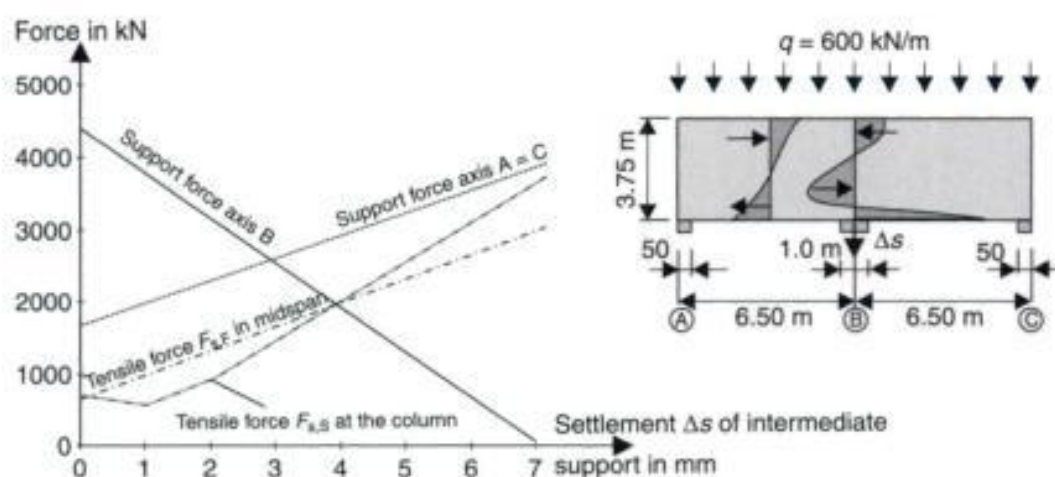


Fig. 3.11 Support forces and tensile forces depending on the settlement of the intermediate support

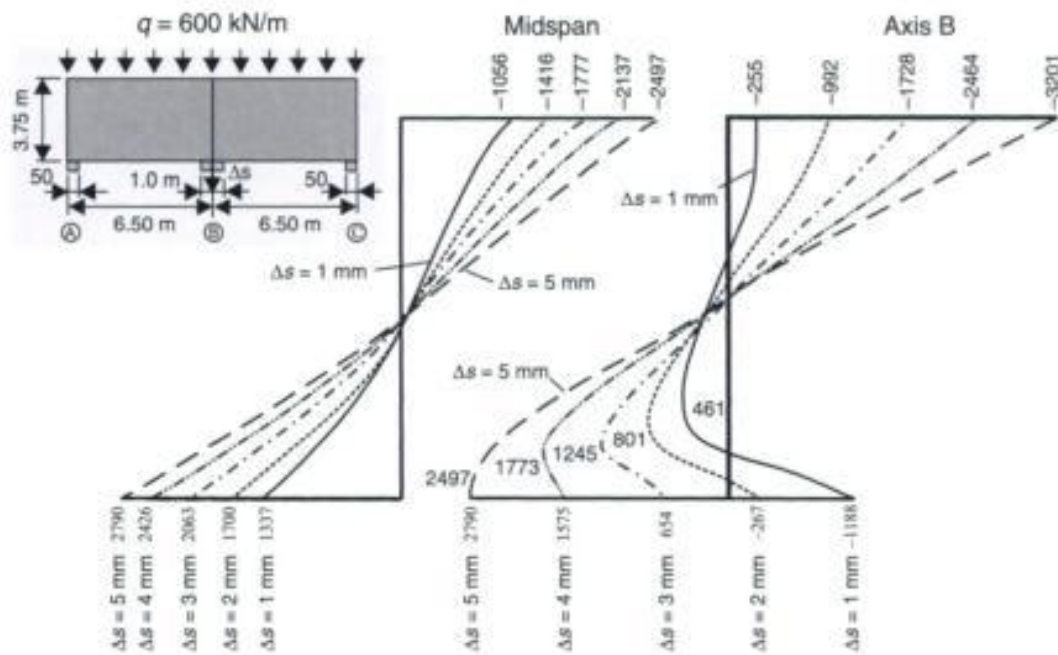


Fig. 3.12 Horizontal membrane forces at the midspan and over the intermediate support B depending on the amount of vertical deflection Δs at axis B

The reactions and the resultant horizontal forces are very considerably influenced by the amount of the settlement at the intermediate support. A deflection of only 2 mm is needed to increase the vertical forces at the end supports by 37% and reduce the reaction at the intermediate support by 38%. The resulting horizontal tensile force is increased by 200% in midspan and 33% at axis B. With increasing deflections, the stress distribution becomes similar to that of a single-span beam with a span length of $2 \times 6.25 = 12.50 \text{ m}$ (see Fig. 3.12).

A deflection of only 7 mm ($=0.001l$) is needed to reduce the reactions at the intermediate support to zero.

3.2.2 Modelling of flexible supports with springs

The above example clearly demonstrates that the stiffness of the supports of a statically indeterminate structure must be considered in the design model. Deep beams are often supported by slender columns or walls. The simplest method to consider the stiffness of the bearing structure is to model them by using individual springs. For simplicity, the column itself is not modelled. This will be shown in the next chapter.

A column has a bending and a normal stiffness. Both should be modelled by individual springs. It should be pointed out that bending

Table 3.3 Equivalent spring stiffness of a column

Normal stiffness	Rotational stiffness	
$F = C_N \cdot \nu$	$M = C_\varphi \cdot \varphi$	
where: $C_N = E_c \cdot A_c / l$	where: $C_\varphi = 3E_c \cdot I_c / l$	where: $C_\varphi = 4E_c \cdot I_c / l$

springs cannot be used in conjunction with plane shell elements, as they have no degree of freedom for rotation (see the following chapter); hence, a different method of modelling the bending stiffness of the columns has to be found.

In general, deep beams are loaded by large vertical forces which require large bearing areas. This continuous support can be modelled by using several spring elements or special boundary elements. The advantage of the latter model is that the elastic support stresses can easily be estimated. These have to be checked in the design.

The axial stiffness of the springs C_N is obtained from the following expression (see Table 3.3):

$$C_N = E \cdot A_c / l$$

where:

- $E \cdot A_c$ is the axial stiffness of column;
- l is the height of column.

As bending springs cannot be used in conjunction with plane shell elements, the rotational stiffness of the column is modelled by using multiple springs, having a given distance from each other (see Fig. 3.13).

The principles are demonstrated on a single-span deep beam (see Fig 3.14). The deep beam is supported on 2 columns ($b/h = 0.24/0.48$ m) which are fully restrained at their base. This results in the

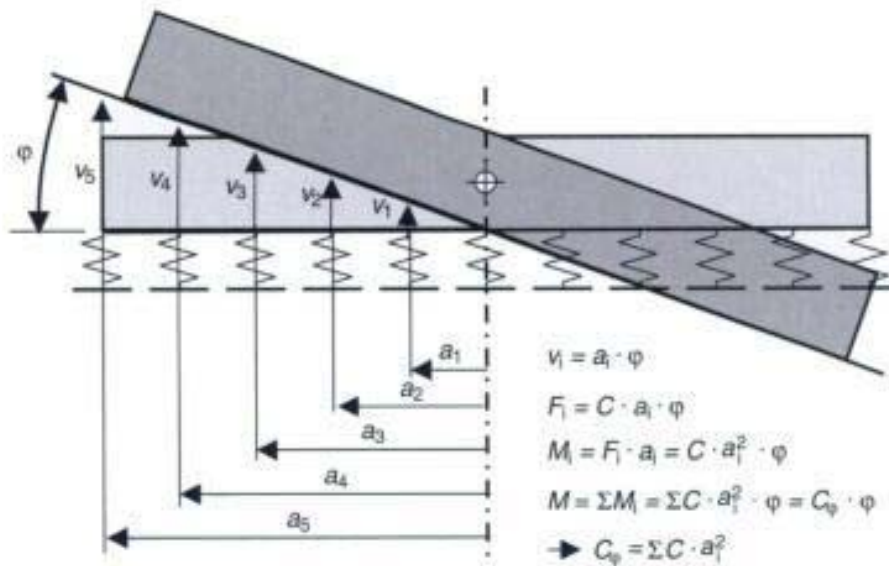


Fig. 3.13 Rotational stiffness resulting from axial springs

following equivalent stiffness for the springs: (concrete grade C 25/30, $E_c = 30\,500\text{ MPa}$).

$$C_N = \frac{E_c \cdot A_c}{l} = \frac{30.5 \cdot 10^6 \cdot 0.24 \cdot 0.48}{3.6} = 976\,000\text{ kN/m}$$

$$C_\varphi = \frac{4 \cdot E_c \cdot I_c}{l} = \frac{4 \cdot 30.5 \cdot 10^6 \cdot 0.24 \cdot 0.48^3 / 12}{3.6} = 75\,000\text{ kNm/m}$$

Two springs are used for each support. The supported nodes are coupled with each other, thus the supported area remains plane before and after loading in the numerical model. The distance of

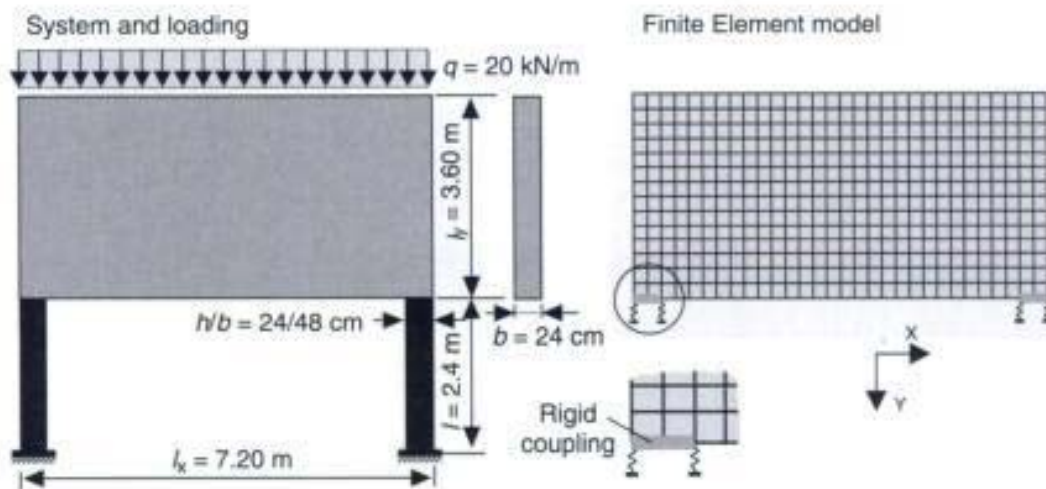


Fig. 3.14 Structure and Finite Element model

the normal springs has to be determined in order to get the correct rotational stiffness C_φ :

$$C_\varphi = 2 \cdot C_N \cdot a_i^2 \Rightarrow a_i = \sqrt{\frac{C_\varphi}{2 \cdot C_N}} = \sqrt{\frac{75\,000}{2 \cdot 976\,000}} = 0.20 \text{ m}$$

where:

a_i is distance of the spring from the centre of the supported area.

For the given structure, it is necessary to use a distance which is smaller than the actual supported width. As this is an exceptional case, the springs are located at the face of the supported area. This results in a distance of 0.48 m between the springs. This model gives a spring force of 31.6 kN and 40.4 kN at the outer spring and the inner spring, respectively. The total vertical force is equal to 72 kN. The resulting bending moment at the top of the column is:

$$M = (40.44 - 31.6)/2 \cdot 0.48 = 2.12 \text{ kNm}$$

The influence of the spring stiffness on the bending moment is shown in Fig. 3.15. It can be seen that in the practical relevant region of $C_N \approx 1000 \text{ MN/m}$, the spring stiffness has a considerable effect on the bending moment at the column head. An infinite stiff support results in a bending moment of $M = 10.3 \text{ kNm}$.

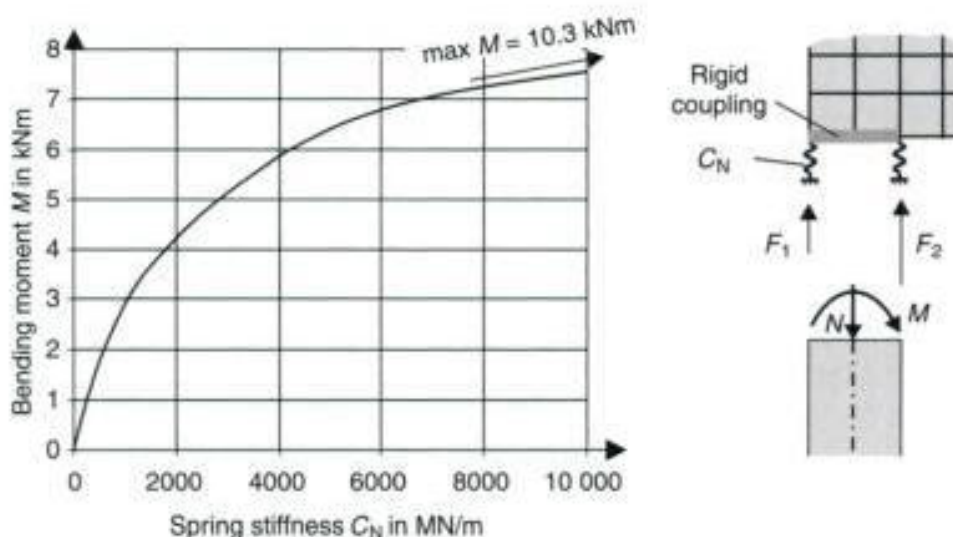


Fig. 3.15 Bending moment at the supports in relation to the normal spring stiffness C_N

3.2.3 Modelling of the columns with beam elements

Instead of using springs, it may be easier to model the whole structure including the shear wall and the columns. The latter one is modelled by beam elements. This has the advantage that the member forces M , V , N and the reinforcement requirements of the column are calculated automatically by the computer program. It is also possible to model the columns using the same plane shell elements as the deep beam (Fig. 3.17). However, this has the disadvantage that the member forces (i.e. the bending moments, shear and normal forces) which are required for the design must be separately calculated by the integration of the stresses in various sections. Both of these models will be further discussed.

The connection of the beam elements with the plane shell elements should be handled with great care, as will be shown in the following example, which uses a single-span deep beam. The columns are modelled with beam elements located on the axis of gravity of the column. The top beam node is stiff connected to the node of the deep beam element at the same location.

The results of the Finite Element analysis are shown in Fig. 3.16. No bending moments can be seen at the column head. This result is not expected, as a rotation of the supported area of the deep beam is likely to happen (note the deflected structure Fig. 3.17). Furthermore, considerable distortions can be seen for the elements in the vicinity of the column heads.

As zero bending moments are highly unexpected at the stiff joint between the column and the deep beam, the same structure is recalculated using plane shell elements for the columns. Figure 3.17 shows the results of this analysis. A rotation of the upper end of the column can be seen which must result in bending moments in the column.

The error of the beam model can be traced back to the fact that plane shell elements have only two degrees of freedom for deflection, v_x and v_y , but no degree of freedom for rotation (Fig. 3.18). Thus, coupling of beam and plane shell elements results in a so-called 'incompatible' element mesh. This means that there is a missing degree of the freedom (rotation) between the two types of elements. Thus, a plane shell element can be used to only estimate membrane forces and not bending moments.

The stiff connection between the column and the deep beam must be modelled by stiff coupling of the top node of the beam element to some nodes of the deep beam (see Fig. 3.19). The rotation of the supported nodes of the deep beam should be identical to the rotation of the upper

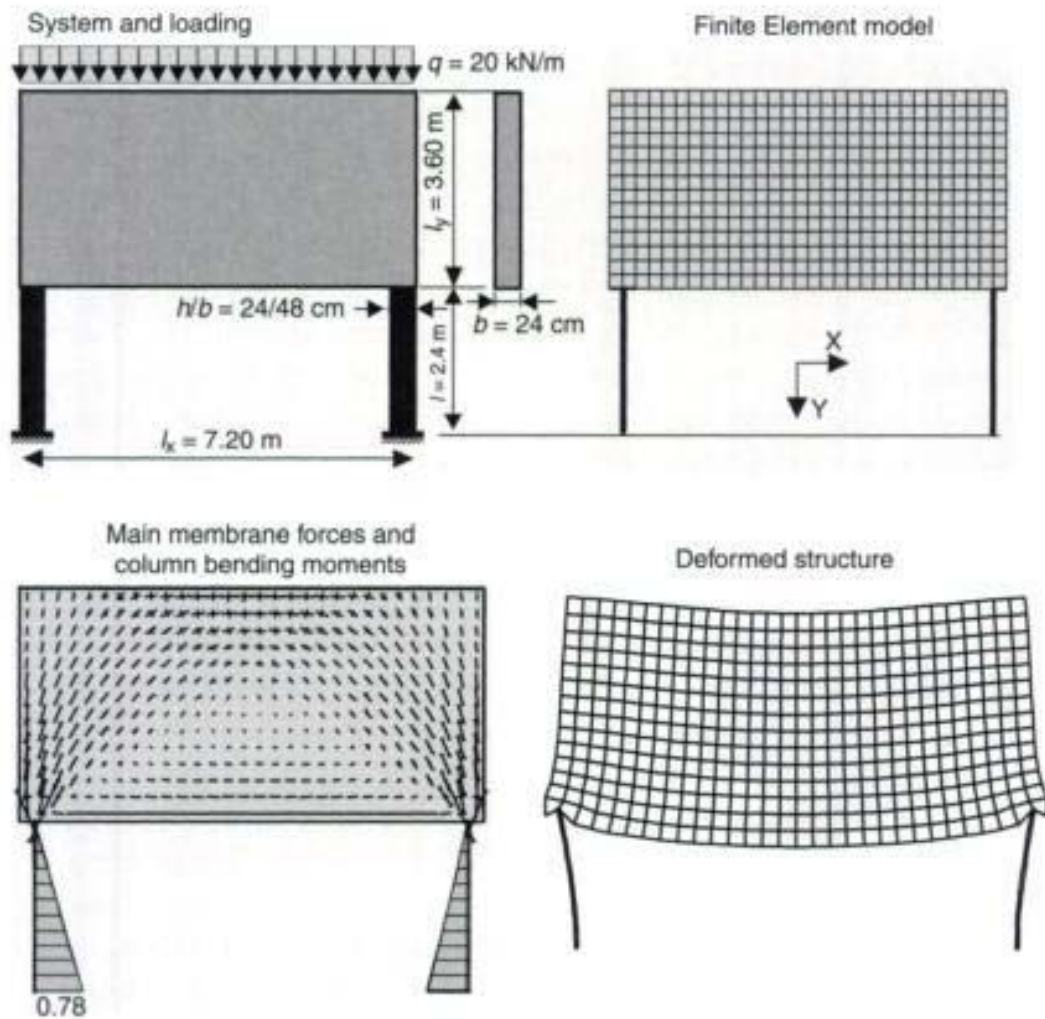


Fig. 3.16 Deep beam supported on two columns (beam elements)

end of the beam element. Distortions of the shell elements above the columns as shown in Fig. 3.16, should be avoided.

The stiff connection can either be modelled with a special coupling of the nodes (Fig. 3.19 left) or by extension of the beam elements into the deep beam (Fig. 3.19 right). Both models only provide an approximation of the real situation. The number of coupled nodes can have a great influence on the bending moments in the column. This is demonstrated by the results shown in Fig. 3.20, where considerable differences between both variants in the calculated bending moments at the column head can be seen. For the case with horizontal coupling a bending moment at the junction of $M = -3.7$ kNm is estimated, whereas for the other model the bending moment is only $M = -2.0$ kNm. The ratio of the first moment with respect to the second one is $3.7/2.0 = 1.85$!

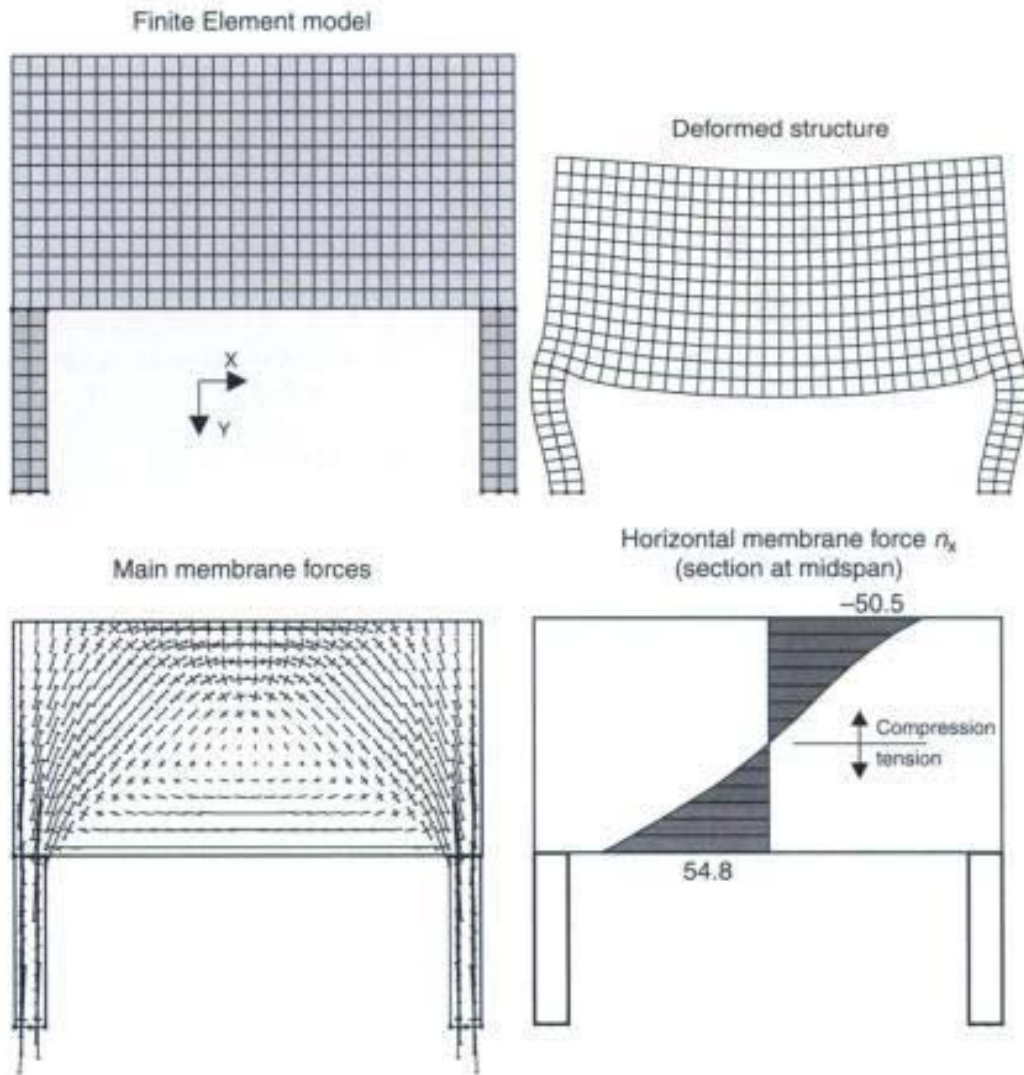


Fig. 3.17 Deep beam supported on columns (plane shell elements)

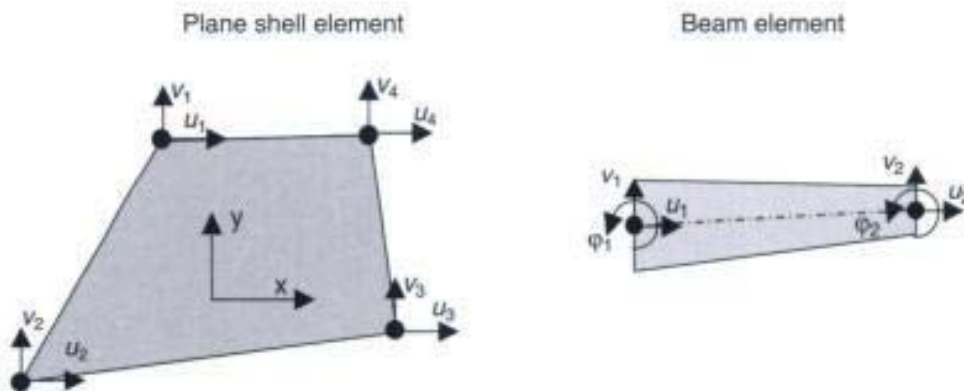


Fig. 3.18 Degrees of freedom of a plane shell and a beam element (two-dimensional)

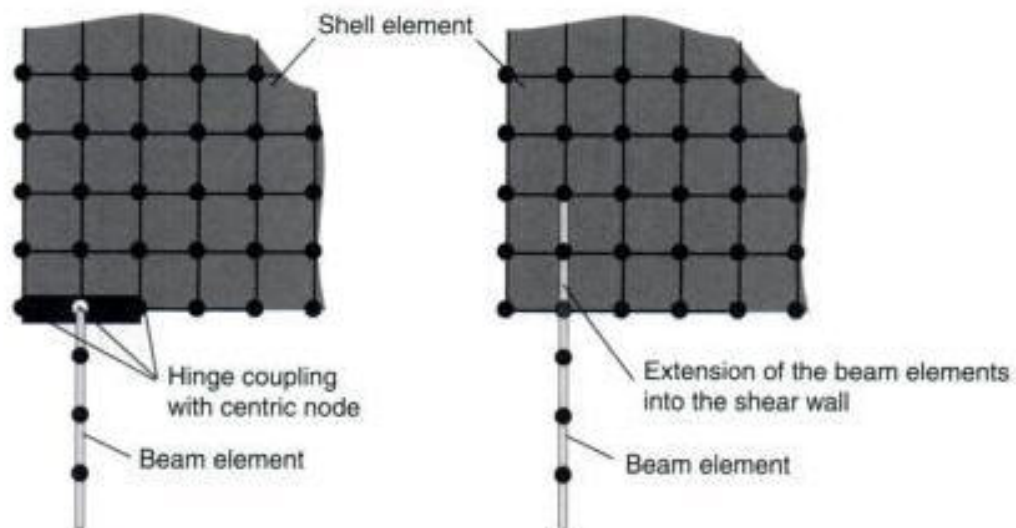


Fig. 3.19 Connection between a beam with a plane shell element

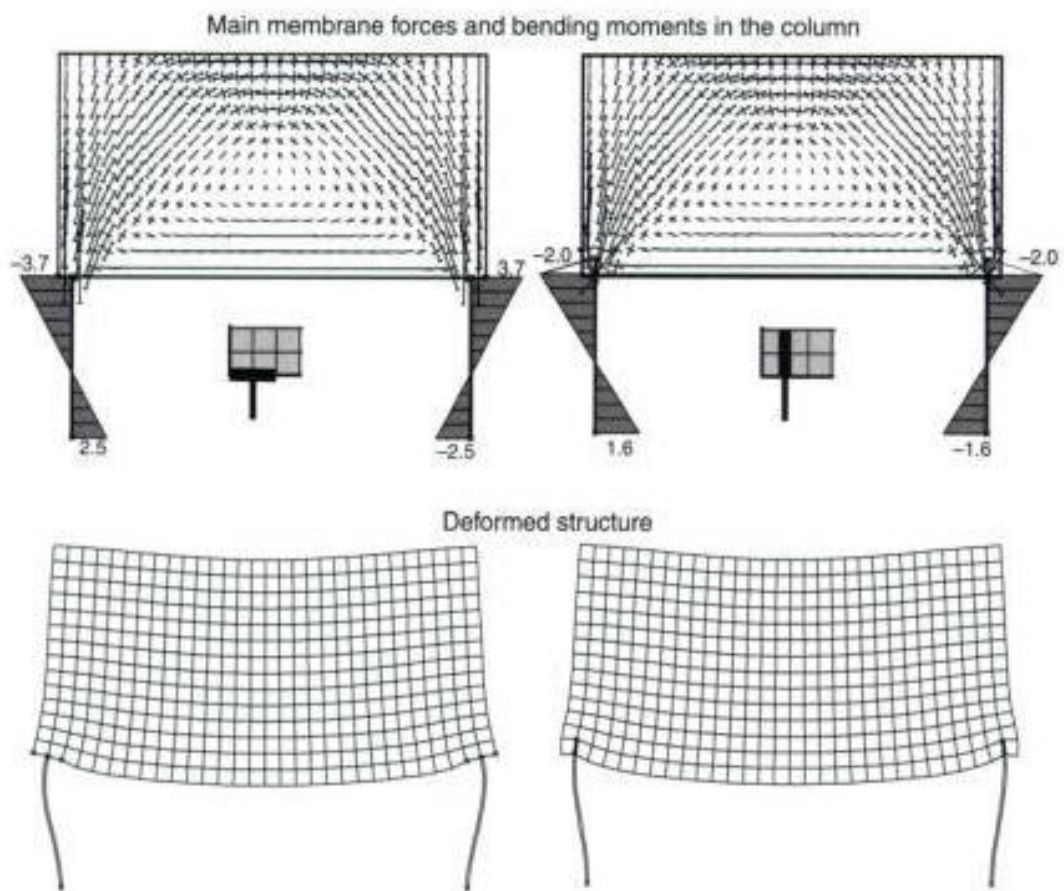


Fig. 3.20 Membrane forces and the deformed structure for two different models (coupling with supported nodes – extension of the beam elements)

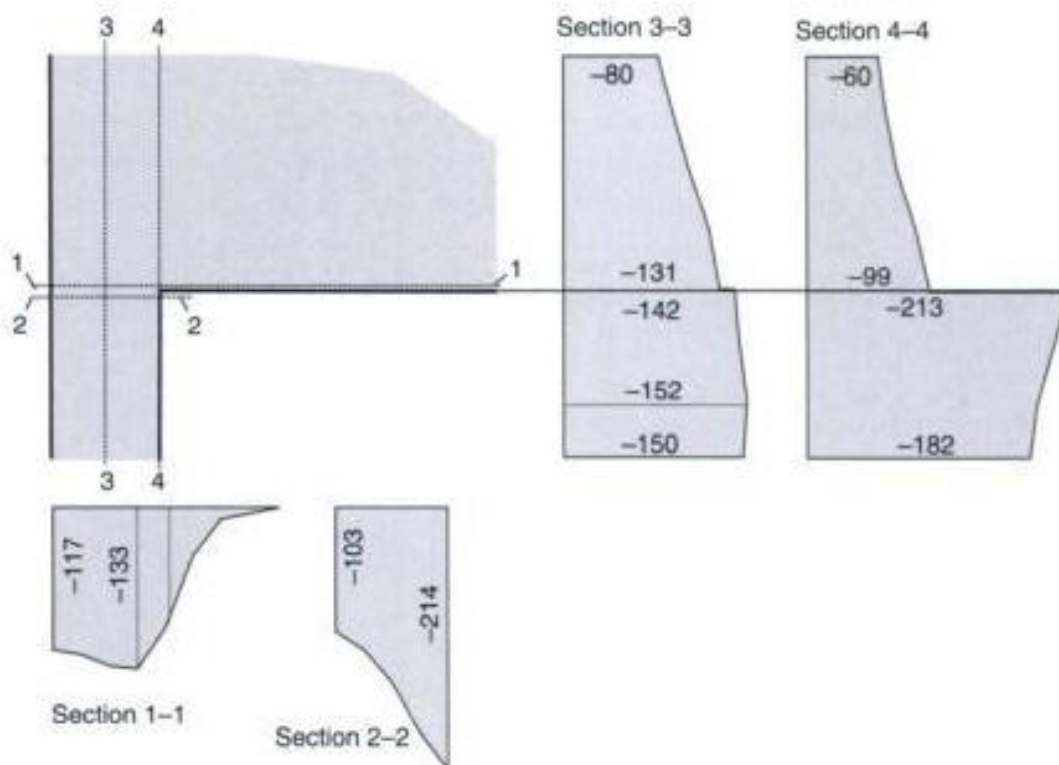


Fig. 3.21 Vertical membrane force n_y in various sections near the corner of a deep beam

Here it should be noted that there are also plane shell elements, which have a rotational degree of freedom (based on Cosserat continuum). However, these elements are rarely implemented in the software programs used for practical design of concrete structures.

A highly refined Finite Element mesh has to be used to obtain a more accurate value for the bending moment. The results of this analysis are shown in Fig. 3.21. The numerical integration of the vertical membrane forces at top of the column (section 2-2) results in a force of $F = 72 \text{ kN}$ ($F = 7.20 \text{ m} \times 20 \text{ kN/m} \times 0.5 = 72 \text{ kN}$) and a bending moment of $M = 2.6 \text{ kNm}$. This value is between the two results from the above models.

An unbalanced distribution of the vertical membrane force n_y in section 4-4 at the inner face of the corner can be seen in Fig. 3.21. This is a result of the simplifications and assumptions of the used numerical model and does not occur in real structures. The corner causes a singularity problem. The unbalanced boundary condition results in high (infinite) stresses resp. membrane forces. If the element size is further reduced, the stresses at the inner face of the corner will become infinite. However, the resulting bending moment is only slightly changed.

The stress distribution in any corner region of plates can only be approximated when using plane elements with a linear-elastic material behaviour. High tensile stresses would cause cracking of the concrete, thus resulting in a redistribution of the internal forces. The same effects occur in the case of large compressive pressures at the inner side of the corner. Therefore, a highly refined element mesh does not model the reality any more precisely than a coarse element mesh.

3.2.4 Horizontal restraint

When modelling deep beams, great care should be taken with regard to horizontal restraints due to the supports. They may result in an arching effect with considerable reduction in the design tensile forces as will be shown in the following example.

The deep beam shown in Fig. 3.22 is a very slender structure, having a width to depth ratio of 1:2. The member can, therefore, also be considered as a normal beam with the assumption of a linear strain distribution over its depth at midspan. The structure is modelled with 14×30 plane shell elements. It is loaded with a vertical uniformly distributed loading of $q = 20 \text{ kN/m}$ at its upper free edge.

Two ultimate support conditions are treated:

- System 1: both supports are fixed in the vertical direction, and only one support is fixed in the horizontal direction;
- System 2: both supports are fixed in both the horizontal and vertical directions.

Figure 3.23 shows the distribution of the main membrane forces n_I and n_{II} and the horizontal membrane force n_x at midspan. Significant differences can be seen between the two models.

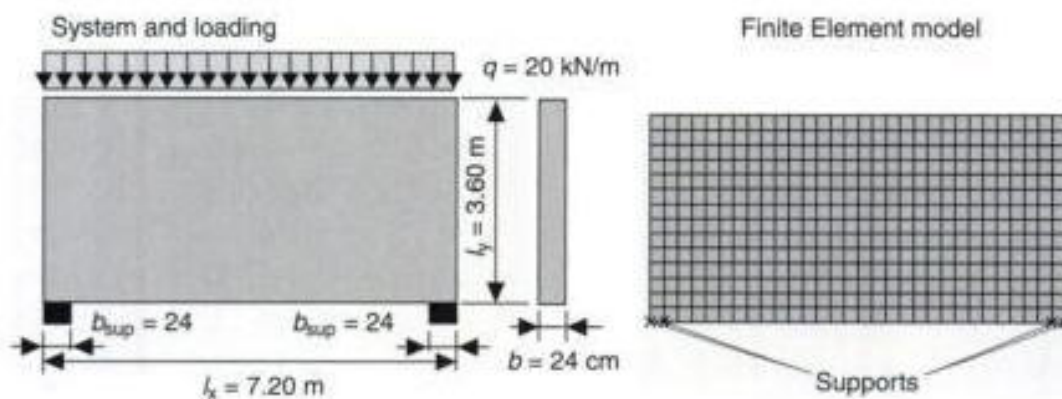


Fig. 3.22 System and element mesh

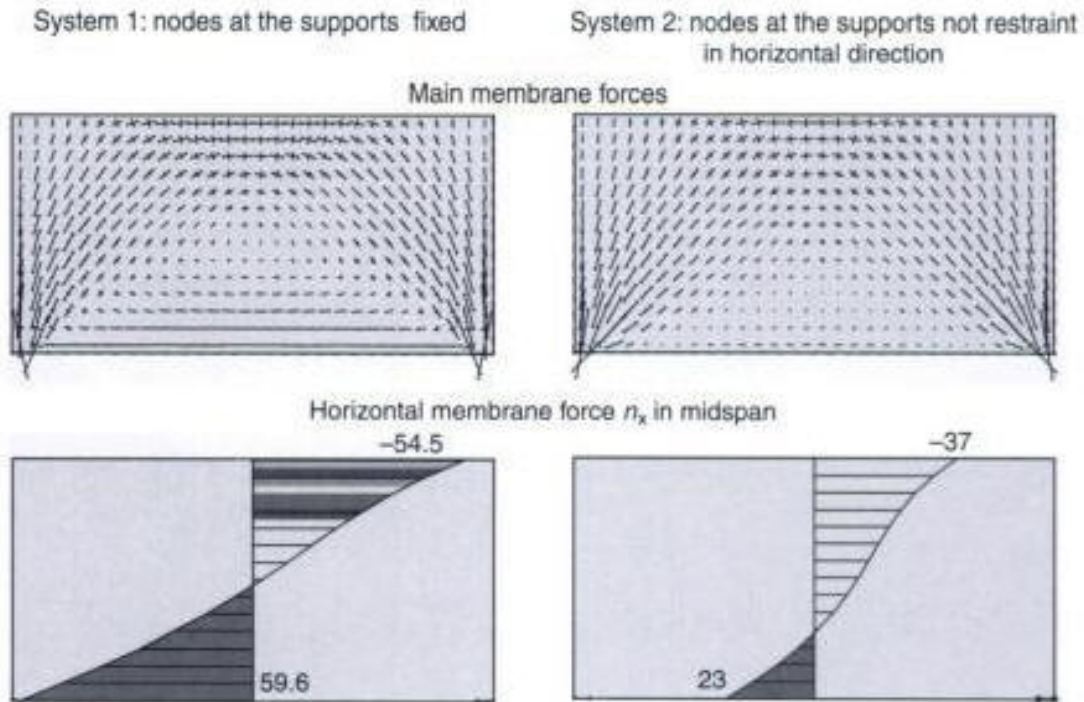


Fig. 3.23 Membrane forces with and without horizontal restraints

If one uses the manual design models provided in DAfStb 240 [10], the calculated tensile force is $F = 53 \text{ kN}$. This is the same value as the resulting tensile force of System 1. If the structure is fully restraint in horizontal direction (System 2) the resulting tensile force in midspan is only 1/5 of the value calculated of System 1, even for this very slender structure.

3.3 Dimensioning of deep beams

As already mentioned in section 3.1, individual dimensioning of each shell element of the whole structure does not result in a useful arrangement of the required reinforcement. This can be seen in Fig. 3.24, which shows the distribution for the required reinforcement as calculated automatically by the computer program for the ULS. The reinforcement requirements are estimated by dividing the total membrane forces in each element by the design yield stress of steel f_{yd} separately for each element. Thus, the horizontal reinforcement is distributed over the depth of the deep beam according to the distribution of tensile membrane force. According to Fig. 3.24, horizontal reinforcement is also required at the top of the wall in the compression zone. Here the software assumes a uniaxial compressed member and calculates the required minimum reinforcement.



Restricted Page

This page is unavailable for viewing ([why?](#)). You may continue browsing to view unrestricted pages, or visit the [About this Book](#) page.

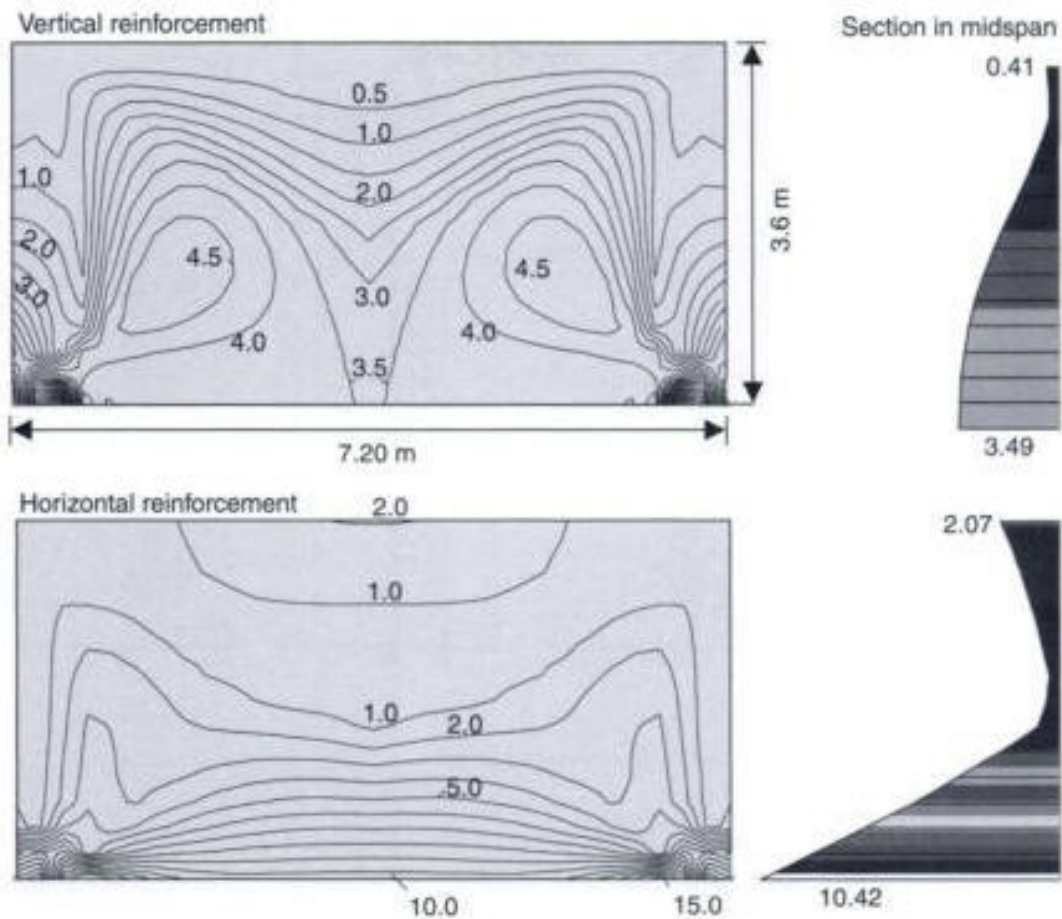


Fig. 3.25 Horizontal and vertical reinforcement (loading with $q = 152.3 \text{ kN/m}$ at the bottom edge)

height which is not greater than $0.1l$ or $0.1h$ (l = span length, h = depth of deep beam).

- The tensile reinforcement should not be staggered as per the tensile stresses. It must be anchored at the supports for a force of $0.8F_{t,\text{span}}$ (where $F_{t,\text{span}}$ is the maximum horizontal tensile force in the field).
- At the intermediate supports of multispan deep beams only straight horizontal bars should be used for the horizontal reinforcement. These bars can overlap where necessary.
- Half of the required horizontal reinforcement over the intermediate supports should go from support to support without any staggering. The rest should have a length of $2 \times 1/3l$ from the end of the support (without further anchorage length).
- Loads acting at the bottom of deep beams, i.e. loads acting in the region of a half circle with a radius of $0.5l$ (where $l \leq h$), including the self weight, should be carried by vertical reinforcement which must have a length of $l \leq h$.

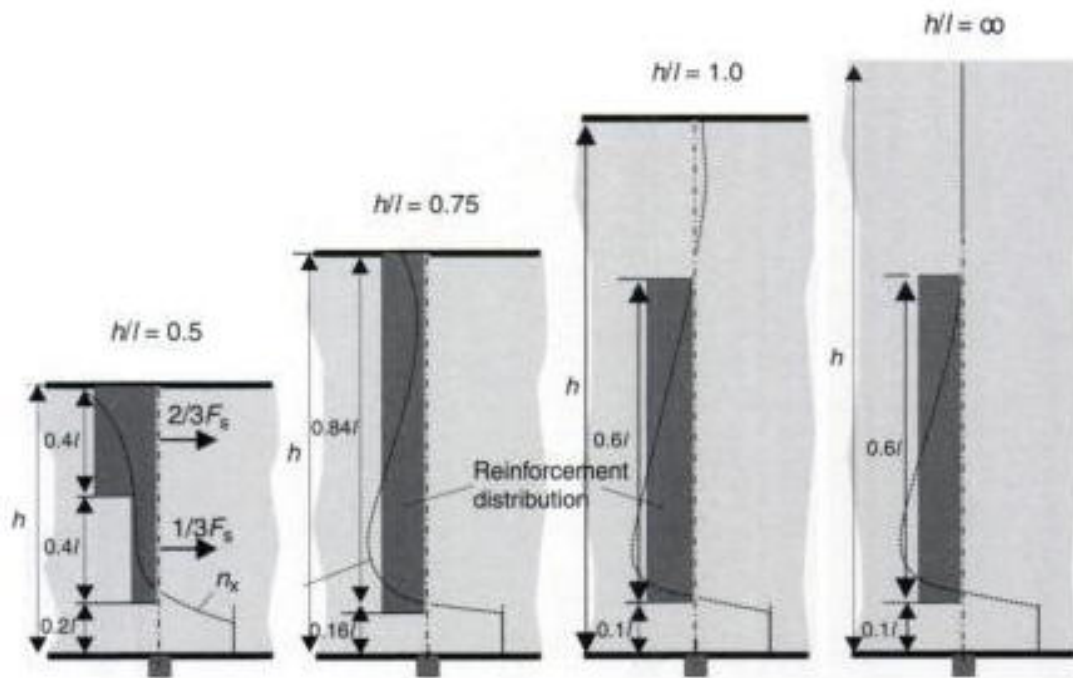


Fig. 3.26 Arrangement of the horizontal reinforcement for the tensile force F_t over the supports of multi-span deep beams [10]

As can be seen from the above list, it is not sufficient to only determine the relevant design forces.

The internal forces of ordinary beams can be estimated by using beam and shell elements. This was already demonstrated in some examples of Chapter 2. Finite Element calculations based on a linear-elastic material behaviour may be useful to determine the flow of forces in discontinuous regions, where the Bernoulli hypothesis is not valid. Examples for this are regions with highly concentrated forces, which occur when anchoring the tendons in prestressed structures, or where there are sudden changes in cross-sectional depths, like halving joints.

In order to demonstrate the problems in the automatic calculation of the required horizontal reinforcement, the following considers a 'simple' single-span beam. The advantage of this simple structure is that the required reinforcement for the ULS can be estimated manually by well-known formulae, whereas for the case of deep beams only approximate methods are available.

The single-span beam has a span length of $l = 20$ m. A uniformly distributed load of $q_k = 20$ kN/m is applied to the structure. This system is symmetric, and therefore only one half of the structure is modelled in order to reduce the amount of required calculations.

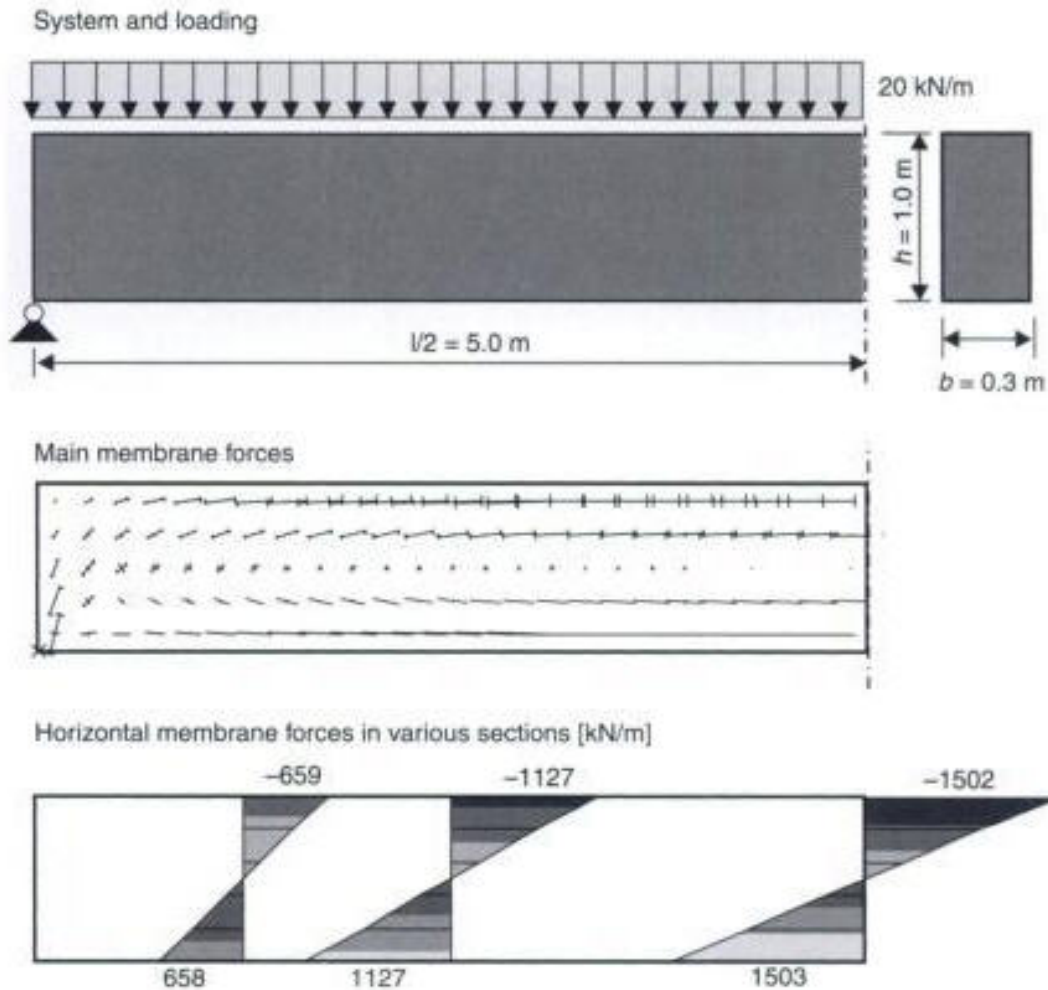


Fig. 3.27 Single-span beam: system, loading and main membrane force distribution

The member forces and the stresses can be simply estimated:

$$M_k = \frac{q_k \cdot l^2}{8} = \frac{20 \cdot 10^2}{8} = 250 \text{ kNm}$$

$$\sigma_{\max} = \frac{M}{W} = \frac{0.250 \cdot 6}{0.3 \cdot 1.0^2} = 5.0 \text{ MN/m}^2$$

$$n_{x,\max} = \sigma \cdot b = 5.0 \cdot 0.3 = 1.5 \text{ MN/m}$$

The manually calculated values are in a very good agreement with the resulting forces of the Finite Element analysis (Fig. 3.27).

A partial safety coefficient of $\gamma = 1.45$ is used for estimating the required bending reinforcement. This gives the required amount of horizontal reinforcement at the midspan (concrete grade C25/30, $f_{yk} = 500 \text{ MPa}$, $b/d/h = 0.30/0.95/1.0 \text{ m}$):

$$\text{moment coefficient } \mu_{Eds} = \frac{M_{Eds}}{b \cdot d^2 \cdot f_{cd}} = \frac{250 \cdot 1.45 \cdot 10^{-3}}{0.3 \cdot 0.95^2 \cdot 25/1.5} = 0.083$$

$$\text{inner lever arm } z = (1 - 0.7 \cdot \mu_{Eds}) \cdot d = (1 - 0.7 \cdot 0.083) \cdot 0.95 \\ = 0.897 \text{ m}$$

$$\text{required reinforcement } req A_s = \frac{M_{Eds}}{z \cdot f_{yd}} = \frac{250 \cdot 1.45}{0.897 \cdot 43.5} = 9.3 \text{ cm}^2$$

The computer program estimates the reinforcement in each element separately. For the lowest element this results in a required horizontal reinforcement of (see Fig. 3.28):

$$req A_s = (n_{x1} + n_{x2})/2 \cdot (h/5) \cdot \gamma/f_{yd} \\ = (1500 + 900)/2 \cdot (1.0/5) \cdot 1.45/43.5 \\ = 8.0 \text{ cm}^2 \text{ (over a depth of 0.2 m!)}$$

Reinforcement for the other elements is shown in Fig. 3.28. If one extrapolates the results in the middle of the bottom elements to the

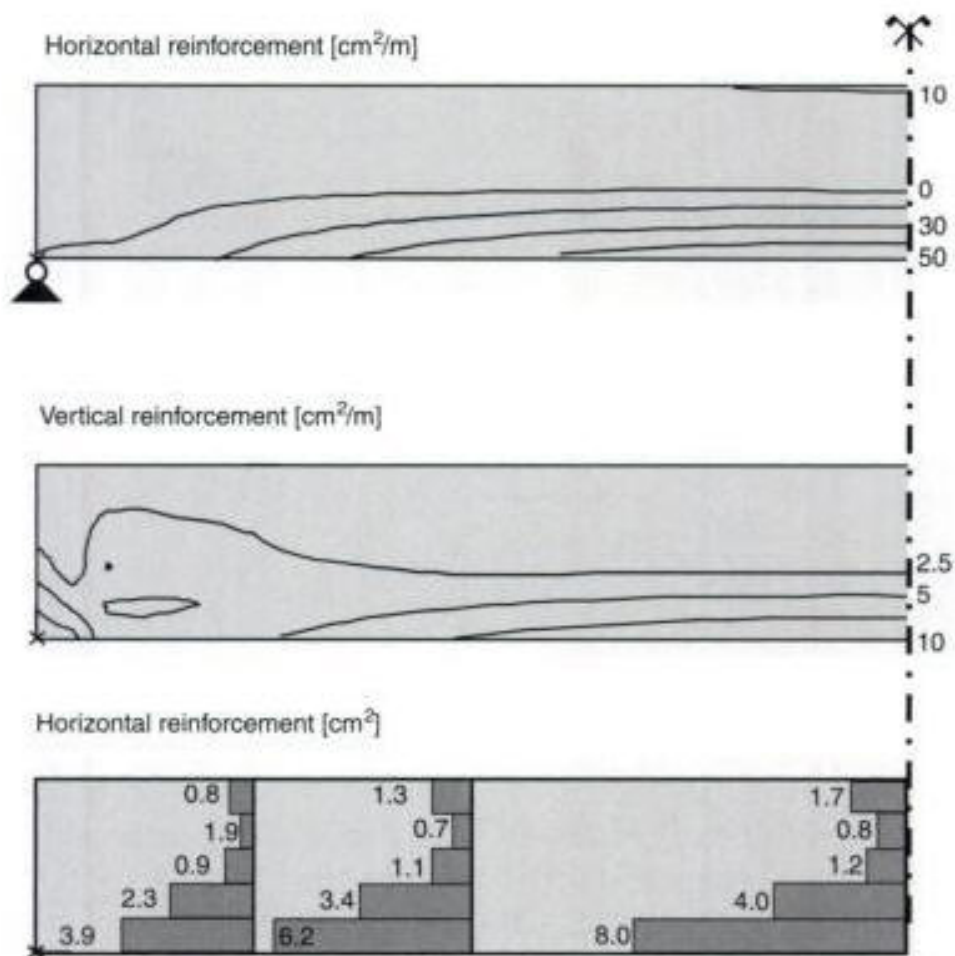


Fig. 3.28 Simply supported beam with uniform loading distribution of the reinforcement calculated by means of a shell model

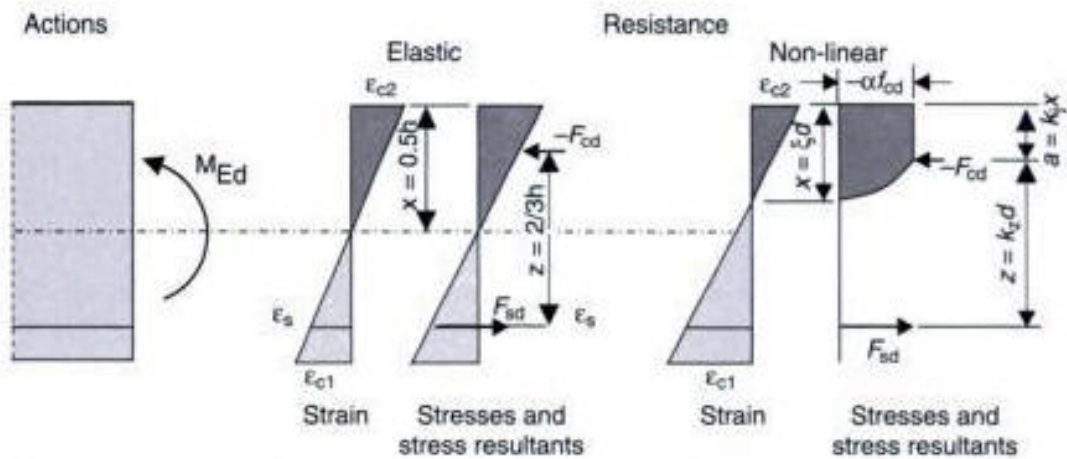


Fig. 3.29 Strain and stress distribution and internal forces of cracked and uncracked members

lower boundary, the estimated maximum reinforcement $A_{s,required}$ would be greater than 50 cm^2 .

The numerical integration of the tensile zone results in a required total reinforcement of:

$$\begin{aligned} req A_s &= (n_{x1} + 0)/2 \cdot (h/2) \cdot \gamma/f_{yd} \\ &= (1500 + 0)/2 \cdot (1.0/5) \cdot 1.45/43.5 \\ &= 12.9 \text{ cm}^2 \end{aligned}$$

Such a numerical calculation not only results in a wrong distribution of the reinforcement, but it is also uneconomical: it overestimates the reinforcement requirements by 39%. This is due to the lever arm of the internal forces of a cracked member which is greater than the one of an uncracked member (see Fig. 3.29).

$$\begin{aligned} \text{Uncracked member (Stage I): } z &= 2/3 \cdot h = 2/3 \cdot 1.0 = 0.667 \text{ m} \\ \text{Cracked member (Stage II): } z &= 0.897 \text{ m (see calc. above)} \end{aligned}$$

This is also true for deep beams. Fig. 3.28 shows the distribution of the vertical reinforcement. The estimated area of stirrups in the critical section at a distance of $1.0d$ from the face of the supports is $a_{s,w} = 5 \text{ cm}^2/\text{m}$. This is much greater than the required value calculated by the manual design. According to EC2, stirrups of area $a_{s,w} = 0.9 \text{ cm}^2/\text{m}$ are sufficient to carry the loads.

In addition, the distribution of the vertical reinforcement in the longitudinal direction is incorrect. According to the numerical analysis

(Fig. 3.28), the vertical reinforcement decreases from the midspan to the supports. This is in contrast to the normal beam theory. In the case of an ordinary single-span beam the shear forces and, thus, the required shear reinforcement increases from the midspan to the supports. The reason for this error in the shell model is the assumption of a linear-elastic uncracked material behaviour. The design for shear of a reinforced or prestressed member is usually based on a strut-and-tie model, with a fully cracked member.

This very simple example of a simply supported beam should demonstrate that the nonlinear material behaviour of concrete as well as the cracking of the composite material 'reinforced concrete', has to be considered in the design. Estimation of the reinforcement requirements by integrating the tensile forces of a linear-elastic model may lead to incorrect and unsafe values.

3.4 Strut-and-tie models

Even if the internal forces of a cracked member cannot be correctly estimated with a linear-elastic shell model, as demonstrated by the above examples, it may be very useful to gain an understanding of the flow of forces in the structure. Linear-elastic Finite Element calculations may and should be used as a basis to develop strut-and-tie models. According to EC2, Part 1, the strut-and-tie model and, especially, the location and orientation of the main compression struts should be similar to that of a linear-elastic Finite Element analysis to avoid major redistribution of forces and cracking.

Strut-and-tie models consist of straight compression and tension struts, which are connected by hinges. The truss model should be statically determined and should represent the main force distribution in the member. Schlaich and Schäfer provide further information regarding this design method [13, 34]. The main principles are explained in the following for a simple single-span deep beam.

At first one has to determine the force distribution in the member. This can be done by means of the force flow method or a linear-elastic Finite Element model. The strut locations are similar to the main compression stresses. The only unknown in the manual analysis for the given single-span deep beam is the location of the horizontal compression strut, respectively the distance z_1 and z_2 (see Fig. 3.30). The horizontal compression and tension struts are located in the centre of the stress field at the midspan. Thus, the increase of the lever arm of the cracked member under ultimate loads is neglected.

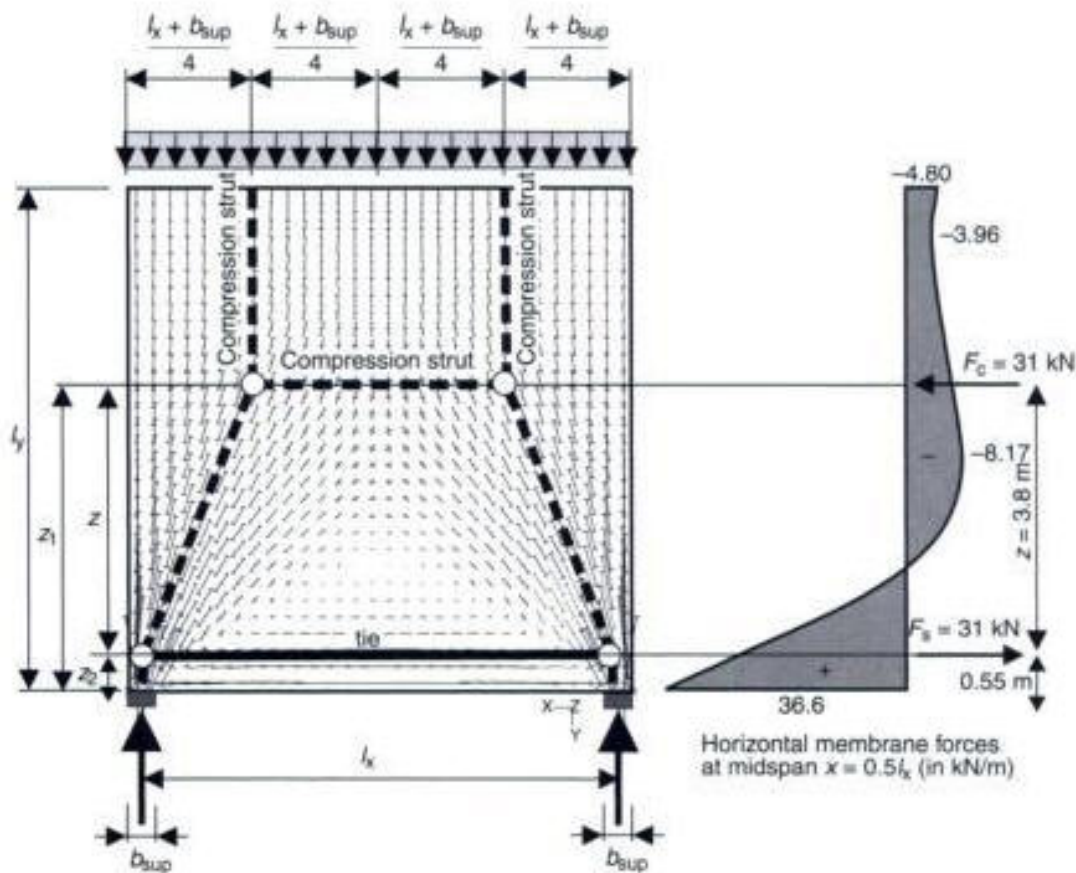


Fig. 3.30 Strut-and-tie model for a single-span deep beam

The strut-and-tie model is a statically determined truss structure. Thus, all forces can be estimated from the geometry of the truss system. The resulting tensile force for the given structure ($l_x = l_y = 7.20$ m; $a = 0.48$ m; $q = 20$ kN/m) is:

$$F_t = \frac{l_x - a}{4} \cdot \frac{q \cdot l/2}{z} = \frac{7.20 - 0.48}{4} \cdot \frac{20 \cdot 7.2/2}{3.8} = 31.8 \text{ kN}$$

The calculated force is nearly identical to the value given in [10]. There is a small difference of 3 kN only (see Table 3.1).

In the above example, the reinforcement requirements are estimated from the resulting tensile forces. But, as will be shown later, this reinforcement can be inadequate with respect to the serviceability of a structure. Fig. 3.31 shows the distribution of the main membrane forces and the resulting strut-and-tie model for a double-span deep beam ($l_x/l_y = 2 \times 7.5/3.65$ m). The model is nearly identical to that of a single-span deep beam. The tensile force at the inner support is the only addition to be considered. The tensile reinforcement at the

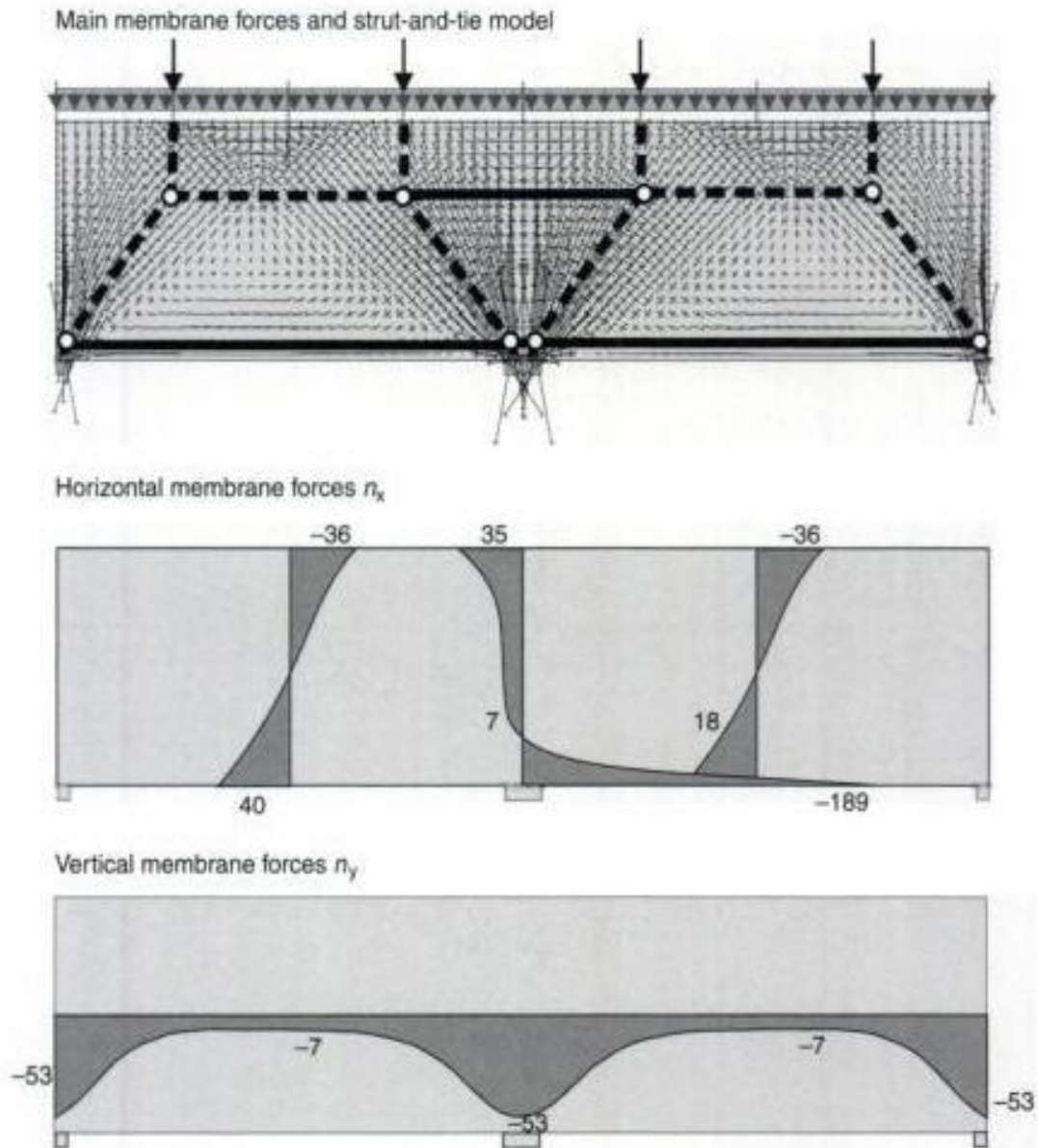


Fig. 3.31 Two-span deep beam ($l_x/l_y = 2 \times 7.5/3.65$ m)

midspan must not be concentrated at the centre axis of the tensile zone but at bottom of the deep beam.

Figure 3.32 shows the same system with a small opening near to the left support. Here the reinforcement calculated from the resulting tensile forces is insufficient. A linear-elastic calculation does not show any vertical tensile forces near the opening. This is in contrast to engineering practice and contradicts with the strut-and-tie model. Vertical reinforcement is required.

Therefore, the nonlinear behaviour of the material has to be considered when developing a strut-and-tie model.

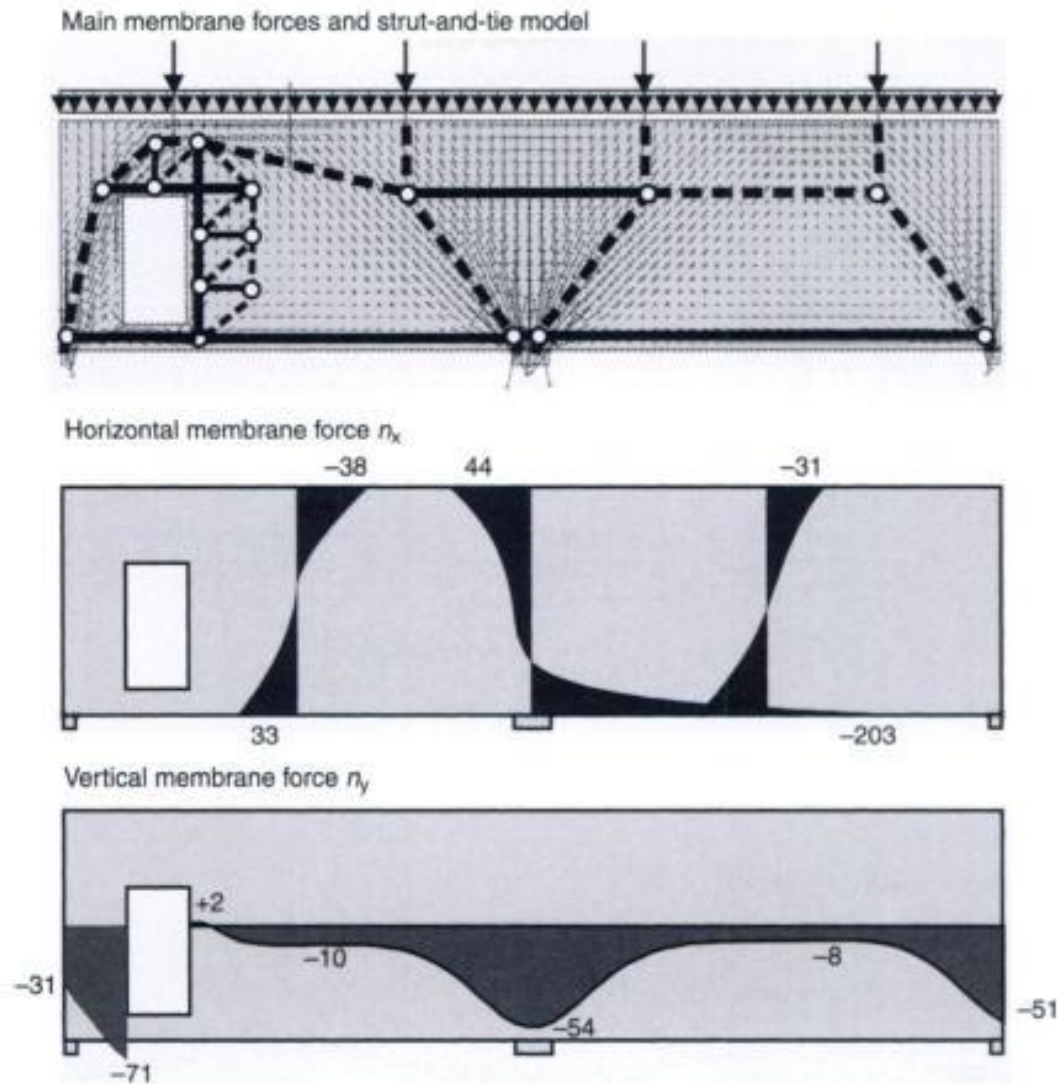


Fig. 3.32 Two-span deep beam ($l_x/l_y = 2 \times 7.5/3.65$ m) with an opening

3.5 Singularities

In shell systems, infinite stresses and deformations (singularities) may be calculated, which are caused by the assumptions of the numerical model. Examples of these singularities are (see Fig. 3.33, Table 3.4):

- corners (free or fully restrained);
- concentrated loads or pin supports.

A Finite Element analysis will always estimate finite results, whereby the maximum stress will increase considerably with any decrease in the element size. The 'exact' calculation of the maximum value of the stresses is generally not required, as the problems are caused by the simplifications of the numerical model, an inaccuracy of the

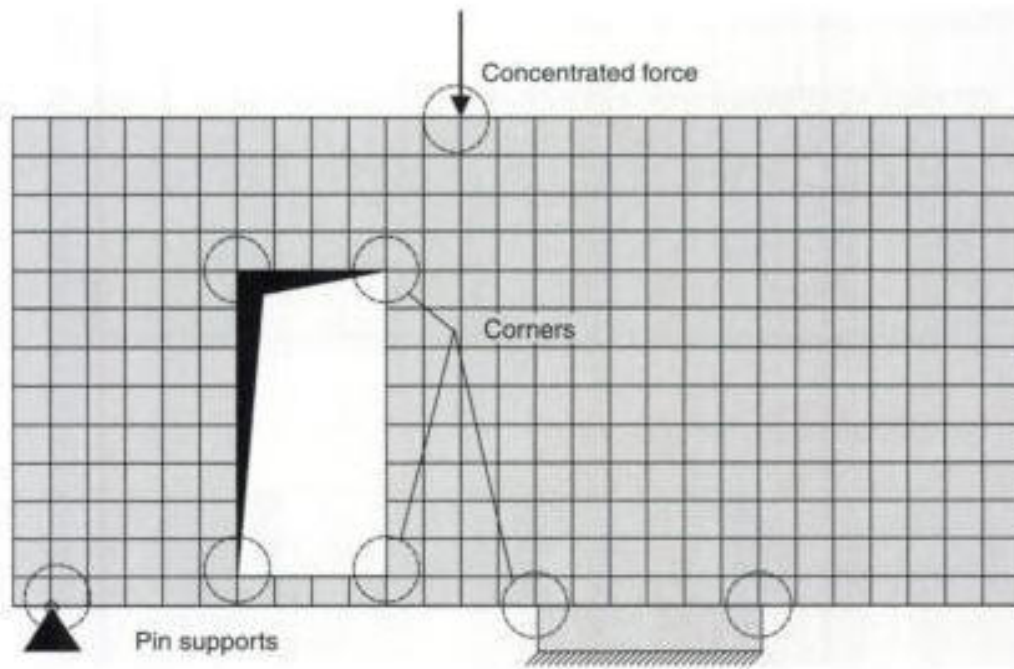


Fig. 3.33 Singularity regions in walls and deep beams

Table 3.4 Singularity regions in plane shell structures (walls and deep beams)

Reactions resp. forces	Displacements	Stresses	Support condition	Stresses infinite for
	Yes	Yes		$\alpha > 180^\circ$
	No	Yes		$\alpha > 180^\circ$
	Yes	Yes		$\alpha > 63^\circ$
	Yes	Yes		$\alpha > 63^\circ$
	No	No		
	No	Yes (σ_x)		
	No	No		
	No	No		

boundary conditions. A real structure does not show any singularities. In the case of high stresses, the material will 'yield'. In tensile regions the concrete will crack. Furthermore, in discontinuity regions the stress distribution is a complex three-dimensional one which will not be modelled with plane shell elements. The main concern will be the good detailing of the reinforcement in the corner regions and in the area of concentrated loading.

Numerical problems with concentrated loads can be avoided if the width of the loaded area is considered. The same is true for pin supports. But any refinement of the numerical model is generally not required, as the stress distribution in these regions is not needed for the design.

Restricted Page

This page is unavailable for viewing ([why?](#)). You may continue browsing to view unrestricted pages, or visit the [About this Book](#) page.

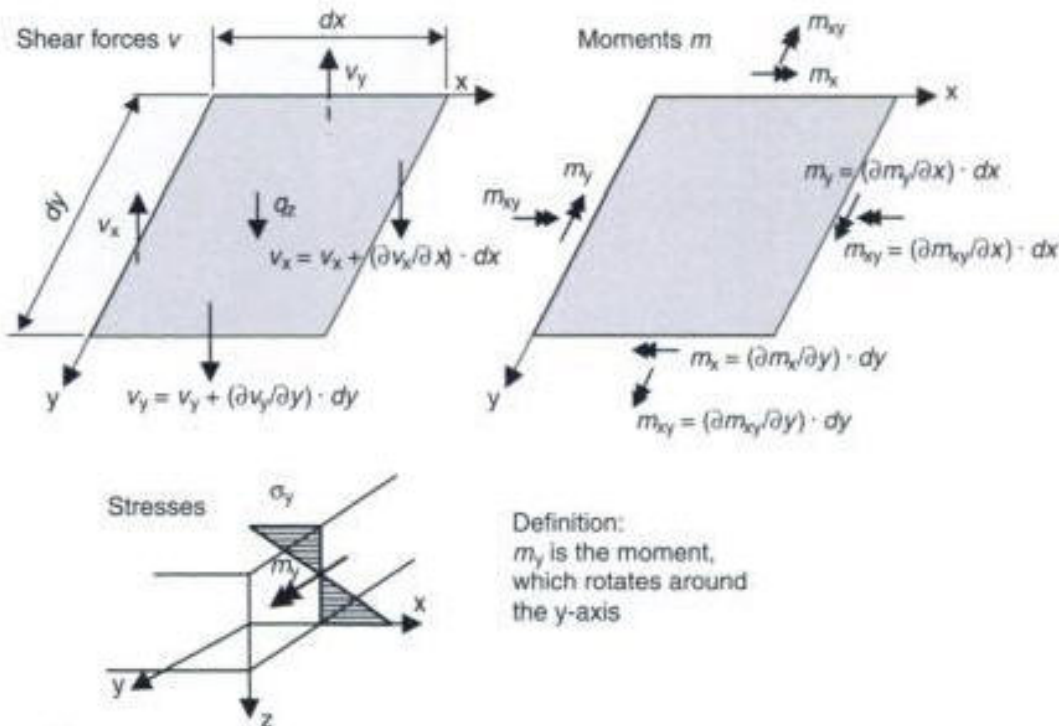


Fig. 4.1 Internal forces and stresses of a finite plate element

- small vertical displacements ($w \ll h$; I. Order theory);
- linear strain distribution over the section depth (Navier);
- no strains at the middle plane (i.e. no normal or membrane forces);
- stresses in normal direction can be neglected;
- plane sections remain plane before and after loading (Bernoulli-Euler).

The basics of a plate analysis are not mentioned any further in this book as extensive information on this topic has been already published [e.g. 23 and 24].

An analytical solution of the partial differential equation $\Delta\Delta w = q/K$ (Kirchhoff slab equation; where K is the flexural rigidity of the plate $K = [E_c h^3] / [12(1 - \nu^2)]$) is only possible for axisymmetric structures and loading, e.g. circular slabs. The shear forces and moments of rectangular slabs can only be estimated by means of numerical methods. The Kirchhoff slab equation was solved by Fourier analysis or Finite Difference approximations [23, 25] and various weighted residual procedures before efficient computer hardware and software were available. Nowadays the Finite Element Method is generally used, as it is more flexible with regard to the boundary conditions and the load arrangements.

Slabs can be analysed manually by means of the strip method. In this approach, the two-dimensional load transfer is simplified to two ordinary beams or a grillage. This simple method is still applied to this

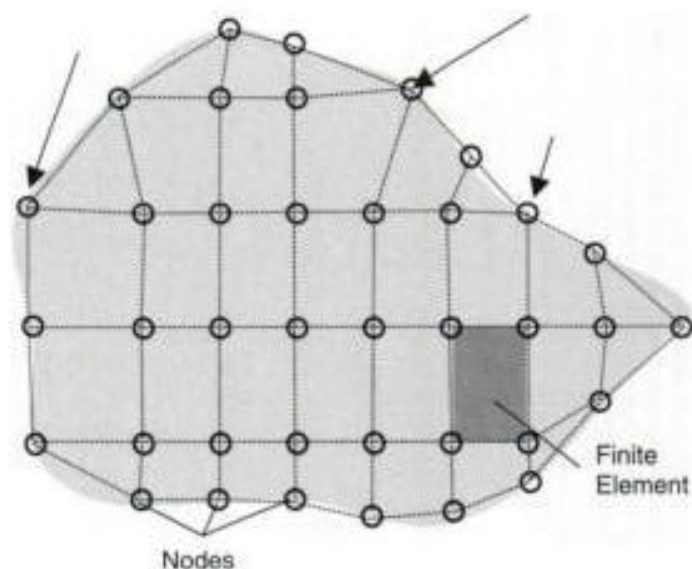


Fig. 4.2 Discretization of a slab

day, as has been shown in section 2.8. Nevertheless, the two-dimensional behaviour of slabs (dispersion of loads) is represented much more accurately by Finite Element models using plate and shell elements.

In recent years the Finite Element Method has become a standard tool for the analysis of spatial structures. The practical applications have dramatically increased with the significant improvement of the software. The graphical pre- and post-processing makes it fast and easy to handle whole buildings, including all slabs, walls, columns, and foundations within one big numerical model. Also the hardware has become much faster. But complex Finite Element models include a big danger, as the collapse of the Sleipner Platform (see section 5.1.1) has impressively demonstrated. Therefore, only simple flat slabs will be mentioned in the following.

In the Finite Element Method, the slab is divided into small finite elements (discretization of a continuum), which are connected to each other by their nodes (Fig. 4.2). The deflections, strains, and internal forces within an element are interpolated from the node displacements by means of so-called form functions, which are mostly polynomials. The form function may but must not fulfil the compatibility conditions at the boundaries between the elements. Therefore, the deformations, strains and stresses, as well as the internal forces may be discontinuous between the elements. The difference of the stresses at the boundaries may be used to verify the quality of the Finite Element model.

A detailed description of the basis of the Finite Element Method is explained in various literature (e.g. [1–3]). Therefore, no further theoretical information regarding the theory is provided here.

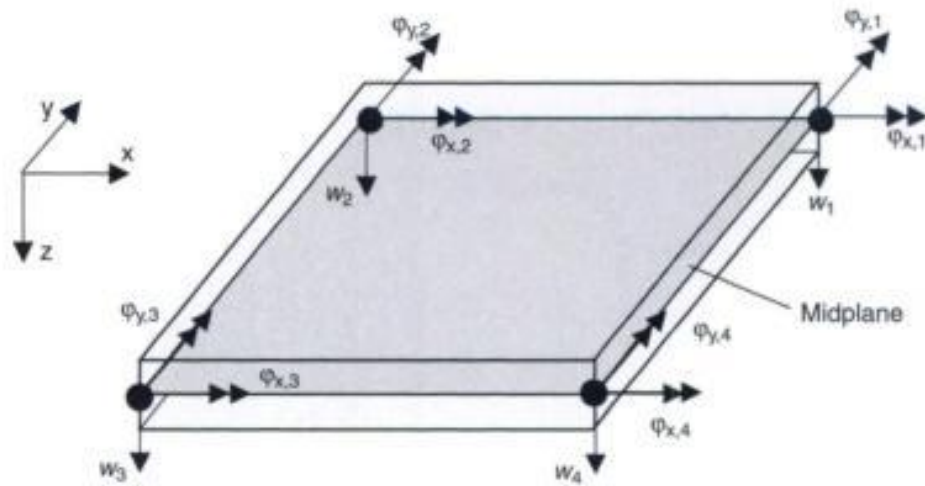


Fig. 4.3 Degrees of freedom of a 4-node plate element

The required effort to generate an adequate Finite Element model has decreased dramatically due to the availability of user-friendly graphical pre-processors. In the near future, it may even be possible to perform the analysis and design of the slab for a 'simple' one-storey residential building (like the one shown in Fig. 4.4) by means of the

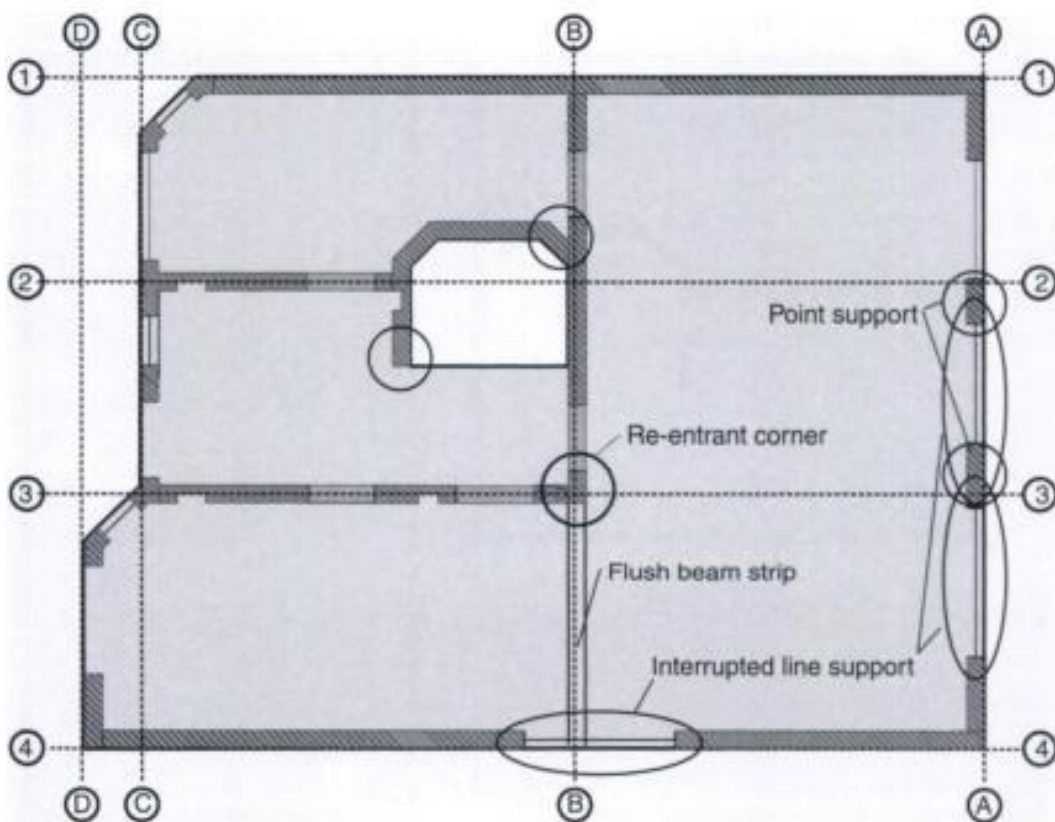


Fig. 4.4 Slab of a simple one-storey residential building

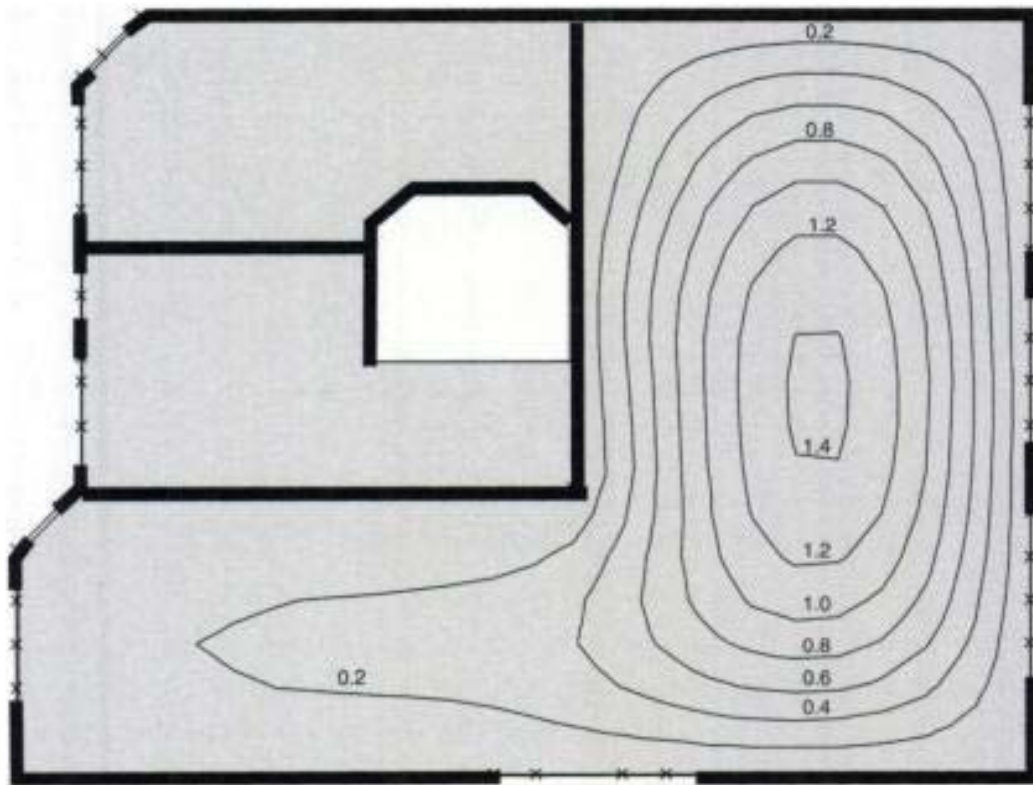


Fig. 4.4a Deflections in mm (linear-elastic material behaviour)

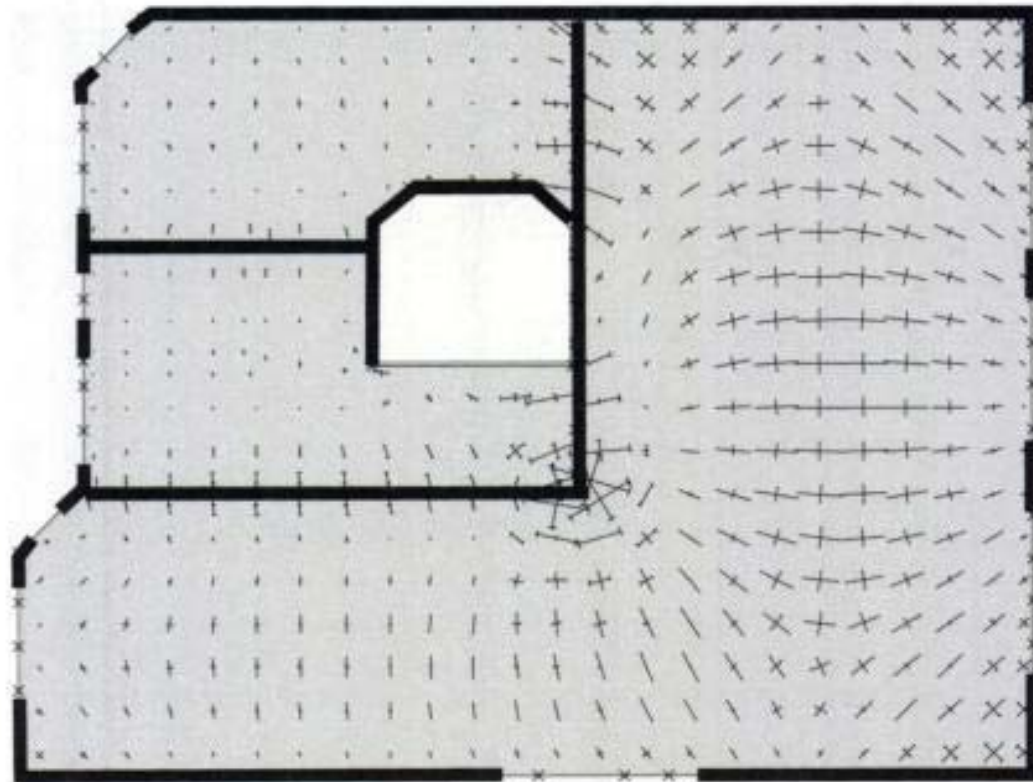


Fig. 4.4b Tensor plot of the principal bending moments



Restricted Page

This page is unavailable for viewing ([why?](#)). You may continue browsing to view unrestricted pages, or visit the [About this Book](#) page.

Finite Element techniques instead of manual calculations. Therefore, one may worry that Finite Element programs will be more and more used by designers without a proper understanding of the method. This problem becomes even worse as a main advantage of the Finite Element Method is that the user does not have to simplify the load transfer of a structure as by manual analysis. Therefore, young engineers without structural experience tend to use the numerical method. This may lead to mistakes in the results which may even cause the collapse of a structure (see section 5.1.1).

It should always be kept in mind that a numerical model is only a simplification of reality. It is only as accurate as its basic assumptions. Therefore, it must be especially understood that the usage of the Finite Element Method requires experience.

When using the Finite Element Method, the following items should always be checked:

- *correct modelling of the support conditions*
 - pin and simple line supports
 - girders (joists)
 - flush beam strips in slabs
 - support by masonry or concrete walls and columns, or elastomer bearings
 - is the slab monolithically fixed to the supports or can uplift occur?
 - discontinuous simple support (e.g. supporting walls which end within the slab)
 - continuously supported on ground.
- *location and orientation of the fixed nodes*
relevant in case of curved boundaries.
- *singularities*
regions where the internal forces and deflections of a slab may become infinite.
- *size of elements*
should be checked in regions with high deformation and stress gradients.
- *numerical–mechanical models*
 - form functions: polynomial functions of first or higher order
 - Kirchhoff or Reissner/Midlin models.

It is not necessary to use complex structures to demonstrate the problems of the Finite Element Method. Even the slab of a simple one-storey residential building (Fig. 4.4) is sufficient. The manual design of this slab can be easily and quickly performed by means of the strip

method. Therefore, this structure is only used here to demonstrate the problems of the Finite Element Method.

The real system is simplified for a Finite Element analysis. A simple line support is assumed underneath all supporting walls (breadth of support neglected), whereby small openings like that of doors or windows are neglected. The slab thickness is $h = 0.18$ m. Concrete grade C20/25 is assumed for the building material. The slab is discretized by 451 plane plate elements. Figures 4.4a to 4.4d show the internal forces and deflections for a uniformly distributed load of $g_d = 5.0 \text{ kN/m}^2$. For simplicity, the most unfavourable arrangements of live loads are not considered here. Very high bending moments and shear forces can be observed in axis B-2 and B-3. The design of the slab for these high bending moments and shear forces is impossible. Even an inexperienced user can recognize this problem. As an engineer, he has to know that the design for such high internal forces is not required. These peaks are caused by simplifications of the numerical model (singularities, see section 4.11). In the following sections such problems in the model for reinforced concrete slabs will be discussed with emphasis on the accurate representation of the support conditions.

Most engineers believe that a 'complex' numerical calculation saves reinforcement, where the structural system is modelled with greater accuracy than in a manual design. This is very often not the case. A comparison between the manual and the Finite Element design of the slab shown in Fig. 4.4 has resulted in a very small or negligible difference in the amount of reinforcement required. Thus, this simple example demonstrates that a more detailed design may not be economical, when considering the great effort required for a numerical analysis and the resulting labour cost of the designer.

4.2 Material parameters – Poisson's ratio

The analysis of a slab is usually based on the linear-elastic isotropic behaviour of the building material concrete. The nonlinear behaviour of concrete and its reduction in stiffness in the case of crack formation are neglected. With this simplification, only two different material parameters, the modulus of elasticity E_c and Poisson's ratio ν , are needed in the design. The modulus of elasticity can be taken either from tests or from codes [6] whereby the creep effect has to be taken into account. Poisson's ratio ν is not an exact value for reinforced concrete. Values varying from $\nu = 0.0$ to $\nu = 0.2$ are generally used.

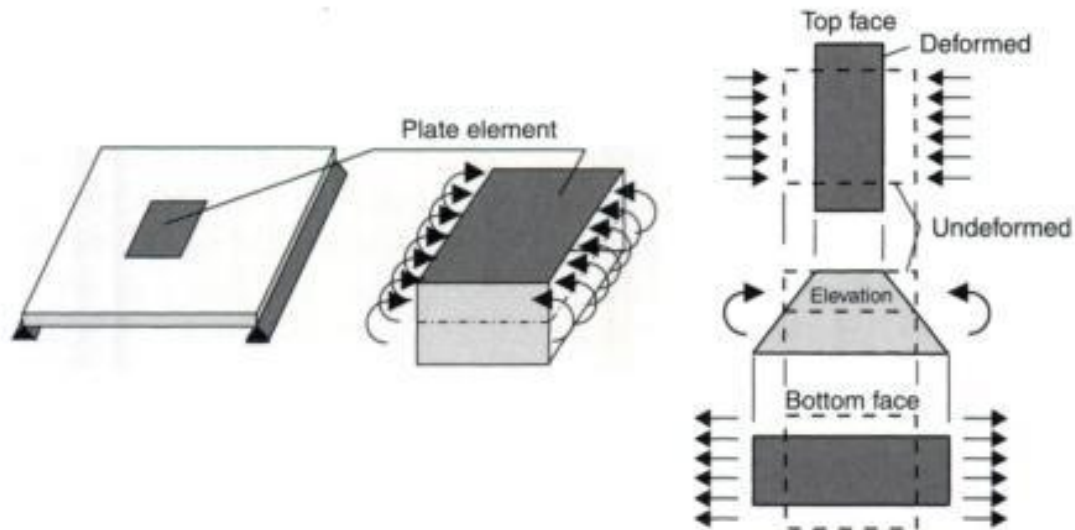


Fig. 4.5 Strain in transverse direction of a linear-elastic plate element under bending (one-way slab)

The Poisson's ratio ν is defined for an elastic member as the ratio between the lateral strain and the axial strain. According to EC2, Part 1 [6] 3.1.2.5.3, the Poisson's ratio in an uncracked compression region of the cross-section may be taken as $\nu = 0.2$, which is the mean value of a 'homogeneous' uncracked concrete under compression. In the tension zone, ν may be assumed to be equal to zero. However, this information is not very helpful as a slab under pure bending always has a compression and a tension zone (Fig. 4.5).

Bittner [26] has conducted theoretical investigations to determine the correct value for Poisson's ratio. He proposed that a value of $\nu = 0.0$ should be used in the design of reinforced concrete slabs. With this value the compressive stresses are underestimated. This is not mostly critical, as the compressive stresses are usually not relevant in the design.

So the structural engineer can choose any value for ν between 0.0 and 0.2 for the design. The influence of Poisson's ratio on the internal forces will be discussed in the following box.

The Kirchhoff plate theory leads to the following expressions, which show the influence of the Poisson's ratio on the bending moments, the shear forces and the corner tie-down force.

Based on these expressions the bending moments m_x and m_y are proportional to Poisson's ratio ν . When ν is decreased, the twisting moment m_{xy} and the corner tie-down force F_e are reduced.

The simplified expressions are verified by a parametric study on a rectangular simply supported slab ($l_x = 5.0$ m, $l_y = 5.0$ to 7.5 m, and

Internal forces according to the Kirchhoff theory

$$m_x = -K \cdot \left(\frac{\partial^2 w}{\partial x^2} + \nu \cdot \frac{\partial^2 w}{\partial y^2} \right) \approx m_x^{\nu=0} + \nu \cdot m_y^{\nu=0} \quad m_{xy} = -K \cdot (1 - \nu) \cdot \left(\frac{\partial^3 w}{\partial x \partial y^2} \right)$$

$$m_y = -K \cdot \left(\frac{\partial^2 w}{\partial y^2} + \nu \cdot \frac{\partial^2 w}{\partial x^2} \right) \approx m_y^{\nu=0} + \nu \cdot m_x^{\nu=0} \quad \nu_x = -K \cdot \left(\frac{\partial^3 w}{\partial x^3} + \nu \cdot \frac{\partial^3 w}{\partial x \cdot \partial y^2} \right)$$

$$F_c = 2 \cdot m_{xy} = 2 \cdot (1 - \nu) \cdot F_c^{\nu=0} \quad \nu_y = -K \cdot \left(\frac{\partial^3 w}{\partial y^3} + \nu \cdot \frac{\partial^3 w}{\partial x^2 \partial y} \right)$$

where:

$$K = \frac{E_c \cdot h^3}{12 \cdot (1 - \nu^2)} = \text{flexural rigidity of the slab} \quad w = \text{deflection of the slab}$$

$$F_c = \text{corner tie-down force (uplifting)} \quad \nu = \text{Poisson's ratio}$$

$h = 0.20$ m), as shown in Fig. 4.6. The internal forces have been estimated for different Poisson's ratios by means of the Finite Element Method. The midspan bending moment m_{ym} is oriented along the longer panel dimension, and increases almost linearly with an increasing Poisson's ratio. This agrees with the expressions listed before. With an increase in Poisson's ratio, the twisting moment m_{xy} and the corner tie-down force F_c decrease linearly. The bending moment m_x and the shear forces are not shown in Fig. 4.6, as they are only slightly affected by Poisson's ratio. The maximum shear force

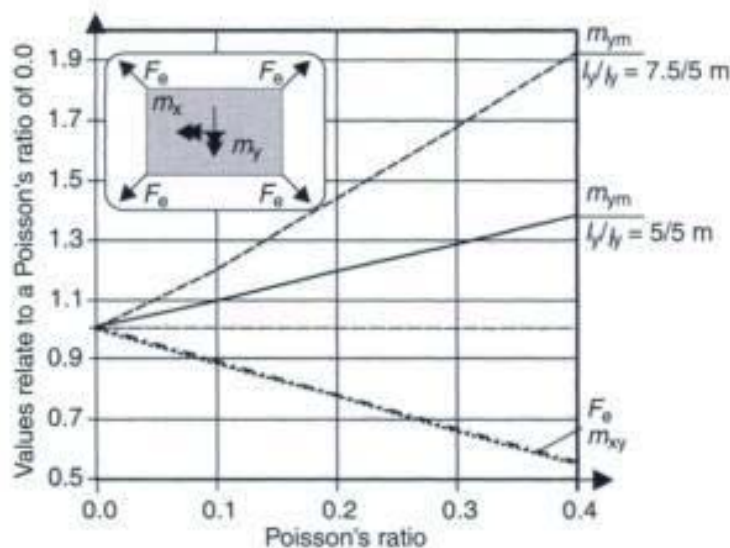


Fig. 4.6 Bending moment m_y , twisting moment m_{xy} , and corner tie-down force F_c for different Poisson's ratios ν ($l_x/l_y = 5.0/5.0$ m and $5.0/7.5$ m, and $h = 0.20$ m)

at the support at midspan decreases by less than 10% if Poisson's ratio increases from $\nu = 0.0$ to $\nu = 0.4$. The maximum deflection at midspan is approximately reduced by 20%.

In slabs, the secondary transverse reinforcement should not be less than 20% of the principal reinforcement [6]. Thus, the value of the Poisson's ratio is often not critical. But this minimum transverse reinforcement has to be considered in the Finite Element design of slabs.

4.3 Support conditions for slabs

Modelling of the support conditions of slabs should be done with great care, as they have a significant influence on the results.

The following support conditions may occur in practice:

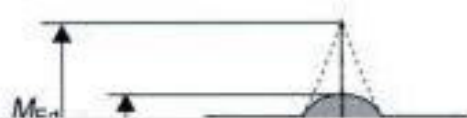
- continuous support of the whole slab or part of it by the ground;
- knife-edge (line) support on walls – free to uplift or fully or partially restrained;
- pin support on columns, e.g. flat slabs.

Normal forces, as well as bending moments, can be transferred if the slab is monolithically connected to the support. The stiffness of the support can be represented either by individual springs or by special boundary elements. In both cases, the rotational stiffness of the springs should be determined with regard to the nonlinear behaviour of the concrete and the reduction of stiffness in case of cracking.

Where the supports have different vertical stiffness values, any possible deflection of the supports should be considered. This can be the case for flat slabs which are supported by columns with different cross-sections or normal forces. Slabs usually have only a small bending stiffness. Thus, the influence of the differential deformation on the internal and support forces can be mostly neglected.

If the slabs are supported on different building materials, having different time-dependant properties, then the time-dependant deformations of the supports (e.g. due to creep or shrinkage) should be considered. A wall made of gypsum – or sand-lime concrete – blocks may become lower with time, whereas the height of a clay-brick wall remains nearly constant. Differential settlements of the foundations should be considered if relevant.

Various numerical models are used in practice to describe the support conditions of slabs. These may result in rather different internal forces in the restraint regions. However, one should not compare the maximum peak values. Only the bending moments and shear forces



Pin support:
smoothed bending moment

Restricted Page

This page is unavailable for viewing ([why?](#)). You may continue browsing to view unrestricted pages, or visit the [About this Book](#) page.

to determine the 'accurate' model of flat slabs, where analytical solutions are not available.

4.4 One-way slab

The following analysis will be carried out on a two-span, simply supported, one-way slab having equal span length of 2×5.0 m (Fig. 4.8). The slab has a constant depth of $h = 0.20$ m. The intermediate support has a breadth of 25 cm. For this simple structure the internal forces can easily be estimated by manual calculations (see Fig. 4.9). These values will be used to verify the numerical results.

Two different load cases are considered:

- Load case 1: uniform loading of $q = 10 \text{ kN/m}^2$ on both spans;
- Load case 2: uniform loading of $q = 10 \text{ kN/m}^2$ on the left span only.

The different models for a support on walls which are used in practice are shown in Fig. 4.10.

- (a) *Three-dimensional model of the whole structure (column and walls) by 3-D elements*

If the whole structure behaves linear elastic then the load-bearing behaviour of the system is modelled with great accuracy by means of a 3-D model. However, the assumption of an uncracked section over the intermediate support is not valid, as it is very likely that the tensile stresses exceed the tensile strength of the concrete. Moreover, a great effort has to be spent to handle a three-dimensional volume or even a two-dimensional shell model, which is often not required. It should be noted that the problems arise when the reinforcement requirements are being estimated. Therefore, in practice, a 3-D shell model is very rarely used.

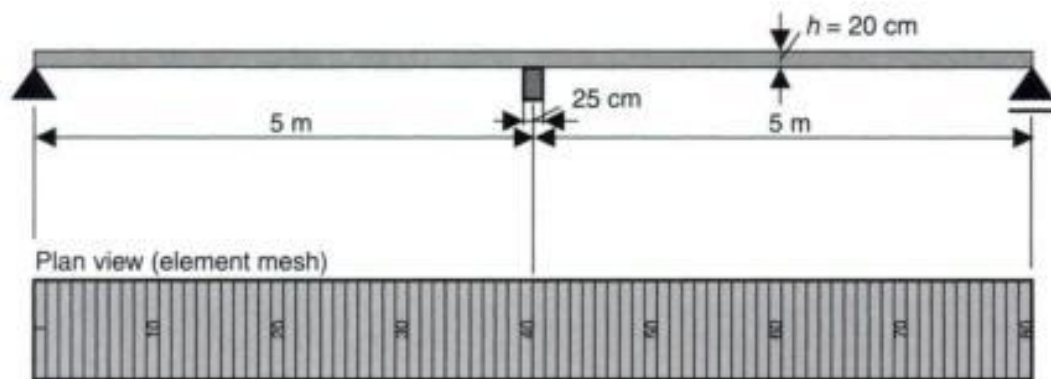
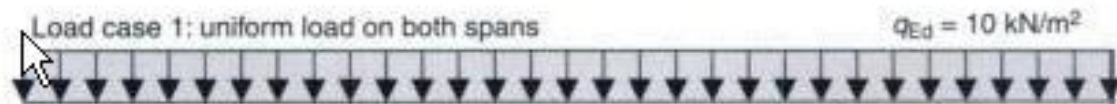


Fig. 4.8 System



Restricted Page

This page is unavailable for viewing ([why?](#)). You may continue browsing to view unrestricted pages, or visit the [About this Book](#) page.

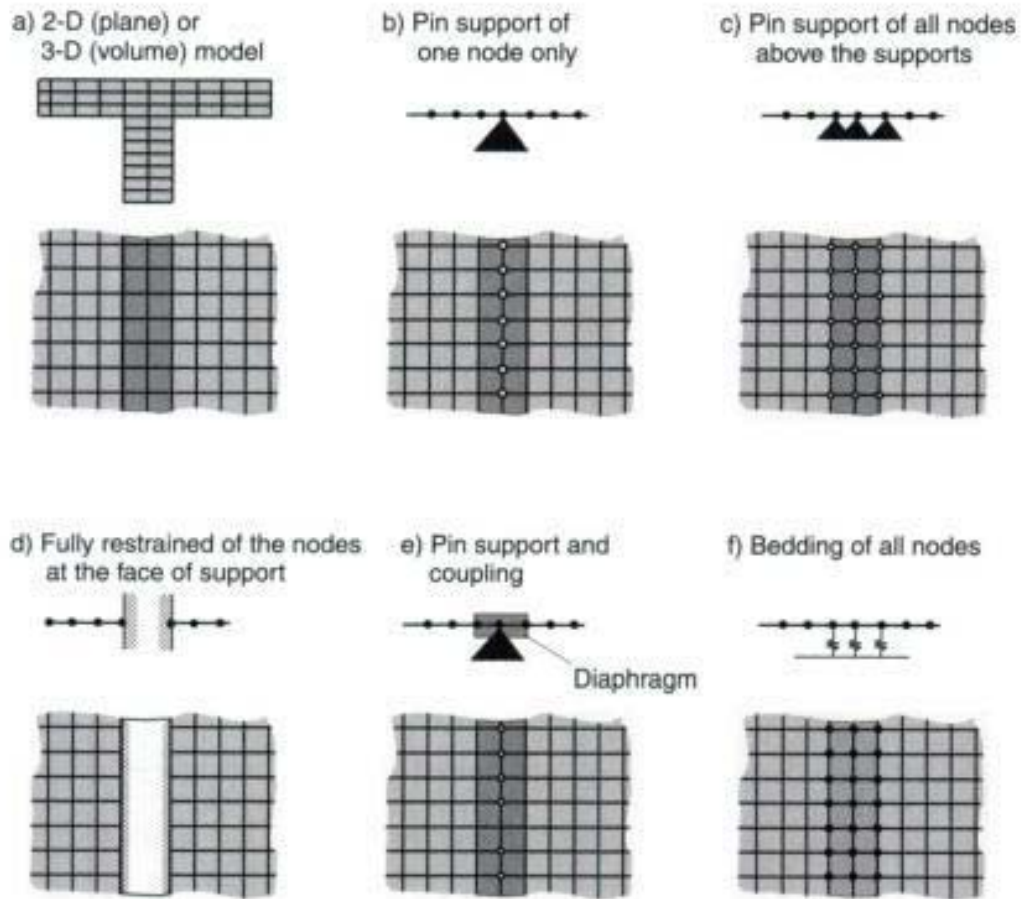


Fig. 4.10 Models for line support of slabs

(e) *Coupling of nodes*

The nodes at the support are coupled with the node in the centre of the support to simulate an infinite stiff element which can rotate around the centre node. This model has already been discussed in section 2.6.3.

(f) *Bedding of the supported elements*

The elements over the wall are elastic supported. A flexible, plane support is simulated.

The different bending moment distributions, resulting from the models described above, are shown in Figs 4.11 and 4.12. The relevant results are further summarized in Table 4.1.

Model B (pin support of one node only) gives a good correlation between the beam and the Finite Element (plate element) results for both load cases. Any further refinement of the element mesh does not change the results. Knife-edge supported one-way slabs do not show any singularities.

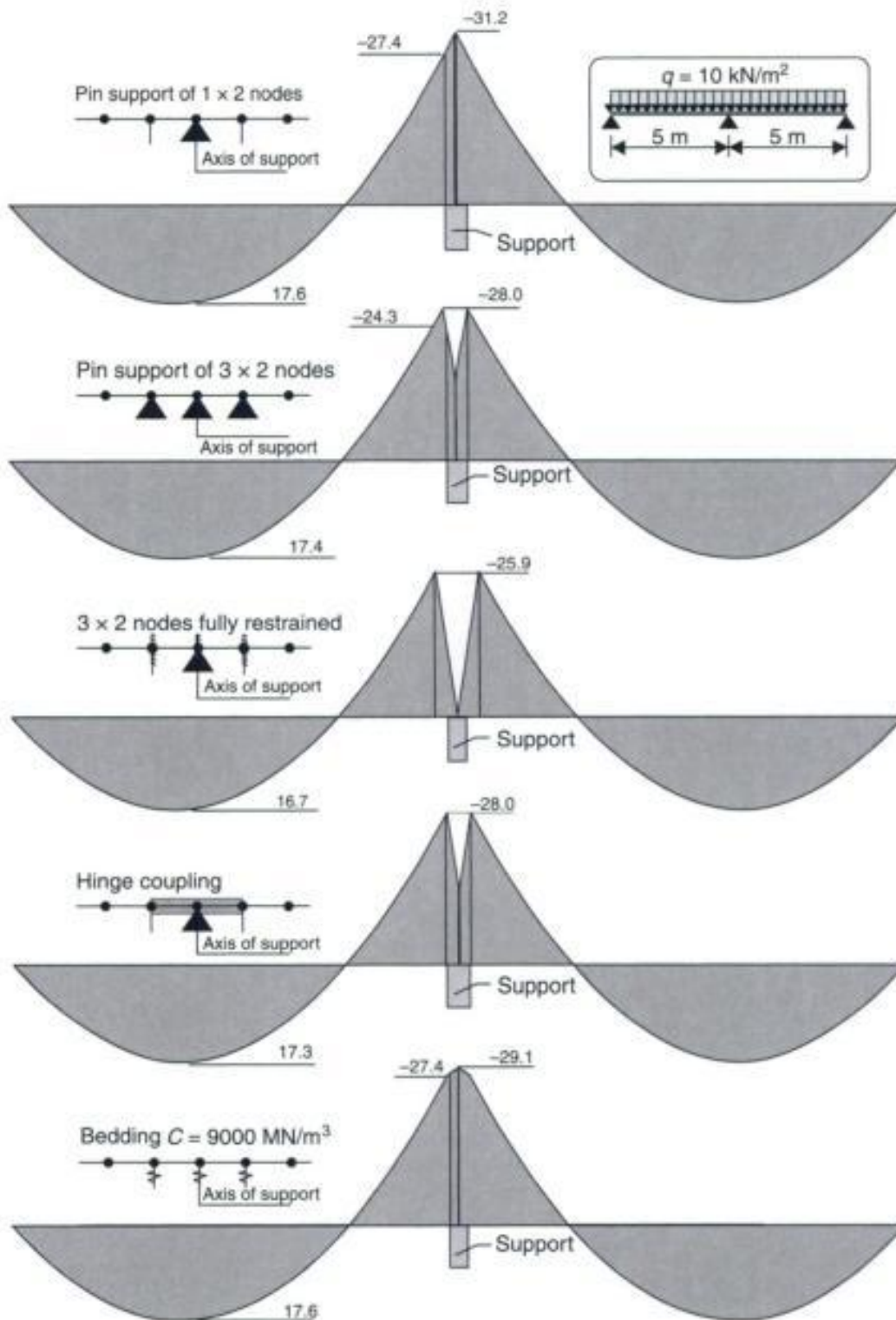


Fig. 4.11 Bending moments – uniform load at both spans – plate elements

If three nodes are restrained in a vertical direction at the support (Model C), the resulting bending moments at the face and those at the centre of the support are underestimated for uniform loading over both spans by 89% and 47%, respectively. On the other hand, if only

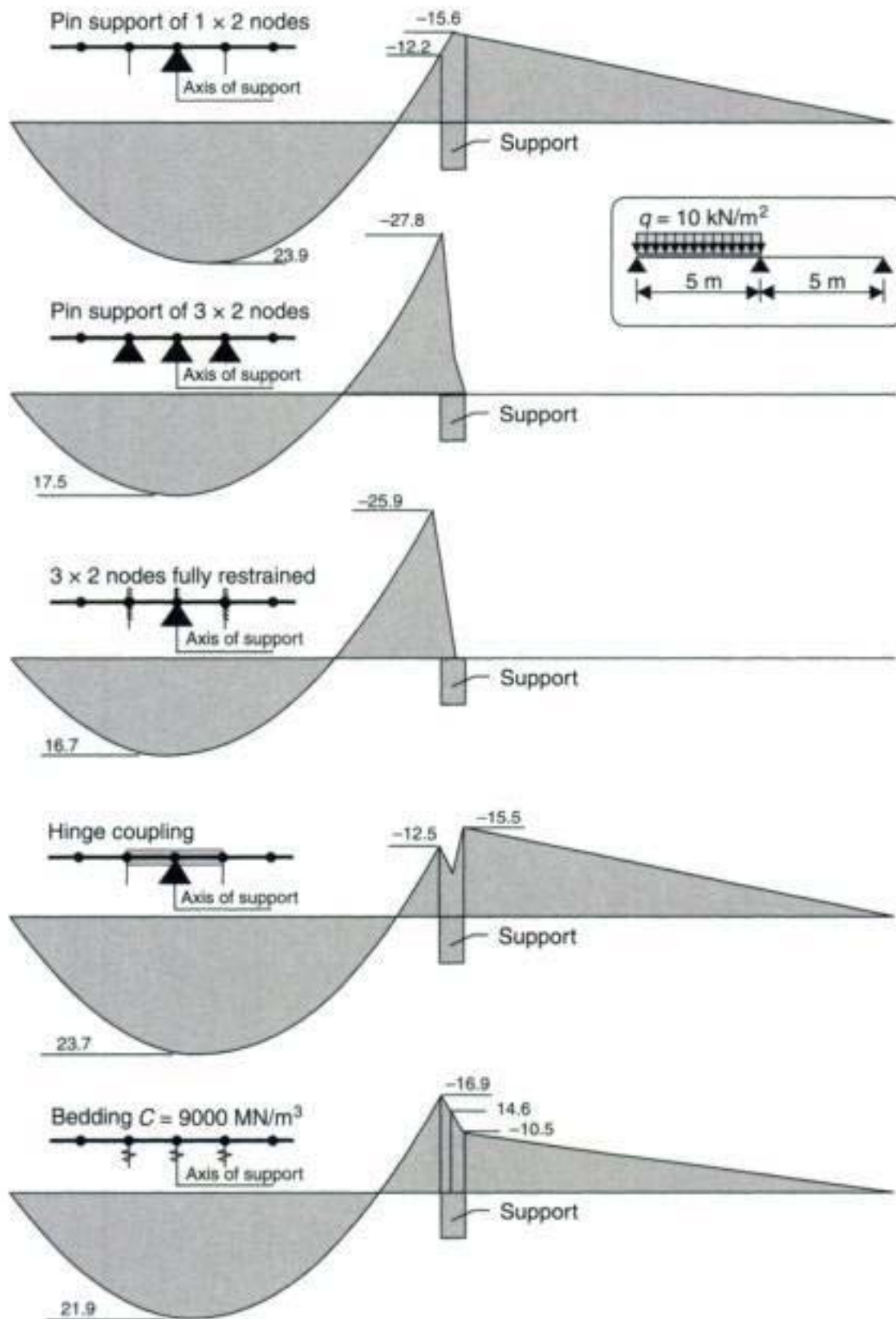


Fig. 4.12 Bending moments – uniform load at left span only – plate elements

one span is loaded, the support bending moment is overestimated by 226%. Therefore, this model should not be used. A further refinement of the element mesh would result in a fully restrained intermediate support. Doubling the number of the elements increases the bending

Table 4.1 Bending moments

Uniform loading on both spans	Field moment max M_F : kNm/m	Moment at the edge of support M_{SA} : kNm/m	Moment at the cl. of support M_{SM} : kNm/m
(b) Pin support of one node	17.6 (100%)	-27.4 (100%)	-31.2 (100%)
(c) Pin support of three nodes above the wall	17.4 (99%)	-24.3 (89%)	-14.5 (47%)
(d) Fully restraint of the nodes at the face of the column	16.7 (95%)	-25.9 (95%)	0
(e) Hinge coupling	17.3 (98%)	-28.0 (102%)	-14.5 (47%)
(f) Bedding ($C = 9 \times 10^6 \text{ kN/m}^3$)	17.6 (100%)	-27.4 (100%)	-29.1 (94%)
Beam analysis (manual)	17.6	-27.3	-29.3/-31.1*

* Smoothed and not smoothed bending moment

Table 4.1 Bending moments (Continued)

Uniform loading on left span only	Field moment max M_F : kNm/m	Moment at the edge of support M_{SA} : kNm/m	Moment at the cl. of support M_{SM} : kNm/m
(b) Pin support of one node	23.9 (100%)	-12.2/-15.2 (99/99%)	-15.6 (99%)
(c) Pin support of three nodes above the wall	17.5 (73%)	-27.8/0 (226/-%)	-7.5 (48%)
(d) Fully restraint of the nodes at the face of the column	16.7 (70%)	-25.9/0 (211/-%)	0
(e) Hinge coupling	23.7 (99%)	-12.5/-15.5 (101/101%)	-14.5 (92%)
(f) Bedding ($C = 9 \times 10^6$ kN/m ³)	21.9 (91%)	-16.9/-10.5 (137/68%)	-14.6 (92%)
Beam analysis (manual)	24.0	-12.3/-15.4*	-15.8

* Moment at left and right face of support

moments by 15% ($M_{sup,face,max} = -28.1$ kNm/m). The influence of the element size decreases by 1% when only one span is loaded.

Restricted Page

This page is unavailable for viewing ([why?](#)). You may continue browsing to view unrestricted pages, or visit the [About this Book](#) page.

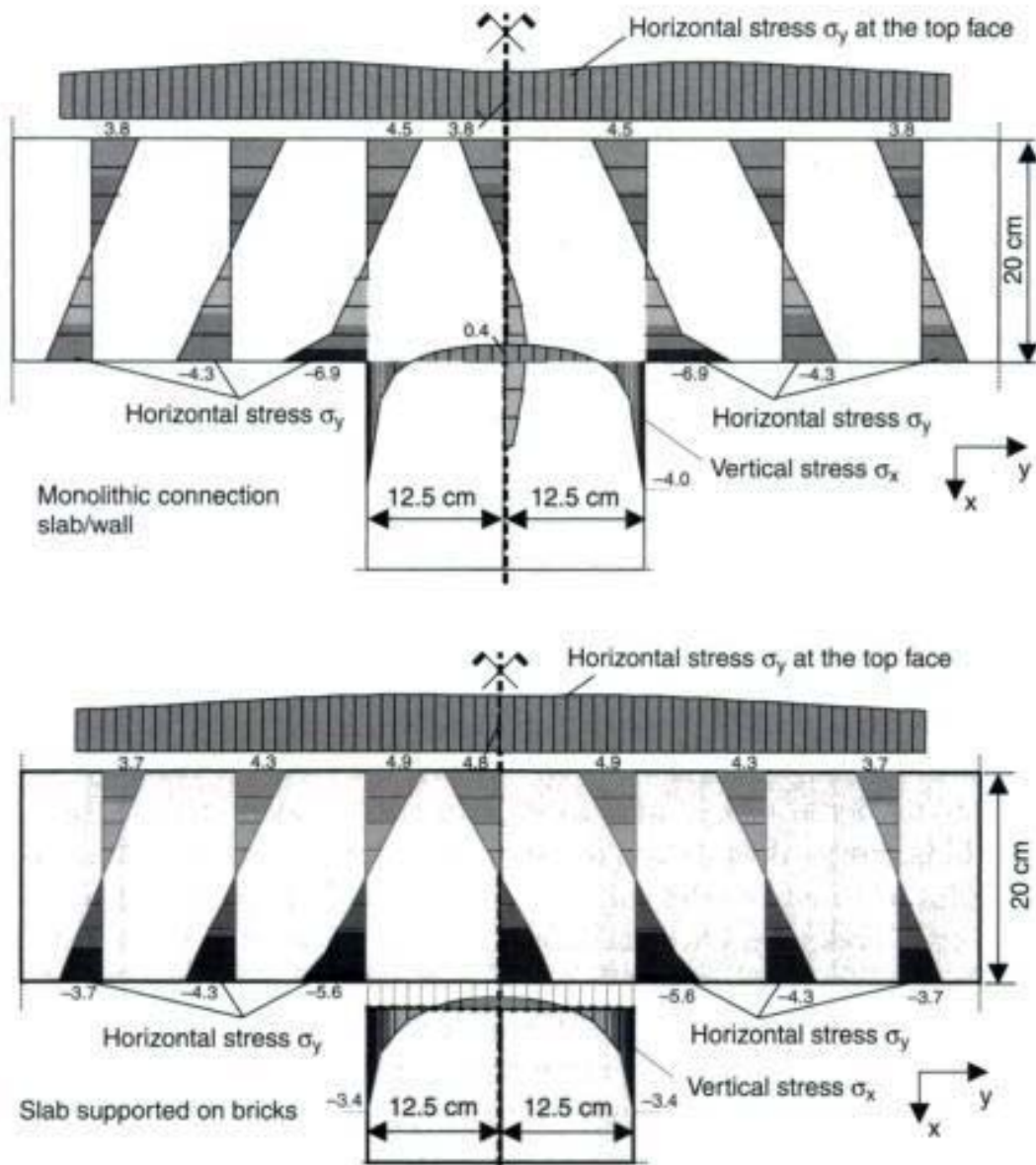


Fig. 4.14 Stress distribution of a one-way slab at the supports

the global deformation of the supporting structure and the resulting force redistribution. The local deformations, the stresses and strains in the slab in the vicinity of the wall with respect to the column head, which are required to determine the 'exact' internal forces, cannot be modelled with this simple approach.

The main assumption of all plate elements, the linear strain distribution, is not valid in the region of the support (see Fig. 4.14). Therefore, the bedding of the elements is an engineering tool, to get a smooth distribution of the bending moments over the support, in a manner similar to those in a manual analysis.

Table 4.2 shows the bending moments for different values of C from $C = 9 \cdot 10^5 \text{ kN/m}^3$ to $C = 9 \cdot 10^7 \text{ kN/m}^3$. The results are not sensitive to the bedding modulus C used for a uniform loading over both spans, as the deflection curve over the support shows a horizontal tangent. On the other hand, when only one span is loaded the bending moments are highly dependant on the value of C (see Table 4.2). A refinement of the element mesh in the support region does not change the internal forces significantly.

A slab has to be designed for both bending and shear. The section at a distance of $1.0d$ from the face of the support is relevant for the shear design for the given direct support of the chosen system. The shear forces are shown in Table 4.3 for different models. A constant static depth of $d = 20-2.5 \text{ cm} = 17.5 \text{ cm}$ is used for comparison.

The results of the various models are similar if both spans are loaded, whereas in load case 2 significant differences can be seen. A restraint of all nodes at the support (Models B and C) results in much higher shear forces in the supported elements (maximum + 13%) of the loaded span. The shear forces are much smaller than the beam values in the unloaded span, and in some models the forces are even zero. This is also the case if the supported elements are bedded.

In conclusion, in order to model a support on walls only the centre node should be fixed to avoid numerical restraints.

In this chapter, the internal forces and moments calculated manually by a beam structure have been used to verify the numerical model. It should be noted that the major assumption of a beam model, a linear strain distribution over the supports, is not valid. This can be seen from Fig. 4.14 where the stresses of a plane shell model (diaphragm) of a one-way slab are shown near the intermediate support for a monolithic connection and a free, not restrained, support ($l = 22 \times 5.0 \text{ m}$).

A nonlinear strain distribution can be seen at the inner face of the support. High compressive stresses are estimated for the fixed connection (singularity). In both cases, the tensile stresses do not increase over the supports. Therefore, it is generally sufficient to use the bending moments at the face of the support for obtaining the smoothed values for design.

Even complex shell models can only approximate the real load-bearing and deformation behaviour of a slab at the supports, as the basic assumption of a linear-elastic material behaviour is not valid in this region. The concrete slab will show some cracks.

cl. of
Nm/m

Restricted Page

This page is unavailable for viewing ([why?](#)). You may continue browsing to view unrestricted pages, or visit the [About this Book](#) page.

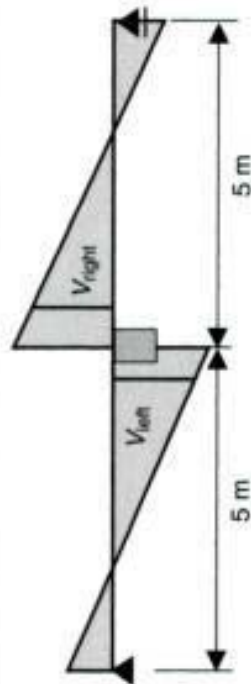
Cl. of
 χ_m/m

Restricted Page

This page is unavailable for viewing ([why?](#)). You may continue browsing to view unrestricted pages, or visit the [About this Book](#) page.

Table 4.3 Shear forces at a distance of $d = 17.5$ cm from the face of the intermediate support

	Uniform loading shear force left/right: kN/m	Uniform load on left span only shear force:	
		Left: kN/m	Right: kN/m
(b) Pin support of one node	28.0 (99%)	24.9 (99%)	3.1 (97%)
(c) Pin support of three nodes above the wall	28.1 (100%)	28.4 (113%)	0.0
(d) Fully restraint of the nodes at the face of the column	28.5 (101%)	28.5 (114%)	0.0
(e) Hinge coupling	28.1 (100%)	24.9 (99%)	3.2 (100%)
(f) Bedding ($C = 9 \times 10^6$ kN/m)	28.0 (99%)	25.8 (103%)	2.2 (69%)
Beam analysis (manual)	28.3	25.1	3.2



4.5 Slabs which can lift from the supports

The design of slabs is usually based on the assumption that the slab cannot lift from the supports. It must be emphasized that even a rectangular, simply supported slab under constant loading will partially lift from the

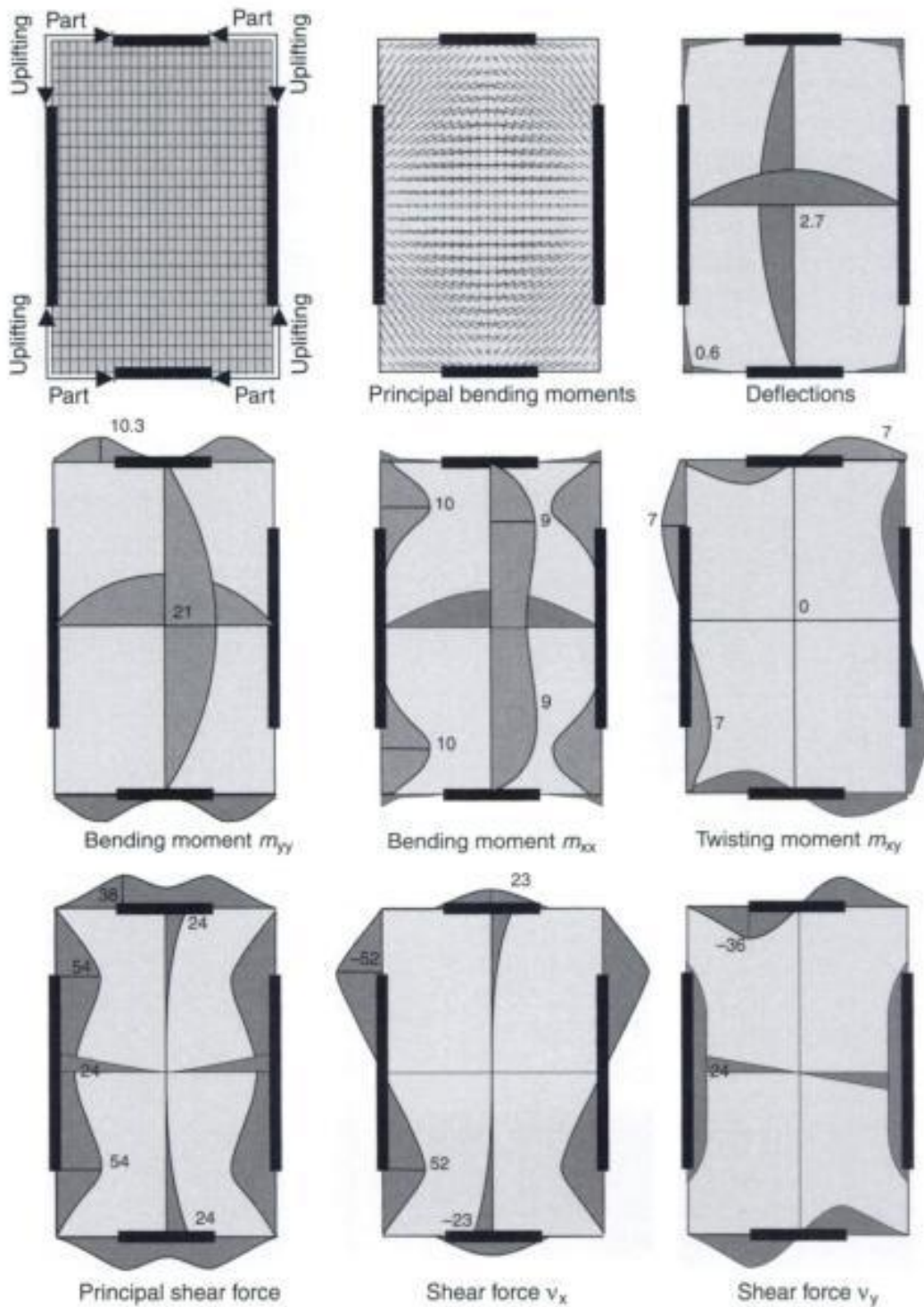


Fig. 4.15 Internal forces and deflections of a rectangular slab free to uplift from the supports under uniform load

Finite element design of concrete structures

supports at its edges. Therefore, one has to consider this effect, if the slab is not fixed to the supports or if the vertical force, e.g. due to walls above, is not sufficiently high to restrain the uplifting forces.

Restricted Page

This page is unavailable for viewing ([why?](#)). You may continue browsing to view unrestricted pages, or visit the [About this Book](#) page.

The internal forces and midspan deflections of a rectangular, simply supported slab which is fixed to the supports and one which can uplift, are given in Table 4.4. If the slab is not restrained in the vertical direction, the bending moments at midspan increase approximately by 13%. The support forces per unit length increase due to the reduced supported length by approximately 38% (shorter side) and 6% (longer side).

4.6 Discontinuous line support

The numerical modelling of discontinuous support of slabs or a wall support which ends in the slab can cause considerable problems. In both cases, infinite shear forces and bending moments are estimated at unsupported edges. This singularity problem is caused by the sudden change of the boundary conditions (see Figs 4.18 and 4.19). Dimensioning of the slab for these 'theoretical' peaks is not required, as they only result from a numerical problem. The basic assumption of a linear strain distribution does not hold near the end of a wall support. The large tensile stresses calculated are reduced due to the cracking of concrete. But an analysis which considers the nonlinear material behaviour and the complicated three-dimensional stress distribution is too difficult and extensive for any practical applications. Hence, three different models may be used to overcome the numerical problem (Fig. 4.16). First, one may neglect the discontinuity of the line support in the numerical model. The design of the opening region has to be done separately on a fully or partially restrained equivalent beam system ('flush beam strip', see Fig. 4.17). This additional effort can be avoided, when the opening is considered in the numerical model.

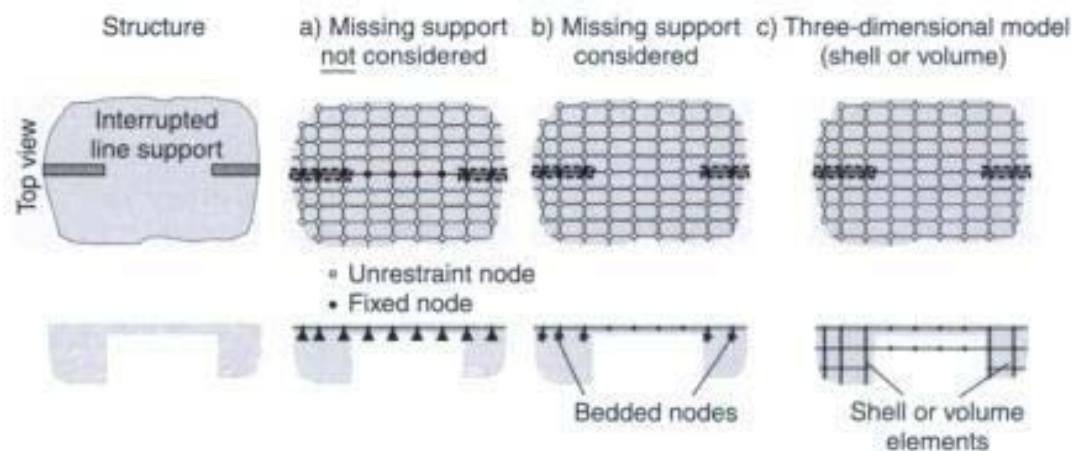


Fig. 4.16 Different models for a discontinuous line support

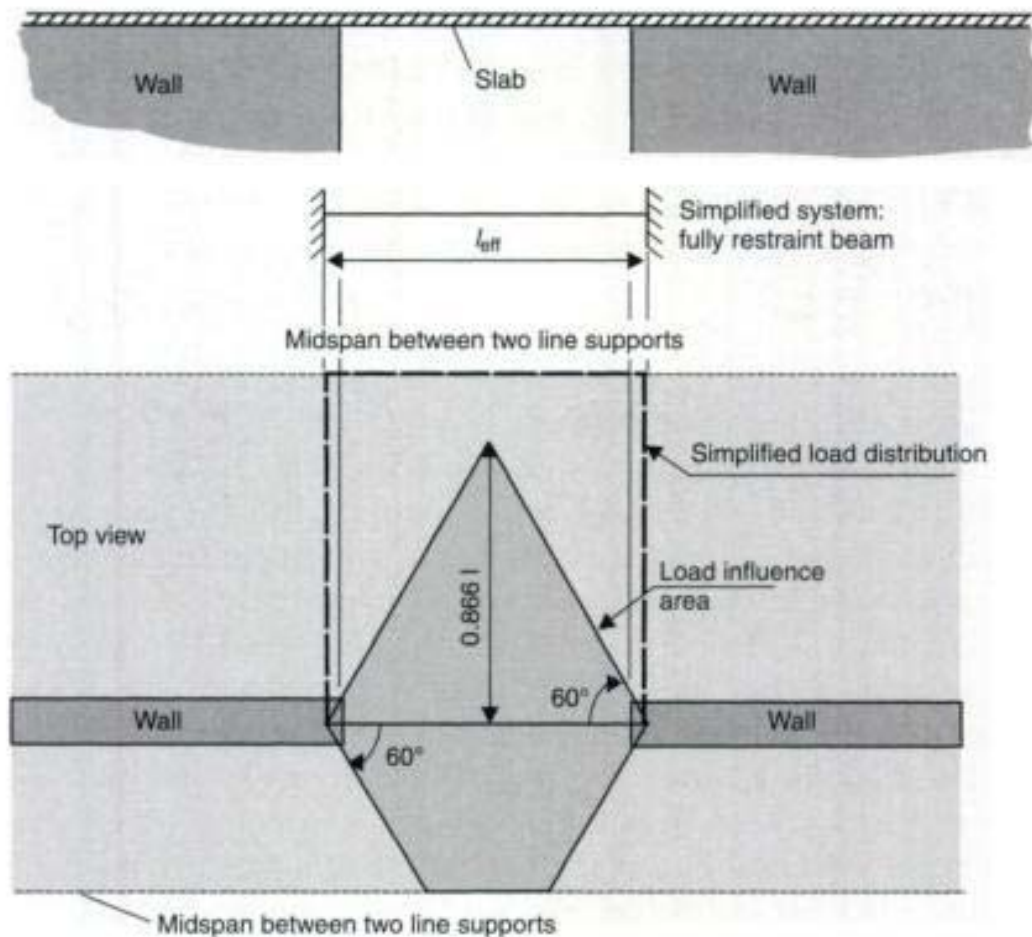


Fig. 4.17 Beam system ('flush beam strip') and load influence areas for a discontinuous line support according to DAfStb Heft 240 [10]

The nodes at the end of the line support may be fully or partially restrained in the vertical direction. Another variation is to use a three-dimensional volume model of the slab and the wall underneath. However, this model is again too extensive and not practical.

In the Finite Element model the missing line supports can be neglected if their length is smaller than 15 times the depth of the slab ($l_{eff}/h < 15$). The dimensioning of this region can be done manually using an equivalent beam system ('flush beam strip') in accordance to DAfStb Heft 240 [10] (see Fig. 4.17). More detailed investigations based on the Finite Element Method are only necessary if the opening length exceeds 15 times of the section depth h of the slab.

'Theoretical' singularities at the unsupported edge can be found if the wall opening is considered by the Finite Element model. These load peaks can be reduced significantly by a soft, elastic support, by elastic bedding of the nodes or the elements, as the results of a comparison calculation demonstrates. Figure 4.18 shows the internal forces for a

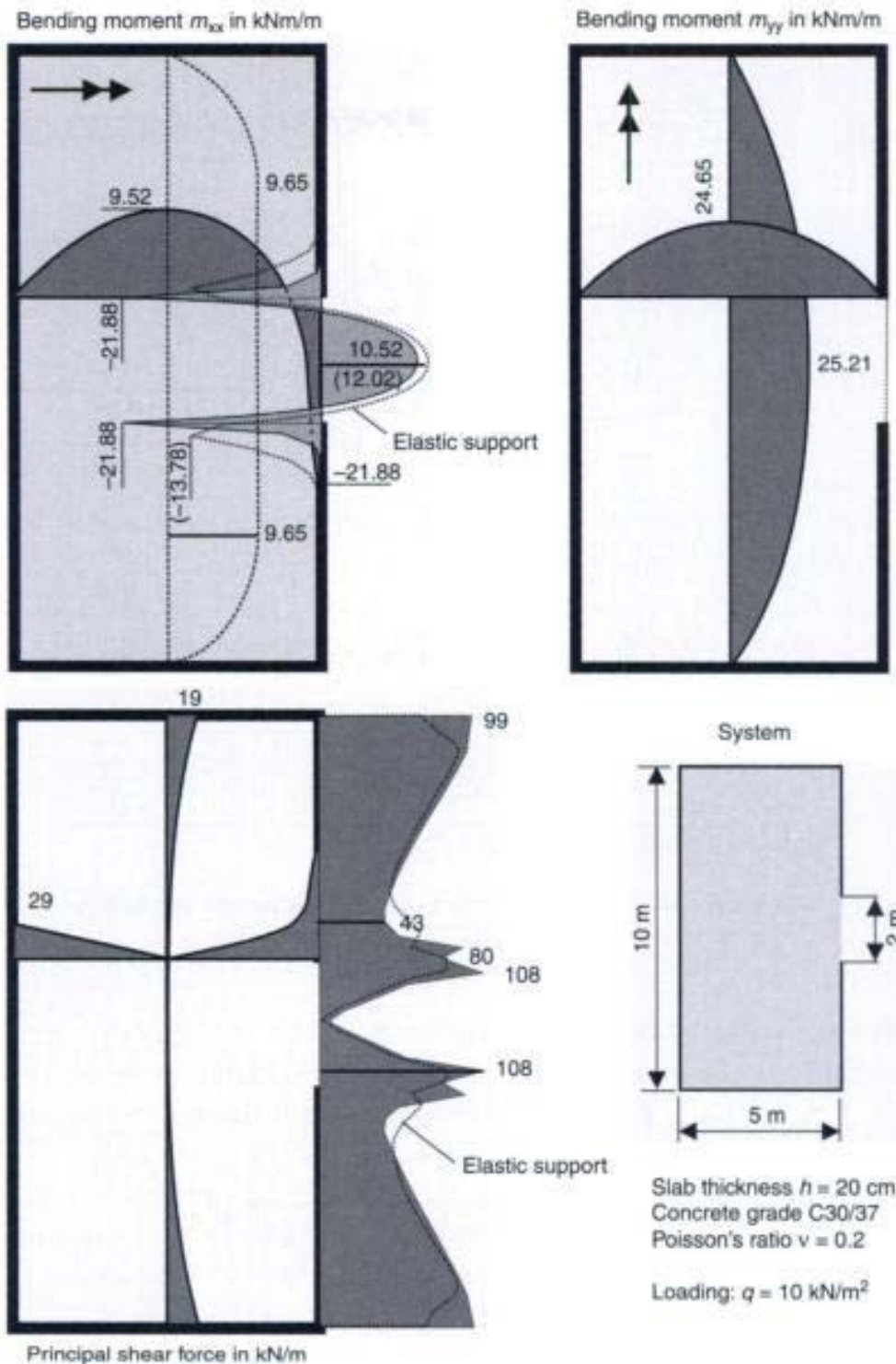


Fig. 4.18 Bending moments and shear forces for a slab with a discontinuous line support

soft and a stiff support. A bedding modulus of $C = 2327$ MN/m² is used, which corresponds to a concrete wall (grade C25/30) with a thickness of $h = 20$ cm and a height of $l = 2.75$ m ($C = E \cdot h/l = 32\,000 \cdot 0.2/2.75 = 2327$ MN/m²).

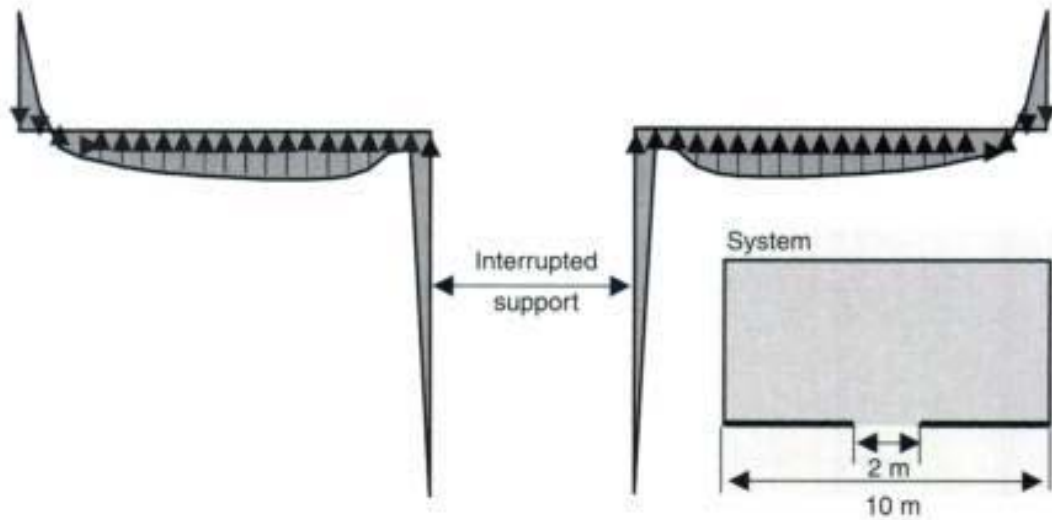


Fig. 4.19 Support forces of the outer wall near the face of the opening (nodes fully restrained in the vertical direction)

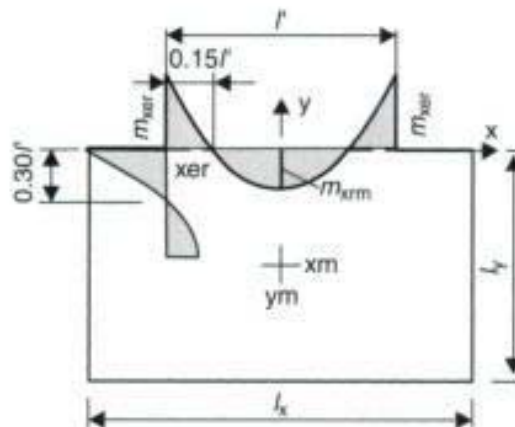
Table 4.5 Modulus of elasticity of different building materials

Concrete	$E_{cm} = 9.5 \cdot (f_{ck} + 8)^{1/3}$
Clay bricks	$E = 3000 \cdot \sigma_0$
Steel	$E_s = 210\,000 \text{ N/mm}^2$

where:

f_{ck} is the characteristic concrete compressive strength in N/mm^2 ;
 σ_0 is the permissible compressive strength of a brick wall.

Table 4.6 Bending moments in the opening region



	Rigid support	Soft support	Stiglat [25]
m_{xm} : kNm/m	10.52	12.02	9.0
m_{xer} : kNm/m	-21.88	-13.78	-42.0

A large reduction in the moment peaks at the unsupported edges can be seen (Fig. 4.18) if the stiffness of the support is considered.

Bending moments for fixed and elastic supports and the values of Stiglat [25] are given in Table 4.6. Stiglat has used the Finite Difference Method and a Poisson's ratio of $\nu = 0.0$ to estimate the internal forces in the region of the missing support. With this assumption the bending moment becomes nearly twice as high as that of the fully restraint supported slab. This large difference may be caused by the influence of the element size. The bending moments at midspan of the Finite Element analysis correspond well to Stiglat's values.

Figure 4.20 shows the bending moment distribution of a slab with a partition wall. For this structure a singularity occurs at the face of the opening. To demonstrate the large influence of the vertical stiffness of the support on the internal forces a very small bedding modulus was used ($C = 50 \text{ MN/m}^2$), which correspond to a wall made of hollow or aerated concrete bricks.

As shown in Fig. 4.20, the peak of the bending moment and the large concentrated shear force at the unsupported edge disappear. This load redistribution causes a considerable increase of the bending moments and the deflections of the slab.

The dimensioning of the slab can be done either with a stiff or elastic support. In the case of a stiff wall it should be noted that a redistribution of the bending moment at the unsupported edge is only possible if the concrete slab cracks. Therefore, reinforcement to limit the crack width should be inserted in the top face of the slab.

It must be emphasized that an elastic support of the slab can only represent the overall deflection behaviour of the supporting wall. The complex three-dimensional stress and strain distribution at the unsupported edges cannot be modelled with plain plate elements based on a linear strain distribution.

4.7 Concrete joist floors

Several variations exist to model joist floors. At first one may consider the joist in the Finite Element model as a stiff vertical continuous support. The resulting support forces are used as external loads for an equivalent T-beam, which may then be analysed manually. This model is based on the assumption of a rigid support, i.e. the stiffness of the joist is much higher than the bending stiffness of the slab.

A more refined model has to be used if this assumption does not apply. The joist has to be discretized together with the slab in the

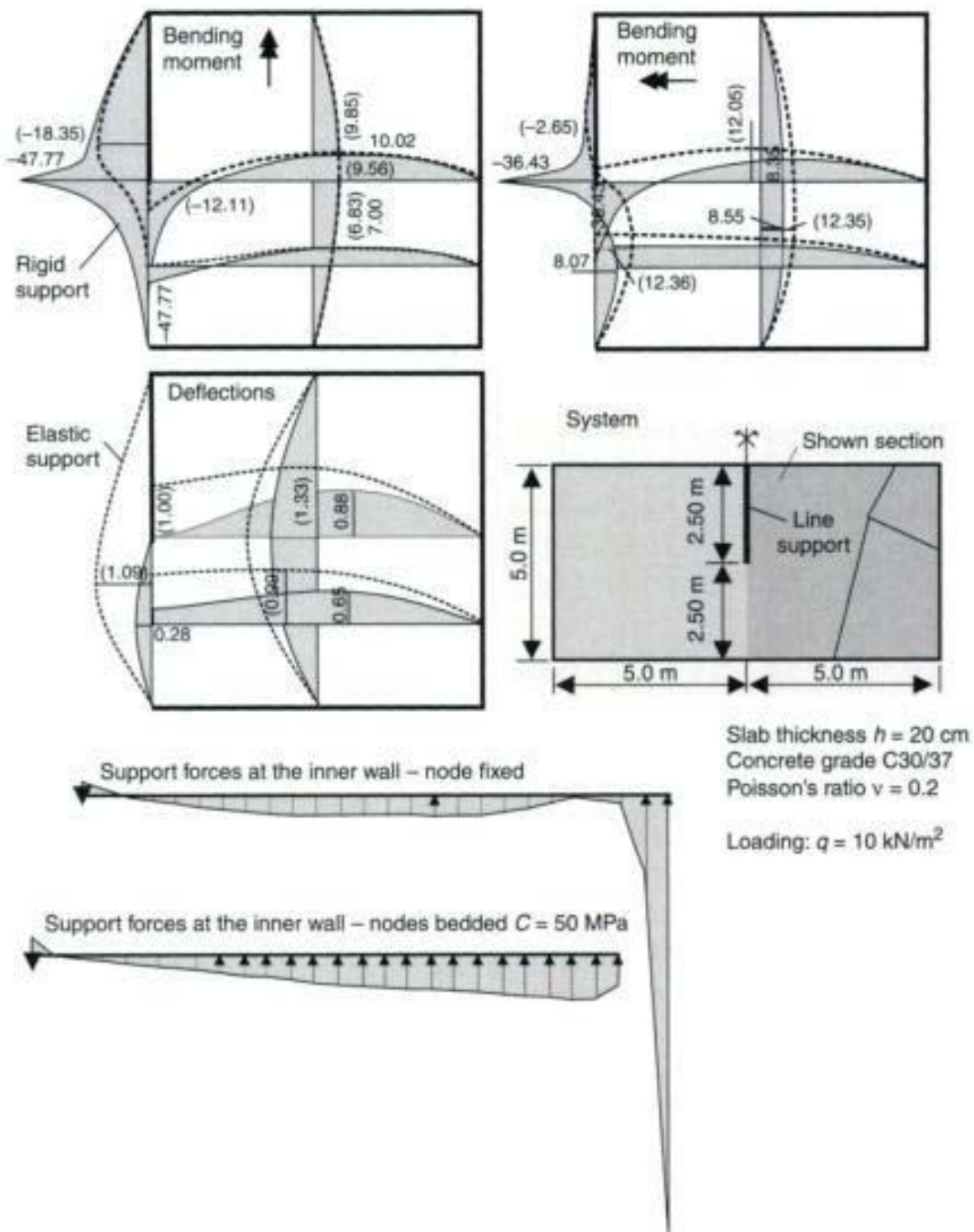


Fig. 4.20 Slab with partition wall

same system. In this case, the real T-beam system is idealized as a slab of constant depth and with an additional separate beam or a plate element having a greater thickness, located at the midplane of the slab. In actual dimensioning, the depth of the equivalent beam element has to be greater as the eccentricity of the joist is not considered. The moment of inertia of the real T-beam should be identical to that of the idealized system. The effective width of the flanges of the joist b_{eff} has to be considered in this calculation. It may be estimated



Restricted Page

This page is unavailable for viewing ([why?](#)). You may continue browsing to view unrestricted pages, or visit the [About this Book](#) page.

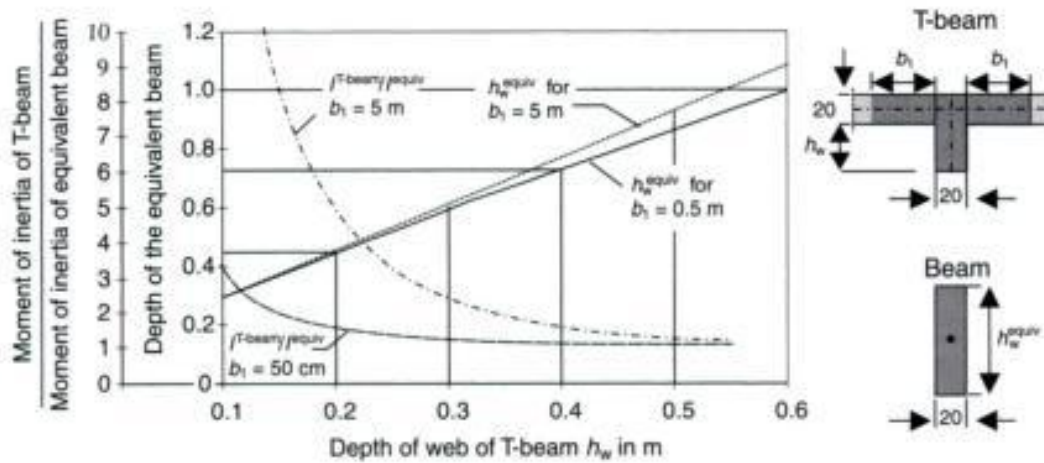


Fig. 4.22 Depth of the equivalent beam h_w^{equiv} and relation of the moment of inertia

4.8 Flat slabs

Flat slab and flat slab plate floors are directly supported on columns. There are no interior beams as supporting elements. They are widely used as flat slab construction is economical (Fig. 4.23). A manual analysis can easily be carried out by the analytical methods given in EC2, Part 1 [6] or in *Heft 240* [10] for regular systems with approximately equal span lengths. The bending moments and shear forces for irregular panels or loadings have to be estimated by means of the Finite Element Method.

The numerical analysis has to model the actual behaviour of the pin support at the columns. Different approaches are available, which will be discussed in the following.

It must be emphasized here that the behaviour of the structure in the region of the columns cannot be calculated exactly due to the underlying assumptions of the Finite Element slab model. In the supported area the strain distribution is very complex. This behaviour cannot be modelled by plate elements which are generally based on a linear strain distribution over their cross-section depth. In Fig. 4.24, the stresses of a circular slab are shown near the supported area. The slab is simply supported at the outer edge and has a circular column at its centre. The slab is subjected to a uniformly distributed load of $q = 10 \text{ kN/m}^2$. The axisymmetric model represents the load-bearing behaviour of a flat slab very well for the region of the column. Even in the case of a rectangular arrangement of the supports the behaviour around the columns is nearly axisymmetric.

An 'exact' determination of the internal forces and the stresses of a pin supported slab is only possible by means of a three-dimensional

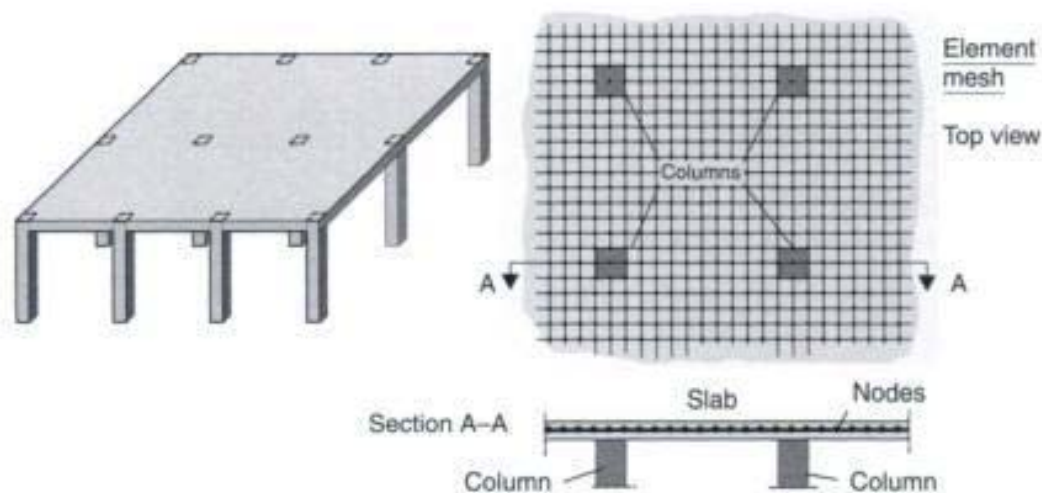


Fig. 4.23 Flat slab

(volume) model. The nonlinear behaviour of the concrete due to cracking has to be considered. Such a complex model of a flat slab is too extensive for practical use. Furthermore, the dimensioning cannot be done automatically by the software.

Therefore, in practice, a two-dimensional plane plate model is used and the columns are modelled by special support conditions. Various models, as shown in Fig. 4.25, can be used. These have already been explained in detail in section 4.3 for a simply supported one-way slab.

(a) Three-dimensional volume model.



Restricted Page

This page is unavailable for viewing ([why?](#)). You may continue browsing to view unrestricted pages, or visit the [About this Book](#) page.

Slabs

a) Three-dimensional
(volume) model

b) Pin support
of one node

c) Pin support of all nodes
above the column



Restricted Page

This page is unavailable for viewing ([why?](#)). You may continue browsing to view unrestricted pages, or visit the [About this Book](#) page.

slab is that the latter is a two-dimensional spatial structure, carrying the loads in two dimensions.

The 'correct' bending moments, shear forces and stresses of a flat slab in the region of the column supports are unknown. Therefore, the results of the various models are examined on a simple structure, using an interior panel of a flat slab with regular panel dimensions of $l_x = l_y = 5.0$ m. For comparison purposes, the bending moment at the face of the column is used. This value is relevant for dimensioning the slab. A uniformly distributed load of $g = 10$ kN/m² is applied to the slab.

Owing to the symmetric structural system and the load arrangement, it is sufficient to only analyse one quarter of the slab and to consider the boundary conditions at the symmetry lines. Therefore, in the following figures only one quarter of the whole slab is shown.

The results of the Finite Element calculations are compared with the values estimated by the widely used equivalent frame [6] and beam method [10]. Here, the bending moments of a flat slab are estimated by means of an equivalent frame or beam system and distributed in transverse direction with factors given in the tables (see Figs 4.27 to 4.29).

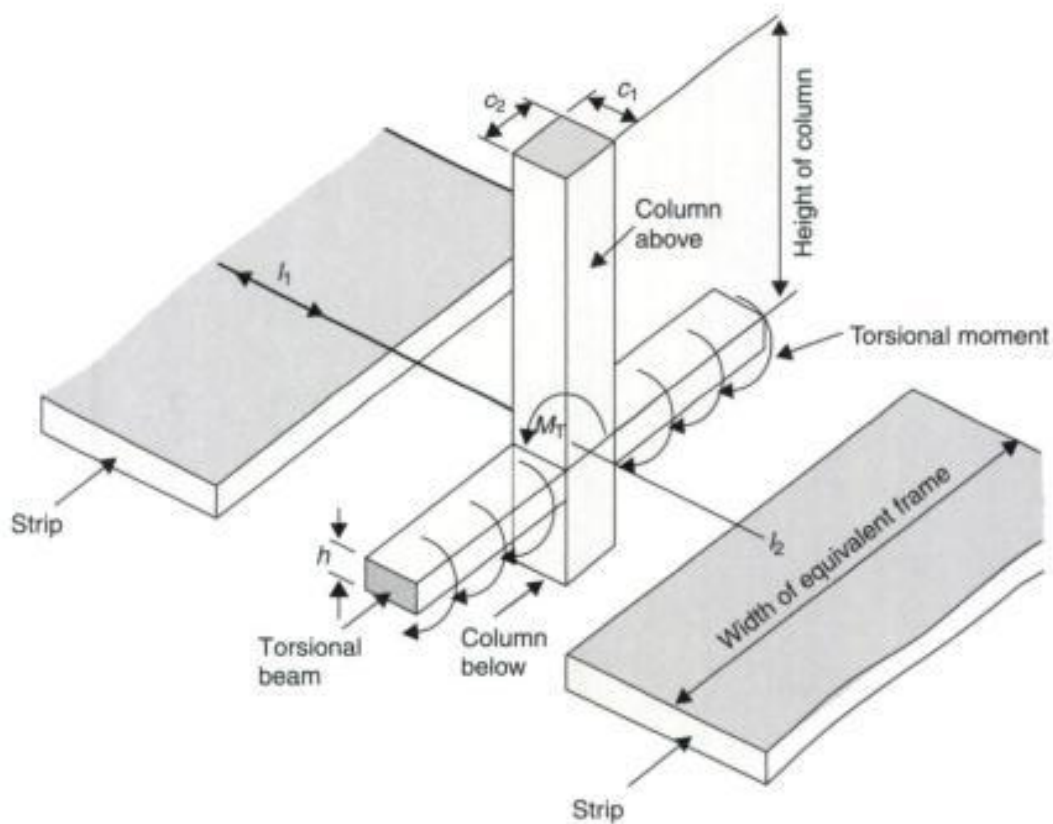
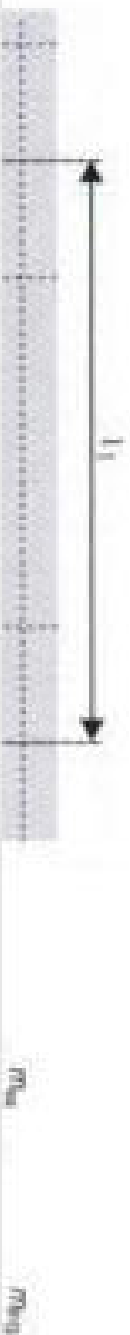


Fig. 4.27 Equivalent frame model of flat slabs

Slabs



Restricted Page

This page is unavailable for viewing ([why?](#)). You may continue browsing to view unrestricted pages, or visit the [About this Book](#) page.

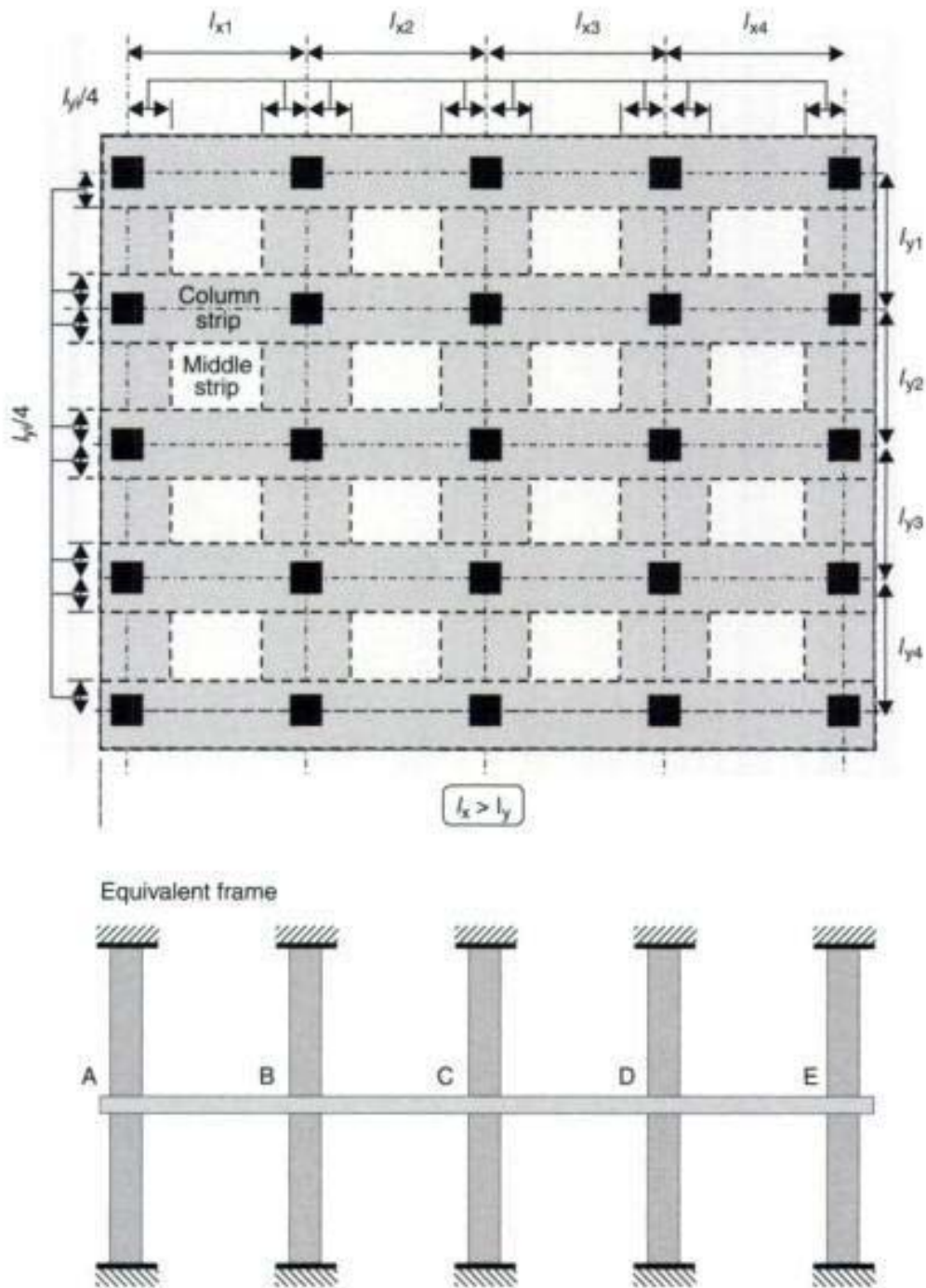


Fig. 4.29 Equivalent frame model of a flat slab according to [6]

Table 4.8 Bending moment in strips

	Negative moments	Positive moments
Column strip	-25.0 to -33.3 kNm/m	+10.4 to 14.6 kNm/m
Middle strip	-16.7 to -8.3 kNm/m	+10.4 to 6.3 kNm/m

uniform load $g = 10 \text{ kN/m}$

where: b_{sup} is the width of column, l is the span length

Support bending moments

in the inner strip above the column:

$$m_{\text{SS}} = k_{\text{SS}}^g \cdot c \cdot g \cdot l_{\text{m1}}^2 + k_{\text{SS}}^q \cdot c \cdot q \cdot l_{\text{m1}}^2$$

$$= \begin{cases} -0.224 \cdot 1.0 \cdot 5^2 = -56 \text{ kNm/m (column 25/25 cm)} \\ -0.160 \cdot 1.0 \cdot 5^2 = -40 \text{ kNm/m (column 50/50 cm)} \end{cases}$$

in the other strip beside the column:

$$m_{\text{SG}} = 0.7m_{\text{SS}} = -39.2 \text{ kNm/m} \quad \text{resp.} \quad -28 \text{ kNm/m}$$

in the field strip:

$$m_{\text{SF}} = k_{\text{SF}}^g \cdot g \cdot l_1^2 + k_{\text{SF}}^q \cdot q \cdot l_1^2 = -0.03 \cdot 10 \cdot 5^2 = -7.5 \text{ kNm/m}$$

Span moments

in the inner strip:

$$m_{\text{FG}} = k_{\text{FG}}^g \cdot g \cdot l_1^2 + k_{\text{FG}}^q \cdot q \cdot l_1^2 = 0.052 \cdot 10 \cdot 5^2 = 13.00 \text{ kNm/m}$$

in the field strip:

$$m_{\text{FF}} = k_{\text{FF}}^g \cdot g \cdot l_1^2 + k_{\text{FF}}^q \cdot q \cdot l_1^2 = 0.041 \cdot 10 \cdot 5^2 = 10.25 \text{ kNm/m}$$

where: k = moment factors (see [10], Tables 3.1–3.5).

The equivalent frame analysis [6] gives bending moments as shown in Table 4.8.

The calculated negative bending moment in the column strip $m_{\text{sup,max}} = -33.3 \text{ kNm/m}$ is significantly less than the value from the equivalent beam method $m_{\text{sup,max}} = -56.0 \text{ kNm/m}$.

The distribution of the bending moments in the direction of the main load bearing is treated first (see Fig. 4.28 bottom). Next, we consider, the distribution of the bending moments in transverse direction (see Fig. 4.28 right).

4.8.1 Pin support of one node

The influence of the element size on the distribution of the bending moments is first examined at the section $y = 0$. The quarter of the interior panel is divided into 4×4 , 8×8 , and 16×16 elements. The size of the element is kept constant in each model for comparison.

There is no refinement of the meshes in the region of the support. Figure 4.30 shows the dimensionless bending moment distribution in the column axis ($y = 0$). It is obvious that a refinement of the element mesh results in a significant increase of the maximum support moment. This can be traced back to a singularity problem caused by the pin support and the concentrated support force. The

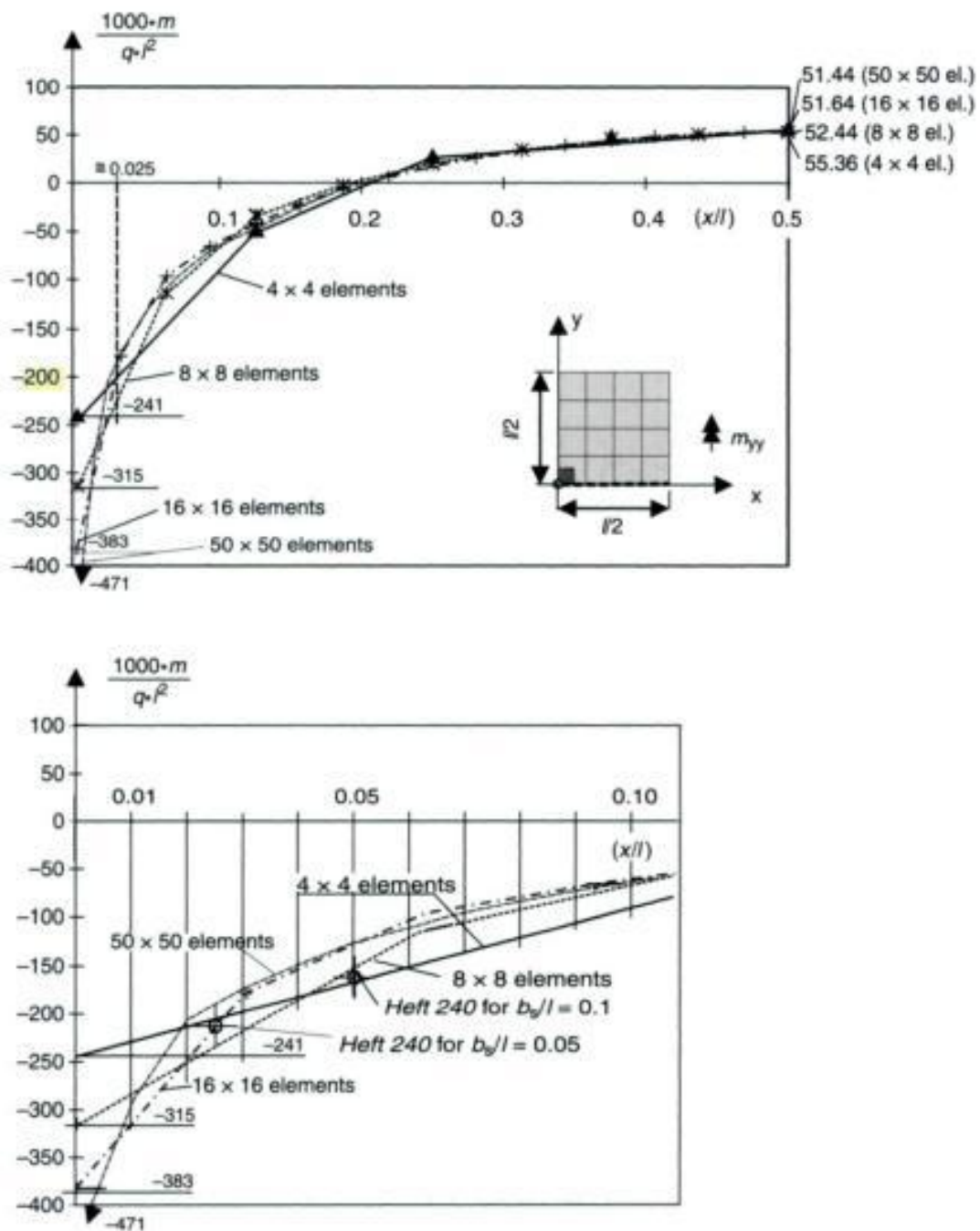


Fig. 4.30 Moment distribution m_{yy} for $y = 0$ in the region of an interior column for different element meshes – pin supported node

bending moment in the span is nearly independent of the element size, except for the very coarse mesh of 4×4 elements.

The moment distribution of the models with 8×8 and 16×16 elements are well matched for the span and up to $x/l \approx 0.06$ from the centreline of the pin support. Consequently, a further refinement of the element mesh would only slightly affect the moments at $x > 0.06l$. Both curves meet in the region of $x/l \approx 0.02$.

The bending moment at the face of the column is needed in the design. Therefore, the considerable differences in the peak moment at the pin support ($m_s = -241$ to -471 kNm/m) are of no practical importance. As illustrated in Fig. 4.30, the results are highly dependant on the element size in the region of $x/l < 0.02$ and $b_{sup}/l < 0.04$. Therefore, a pin supported node should not be used for a column width of $b_{sup} < 0.04l$. Such slender columns (e.g. $b_{sup} < 20$ cm for $l_{slab} = 5$ m) are rarely used in practice.

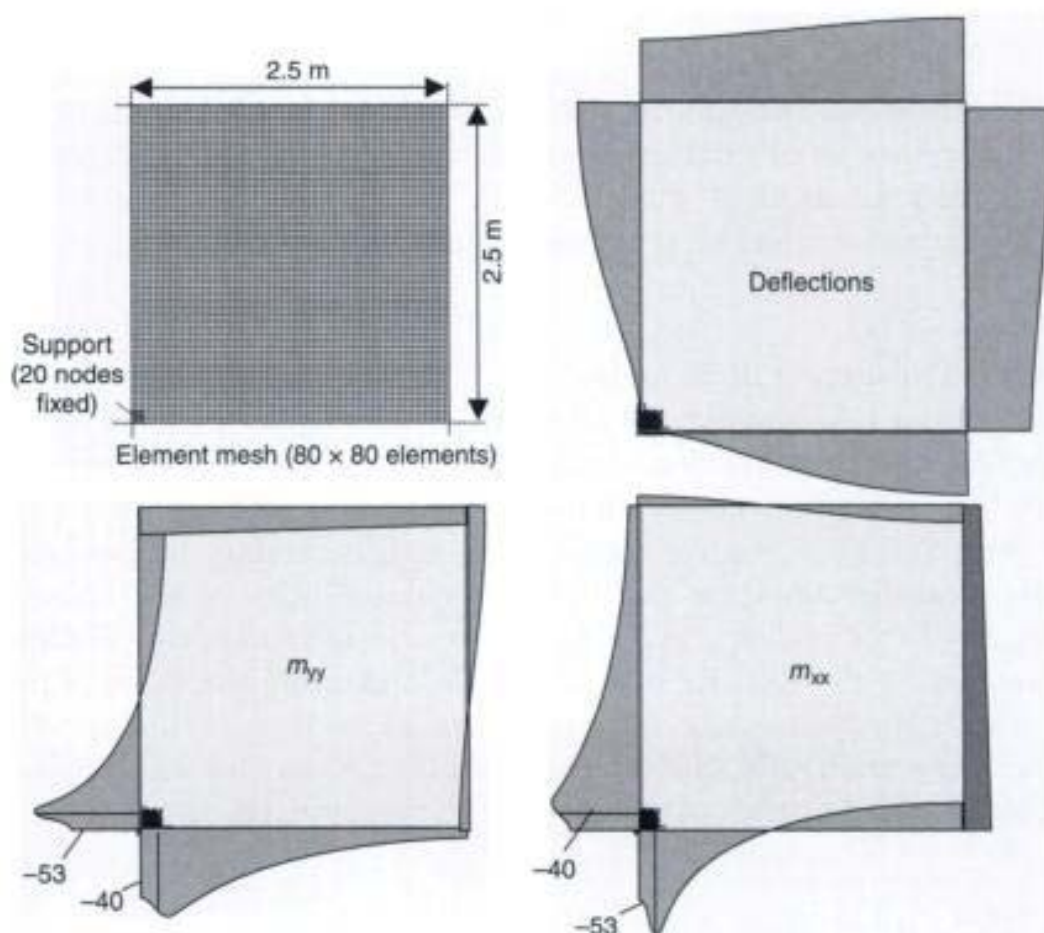


Fig. 4.31 Element mesh, bending moments and deflections of a flat slab – all nodes above the column fixed in vertical direction

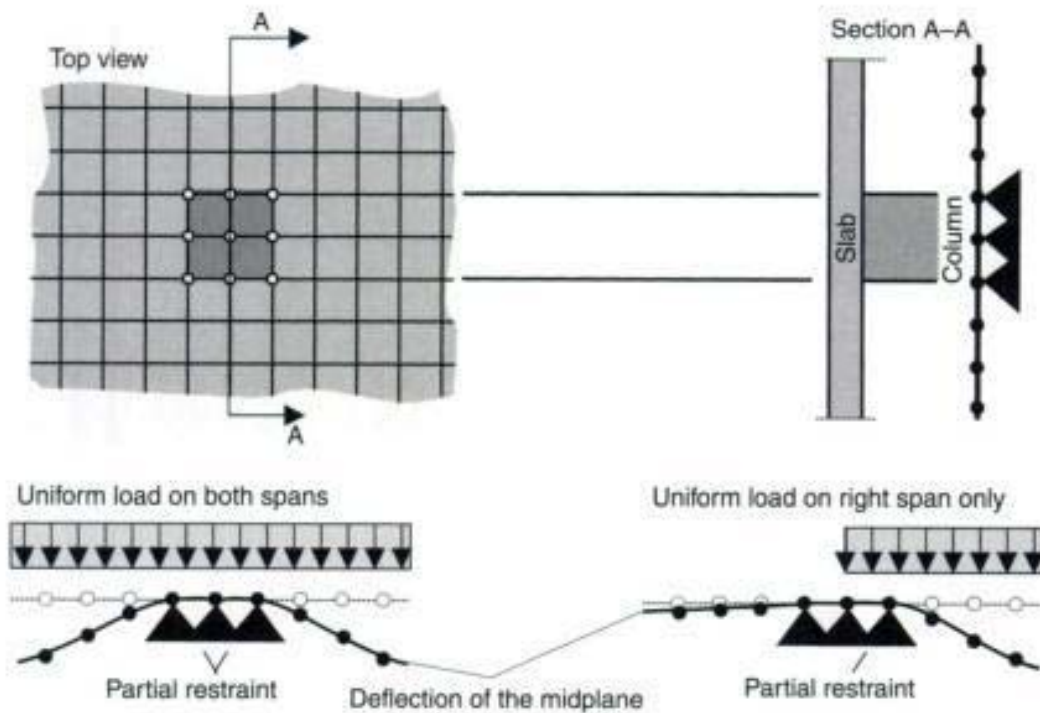


Fig. 4.32 Restraint caused by the pin support of all nodes above the column

Furthermore, one can see that the maximum bending moments at the supports for all meshes correlates well with values calculated by the analytical method given in [10]. This is not surprising as the moment factor k had been estimated for a pin supported plate.

4.8.2 Pin support of all nodes

The slab is fully restrained if all nodes at the column are fixed in the vertical direction. This mis-modelling is important for asymmetric loading, as has been shown for a one-way slab (see section 4.4).

Figure 4.33 shows the distribution of the bending moments in the symmetry lines for two different cross-sections of the column ($b_{sup} = 25$ cm and $b_{sup} = 50$ cm). It can be seen that the bending moments in the span are only slightly dependant on the width of the column. In contrast the internal forces at the face of the column increase considerably when the width of the column becomes smaller. This is caused by the concentration of the support reactions.

4.8.3 Fully restraint of all nodes

If, in addition to the previous example, the rotation of all supported nodes is restrained then there is a high moment peak at the column.

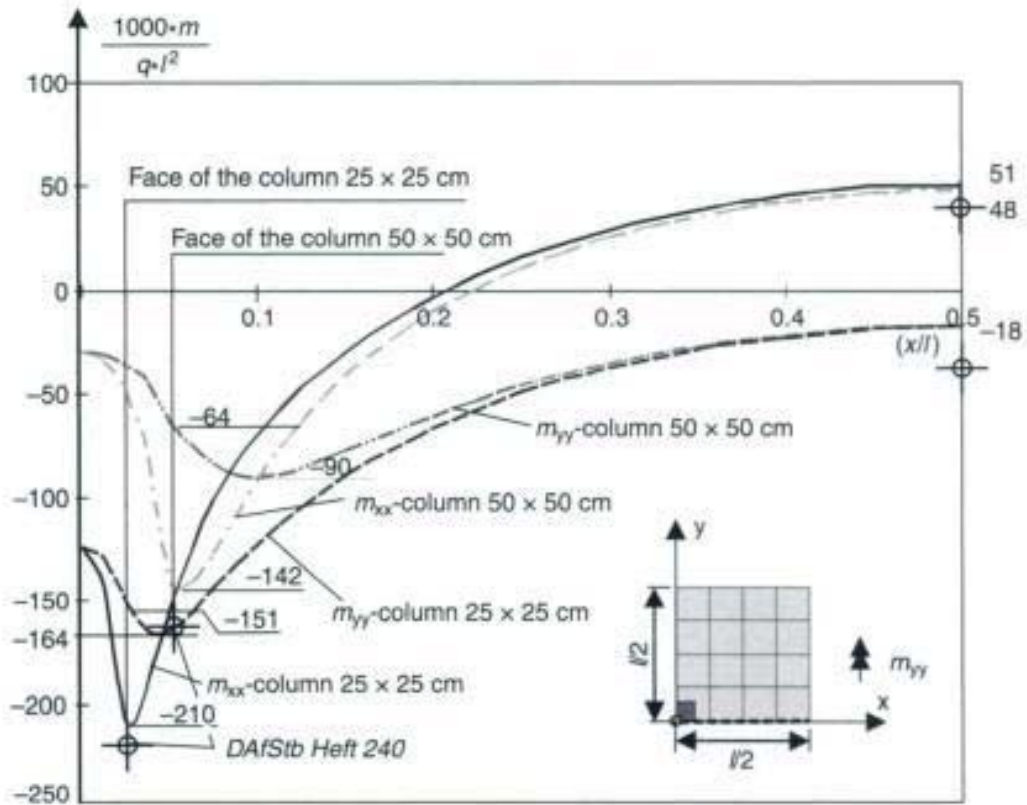


Fig. 4.33 Bending moment m_{yy} and m_{xx} in the section $y = 0$ – pin support of all nodes above the column

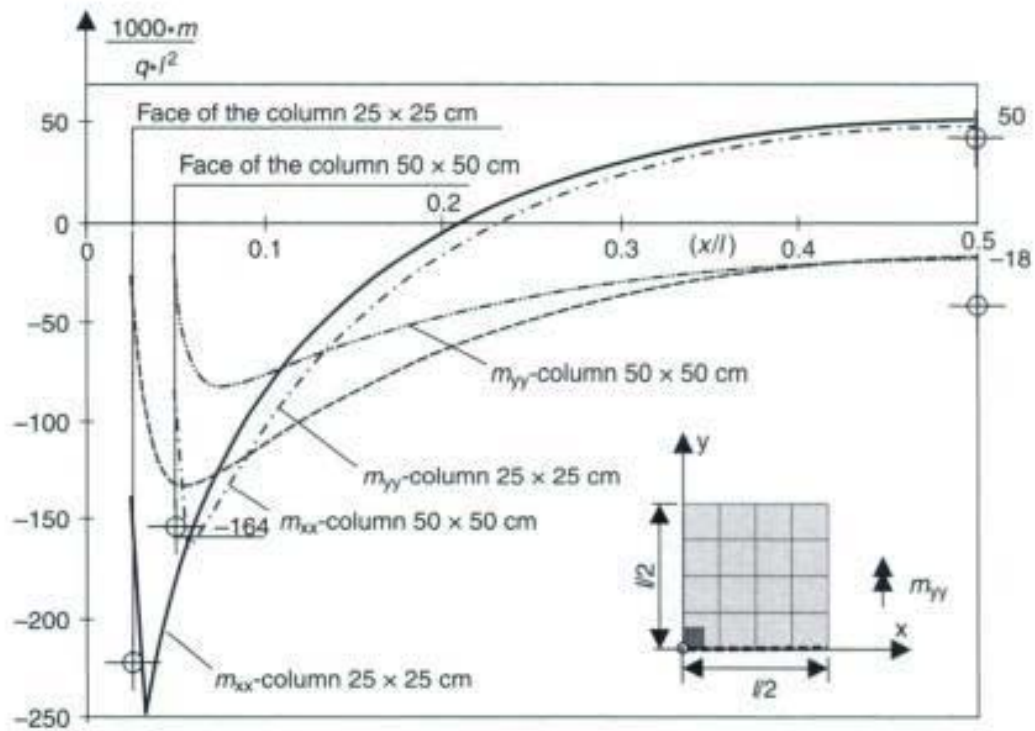


Fig. 4.34 Bending moment m_{yy} and m_{xx} in the section $y = 0$ – all nodes above the column are fully restraint

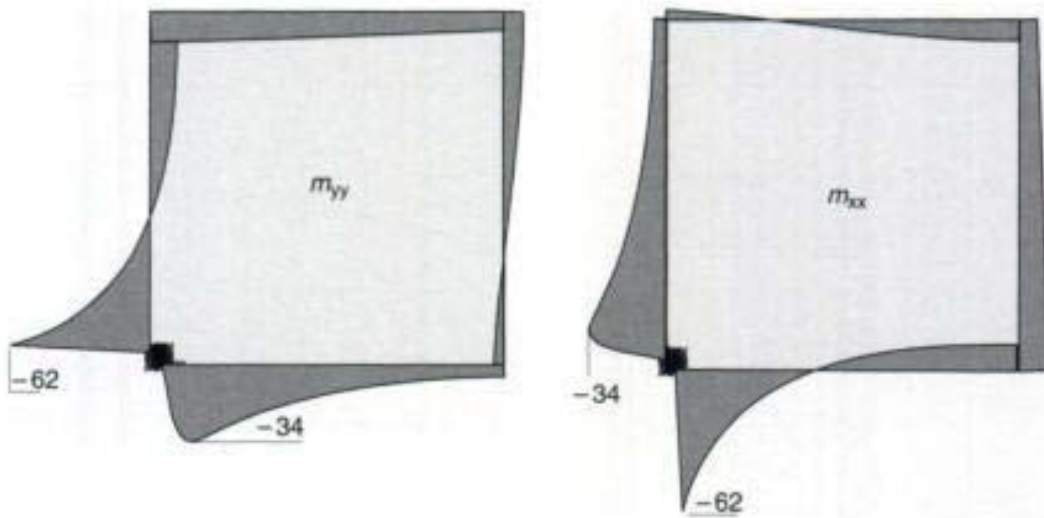
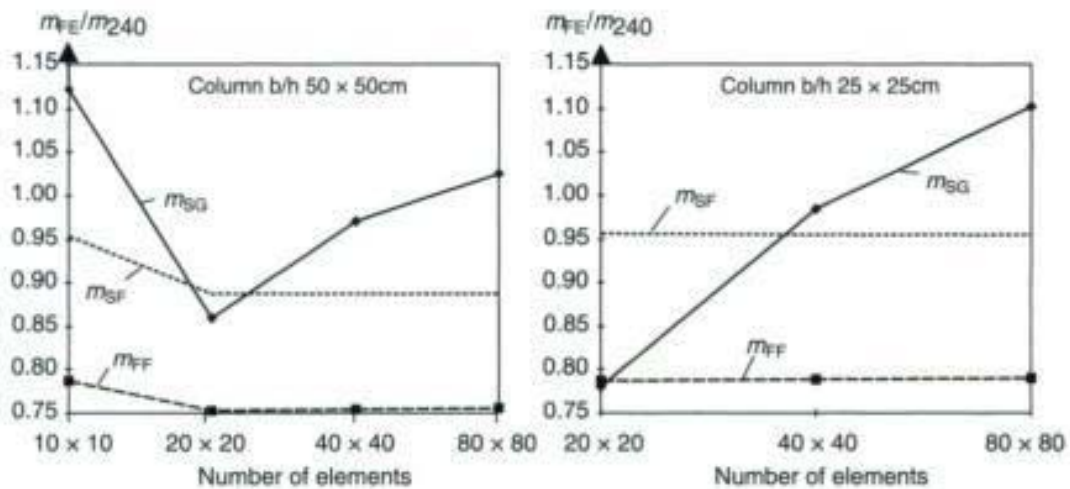


Fig. 4.35 Bending moment in the symmetry lines – all nodes above the column are fully restraint

The maximum value is not located at the face of the column. The elements over the support are free of any internal forces as their nodes are fully restrained.

As illustrated in Fig. 4.36, the size of the elements has a great influence on the maximum support bending moment. The bending



where:

- m_{SG} is the support bending moment in the inner strip
- m_{SF} is the support bending moment in the field strip
- m_{FF} is the span moment in the field strip
- m_{FE} are the moments from FE analysis
- m_{240} are the moments according to Heft 240 [10]

Fig. 4.36 Bending moment near the face of the column for different refined element meshes; column size 25 x 25 cm and 50 x 50 cm – all supported nodes fully restrained

moments near the face of the column (maximum value) are compared for various mesh refinements with the values calculated according to [10].

4.8.4 Elastic bedded elements

The problem of estimating the correct bedding modulus C has already been discussed in section 4.4. It has to be noted that the bedding of the elements above the column results in a partial restraint of the slab, as is the case when all nodes are restrained in the vertical direction. For a very high bedding modulus C , the same effects occur as for fully restrained nodes.

Figure 4.37 shows the moment distribution in the column axis for a bedding modulus of $C = 9000 \text{ MN/m}^3$. 40×40 elements are used for a quarter of the slab. The column has a cross-section of $25 \times 25 \text{ cm}$. Hence 2×2 elements and 4×4 elements for a column of $50 \times 50 \text{ cm}$ are bedded. The results of the numerical analysis do not change much if the element mesh is further refined.

The desired smoothed distribution of the bending moment over the column can be seen in Fig. 4.37. The maximum bending moment decreases with the size of the column. A good correlation of the results with the values provided by Heft 240 [10] is obtained.

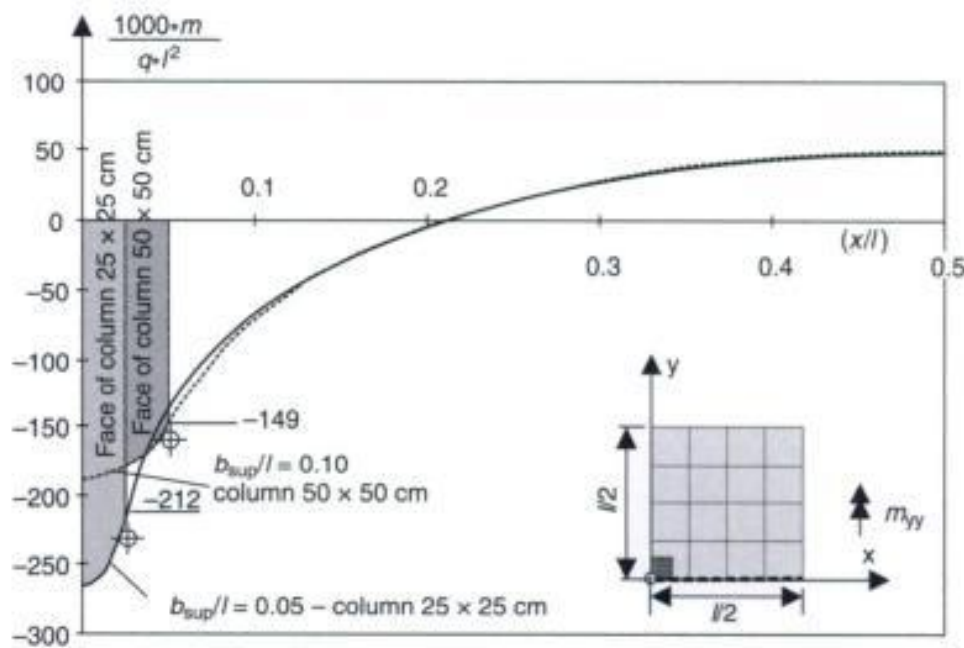


Fig. 4.37 Bending moment in section $y = 0$ – elastic bedded elements

Finite element design of concrete structures

As shown by the parametric study with different bedding modulus C , only the maximum bending moment at the support is dependant on the
difference of the moment (see Fig. 4.28). A. C. Abou-Elkhair, Ph.D., Lecturer

Restricted Page

This page is unavailable for viewing ([why?](#)). You may continue browsing to view unrestricted pages, or visit the [About this Book](#) page.

In contrast to the previously mentioned model, the rotation of the nodes (φ_{x_1} , φ_{y_1} , φ_{z_1}) are not combined for a hinged coupling. Only the

Restricted Page

This page is unavailable for viewing ([why?](#)). You may continue browsing to view unrestricted pages, or visit the [About this Book](#) page.

Finite element design of concrete structures



Restricted Page

This page is unavailable for viewing ([why?](#)). You may continue browsing to view unrestricted pages, or visit the [About this Book](#) page.

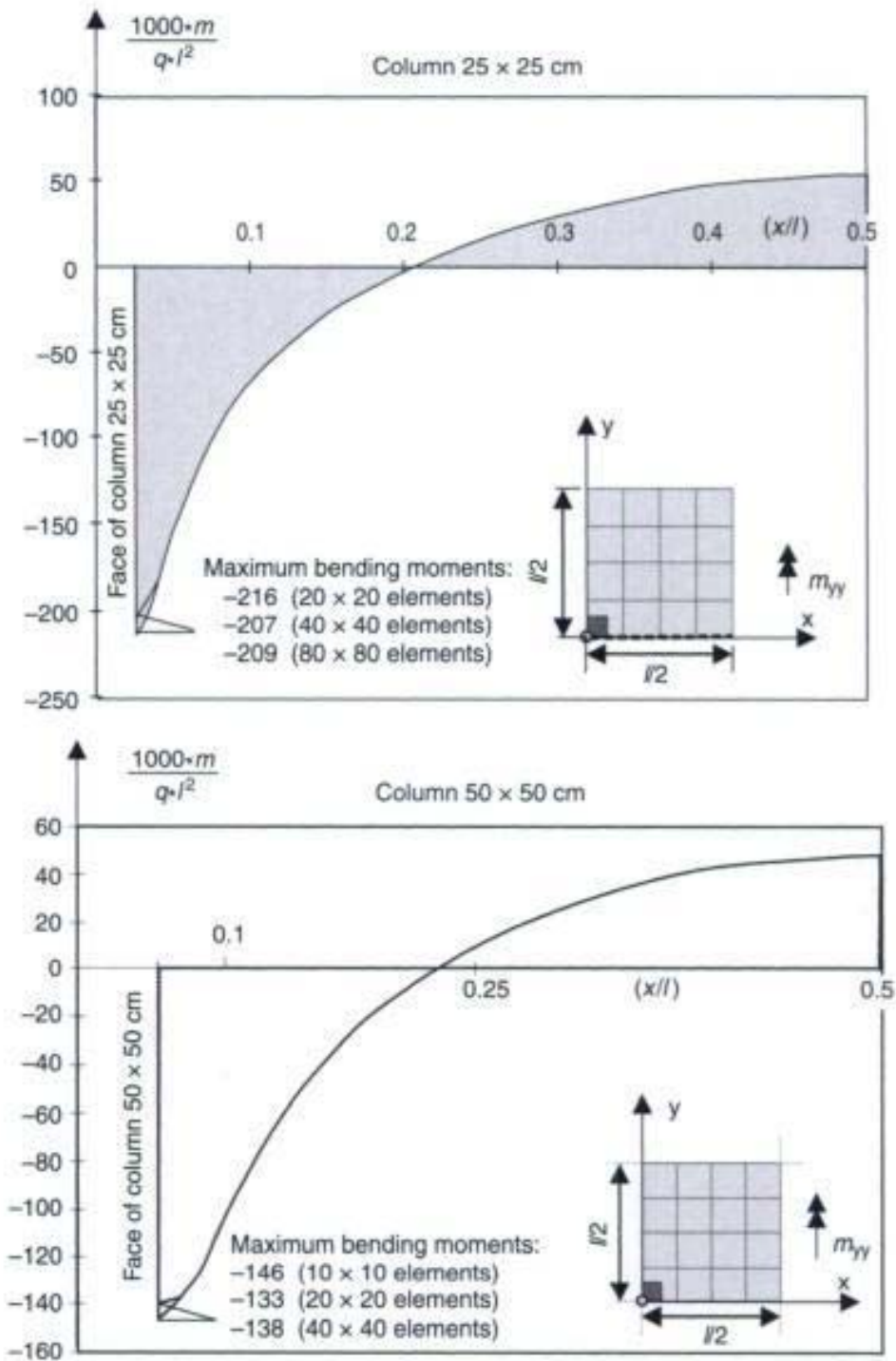


Fig. 4.39 Bending moment in section $y = 0$ – hinged coupling of the nodes

done in the centre of the elements and not at the nodes. A parabolic smoothed bending moment distribution over the support should be used if there is no monolithic connection between the slab and the column.

Table 4.9 Span and support bending moments for a flat slab according to different models ($b_{\text{sup}} = 25 \text{ cm}$, $l_x = l_y = 5 \text{ m}$, 40×40 elements)

Span moments	DAfStb [10] (manual analysis)	Pin support of 1 node	Pin support of 3 nodes	Bedding	Hinged coupling
Inner strip 1 m_{FG}	13.0 (13.0)* (100%)	12.9 (99%)	12.7 (98%)	12.8 (99%)	12.7 (98%)
Field strip m_{FF}	10.3 (8.75)* (100%)	8.3 (81%)	8.2 (80%)	8.3 (81%)	8.2 (80%)
Support moments (at the face)	DAfStb [10] (manual analysis)	Pin support of 1 node	Pin support of 3 nodes	Bedding	Hinged coupling
Inner strip 1 (face) m_{SS}	-56.0 (-44.8)* (100%)	-63.3 (113%)	-41.2 (74%)	-59.1 (106%)	-41.2 (74%)
Inner strip 2 m_{SG}	-39.2 (-29.2)* (100%)	-32.3 (82%)	-30.6 (78%)	-31.7 (81%)	-30.6 (78%)
Field strip m_{SF}	-7.5 (-10.4)* (100%)	-4.6 (61%)	-4.5 (60%)	-4.6 (61%)	-4.5 (60%)

* Values in parentheses: equivalent girder system according to [10]

4.8.8 Slab – edge column connection

In general the bending stiffness of interior columns can be neglected, but this does not apply to edge or corner columns. The partial restraint of the slab can be modelled by torsional springs or by bedding of the support elements. A spring stiffness of $C = 3EI/l$ and $C = 4EI/l$ may be used for a column which is pin ended on the base and a fully restrained column, respectively (Fig. 4.41). The upper boundary value is gained if all nodes are fully restrained. The reduction of stiffness of a cracked member relative to the elastic value should be considered.

The node in the centre of the supported area is fixed for a pin support. Thus, a small cantilever slab is created which shows bending moments perpendicular to the free edge.

The following calculations are carried out on a simple system, a rectangular flat slab with equal span length $l_x = l_y = 5.0 \text{ m}$ supported by four edge columns (25/25 cm). Due to this being a symmetric system, only a quarter has to be modelled. A uniform load of $q = 10 \text{ kN/m}^2$ is applied.

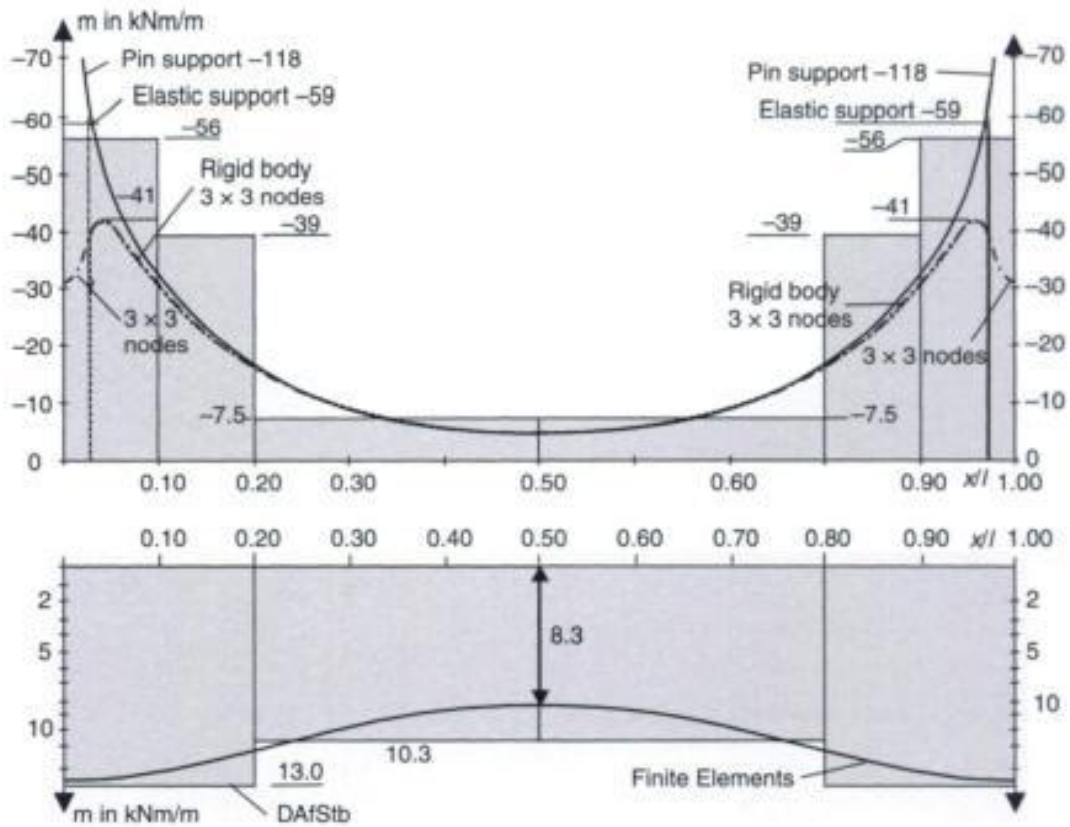
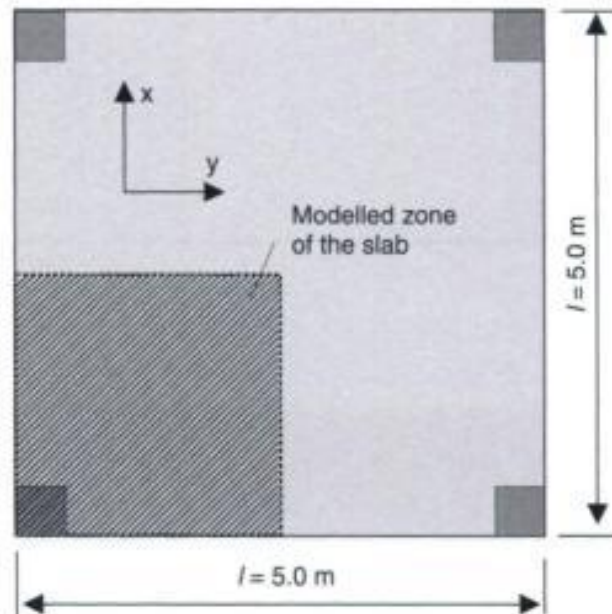


Fig. 4.40 Transverse distribution of the bending moment perpendicular to the main load transfer direction according to DAFStb [10] (shaded area) and the Finite Element Method



Bedding moduli between $C = 9 \cdot 10^6 \text{ kN/m}^3$ and $27 \cdot 10^6 \text{ kN/m}^3$ are used. The first value corresponds to the normal stiffness $C_N = E/l$ of a

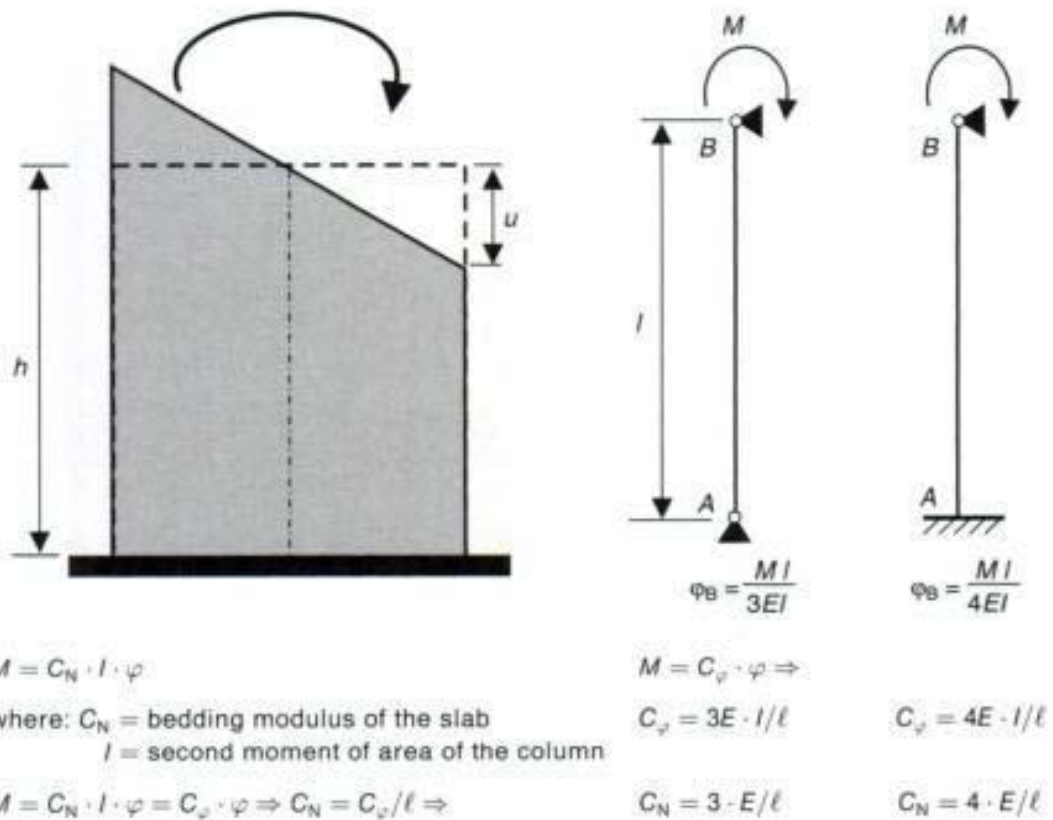


Fig. 4.41 Bedding modulus C_N to model the bending stiffness of a column

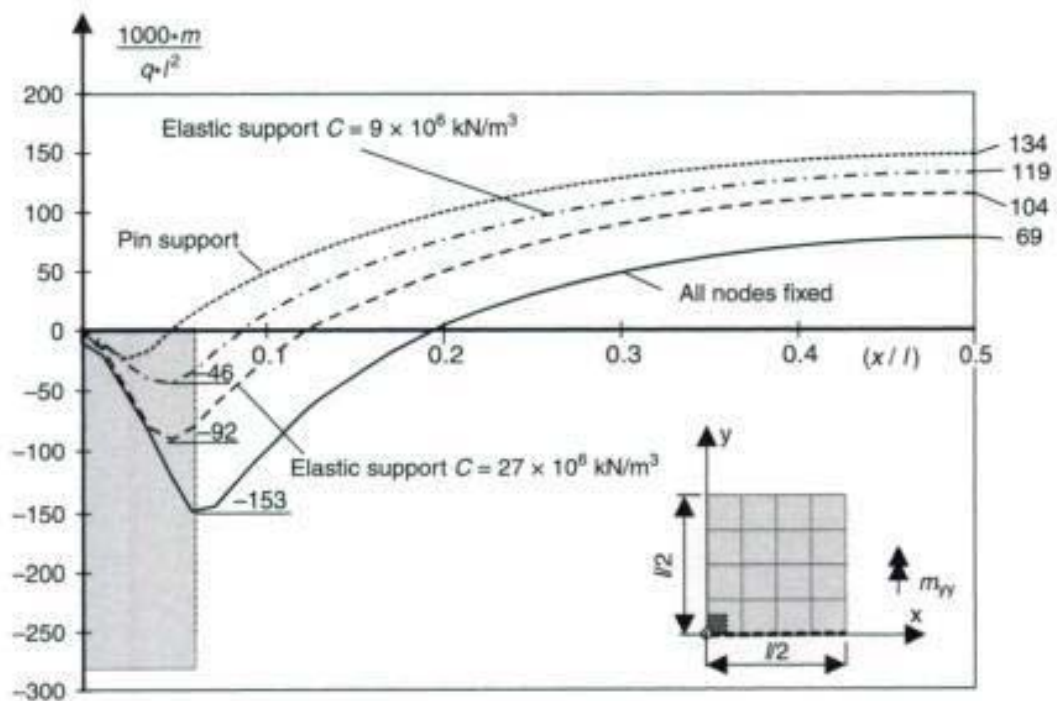


Fig. 4.42 Bending moment m_{yy} in section $y = 0$ of an edge supported slab for different bedding moduli C

3.55 m high column with a Young's modulus of $E_C = 32\,000\text{ MN/m}^2$ (concrete grade C30/37). If the bending stiffness is considered, a value of $C_N = 3E/l = 27 \cdot 10^6\text{ kN/m}^3$ has to be used.

Figure 4.42 shows the bending moment distribution m_{yy} at the edge of the slab ($y = 0$) for different models. The moment at the face of the column and at midspan is very sensitive to the numerical model of the support.

The span moment at the outer edge of the slab is 30% greater if bedded elements are used instead of a pin support. Significant differences can be observed at the relevant sections for design at the face of the column. The extreme values are 0 kNm/m to -38 kNm/m .

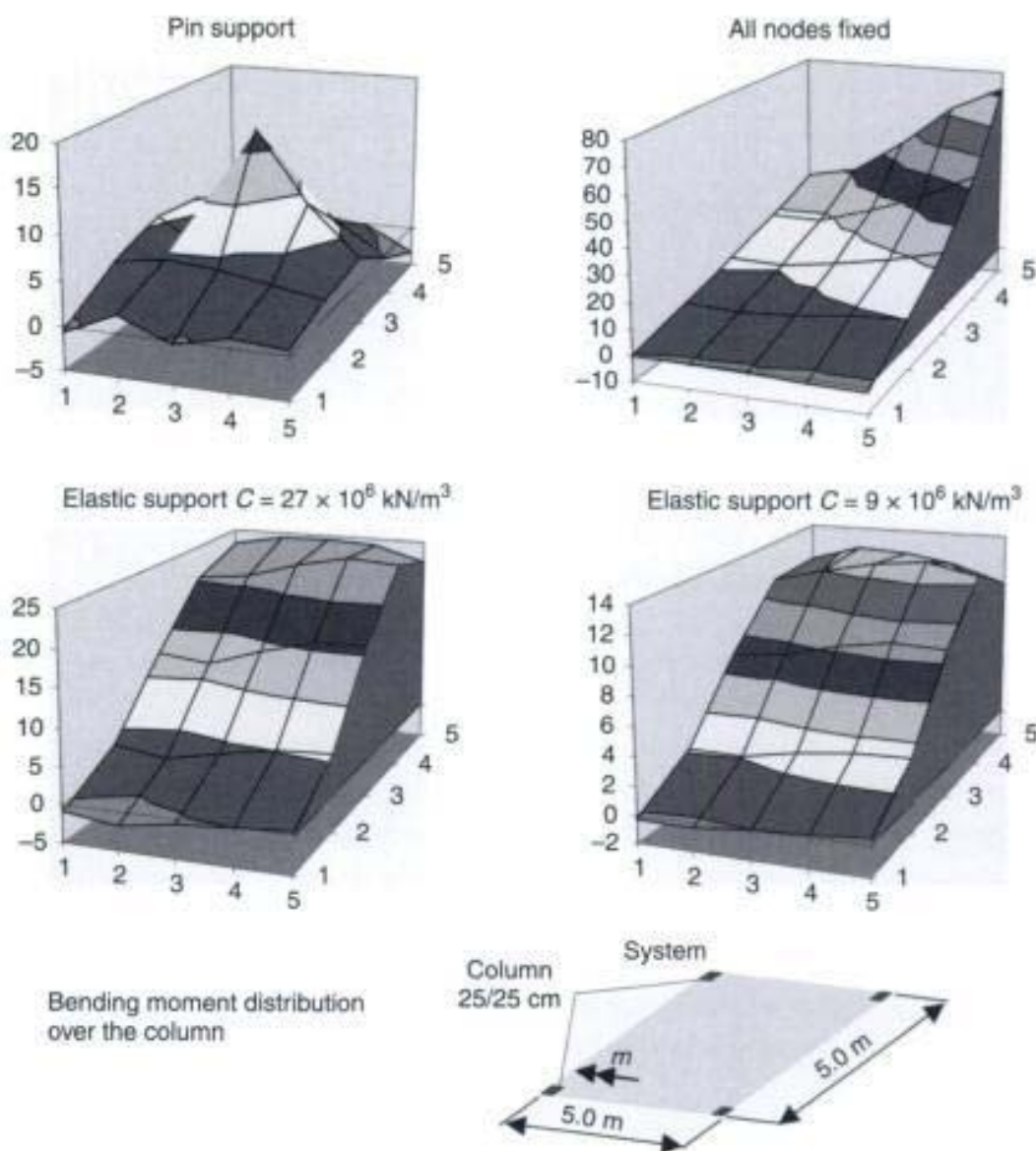


Fig. 4.43 Bending moments at an edge column for different models and bedding moduli C (thin shell elements)

These differences become clear, when the three-dimensional distribution of the bending moments above the column is checked. The peak values are not located on the symmetry axis. The largest bending moment is between $m = -14 \text{ kNm/m}$ for bedded elements with $C = 9000 \text{ MN/m}^3$ and $m = -73 \text{ kNm/m}$ for fixed nodes.

4.9 Foundation slabs

Foundation slabs are spatial concrete structures which distribute the load of the structure before transferring it into the ground. Thus, the ground pressure is mostly reduced in comparison to footings.

The following foundation types are used in practice:

- (a) *Footings*
used for high concentrated forces (e.g. those resulting from column loadings).
- (b) *Strip foundations*
used beneath walls or series of columns.
- (c) *Foundation slabs*
used under buildings as load-bearing elements and for watertight structures.

The design of a strip foundation in the direction of the longitudinal axis can be done by means of an elastically supported beam model. The member forces in the transverse direction can be determined either analytically if the deformation of the structure can be neglected, or by means of a two-dimensional plate model (see section 4.9.2).

The internal forces of a foundation slab are mostly determined by means of the stiffness modulus method. The inaccuracies of this approach have already been discussed in section 2.4. The main advantage of this model lies in the fact that the bedding behaviour can easily be implemented within the element functions. Thus, no contact or interface elements are required which simplifies the mesh generation and the numerical analysis. Furthermore, a two-dimensional plane Finite Element model is sufficient whereas the constraint modulus method requires a three-dimensional model of the structure and the ground or an iterative solution. The following calculations are based on the stiffness modulus method.

4.9.1 Footings

Footings are used under high concentrated loads, for example those caused by columns. The panel dimensions necessary for these

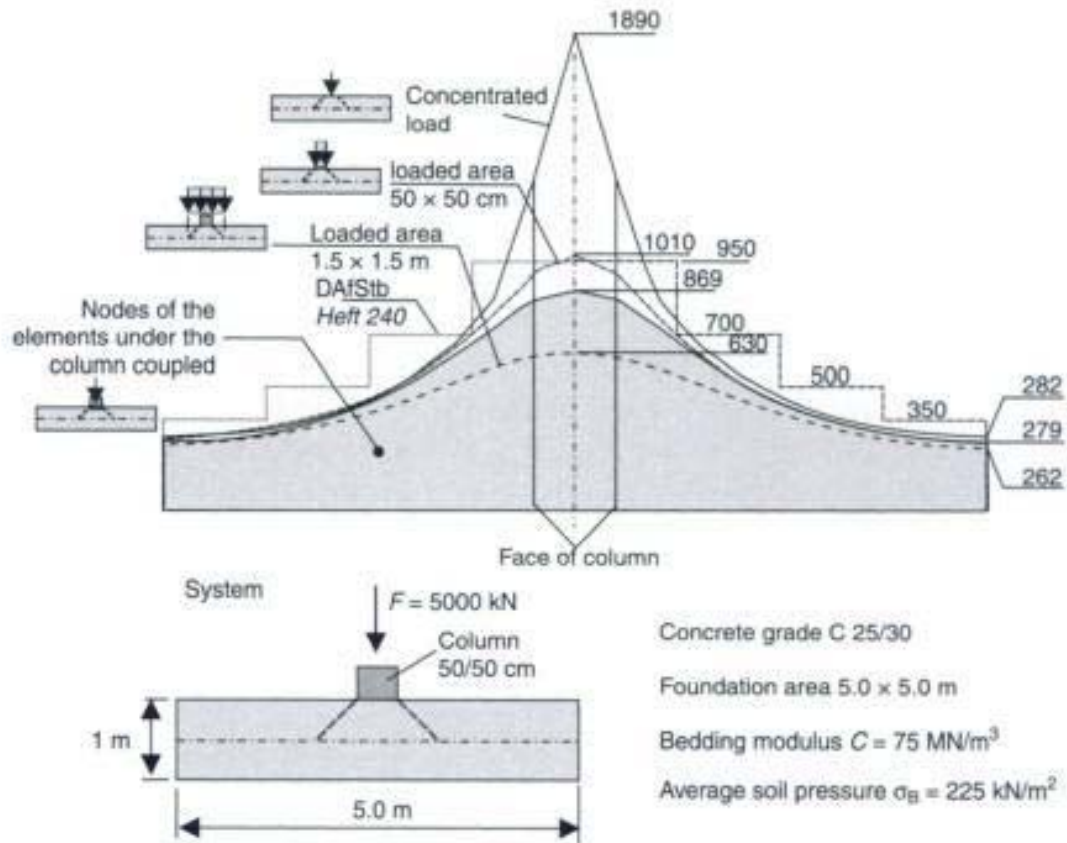


Fig. 4.44 Moment distribution of a single-slab foundation

foundations are mostly determined by the permissible soil pressures. The slab depth is fixed by the design for bending or by punching. For small loads, massive block foundations can be used which may not be reinforced. Such structures can be designed by means of strut-and-tie models. Numerical analysis is not required.

The following example focuses on the design of the foundation slabs. The internal forces can be calculated by means of a Finite Element model or simplified analytical methods, like the equivalent strip method given in [10]. Hence different models are available to verify the results.

The columns, which transfer the load to the foundation, can be modelled with different approaches like those used for flat slabs. The variants are (Fig. 4.44):

- a concentrated single loading;
- uniform loading over the area of the column (50/50 cm);
- uniform loading, extension of the loaded area to the midplane of the slab (1.50/1.50 m);

- hinge coupling of the elements in the column area with the node at the centre of the column (coupled area is equal to column dimensions, 50/50 cm).

Figure 4.44 shows the bending moment distribution in the symmetry axis calculated for the different models. The rectangular slab with $l_x = l_y = 5.0\text{ m}$ is loaded by a concentrated force of $F = 5000\text{ kN}$. The stepped curve is calculated with the simple analytical model given in [10]. With the given Finite Element model, a single concentrated load results in a very high moment peak (singularity) of $m_{\max} = 1890\text{ kNm/m}$. If the load is distributed over the area of the column ($m_{\max} = 1010\text{ kNm/m} = 100\%$), it results in only half of this value. A coupling of the elements under the column results in a further decrease in the maximum moment by approximately 14%. A bending moment of $m_{\max} = 630\text{ kNm/m} = 62\%$ is obtained, when the column load is dispersed up to the midplane of the foundation slab at an angle of 45° , resulting in a loaded area of $1.50 \times 1.50\text{ m}^2$. It can be observed that the size of the loaded area has a significant influence on the bending moment distribution.

The correct model and the correct loaded area can only be found by verification with experimental results or by means of a three-dimensional Finite Element analysis. The main bending moments show an axisymmetric pattern in the column region as can be seen in Fig. 4.45. Thus, an axisymmetric model (diaphragm) and not a three-dimensional model is sufficient to determine the correct

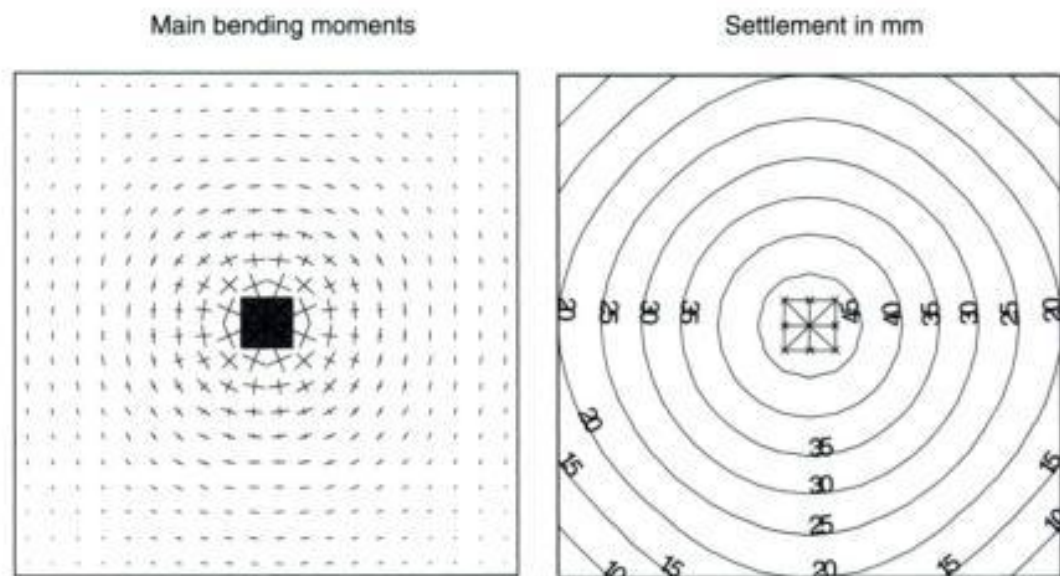


Fig. 4.45 Main bending moments and settlements

Slabbs



Restricted Page

This page is unavailable for viewing ([why?](#)). You may continue browsing to view unrestricted pages, or visit the [About this Book](#) page.

3926 KN

Restricted Page

This page is unavailable for viewing ([why?](#)). You may continue browsing to view unrestricted pages, or visit the [About this Book](#) page.

Slabs



Restricted Page

This page is unavailable for viewing ([why?](#)). You may continue browsing to view unrestricted pages, or visit the [About this Book](#) page.

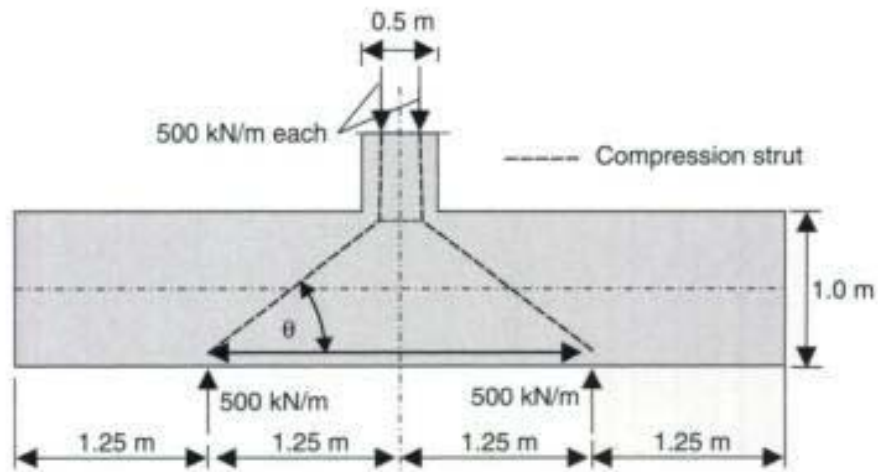


Fig. 4.51 Simple strut-and-tie model of a strip foundation in transverse direction

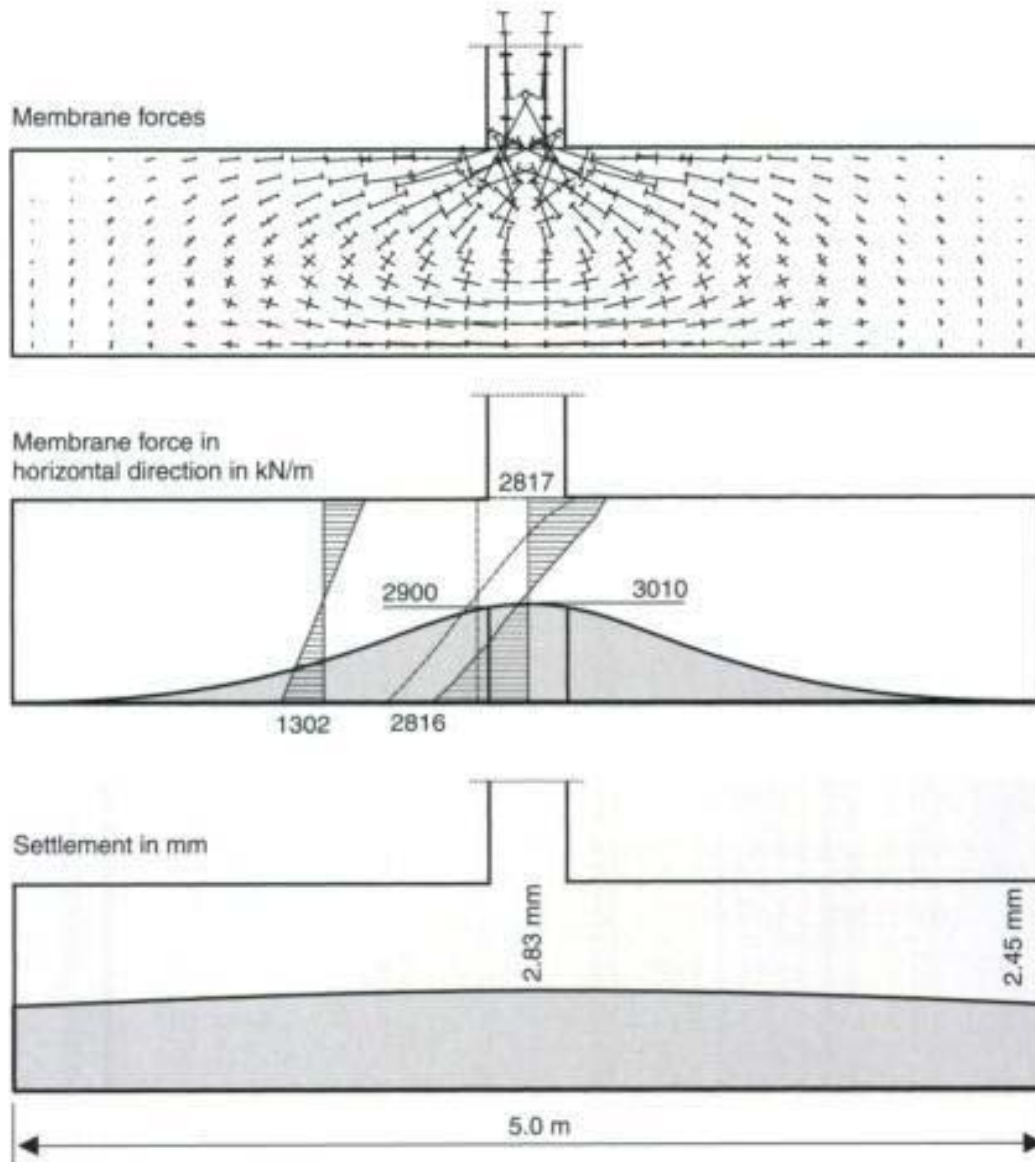


Fig. 4.52 Strip foundation – membrane forces and settlements

4.10 Skewed slabs

The previous sections only focus on rectangular slabs or flat slabs. These simple structures have been used to demonstrate the basic problem of finding an adequate model for the supports and the loaded area. In practice more complicated slab systems are built, which have complex support conditions and irregular layout (Fig. 4.53). It is one of the most important advantages of concrete that structures can be built in arbitrary shapes.

Skewed slabs with two simply supported opposite sensibly parallel edges and two free edges are often used for single-span bridges. A line support results in infinite shear forces and bending moments in the obtuse corner. This can be seen in Fig. 4.54, which shows the distribution of the internal forces at a simply supported edge. The slab has a width of 13 m and an angle of 45° to the supported axis. The singularity of the support forces can be seen clearly.

The peak moments can be reduced significantly, if the stiffness of the individual bearings is considered. In Fig. 4.54 the internal forces are plotted for a slab with three elastomer bearings ($50 \times 25 \text{ cm}^2$, height $h = 10 \text{ cm}$) on each side. The main shear force in this system is one third of that of the simple continuous supported slab. The bending moment m_{yy} in transverse direction is increased from -234 kNm/m to -409 kNm/m . This is caused by the transverse bending of the slab

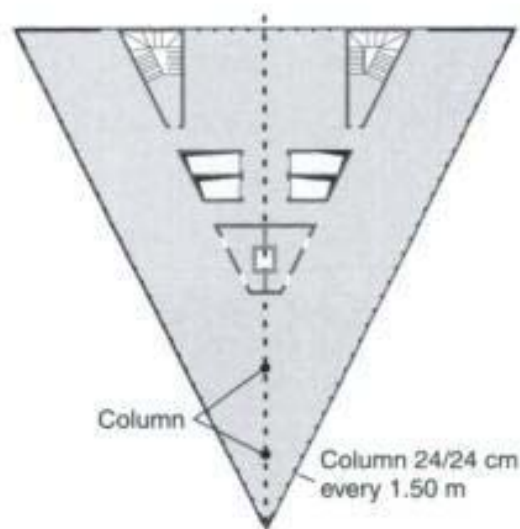


Fig. 4.53 Triangular slab of an office building

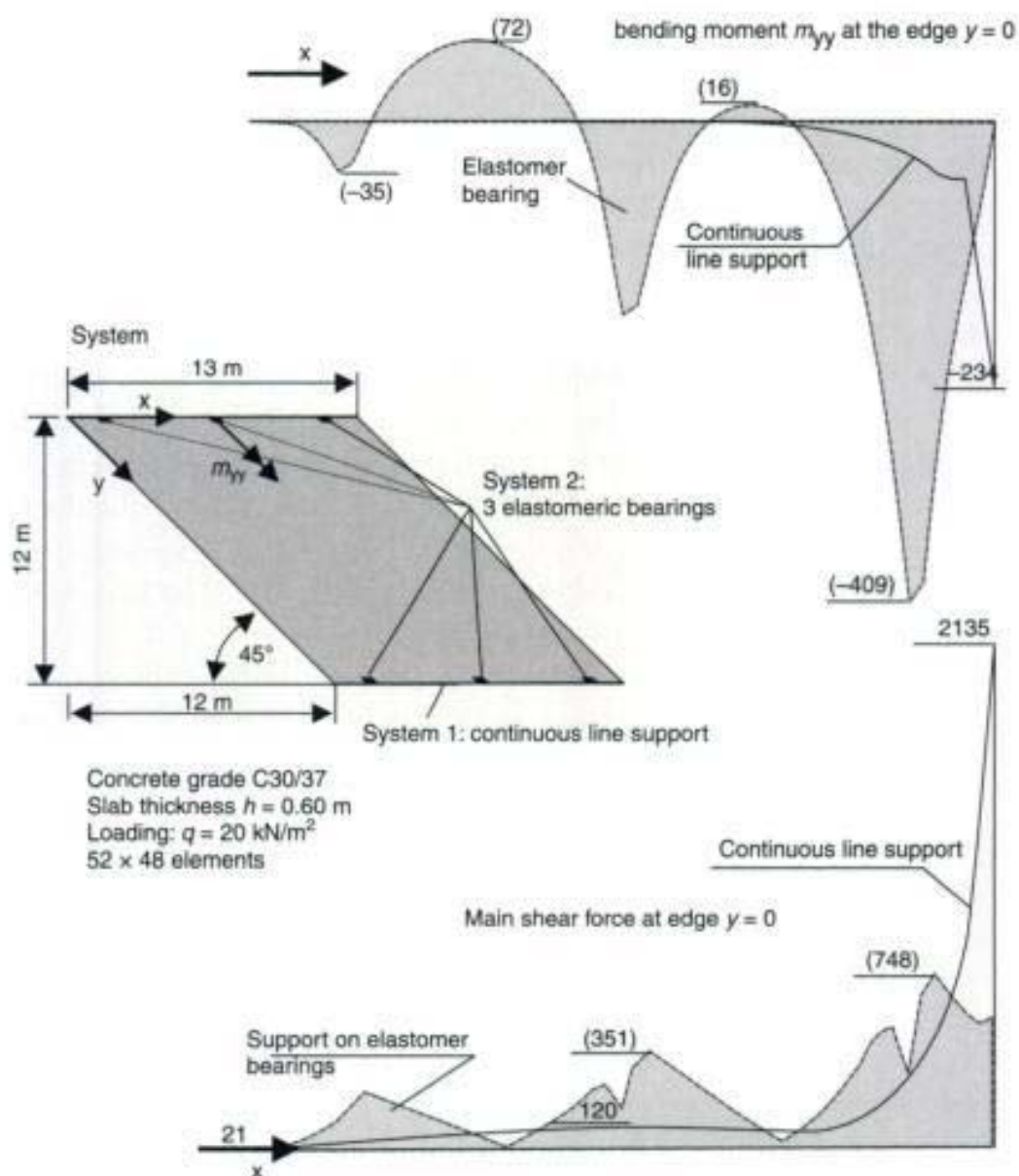


Fig. 4.54 Bending moment and main shear force at the supported edge of a skewed slab

Table 4.10 Internal forces and deflections at midspan ($y = 0.5l = 6$ m)

	Rigid support		Elastomer bearings	
	Centre	End	Centre	End
Bending moment m_{yy} : kNm/m	0	131	-29	121
Bending moment m_{xx} : kNm/m	397	195	414	196
Shear force v : kN/m	0	331	0	406
Deflection w : mm	11.5	14.7	18.6	20.6

due to the single bearings. The transverse bending moment can be reduced if the number or the size of the bearings is increased.

The internal forces at the midspan are almost independent of the support conditions, as shown by the figures given in Table 4.10.

4.11 Singularities

Singularity problems may arise in linear-elastic slab calculations as has been previously shown. Some problems can be avoided by an elastic support or an extension of the loaded area. Singularities may occur in the regions of (Fig. 4.55):

- walls which end within a slab (section 4.6);
- discontinuous line supports (section 4.6);
- pin support (section 4.8);
- obtuse corners (section 4.10).

Two more singularity regions which are relevant in practice are treated next:

- openings;
- re-entrant corner ($\alpha \geq 90^\circ$);
- concentrated loads.

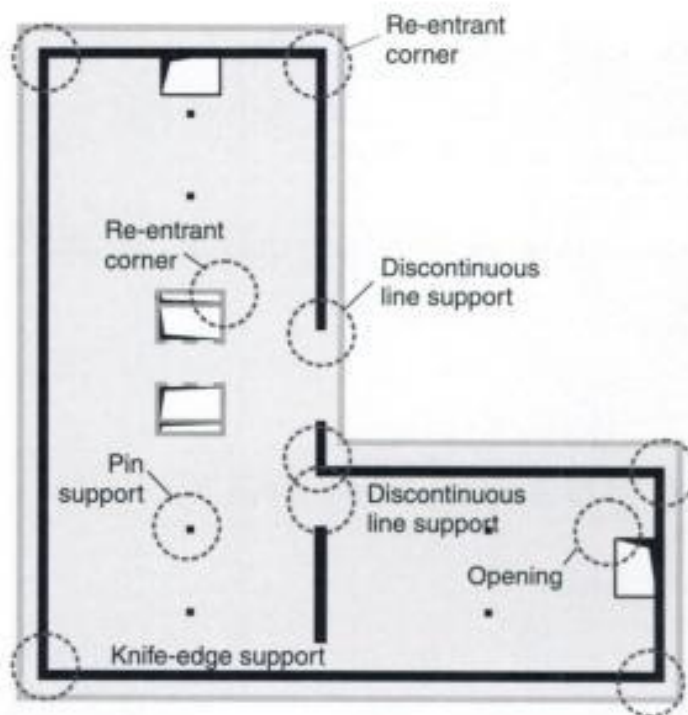
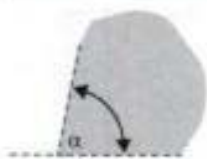










Fig. 4.55 Singularities

Table 4.11 Singularities of FE-models based on Kirchhoff plate elements

Support condition	Moments	Shear forces
	$\alpha > 180^\circ$	$\alpha > 78^\circ$
	$\alpha > 90^\circ$	$\alpha > 51^\circ$
	$\alpha > 90^\circ$	$\alpha > 60^\circ$
	$\alpha > 95^\circ$	$\alpha > 52^\circ$
	$\alpha > 129^\circ$	$\alpha > 90^\circ$
	$\alpha > 180^\circ$	$\alpha > 126^\circ$
<p>----- free edge</p> <p>———— hinge support</p> <p>===== fully restraint</p>		
Loading	Displacement, rotation	Internal forces
	No	Yes (m_x, m_y, v_x, v_y)
	Yes ($\varphi_y = \frac{dw}{dx}$)	Yes (m_{xy}, v_y)
	No	Yes (v_x)

Copyrighted Material

Slabs

Singularities are caused by simplifications of numerical models [31].
The assumption of a linear strain distribution over the section depth

Restricted Page

This page is unavailable for viewing ([why?](#)). You may continue browsing to view unrestricted pages, or visit the [About this Book](#) page.

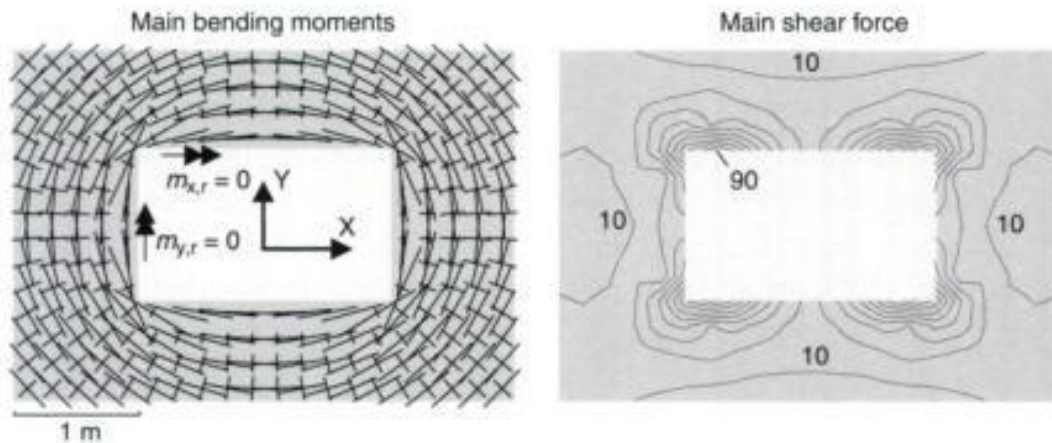


Fig. 4.57 Main bending moments and shear forces in the region of an opening

The maximum peak value depends on the size of the relevant elements. Only a small region near the corner is influenced by the singularity (see Fig. 4.56).

The distribution of the principal bending moments and shear forces in the region of an opening is shown in Fig. 4.57. The high increase of the shear force in the corner indicates a singularity problem. The shear design of the slab is not possible (and not required) for these peak values.

Singularity problems can be avoided by smoothing the edges, by rounding the corners in the Finite Element model. However, this effort is not required in practice, as shown by the previous analyses.

4.11.2 Re-entrant corners ($\alpha \geq 90^\circ$)

Figure 4.58 shows the distribution of the main bending moments in the region of a cantilever slab, where two supporting walls meet at right angles. The singularity can be clearly seen. This problem can be solved, if the vertical stiffness of the walls is considered in the numerical model (see Fig. 4.58). The bedding modulus at the supports is chosen though the vertical deflection of the slab under the wall is less than 0.8 mm in this example. Even with this small value the shear forces and the bending moments are reduced by a factor of 3 and 2, respectively, relative to those of a slab with rigid supports.

4.11.3 Concentrated loads

In the linear-elastic Kirchhoff slab theory, infinite internal forces are calculated under a point load (see Fig. 4.59), whereas the deflections

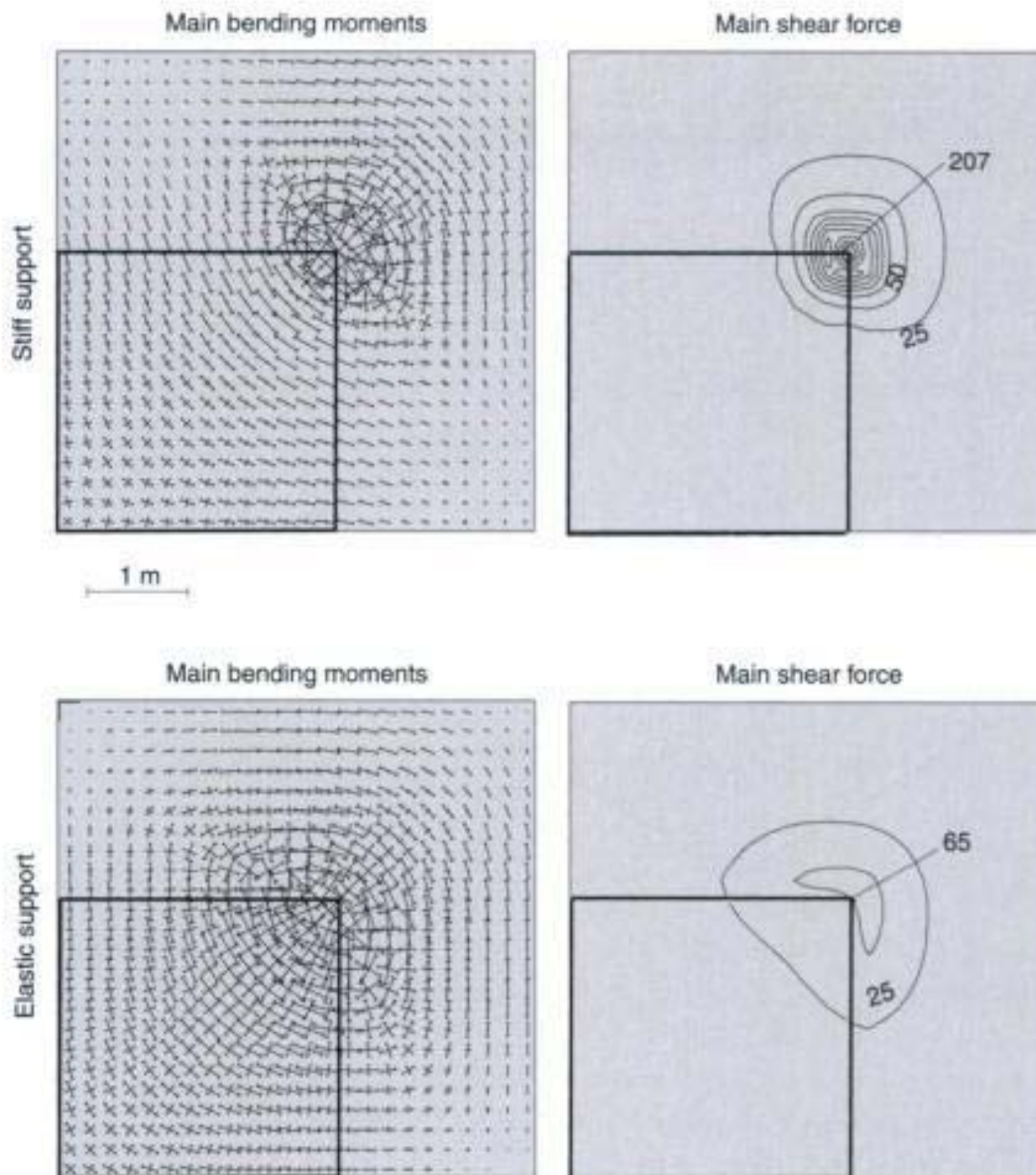


Fig. 4.58 Internal forces of a slab which is supported by two perpendicular walls – no supports at the outer edges.

are limited. This singularity problem can easily be solved by a spreading of the loaded area. This will be shown in the following.

Concentrated loads may occur, for example on a deck slab of hollow box or T-beam bridges. The internal forces due to truck loading are calculated using a simplified system of a partially restrained equivalent slab (see Fig. 4.60), as in practice a 3-D Finite Element model of the whole structure is too extensive. A detailed estimation of the effective span length is not required with regard to the assumptions of the model. The torsion stiffness may be estimated by separate manual calculations,

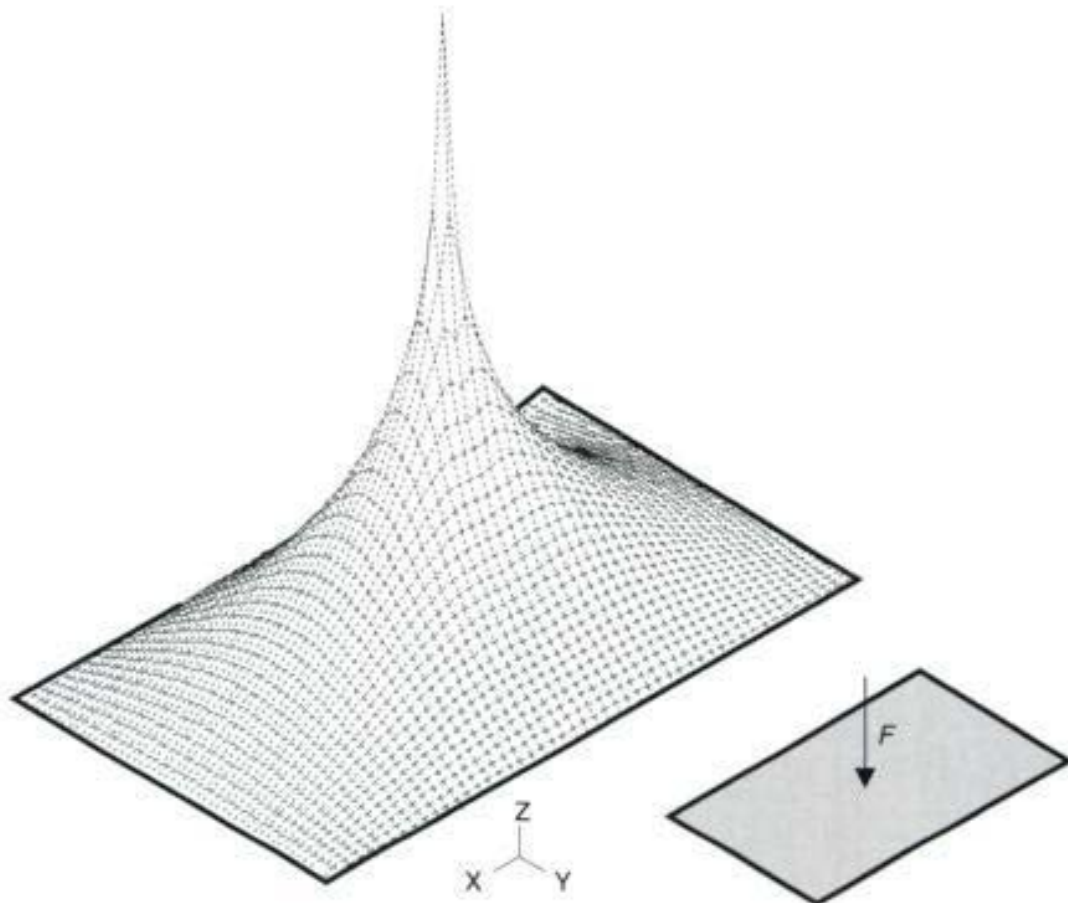


Fig. 4.59 Moment distribution of a rectangular slab loaded by a point load at the midspan

e.g. using an equivalent beam model. It depends not only on the structural system but also on the type of the loading.

The point load has to be distributed up to the midplane to avoid singularities (Fig. 4.61).

Figure 4.62 shows the significant influence of the loaded area on the bending moments. Here the bending moments for a total force of $F = 100 \text{ kN}$ and a loaded area of $0 \times 0 \text{ cm}^2$, $24 \times 20 \text{ cm}^2$, and $60 \times 96 \text{ cm}^2$ are plotted. The slab has an effective span length of $l_{\text{eff}} = 6.0 \text{ m}$ and a constant thickness of $h = 20 \text{ cm}$. The inclined haunches near the webs are neglected.

A Finite Element analysis of the deck slab is required if more accurate internal forces are needed for design or in the case of special load arrangements. Tables in literature and influence lines provided by Homberg and Ropers [19] and Homberg [20] can be used for standard conditions. The determination of the internal forces by means of tables may be time-consuming as various values have to be interpolated; thus, a Finite Element analysis may become economical.

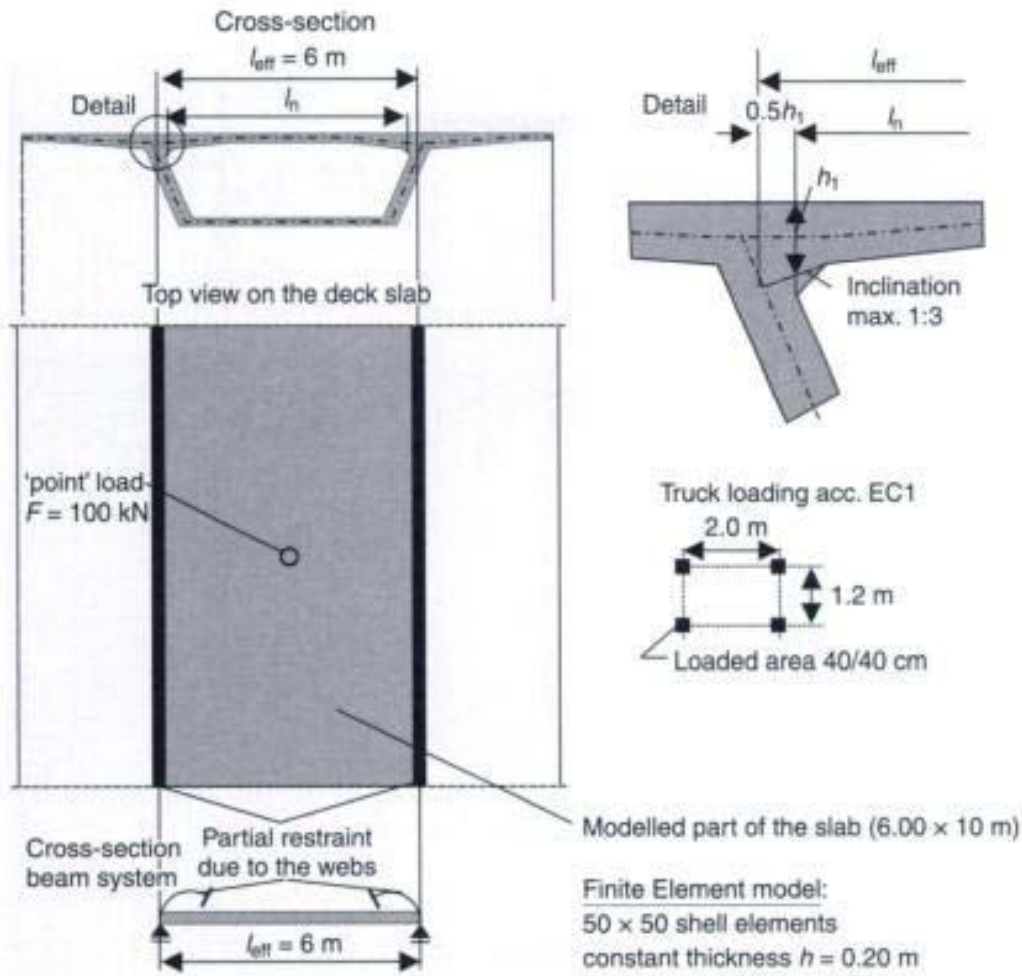


Fig. 4.60 Equivalent slab model for the deck of a hollow box girder bridge

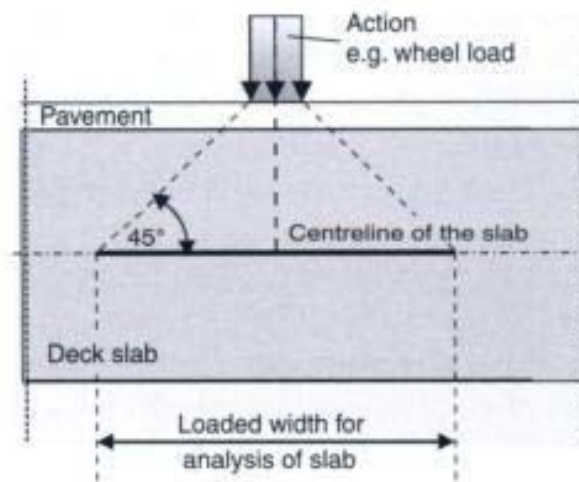


Fig. 4.61 Dispersion of concentrated loads up to the midplane

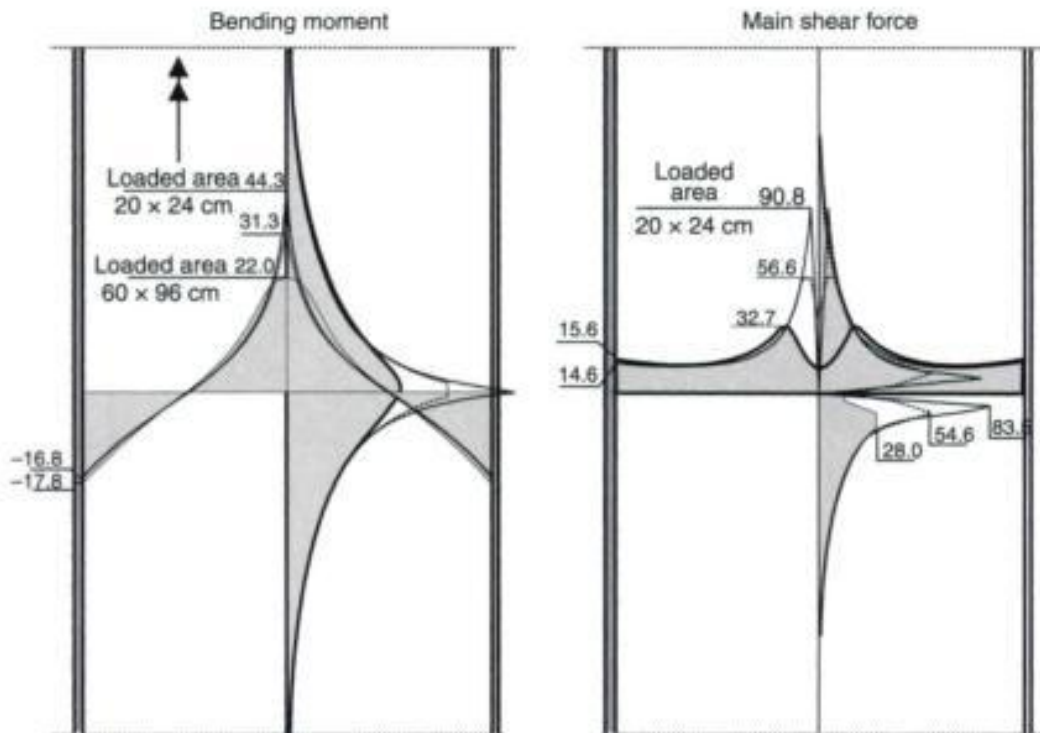


Fig. 4.62 Moment and shear force distribution of a plate strip loaded by a force of $F = 100$ kN at midspan – different loaded areas

4.12 Discretization – generation of the element mesh

Nowadays, the generation of the element mesh is done by means of graphical pre-processors. The effort is considerably less than a manual input. Also, input errors, caused by incorrect node coordinates or restraints, are mostly avoided by the visual control.

An automatic mesh generation can only consider the main geometrical boundaries. Refinements are required in regions of great stress gradients, and have to be done manually by the user if no adaptive mesh refinement tools are available. Hence, the mesh generation requires sufficient experience and skills in use of the Finite Element Method and knowledge of material properties too.

The problems of mesh generation are demonstrated by the following two practical examples.

4.12.1 Location of the restraint nodes

The support nodes of simply supported circular slabs should be located exactly on the outer circumference. Even small differences may result in a partial restraint of the slab even in the case of hinge support. This problem is demonstrated on a simple example.

*Image
not
available*

Restricted Page

This page is unavailable for viewing ([why?](#)). You may continue browsing to view unrestricted pages, or visit the [About this Book](#) page.

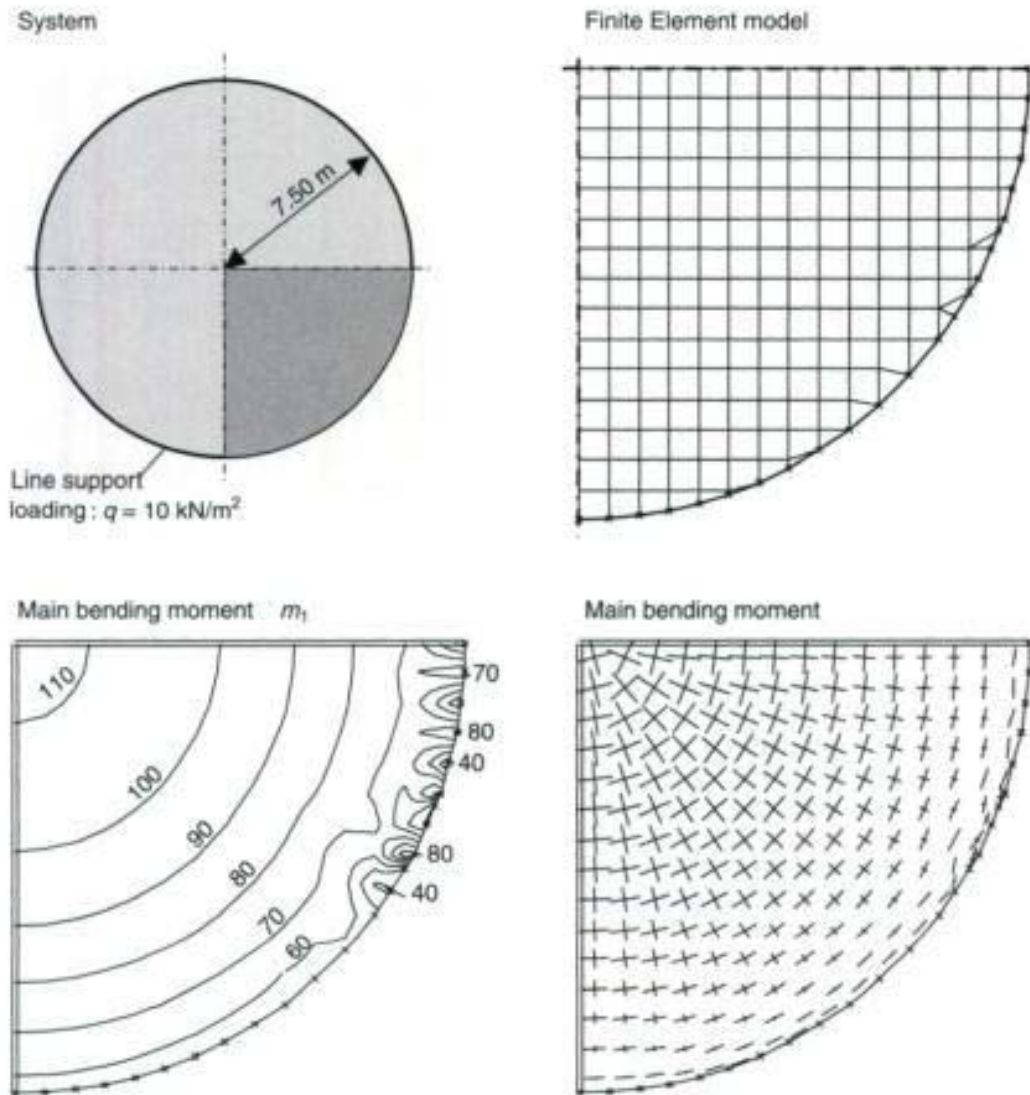


Fig. 4.64 Circular slab – boundary nodes not accurately placed on the outer circumference

Figure 4.64 shows the Finite Element mesh and the resulting main bending moments. Due to the symmetry conditions it is sufficient to only model a quarter of the whole slab.

The orientation of the main bending moments at the upper edge of the slab is surprising. A support moment of $m_1 = 80 \text{ kNm/m}$ has been calculated. This moment is 70% of the maximum bending moment in the centre even for a structure which is supported by hinges.

This error is caused by the faulty location of the supported nodes. The fixed nodes at the upper right of the slab are located in a sawtooth manner, 1 mm away from the circle. Even this small value, equivalent to 1/1500 of the diameter, has a significant influence on the bending moments. The same problem arises in rectangular slabs, for cases where the fixed nodes are not located accurately on a straight line.

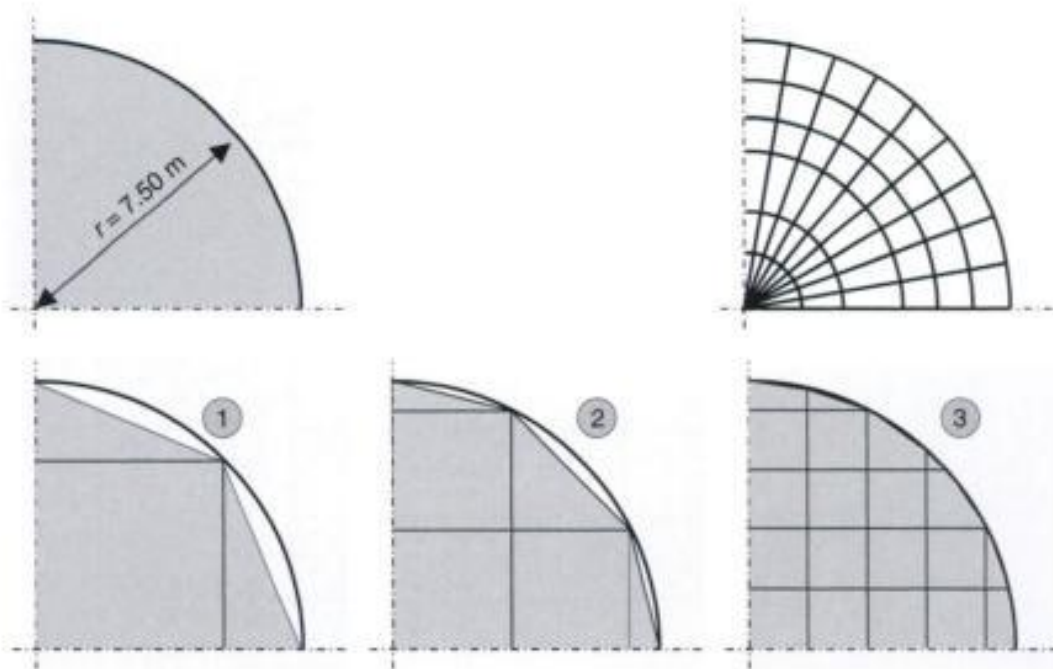


Fig. 4.65 Finite Element meshes for a circular slab – various number of elements

This example has impressively shown that the fixed nodes should be precisely located at the curved boundary.

Very often only the graphical output of a Finite Element analysis is checked. Errors in node coordinates, like those referred to above, can then hardly be noticed. Therefore, the checking of a Finite Element analysis should not be restricted only to the graphical output of the software.

4.12.2 Size of the elements

A sufficient number of elements have to be used in order to model the real deformation characteristics and the load-bearing behaviour of a structure. This has to be considered particularly for curved boundaries as will be shown on the simply supported circular slab under uniform load of $q = 10 \text{ kN/m}^2$, mentioned previously.

Figure 4.66 shows the bending moment distribution and the deflection in the centre of the slab for different number of elements. The correct values can be estimated analytically.

bending moment in the centre

$$m_l = \frac{q \cdot r^2}{16} (3 + \nu) = \frac{10 \cdot 7.5^2}{16} (3 + 0.2) = 112.5 \text{ kNm}$$

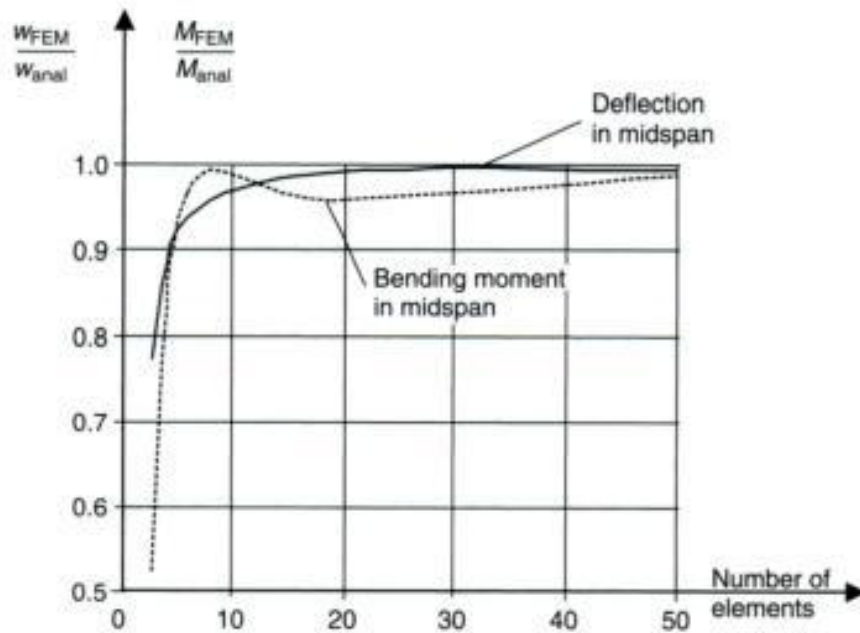


Fig. 4.66 Deflections and bending moment in the centre of a circular simply supported slab for different number of elements

deflection in the centre

$$\begin{aligned}
 w &= \frac{(5 + \nu) \cdot q \cdot r^4}{64 \cdot (1 + \nu) \cdot \frac{E \cdot h^3}{12 \cdot (1 - \nu^2)}} \\
 &= \frac{(5 + 0.2) \cdot 10 \cdot 7.5^4}{64 \cdot (1 + 0.2) \cdot \frac{34 \cdot 10^6 \cdot 0.5^3}{12 \cdot (1 - 0.2^2)}} \cdot 10^3 = 5.8 \text{ mm}
 \end{aligned}$$

The results show that only $4 \times 6 = 24$ elements are required for the whole slab in order to get satisfactory results.

Nowadays, due to the increasing computer capacity, the size of the numerical model or the number of elements does not usually play an important role. Therefore, modelling is often done quickly, without sufficient attention paid to the relevant details. What may be considered as unimportant details, such as a one-way cantilever slab or a small opening in a flat slab near a column support, are not noticed. However, these are the regions where high gradients of the internal forces may occur.

The problems, due to neglecting such 'unimportant' details, are demonstrated by a simple cantilever slab. This is not a theoretical example. Such a problem had occurred in a real big slab, whereas, unfortunately, the mistake had only been noticed after the slab had been poured with insufficient reinforcement. Excessive retro fitting was required. The

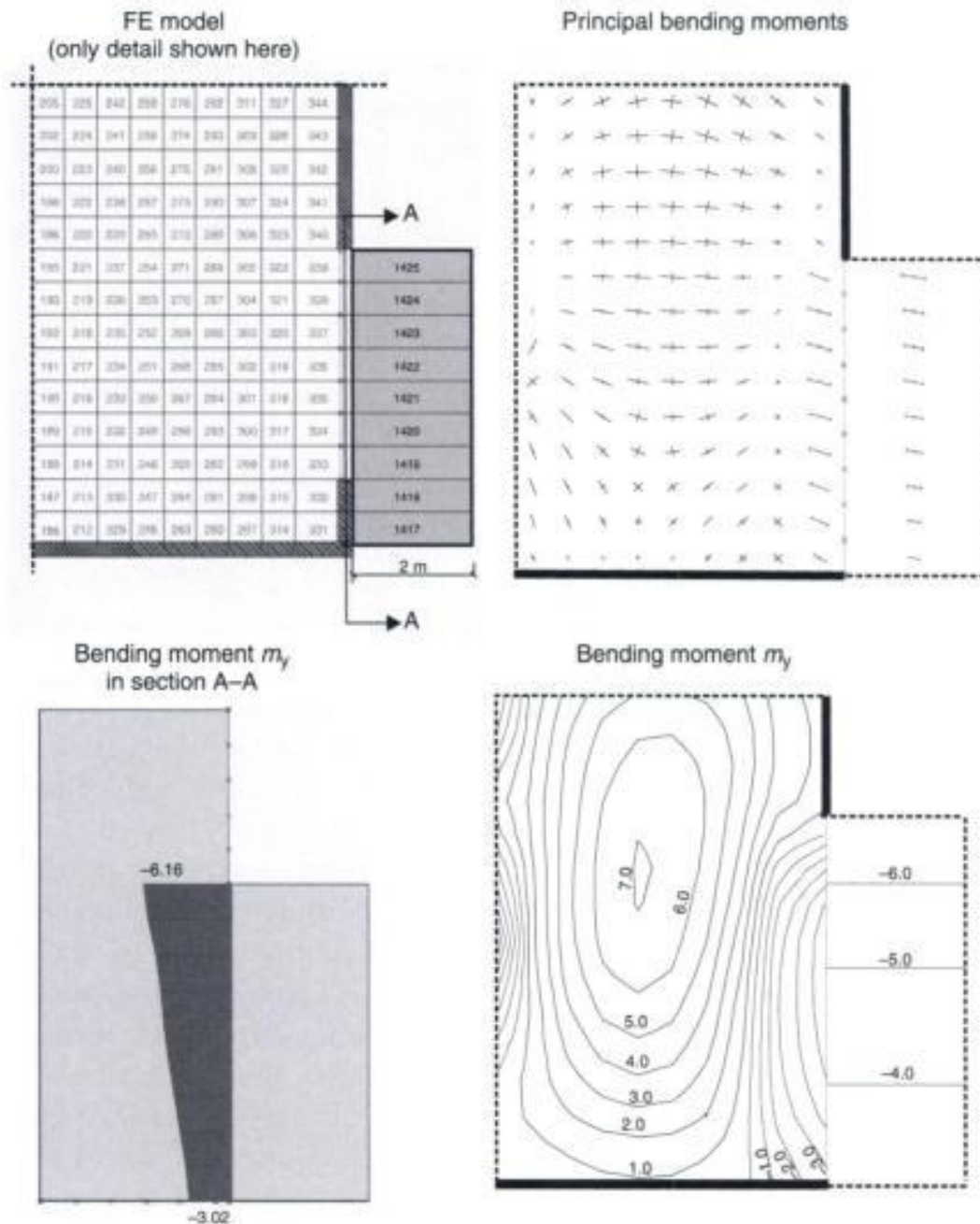


Fig. 4.67 Bending moments in the region of the balcony

system and the element model are shown in Fig. 4.67 (the full system is shown in Fig. 4.4). The balcony had been only modelled with one element layer, as it has a simple one-way load-bearing behaviour. A uniform load of $q = 5 \text{ kN/m}^2$ is applied on the whole slab. This results in a support bending moment of the equivalent cantilever beam of $m_s = 5 \times 2 \times 1 = -10 \text{ kNm/m}$. Values between $m_s = -3$ and $m_s = -6 \text{ kNm/m}$, which are much smaller than the analytical ones, are calculated by the Finite Element Method. The differences are caused by the linear form functions of the four-noded element used, which results

Finite element design of concrete structures

in constant internal forces within an element. Thus, only the values in the centre of the element are calculated and not the values required for design at the boundaries. The disadvantages of the slab panel design are that

Restricted Page

This page is unavailable for viewing ([why?](#)). You may continue browsing to view unrestricted pages, or visit the [About this Book](#) page.



Restricted Page

This page is unavailable for viewing ([why?](#)). You may continue browsing to view unrestricted pages, or visit the [About this Book](#) page.

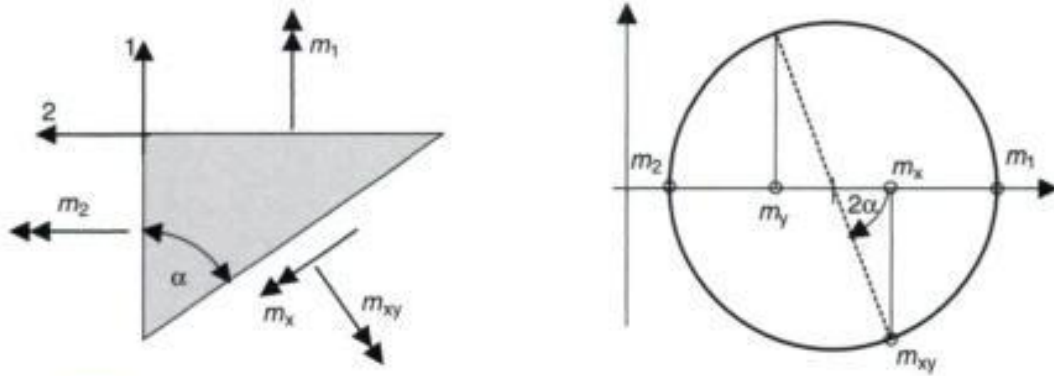


Fig. 4.69 Transformation of the bending moment

It should be noted that the codes specify a minimum transverse reinforcement (20% of the maximum reinforcement in the main load-bearing direction). Thus, the value k_t should always be greater than 0.2. Furthermore, for $\alpha \geq 25^\circ$ the reinforcement should be distributed in the orthogonal directions, as illustrated in Fig. 4.70. In this figure, the bending moment, m_2 , is always greater than that caused by the external actions. The design bending moments in the direction of the reinforcement bars can be estimated by using the following expressions:

$$m_y = k \cdot m_1 = \frac{1}{\cos^2 \alpha + k_t \cdot \sin^2 \alpha} \cdot m_1$$

$$m_x = k_t \cdot m_y$$

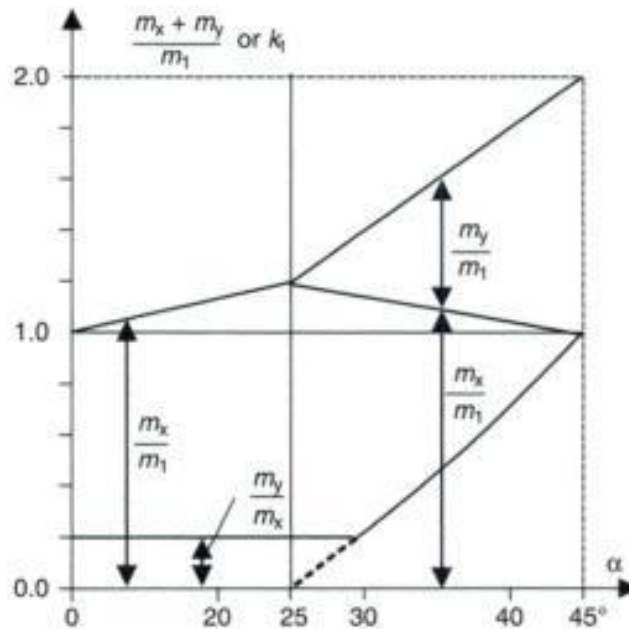


Fig. 4.70 Distribution of the main bending moment in the direction of the reinforcement bars

4.13.2 Model of Baumann

The design for the bending of a slab is transferred to the design of a plane plate (disk) for normal forces (Fig. 4.71) [36].

The forces in the reinforcement results from the equilibrium conditions on a plane plate element (see Fig. 4.73). The angle of the cracks φ is determined by the principle of the minimum energy. A linear-elastic material behaviour is assumed.

$$\cot^4 \varphi_1 + \cot^3 \varphi_1 \cdot \frac{\tan \alpha + k \cdot \cot \alpha}{1 - k} - \cot \varphi_1 \frac{\cot \alpha + k \cdot \tan \alpha}{\lambda \cdot (1 - k)} - \frac{1}{\lambda} = \frac{\nu}{\lambda} (1 - \cot^4 \varphi_1)$$

where:

$$\lambda = \frac{a_{sx}}{a_{sy}}; \quad \nu = \frac{a_{sx}}{h} \cdot \frac{E_s}{E_c}$$

$$k = m_2/m_1 = n_2/n_1$$

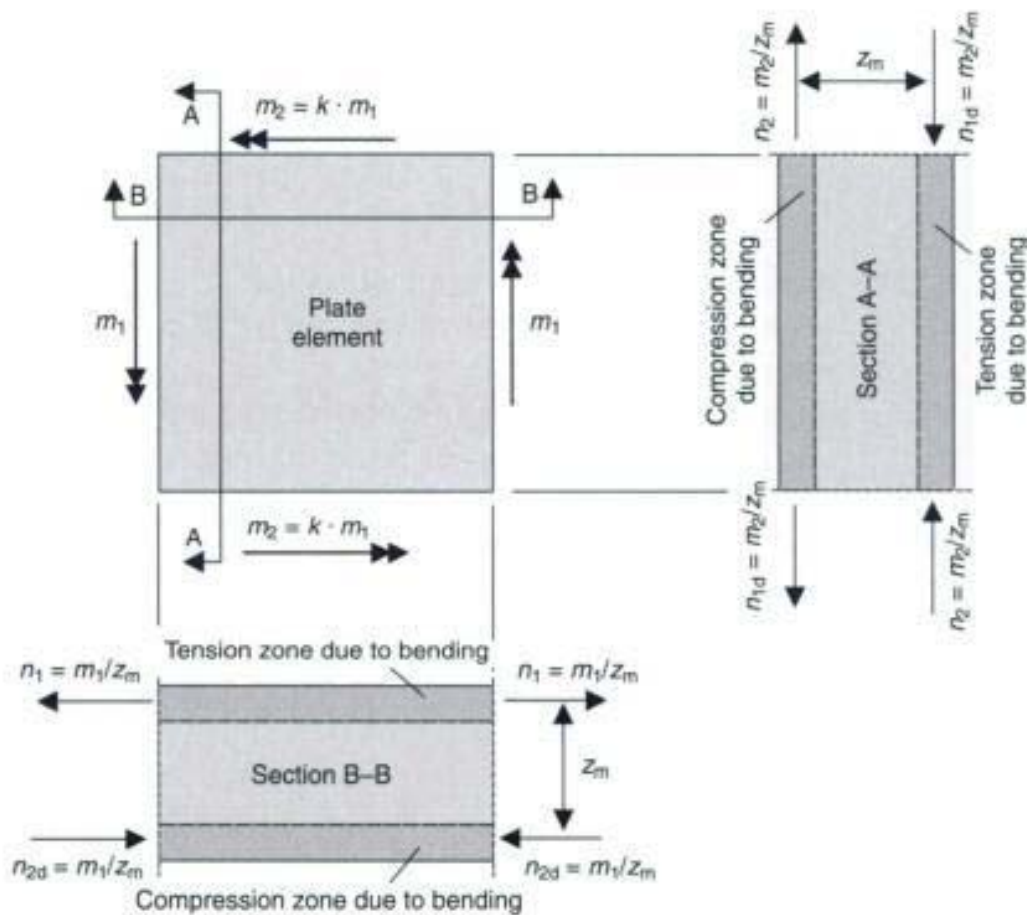


Fig. 4.71 Transfer of bending moments into normal forces in an equivalent disk

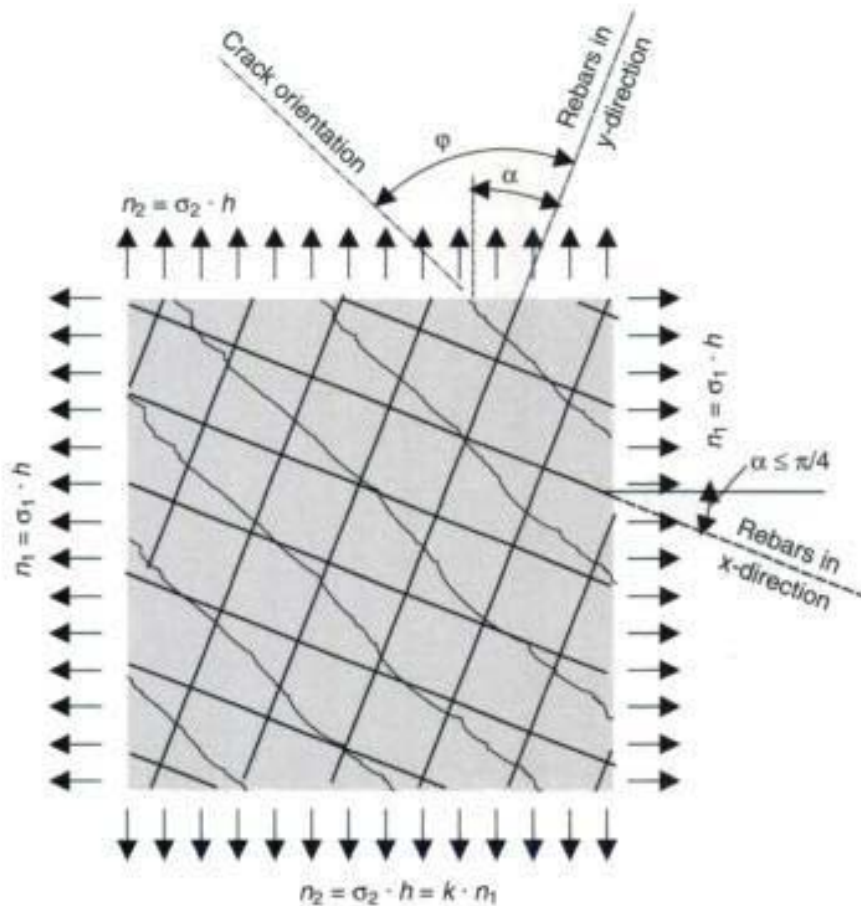


Fig. 4.72 Definition of angles α and φ

m_1 and m_2 are the principal bending moments

α angle between direction of rebar (y) and main tensile force n_1 ($\alpha \leq 45^\circ$);

φ angle between direction of rebar (y) and cracks;

φ_1 angle between direction of rebar (y) and cracks, if the shear forces are neglected;

φ_2 angle between direction of rebar (y) and cracks, if the steel is yielding.

If the reinforcement in both directions reaches the yielding point, the angle of the crack φ_2 is obtained from the following expression:

$$\tan \varphi_2 = -C + \sqrt{C^2 + \lambda}$$

where:

$$C = \frac{1 + \tan^2 \alpha \cdot (k - \lambda) - k \cdot \lambda}{2 \cdot \tan \alpha \cdot (1 - k)}$$



Restricted Page

This page is unavailable for viewing ([why?](#)). You may continue browsing to view unrestricted pages, or visit the [About this Book](#) page.

The following expressions are used to determine the forces in the reinforcement F_{sx} and F_{sy} and the compressive force F_c :

k	$k = n_2/n_1 \geq \tan(\alpha + \pi/4) \cdot \tan \alpha$	$k = n_2/n_1 < \tan(\alpha + \pi/4) \cdot \tan \alpha$
$\varphi =$	$\pi/4$	$\varphi = \arctan \left[\frac{k - 1}{\tan \alpha + k \cdot \cotan \alpha} \right]$
$F_{sx} =$	$n_1 + \frac{n_1 - n_2}{2} \cdot \sin 2\alpha \cdot (1 - \tan \alpha)$	$\frac{n_2}{\sin^2 \alpha + k \cdot \cos^2 \alpha}$
$F_{sy} =$	$n_2 + \frac{n_1 - n_2}{2} \cdot \sin 2\alpha \cdot (1 + \tan \alpha)$	$= 0$
$F_c =$	$(n_1 - n_2) \cdot \sin 2\alpha$	$(n_1 - n_2) \cdot \sin 2\alpha / \sin 2\varphi_{0y}$

4.13.3 Model of Eurocode 2

The Eurocode 2 (EC2) model [6] is also based on a transformation of the bending moments into the direction of the reinforcement (Fig. 4.74). The results agree with the Baumann model if: $m_x \geq |m_{xy}|$.

4.13.4 Comparison of the different models

Figure 4.75 shows a comparison of the reinforcement required for the ULS design, according to the above-mentioned models for

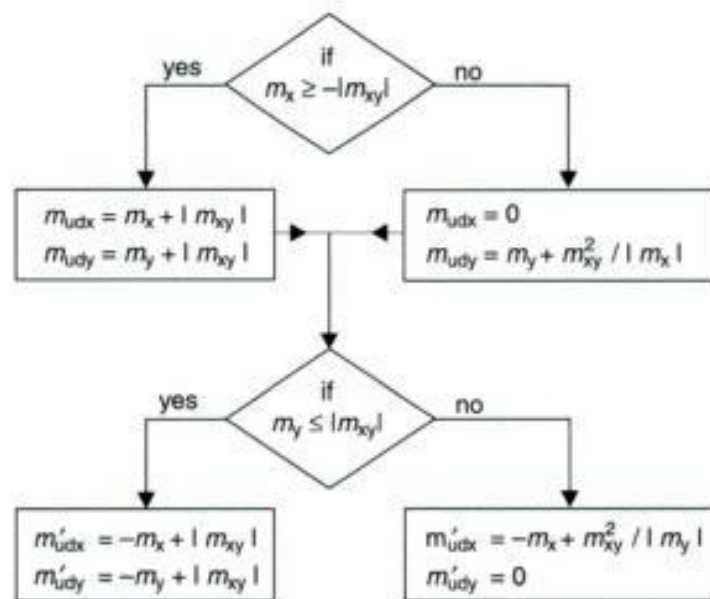


Fig. 4.74 Dimensioning of slabs according to EC2, Part 1, A 2.8 [6]

Slabs



Restricted Page

This page is unavailable for viewing ([why?](#)). You may continue browsing to view unrestricted pages, or visit the [About this Book](#) page.

rectangular slabs under uniform load. These values can be used to verify a Finite Element model. However, the differences in the numerical models, assumptions, and simplifications have to be considered. While most tables have been calculated in accordance to the Kirchhoff plate theory, the Finite Element software is generally based on the more consistent plate theory of Reissner/Midlin. The main difference between the two approaches is in the shear deformation. The Kirchhoff approach neglects shear deformations, while these are taken into

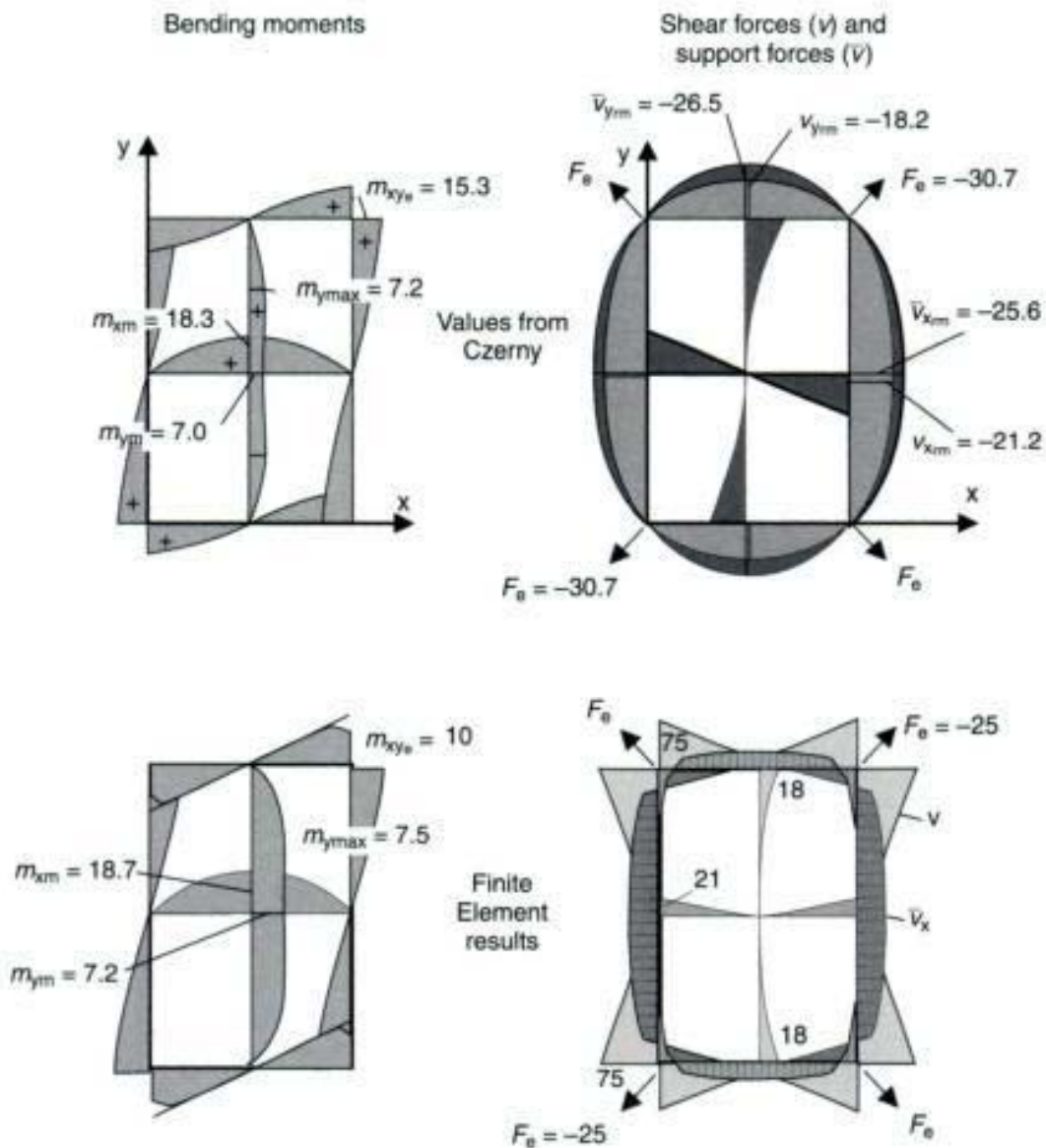


Fig. 4.76 Bending moments and shear forces of a simply supported rectangular slab under uniform load calculated by the Finite Element Method and with Czerny tables [11]

Table 4.12 Comparison of the internal force, support forces and deflection

Concrete Reinforced Concrete Prestressed Concrete

Restricted Page

This page is unavailable for viewing ([why?](#)). You may continue browsing to view unrestricted pages, or visit the [About this Book](#) page.

Table 4.13 Internal forces of a simply supported rectangular slab under uniform load (according to Czerny [11])

	$l_y/l_x = 1.0$	1.05	1.1	1.15	1.20	1.25	1.30	1.35	1.40	1.45	1.50	
m_{sm}	$= q \cdot l_x^2$	27.2	24.5	22.4	20.7	19.1	17.8	16.8	15.8	15.0	14.3	13.7
$m_{y,max}$	$= q \cdot l_x^2$	27.2	27.5	27.9	28.4	29.1	29.9	30.9	31.8	32.8	33.8	34.7
$m_{y,min}$	$= q \cdot l_x^2$	21.6	20.6	19.7	19.0	18.4	17.9	17.5	17.1	16.8	16.5	16.3
F_e	$= q \cdot l_x^2$	10.8	10.3	9.85	9.5	9.2	8.95	8.75	8.55	8.4	8.25	8.15
$v_{x,sm}$	$= q \cdot l_x$	2.96	2.87	2.78	2.71	2.64	2.58	2.52	2.47	2.43	2.39	2.36
$\bar{v}_{x,sm}$	$= q \cdot l_x$	2.19	2.15	2.11	2.07	2.04	2.02	2.00	1.98	1.97	1.96	1.95
$v_{y,sm}$	$= q \cdot l_x$	2.96	2.92	2.89	2.86	2.84	2.82	2.80	2.78	2.76	2.75	2.75
$\bar{v}_{y,sm}$	$= q \cdot l_x$	2.19	2.14	2.09	2.05	2.02	1.99	1.96	1.94	1.92	1.90	1.89
f_m	$= \frac{q \cdot l_x^4}{E \cdot h^3}$	0.0487	0.0536	0.0584	0.0631	0.0678	0.0728	0.0767	0.0809	0.0850	0.0890	0.0927

	$l_y/l_x = 1.50$	1.55	1.60	1.65	1.70	1.75	1.80	1.85	1.90	1.95	2.00	
m_{sm}	$= q \cdot l_x^2$	13.7	13.2	12.7	12.3	11.9	11.5	11.3	10.8	10.6	10.4	
$m_{y,max}$	$= q \cdot l_x^2$	34.7	35.4	36.1	36.7	37.3	37.9	38.5	39.4	39.8	40.3	
$m_{y,min}$	$= q \cdot l_x^2$	16.3	16.1	15.9	15.7	15.6	15.5	15.4	15.3	15.2	15.1	
F_e	$= q \cdot l_x$	8.15	8.05	7.95	7.85	7.80	7.75	7.70	7.65	7.6	7.55	
$v_{x,sm}$	$= q \cdot l_x$	2.36	2.33	2.30	2.27	2.25	2.23	2.21	2.18	2.16	2.15	
$\bar{v}_{x,sm}$	$= q \cdot l_x$	1.95	1.94	1.93	1.92	1.92	1.92	1.92	1.92	1.92	1.92	
$v_{y,sm}$	$= q \cdot l_x$	2.75	2.74	2.73	2.73	2.73	2.72	2.72	2.71	2.70	2.70	
$\bar{v}_{y,sm}$	$= q \cdot l_x$	1.89	1.88	1.87	1.86	1.85	1.84	1.83	1.82	1.82	1.82	
f_m	$= \frac{q \cdot l_x^4}{E \cdot h^3}$	0.0927	0.0963	0.0997	0.1029	0.1060	0.1093	0.1118	0.1145	0.1169	0.1195	0.1215

Note: h is the slab thickness

Restricted Page

This page is unavailable for viewing ([why?](#)). You may continue browsing to view unrestricted pages, or visit the [About this Book](#) page.

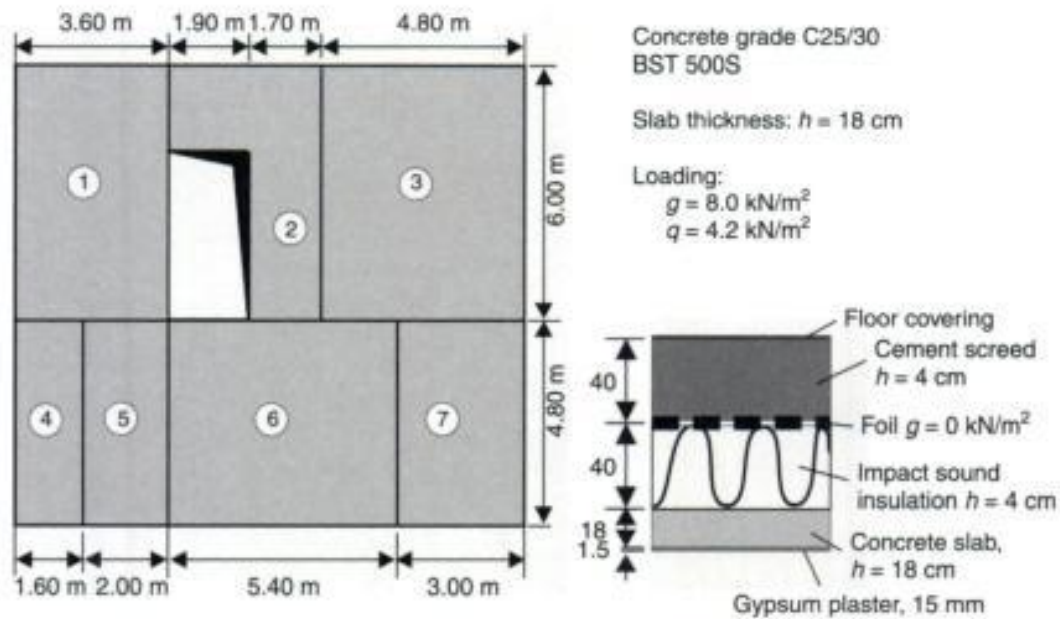


Fig. 4.77 Structure and loading

model. This structure had been used in the original publication [27], but the loads and the thickness of the slab have been increased to represent the up-to-date conditions.

Figures 4.78 and 4.79 show the bending moment distribution calculated by the Finite Element Method in both axes for various sections. Figure 4.80 shows the comparison of the bending moments in the relevant sections. A good agreement in the field bending moments can be seen for both calculations using the simple manual method and the Finite Element Method. The support bending moments are generally greater due to the assumption of high restraints (between 50% and 100%).

It should be noted that the minimum bending moments given in EC2, Part 1 [6] are relevant in the small slabs Nos. 4 and 5 and not the values from the linear-elastic Finite Element model. The minimum internal forces always have to be considered in addition to a Finite Element analysis.

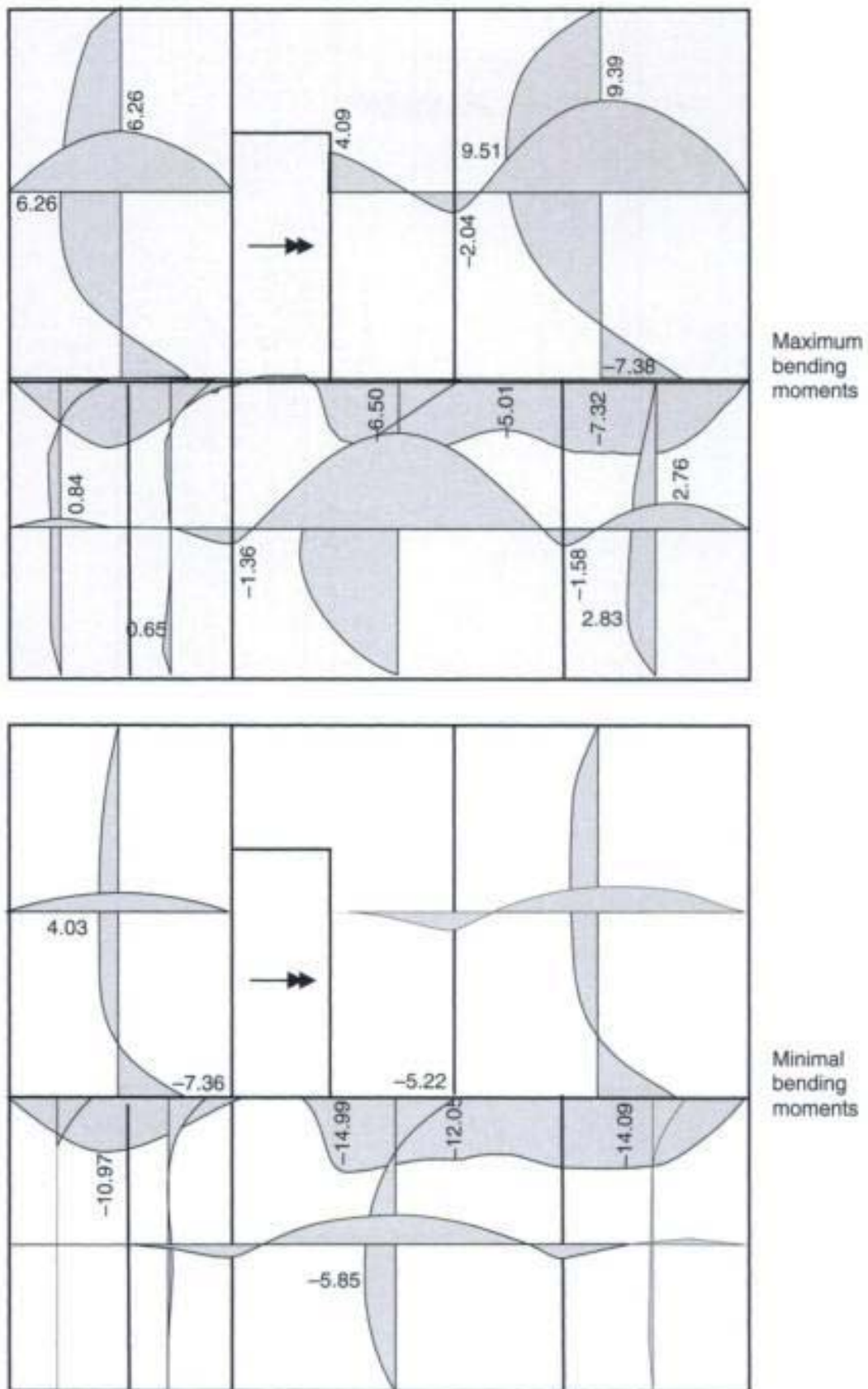


Fig. 4.78 Bending moment distribution in various sections (Finite Element analysis)

Copyrighted Material

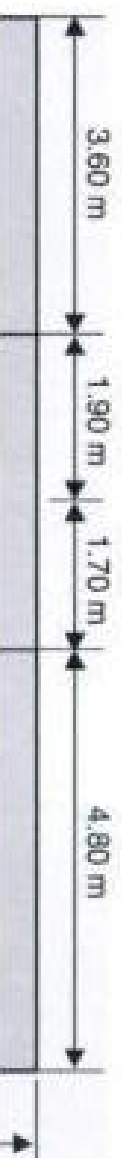
Finite element design of concrete structures



Restricted Page

This page is unavailable for viewing ([why?](#)). You may continue browsing to view unrestricted pages, or visit the [About this Book](#) page.

Slabs



Restricted Page

This page is unavailable for viewing ([why?](#)). You may continue browsing to view unrestricted pages, or visit the [About this Book](#) page.

Restricted Page

This page is unavailable for viewing ([why?](#)). You may continue browsing to view unrestricted pages, or visit the [About this Book](#) page.

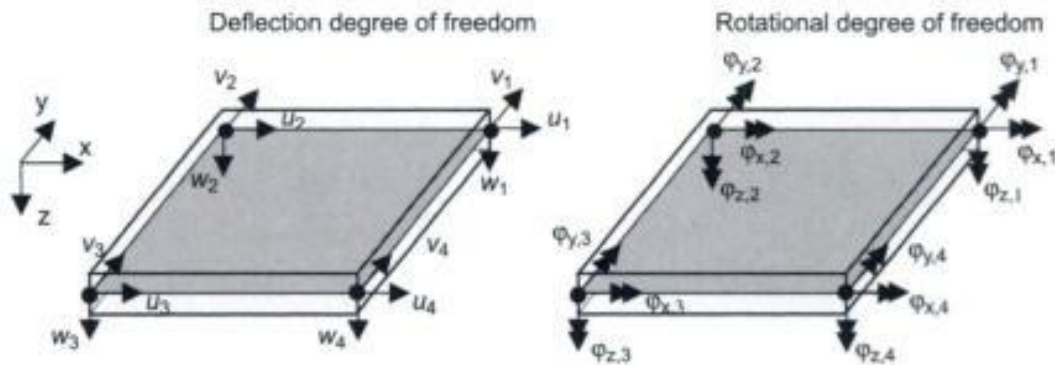


Fig. 5.1 Nodal degrees of freedom of a flat thin shell element

5.1.1 Collapse of the Sleipner Platform

The problems of **Finite Element** calculations can be well demonstrated in respect of damage or failures of structures due to errors in the numerical analyses. Unfortunately, due to a lack of interest in demonstrating such design errors, so far only a few of such cases have actually been published.

A good example of the failure of a **concrete structure**, caused by an erroneous numerical analysis, was the collapse of the offshore oil platform 'Sleipner A'. Further detailed data is available in the literature [4, 5, 32]. This so-called Condeep-type platform consists of 24 cylindrical caisson cells, each with an internal diameter of 24 m, which were closed at top and bottom by a dome (see Fig. 5.2). These cells were used as buoyancy during the construction and the shipping of the platform to its final location. The steel deck (total weight 40 000 tons) rested on four shafts, each having a minimum internal diameter of 12 m. The **structure** had a total height of 110 m. It was designed to operate at a location with a water depth of 82 m. The 'Sleipner A' platform was the twelfth in a series of gravity-based structures built for use in the exploitation of hydrocarbons in the North Sea. There was no significant difference between this platform and the earlier platforms of the Condeep type.

The **structure** collapsed during installation. The construction of this type of platform is carried out in three phases. In the first phase, the lower part of the foundation **structure** is built in a dry dock. Then the dry dock is flooded and the **structure** is shipped to a deep-water construction berth, where the rest of the cylindrical caisson cells and the four shafts are erected. Finally, the whole platform is lowered to nearly the sea water level by partially flooding the cylindrical caisson cells, and the steel deck is lifted on the shafts and fixed in place.

Finite element design of concrete structures



Restricted Page

This page is unavailable for viewing ([why?](#)). You may continue browsing to view unrestricted pages, or visit the [About this Book](#) page.

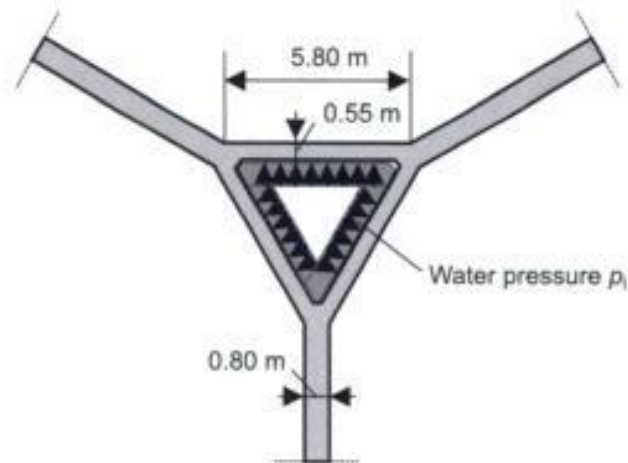


Fig. 5.3 Detail 'A' – tricell

- erroneous **Finite Element** analysis;
- insufficient reinforcement and bad detailing of the tricell walls.

The bad detailing of the intersection between the cell walls can be seen in Fig. 5.5. The T-headed bar of diameter $d_s = 25$ mm, was not anchored in the compression region of the walls. More information about this problem is given in the available literature (e.g. [4, 5]).

The errors in the **Finite Element** analysis of the platform lay in an insufficient discretization, and poor geometrical shaping of some elements in the tricells (Fig. 5.6). Simplifications had been made with

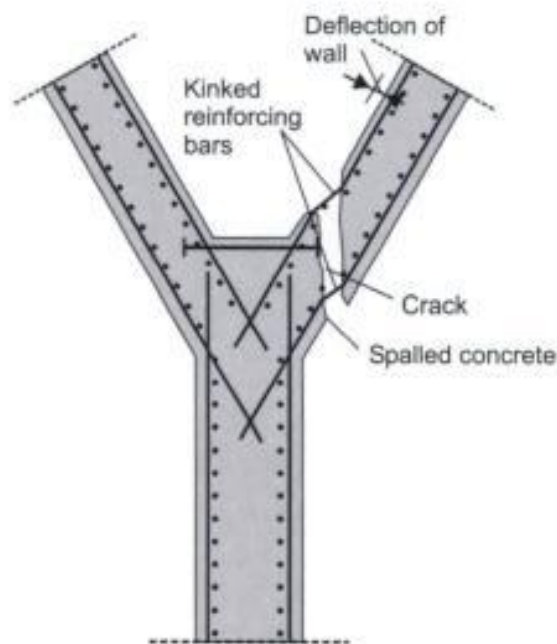


Fig. 5.4 Failure mode

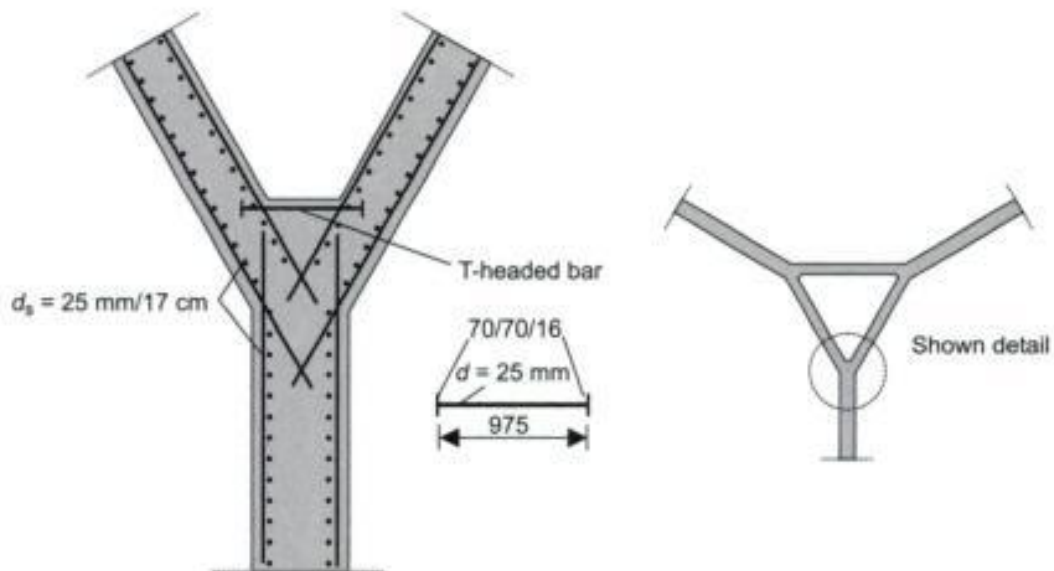


Fig. 5.5 Arrangement of the reinforcement in the intersection of the caisson cells (tricells)

regards to the number and shape of the elements, due to the size and complexity of the structure and the limited computer capacity. This had resulted in incorrect modelling of the load-bearing behaviour of the tricells. The walls of the cells had been modelled by only two element layers.

Using a coarse finite element mesh, the internal tensile forces, that is the shear forces at the wall supports, are underestimated by nearly 50%. Due to the large amount of input and output data of the three-dimensional model used, this mistake was not recognized by the designers.

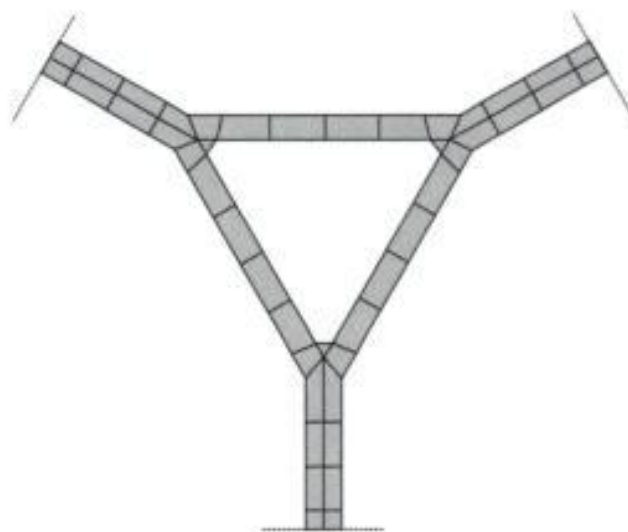


Fig. 5.6 Element mesh of the tricells

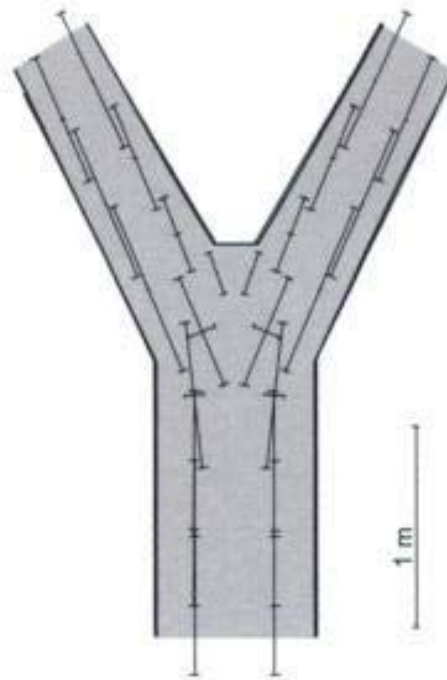


Fig. 5.7 Main membrane forces

The basic model problem is demonstrated by the following parametric study. For simplicity, a flat shell model is used.

Figure 5.7 shows the distribution of the main membrane forces in the region of the wall intersections. The inclination of the compression struts result in a high tensile force, which should be carried by the T-headed bars. However, the size of this force is highly dependant on the size of the elements, as can easily be demonstrated by calculations with various mesh sizes. Figure 5.8 shows the distribution of the horizontal tensile force in the walls for different mesh refinements (see Fig. 5.9).

With a very coarse mesh there appears to be no tensile force in the intersection region (mesh No. 1). Refinements result in a large increase in the horizontal force resultants (see Table 5.1). It should be noted that the results are highly dependant on the element type used and the element size.

What are the conclusions of this failure [33]? Complicated shell models with various arbitrary loadings can hardly be checked by a manual analysis of simplified equivalent structures, whereas this is possible for flat plates and shear walls. Furthermore, the checking of the equilibrium condition of the external and support forces is not sufficient. Other checks have to be performed for shells with complicated shapes.

The essential problem in the numerical analysis of the platform was that the element mesh used was not able to model the real deformation characteristics and load-bearing behaviour of the structure. The element

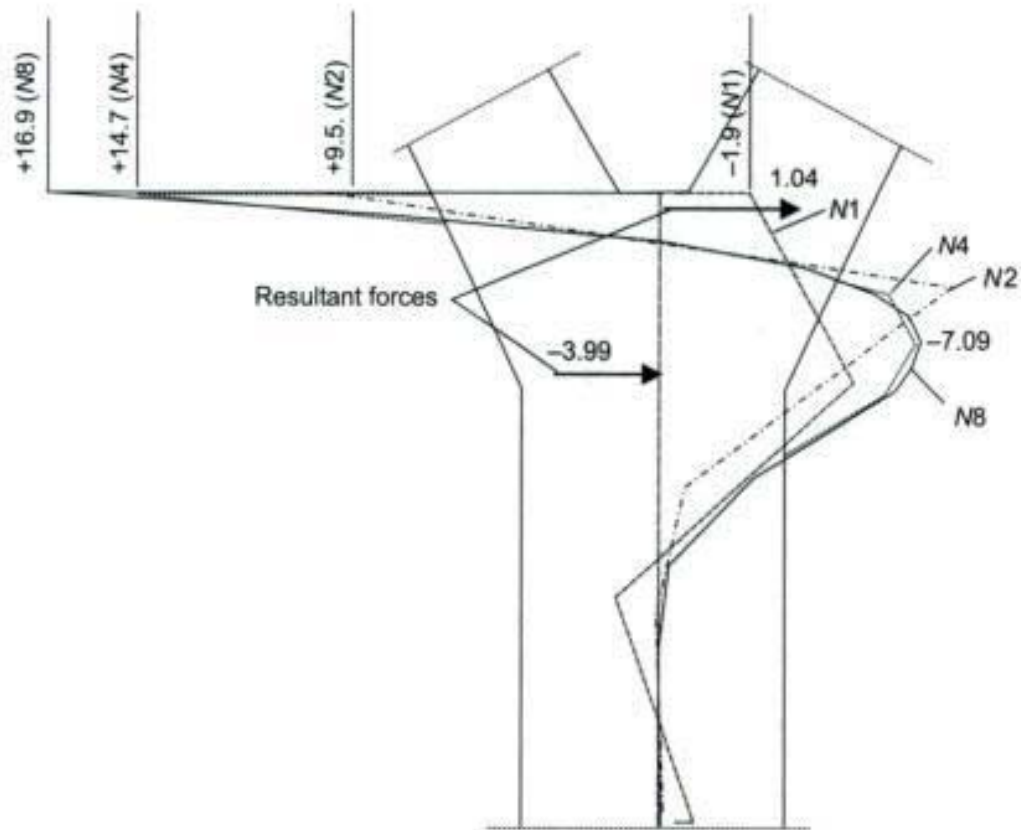


Fig. 5.8 Distribution of the horizontal membrane force in the wall

size used was too large, furthermore, the assumption of linear-elastic behaviour did not hold for all sections of the structure.

Thus, each structure has to be checked for regions where the assumptions of the numerical model do not apply. Detailed knowledge of both the Finite Element Method and the material behaviour are required for this task. Numerical algorithms like the automatic mesh refinement cannot compensate for the knowledge of the user. They are often not able to detect critical sections when the element mesh used is too coarse.

Critical regions of the structure can be analysed separately from the whole structure by means of, for example, strut-and-tie models or refined Finite Element models (substructure method). The resultant forces at the outer surface of the substructure can then be applied to a global model.

5.1.2 Patch loads on shells

The design of a huge offshore platform is very specialized and not a routine task. However, model problems can appear even on simple

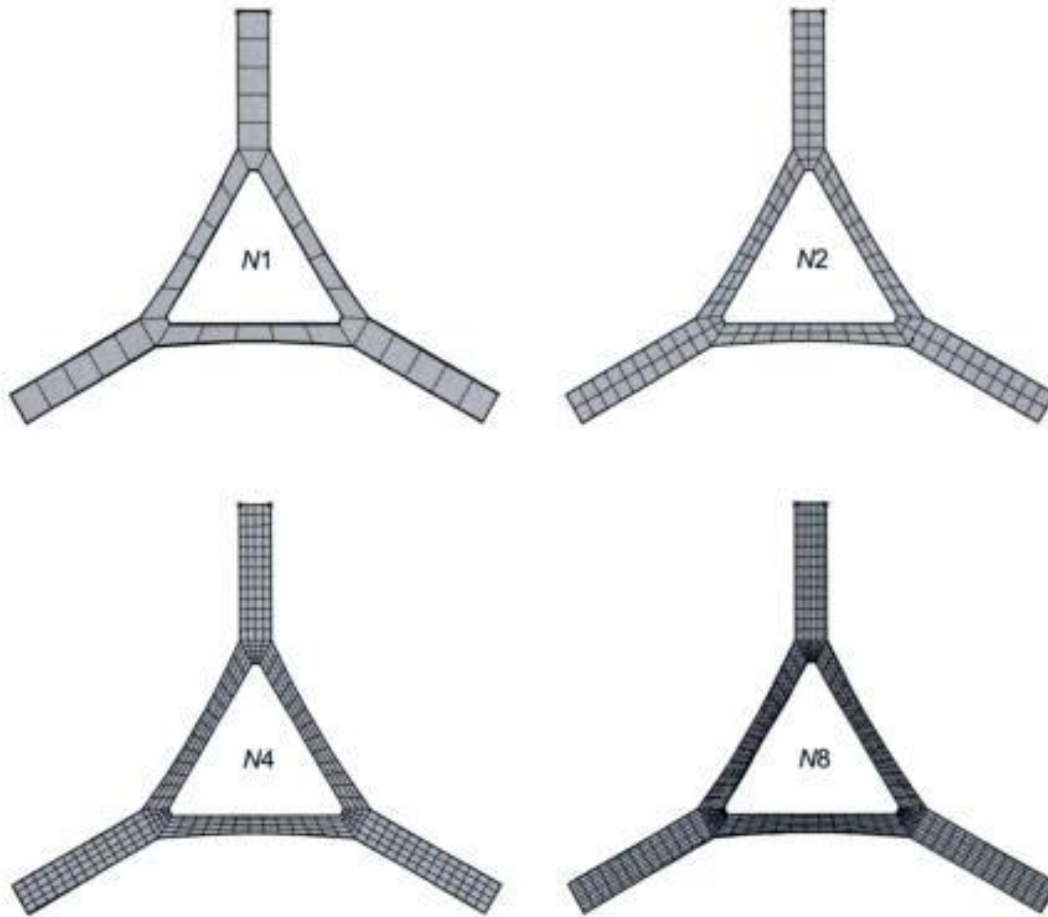


Fig. 5.9 Element meshes for the tricells

Table 5.1 Resultant tensile force for various element meshes

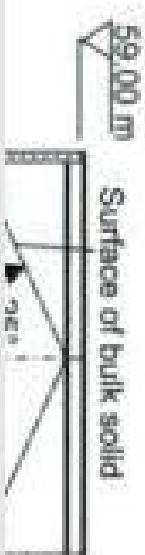
Element mesh	N1	N2	N4	N8
Resultant tensile force T_1 in MN/m	-2.0	0.75	0.99	1.04

cylindrical shells. The following demonstrates this on a cylindrical silo (see Fig. 5.10).

The cylindrical bin, which is used for storage of fly ash, has a height of 59 m and an inner diameter of 24.4 m. The following analysis is carried out on a simplified model. Only the cylindrical shaft is modelled. The inverted cone and the partial restraint of the walls in the pile foundation are neglected.

For axisymmetric structures, three-dimensional models are only required if unsymmetric loads have to be applied. This is the case for most silo structures. The main loading of a silo results from the bulk material inside the bin, which can be estimated from various codes

Finite element design of concrete structures



Restricted Page

This page is unavailable for viewing ([why?](#)). You may continue browsing to view unrestricted pages, or visit the [About this Book](#) page.

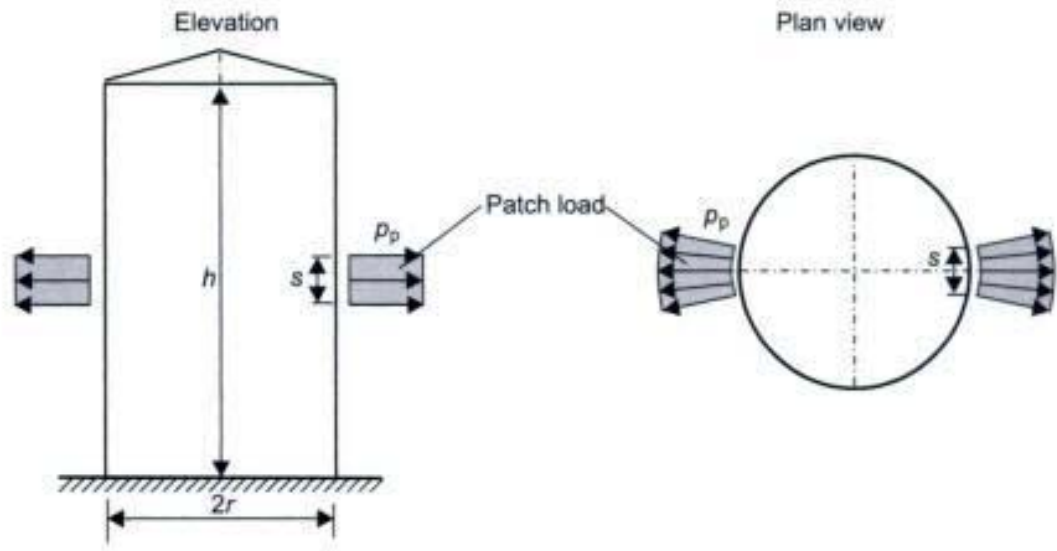


Fig. 5.11 Patch load according to EC1, Part 4 [28]

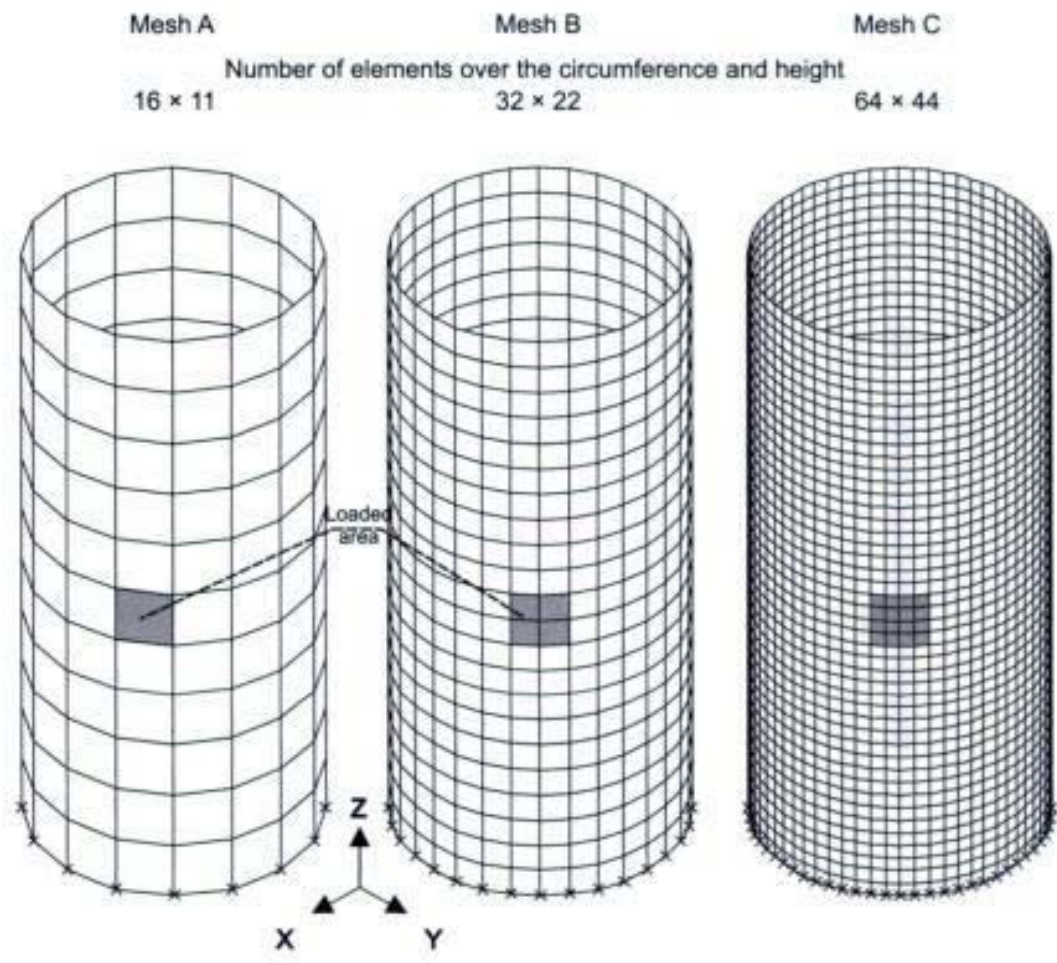


Fig. 5.12 Element meshes

Copyrighted Material

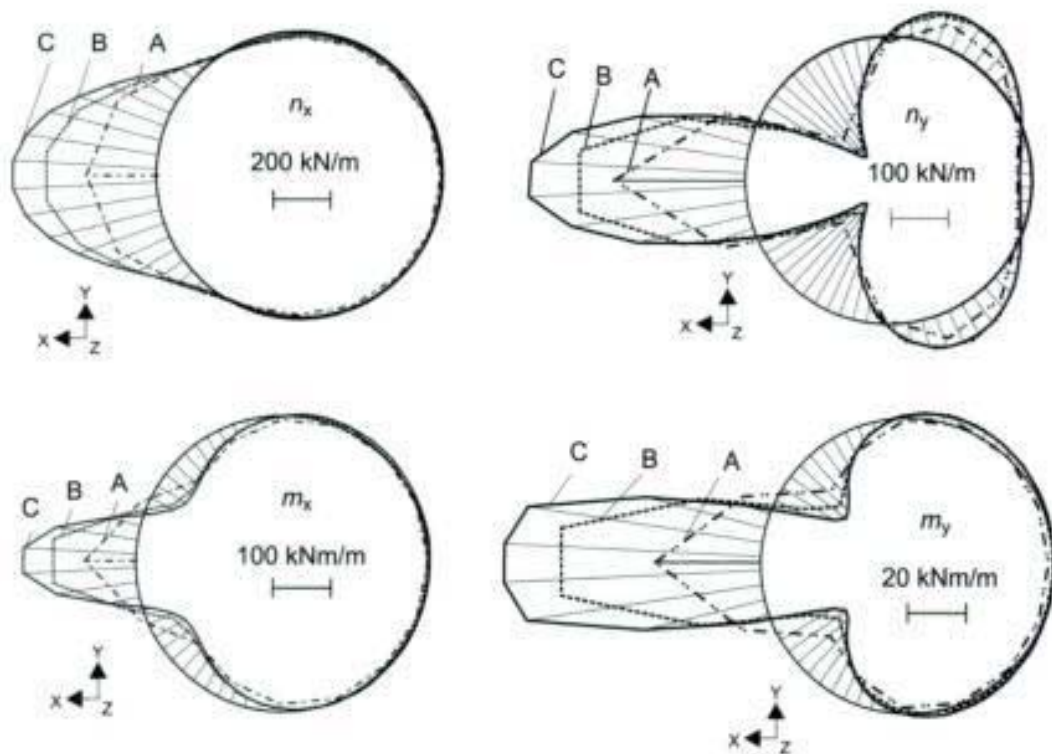


Fig. 5.13 Internal forces in a horizontal section at $z = h/2 = 28\text{ m}$ (element values)

mesh No. 3. A uniform horizontal patch load of $q = 100\text{ kN/m}^2$ is applied to the walls.

The internal forces under the patch load increase considerably with an increase in the number of the elements, as can be seen in Fig. 5.13. Table 5.2 gives the maximum values of the internal forces. The maximum bending moment, calculated with the coarse element mesh A, is only $\frac{1}{3}$ of that of mesh C. Calculating the reinforcement requirements using

Table 5.2 Maximum internal forces (nodal value)

		Mesh A	Mesh B	Mesh C	Hennig [29]	
n_x in kN/m	min	-97 (86%)	-106 (94%)	-113 (100%)	-	-
	max	244 (39%)	492 (79%)	627 (100%)	424 (68%)	
n_y in kN/m	min	-487 (85%)	-556 (97%)	-571 (100%)	-540 (95%)	
	max	273 (71%)	356 (92%)	387 (100%)	-	-
m_x in kNm/m	min	-50 (78%)	-68 (106%)	-64 (100%)	-	-
	max	93 (44%)	202 (97%)	209 (100%)	188 (90%)	
m_y in kNm/m	min	-15 (63%)	-22 (92%)	-24 (100%)	-	-
	max	36 (31%)	114 (98%)	116 (100%)	120 (103%)	

n_x, m_x = internal forces in circumferential direction.

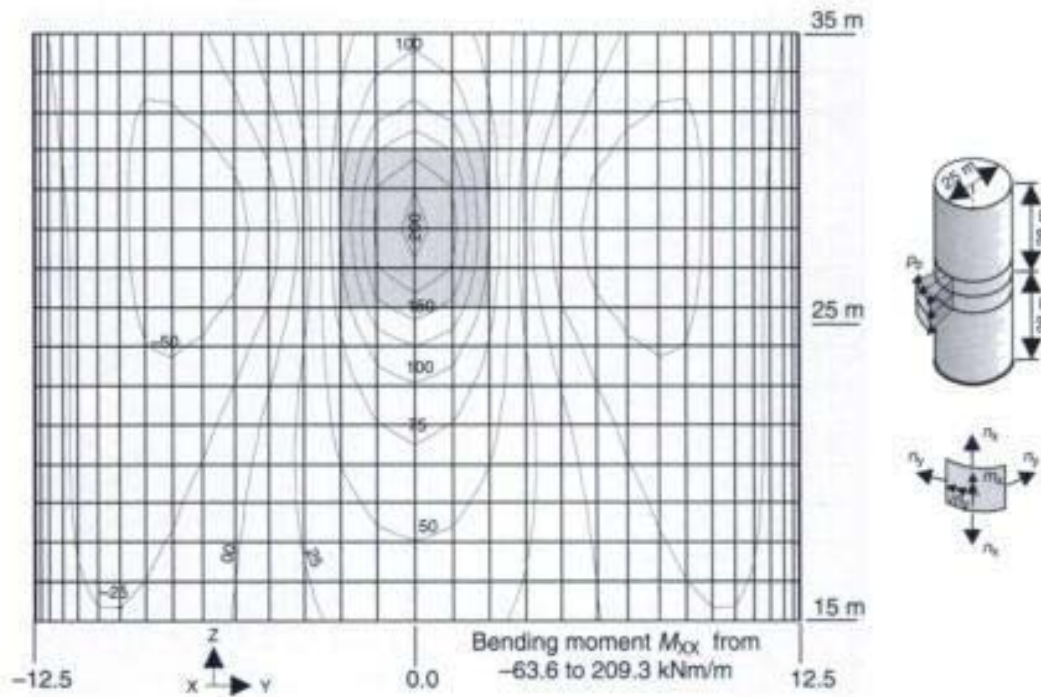


Fig. 5.14 Contour plot of the bending moment m_x in circumferential direction (mesh C)

such considerably lower value for the bending moments would result in a lack of safety.

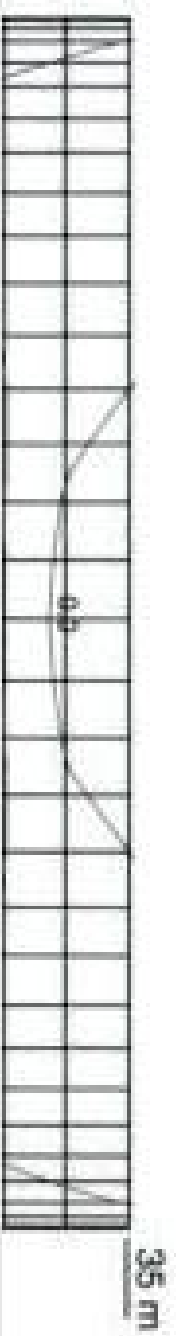
Due to the large uncertainty in the actual loading conditions, a high accuracy in the analysis is not required. The patch load represents only a rough idealization of the non-uniform pressure distribution in the silo bin in the circumferential direction caused by the granular bulk material. In this respect, an extensive three-dimensional finite element shell analysis is only useful in special cases. Table 5.2 shows that a simple manual analysis of the maximum bending moments, using the parameters published by Hennig [29], gives a good agreement with the Finite Element analysis.

As previously mentioned, the patch load represents a rough simplification of the real pressure distribution. Therefore, nonlinear calculations are not permissible, as the theoretical bending moments in the walls would be considerably reduced relative to the actual moments.

5.2 Continuous slab beam girder systems – T-beams

T-beams are widely used in concrete structures, whether as a main longitudinal girder in bridges or as the support (joist) of slabs (see sections 2.8.2 and 2.8.3). An analysis can easily be carried out manually

Finite element design of concrete structures



Restricted Page

This page is unavailable for viewing ([why?](#)). You may continue browsing to view unrestricted pages, or visit the [About this Book](#) page.

forces in the plate analysis can then be used as loading for the T-beam girder to calculate the internal forces and dimensioning of the T-beam.

Restricted Page

This page is unavailable for viewing ([why?](#)). You may continue browsing to view unrestricted pages, or visit the [About this Book](#) page.

Finite element design of concrete structures



Restricted Page

This page is unavailable for viewing ([why?](#)). You may continue browsing to view unrestricted pages, or visit the [About this Book](#) page.

5.2.1.3 Model C: Replacement of the web by additional beam elements at the midplane of the slab

Restricted Page

This page is unavailable for viewing ([why?](#)). You may continue browsing to view unrestricted pages, or visit the [About this Book](#) page.

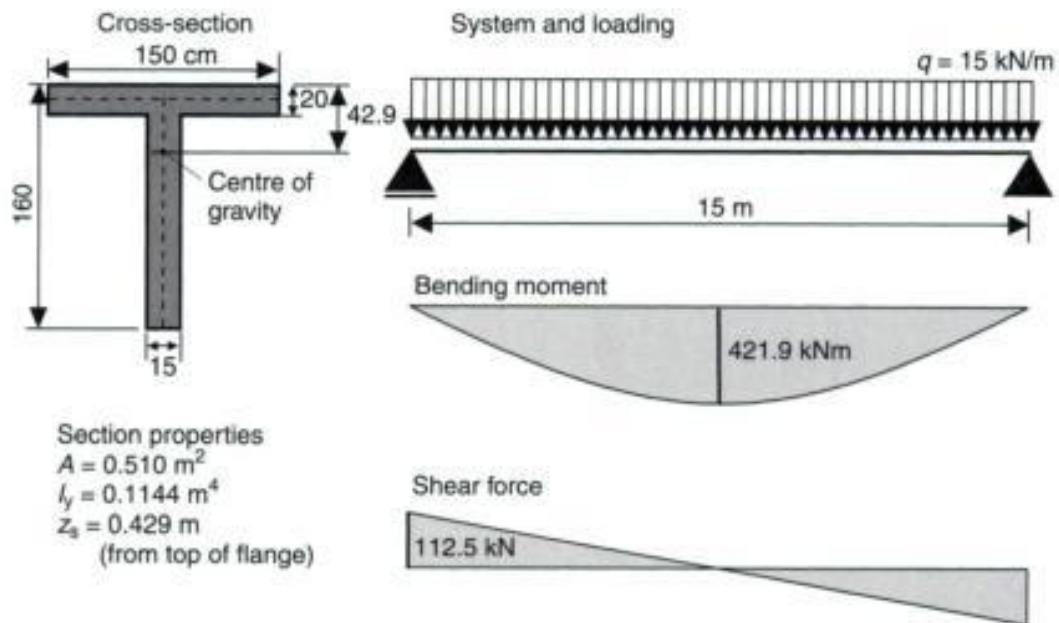


Fig. 5.18 T-beam: system, loads, internal forces (beam model)

5.2.2 Comparison calculations with the different models

The results of the different approaches will be compared on a very simple structure, a simply supported single span T-beam (span width of $l = 15$ m) under a uniform load of $q = 15$ kN/m (see Fig. 5.18). The internal forces can easily be manually calculated by means of a girder system, as the whole flange is under constant compression ($b_{\text{eff}} = b_{\text{fl}}$). This manual analysis results in the following maximum stresses in midspan of the T-beam.

$$\begin{aligned} \sigma_c &= \frac{M}{I} \cdot z = \frac{421.9}{0.1144} \cdot \begin{pmatrix} -0.429 \\ -0.229 \\ 1.171 \end{pmatrix} \\ &= \begin{cases} -1582 \text{ kN/m}^2 & \text{(top)} \\ -845 \text{ kN/m}^2 & \text{(lower face of flange)} \\ +4310 \text{ kN/m}^2 & \text{(bottom)} \end{cases} \end{aligned}$$

These values serve as reference for the other models.

The results of the shell model are shown in Figs 5.19 to 5.21. The structure and the loading are symmetric. Therefore, it is sufficient to model only half of the whole structure and to consider the special boundary conditions at midspan. The web and the flange are each modelled by 20×50 elements. A pin support, which results in infinite

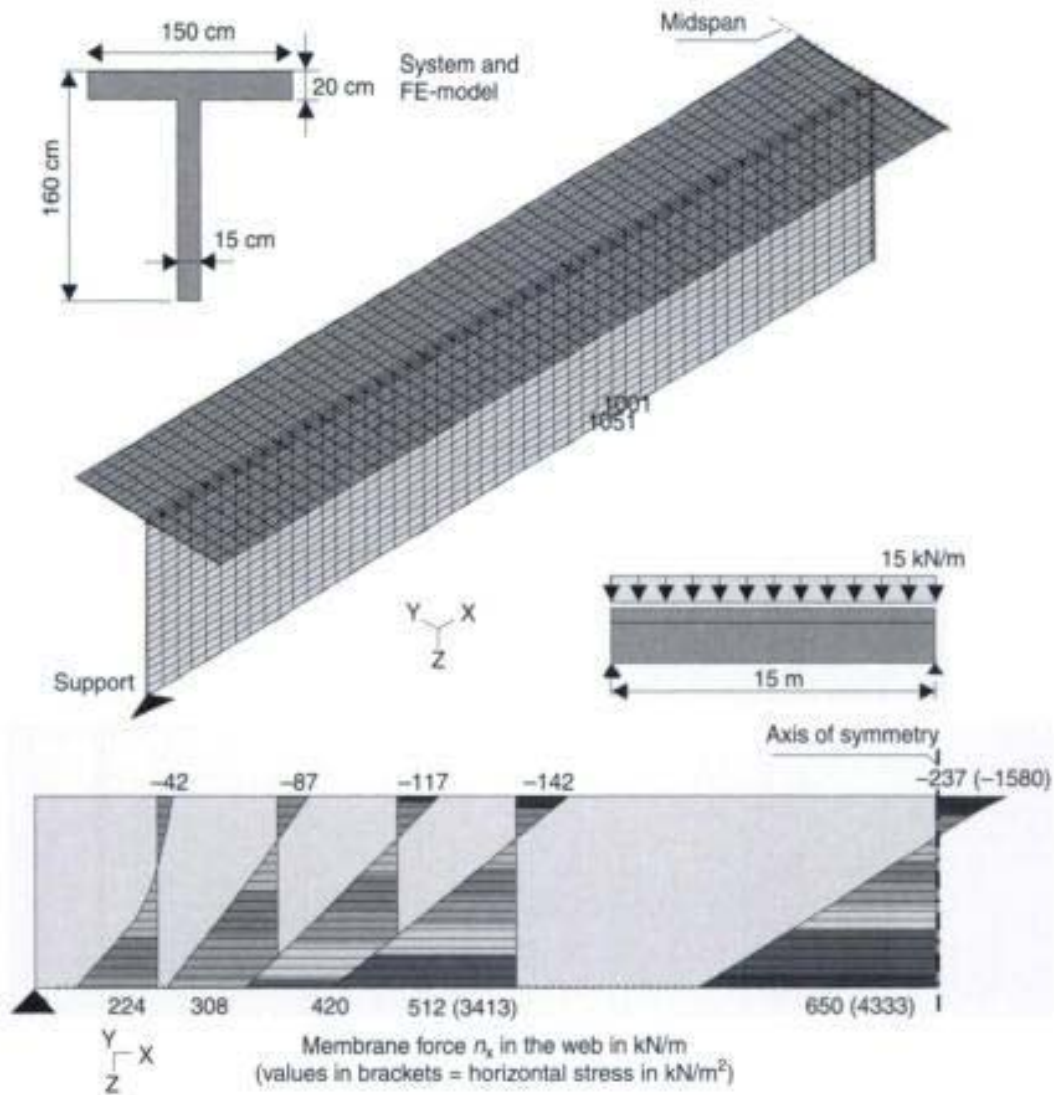


Fig. 5.19 Shell model

forces in the vicinity of the restraint, and not a continuous bedding is used, as the internal forces near the supports are of no further interest. A uniform load of $q = 10 \text{ kN/m}^2$ is applied to the flange.

The distribution of the horizontal membrane forces and the horizontal strains across the section depth are linear except near the supports (Fig. 5.19). The main assumption of any beam analysis, the linear strain distribution over the depth of the section, is valid for almost the whole structure. Therefore, it is not surprising that the normal stresses of the Finite Element model correspond well to the results of the beam analysis (stresses at the upper and lower edge of the section at midspan ($\sigma^{\text{top}} = -1580 \text{ kN/mm}^2$; $\sigma^{\text{bottom}} = +4333 \text{ kN/mm}^2$, see Fig. 5.19).

The compressive stresses, $\sigma_x = n_x/h_f$, in the flange increase parabolically from the support axis to midspan in agreement to the bending

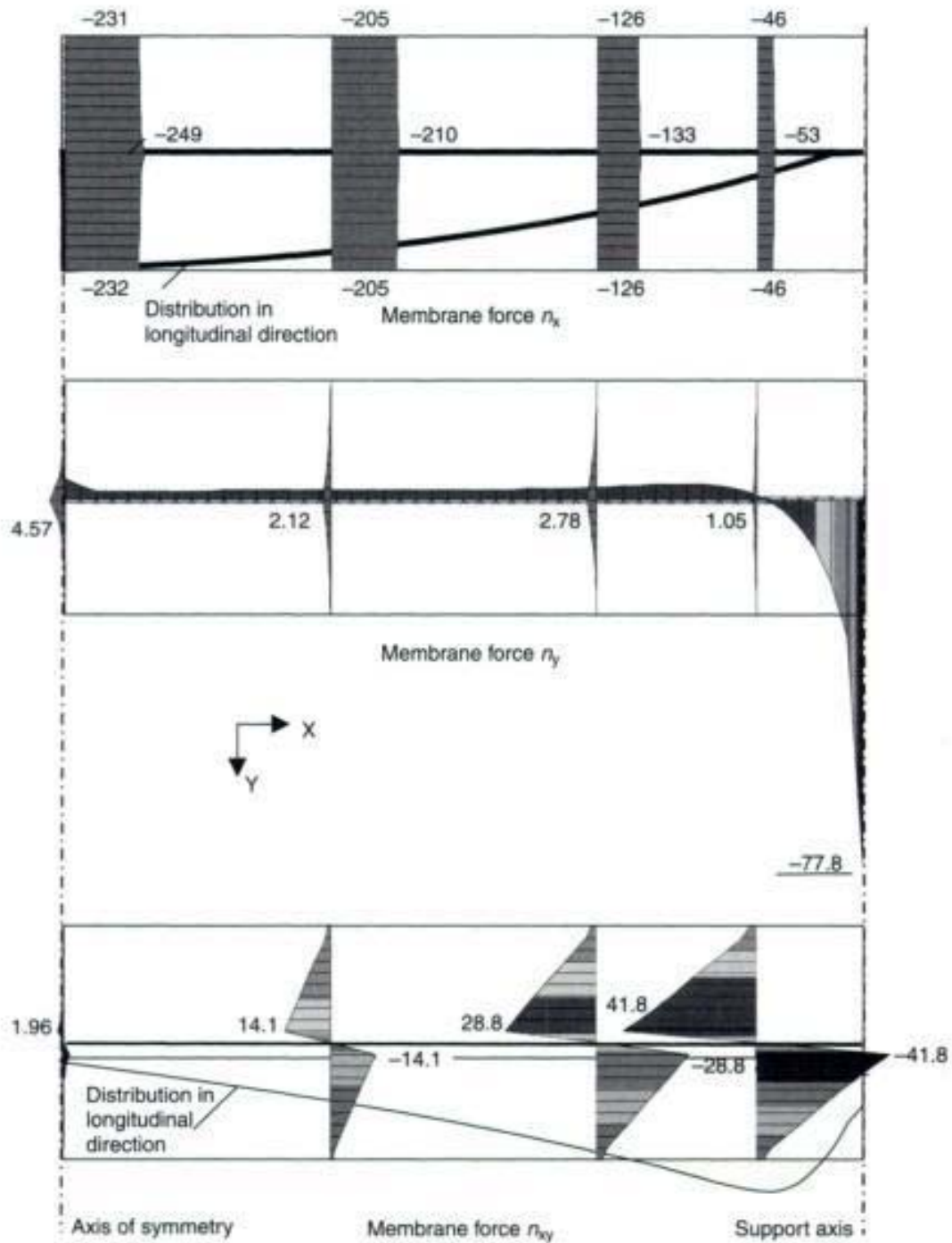


Fig. 5.20 Membrane forces n_x , n_y , n_{xy} in the flange in different sections

moment distribution (Fig. 5.20). The support force causes high transverse compressive stresses $\sigma_y = n_y/h_f$ in the flange, at the end of the beam (Fig. 5.20 middle). The membrane shear forces, n_{xy} , in the flange are greatest at the intersection with the web. They decrease in a longitudinal direction to zero at midspan. Consequently, the shear force is not constant as assumed in most models for shear design of a flange in transverse direction (see, e.g., [6], section 4.3.2.5).

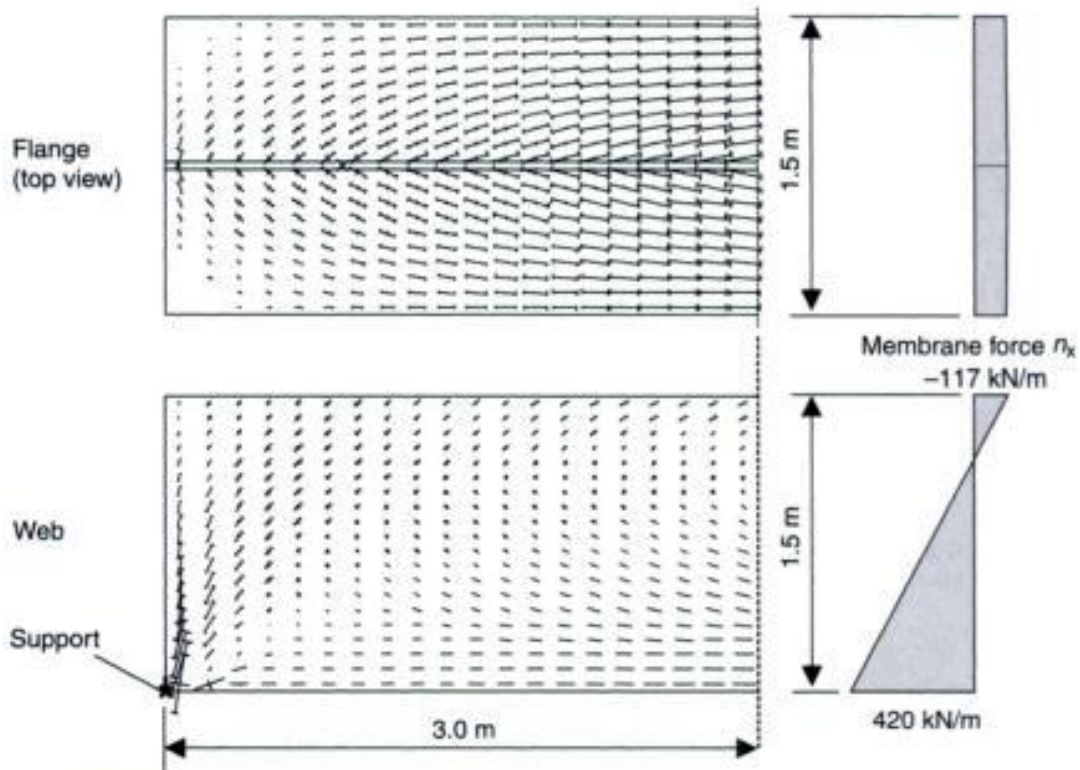


Fig. 5.21 Main membrane forces in the support regions

A three-dimensional folded slab model of a T-beam is, in general, too extensive for most practical cases, especially as the dimensioning task is difficult (see, e.g., shear walls). However, shell models are very helpful to determine the flow of forces in a structure and to evaluate an accurate strut-and-tie model (see section 5.2.3).

Figure 5.22 shows a model with beam elements located in the midplane of the plate. An equivalent depth of $h^{\text{equiv}} = 2.09$ m and a width of $b_w = 0.15$ m (the same as a real web) can be calculated for the given dimensions of the T-beam. The models with an eccentric beam element are shown in Figs 5.23 and 5.24.

The total internal forces of the T-beam are calculated by summation of the beam forces N_{beam} , M_{beam} and the membrane forces in the shell n_x , m_x . The latter values are gained by numerical integration.

Edge stresses of a beam:

$$\sigma_c = N/A \pm M/W$$

Edge stresses of a slab:

$$\sigma_c = \frac{n_x \cdot b_F}{A} \pm \frac{m_{xx} \cdot b_F}{W} = \frac{n_x}{h_f} \pm \frac{m_{xx} \cdot 6}{h_f^2}$$

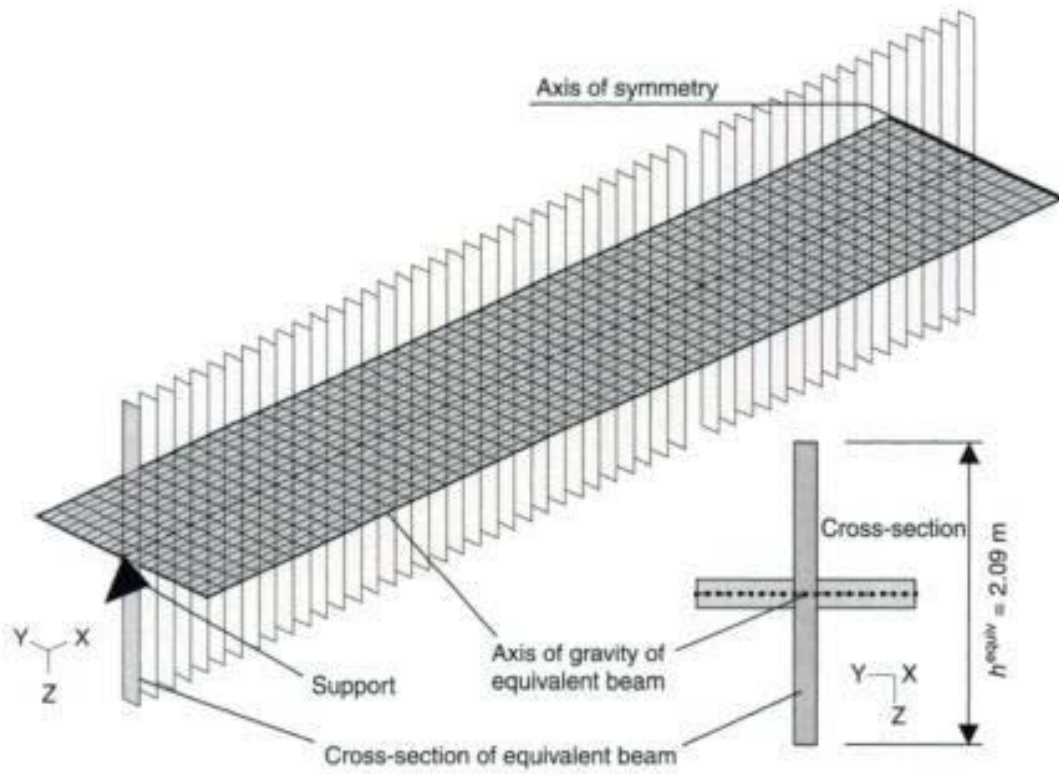


Fig. 5.22 Model C: plate elements (flange) with central equivalent beam elements (web)

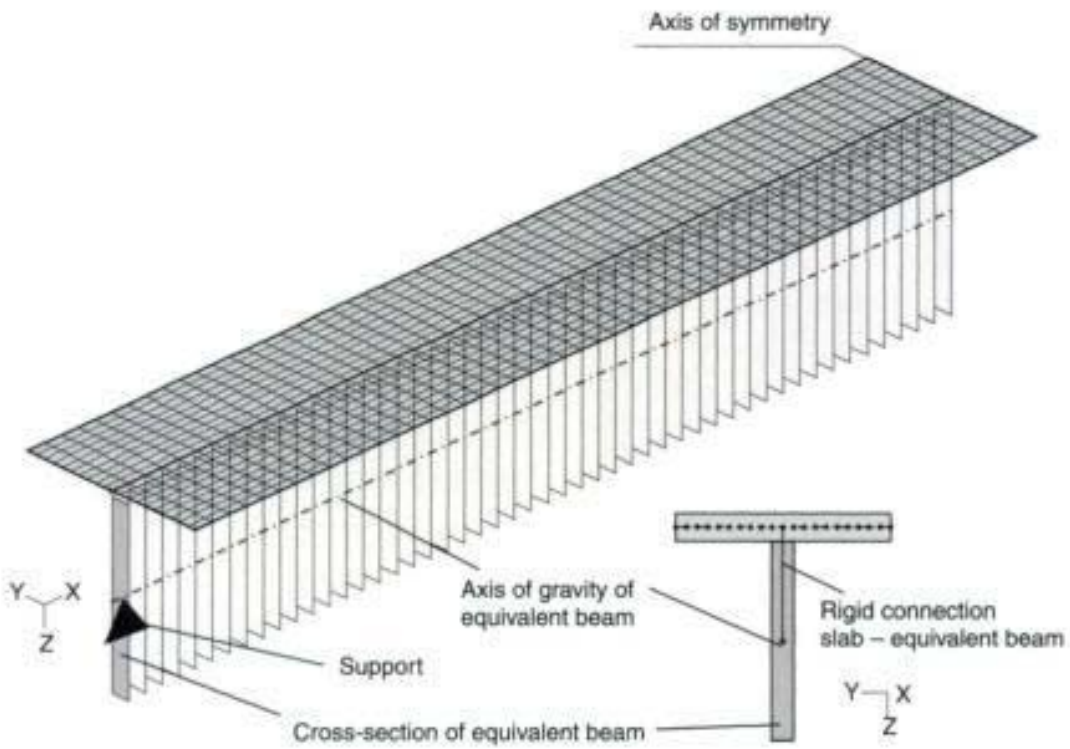


Fig. 5.23 Model D1: shell elements (flange) with eccentric beam elements (web)

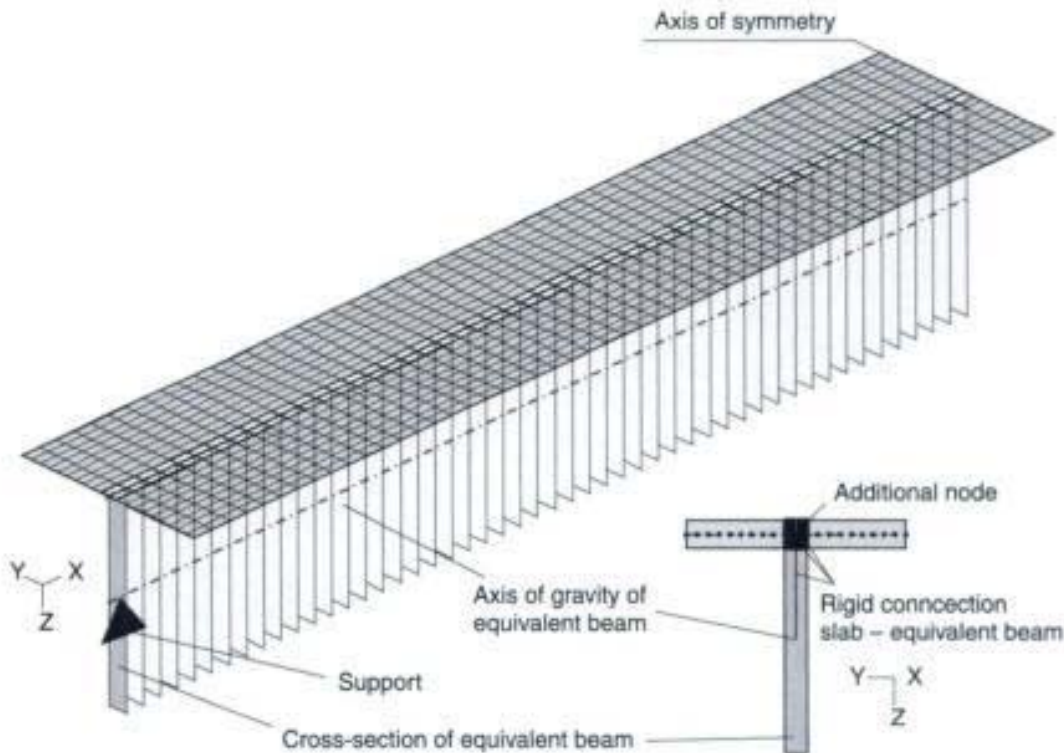


Fig. 5.24 Model D2: shell elements (flange) with eccentric beam elements (web)

Total normal force of T-beam:

$$N_{\text{tot}} = N_{\text{beam}} + N_{\text{slab}} = N_{\text{beam}} + n_{\text{slab}} \cdot b_{\text{flange}}$$

Total bending moment of T-beam:

$$M_{\text{tot}} = M_{\text{beam}} + N_{\text{beam}} \cdot z_{\text{beam}} + m_{\text{slab}} \cdot b_{\text{flange}} + n_{\text{slab}} \cdot b_{\text{flange}} \cdot z_{\text{slab}}$$

where:

b_w, b_f is the width of web and flange

h_w, h_f is the depth of web and flange

z is the distance between the centre of gravity of the flange or the web to that of the T-beam

The results of the various approaches are summarized in Table 5.3. A very good agreement between all three different numerical models and the values of the manual analysis can be observed. The small differences between the results are caused by rounding errors. The distributions of the edge stresses are shown in Fig. 5.25.

The bending bearing behaviour is well represented in all the models. No differences in the deflection of the girder can be observed.

Table 5.3 Member forces at midspan over the section depth of different models (dimensions kN and m)

Model	N_{slab}^{beam}	M_{slab}^{beam}	b m	h m	z m	σ_{top} kN/m ²	σ_{bottom} kN/m ²	N_{slab}^{beam}	M_{slab}^{beam}
C	0.0	418.5	0.15	2.09	0	-3832	+3832	0.0	418.5
	0.0	2.42	1.5	0.2	0	-363	+363	0.0	3.63
	Total								0.0
D1	366.1	126.0	0.15	1.40	1.171 - 0.7	-849	+4335	366.1	126.0 + 172.4
	-244.0	2.42	1.5	0.2	0.429 - 0.1	-1584	-856	-366.0	3.63 + 120.4
	Total								0.1
D2	330.0	189.0	0.15	1.60	0.8 - 0.429	-1578	+4328	330.0	189.0 + 122.4
	-245.0	2.43	1.5	0.2	0.429 - 0.1	-1587	-859	-366.0	3.3 + 108.8
	Total								-0.8

As it was expected, the stress distributions in the slab and in the equivalent girder of Model C are completely different from the other cases (see Fig. 5.25). These values cannot be used in design (e.g. checking the edge tensile stresses in the serviceability limit state for partial prestressed structures). In contrast, the stresses of Model D agree well with that of the T-beam girder, both in the web and the flange.

In Model D, single forces and single bending moments are introduced in the nodes due to the local coupling of the beam and shell elements.

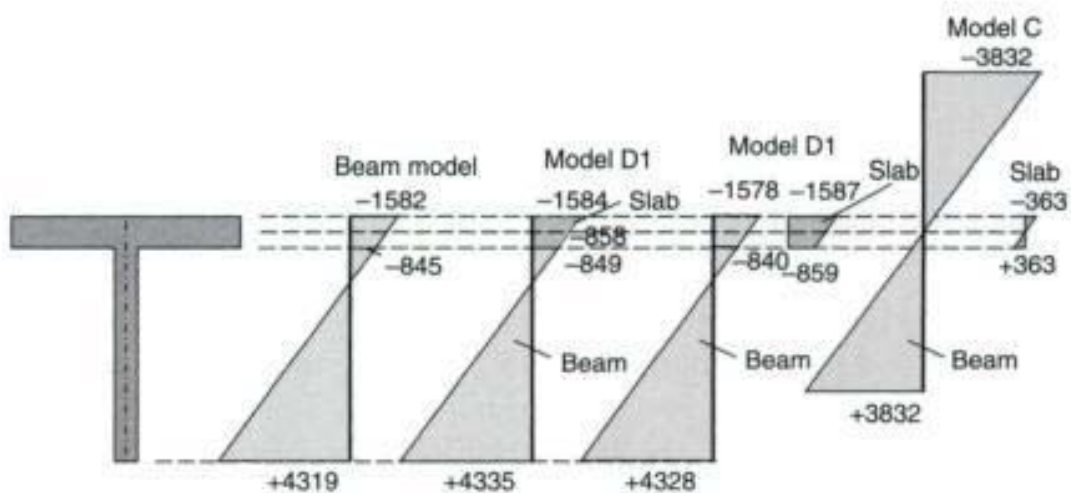


Fig. 5.25 Stress distribution in midspan over the section depth of different models [kN/m²]



Restricted Page

This page is unavailable for viewing ([why?](#)). You may continue browsing to view unrestricted pages, or visit the [About this Book](#) page.

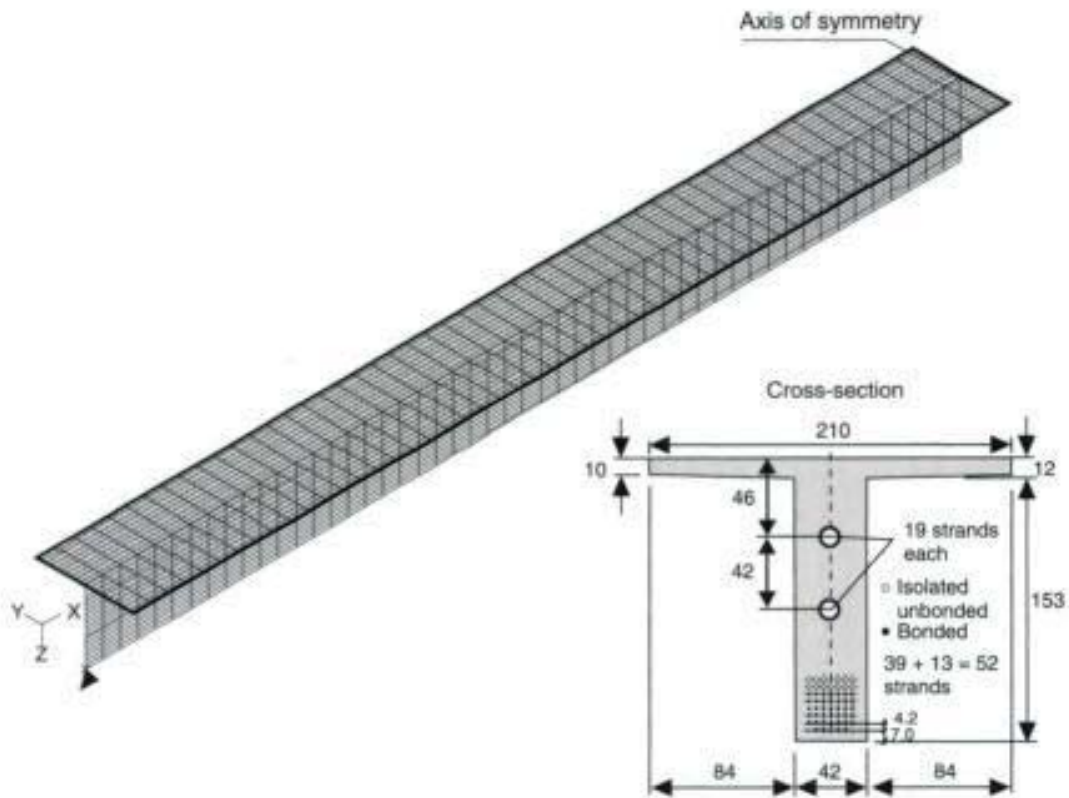


Fig. 5.27 Structure and Finite Element model

on the flow of forces is useful. A 3-D Finite Element shell analysis can be helpful in this task.

This will be shown for a single precast beam of the concrete T-beam bridge shown in Fig. 5.27 (see also Figs 2.96 and 2.97). This system has already been explained in section 2.8.3. The beam has a span length of $l = 38$ m. The following calculation only considers the prestressing forces. The T-beam girder was stressed by 52 straight tendons of grade ST 1570/1770.

The analysis can be restricted to half of the system, as the structure and the loading are symmetric. Shell elements of 20×50 are used for the web and the flange.

The results of the shell analysis are shown in Figs 5.28 and 5.29. The strut-and-tie model was adapted to the orientation of the main membrane forces. The large transverse tensile stresses in the flange at the support region are clearly shown in Fig. 5.29.

The above-mentioned analysis was based on a linear-elastic material behaviour. This applies mostly to the web, as almost no tensile stresses occur under prestressing; nevertheless, force redistributions may happen in the flange due to cracking.

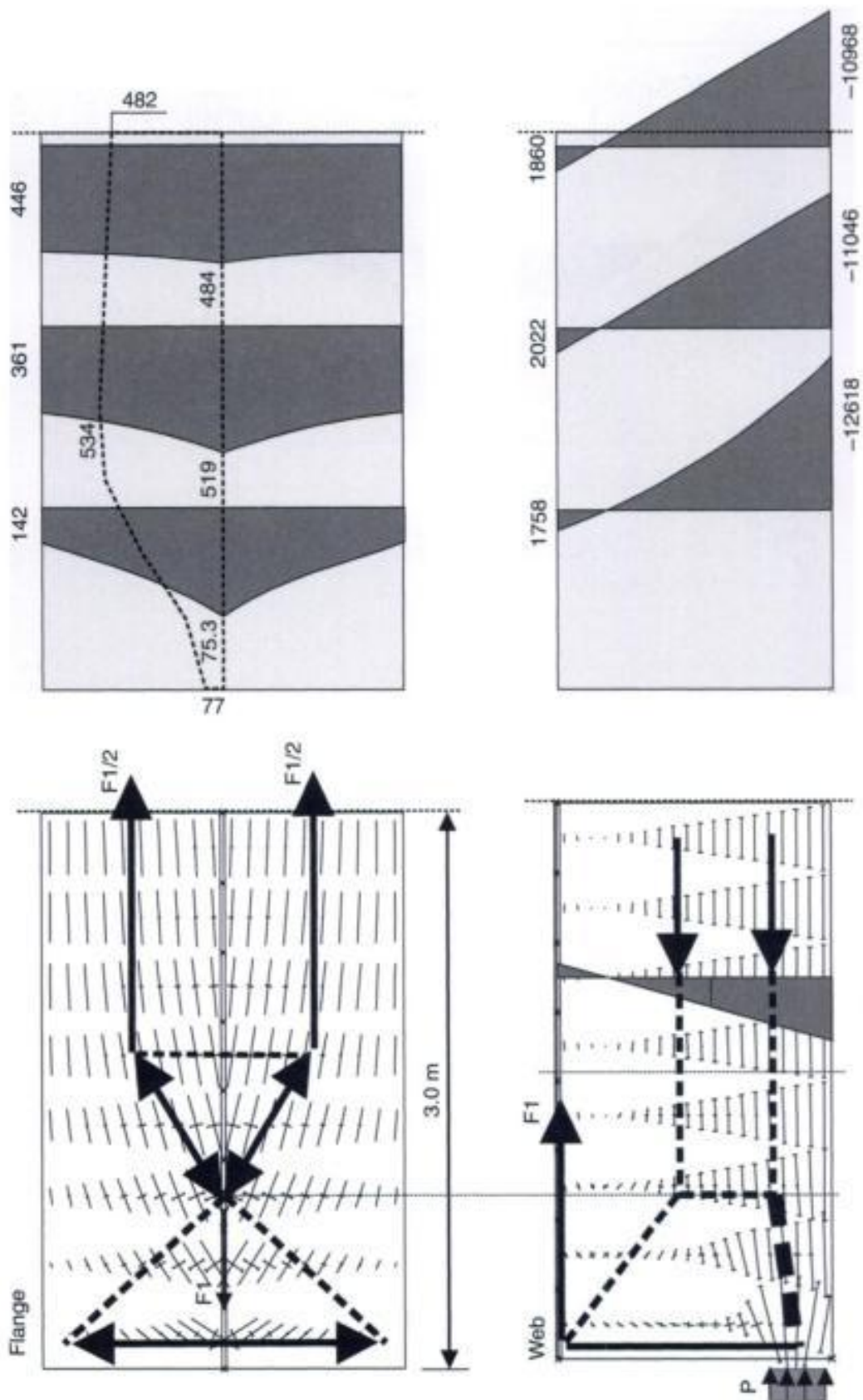


Fig. 5.28 Main membrane forces at the end of the girder ($l = 3.0$ m) and membrane forces in longitudinal direction in various sections – strut-and-tie model

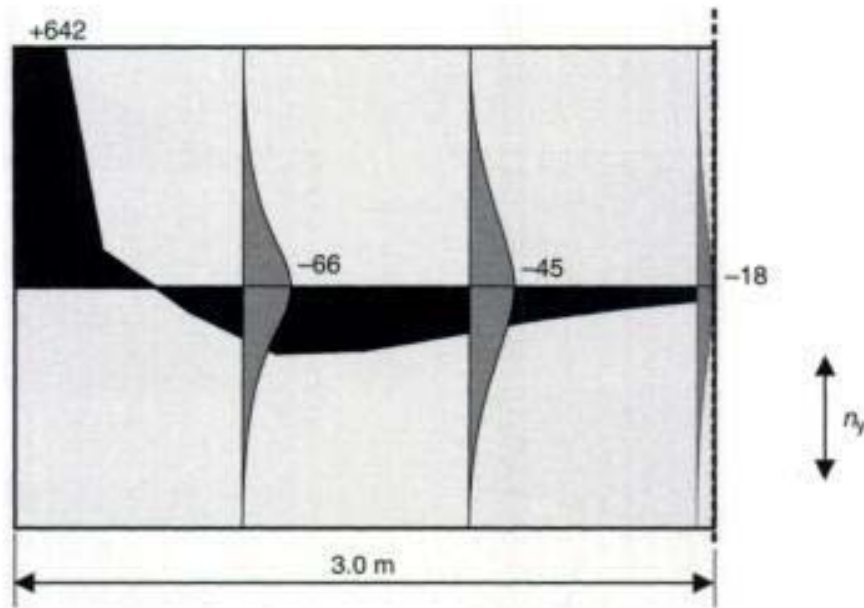


Fig. 5.29 Distribution of the membrane forces in transverse direction in the flange near the end of the beam (top view)

5.3 Composite structures

The model – flat shell with eccentric beam – can be used for the analysis of composite structures. Construction stages can be considered by activating the relevant load-bearing parts of the structures, i.e. the elements. The shear forces in the joint are obtained directly from the coupling forces in the nodes. Time dependant characteristics of the concrete can be considered in the analysis.

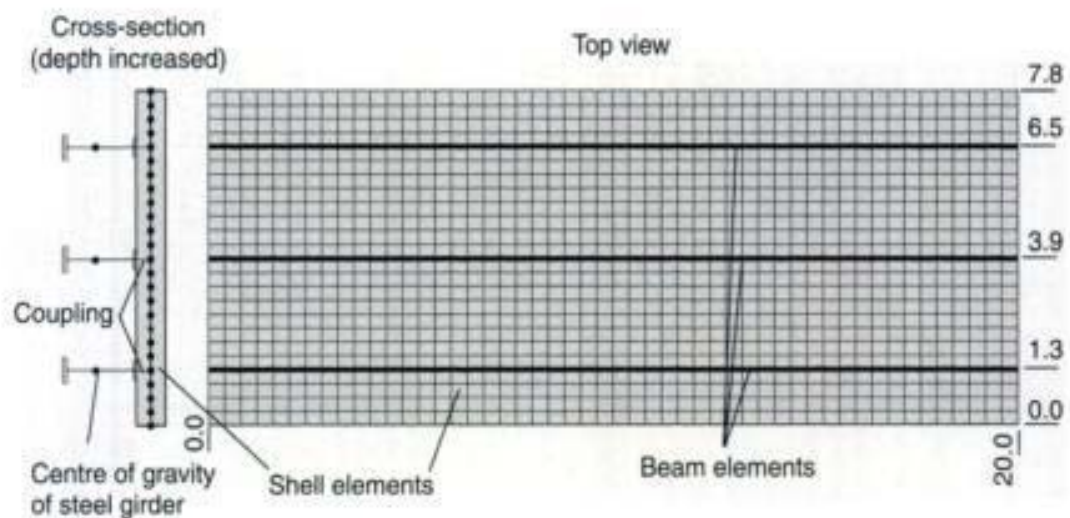


Fig. 5.30 Composite structure – Finite Element model

5.4 Singularities

Singularities of the internal forces can be observed in shell structures as well as in plate systems. They are caused by the same numerical errors. Therefore, only one practical problem – single forces on shell structures – is discussed in the following example.

As explained already for plate structures, single forces should only be applied to a Finite Element shell model, if the internal forces close to

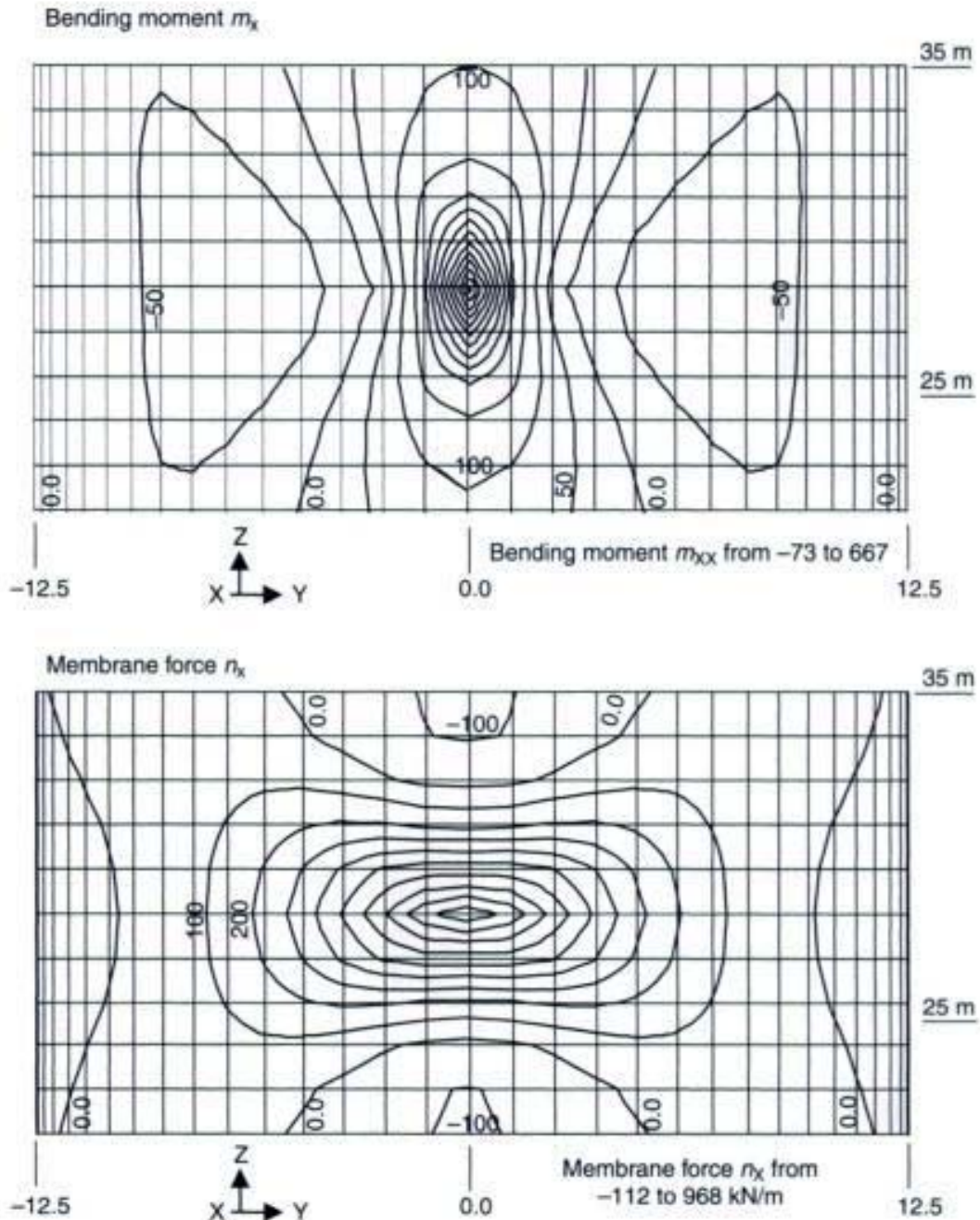


Fig. 5.31 Bending moment m_x and membrane force n_x in the loaded area (point load)

Table 5.4 Internal forces (mesh: 64×44 elements) loaded area – single force

	n_x in kN/m		n_y in kN/m		m_x in kN/m		m_y in kN/m	
	min.	max.	min.	max.	min.	max.	min.	max.
Loaded area 5×5 m $q = 100$ kN/m	-113	627	-571	387	-64	209	-24	116
Point load $Q = 2500$ kN	-117	968	-590	576	-73	667	-31	541

n_x, m_x membrane force and bending moment in circumferential direction

the loaded area are not needed for design. Otherwise, the estimation of high bending moments and membrane forces close to the concentrated load may result in an uneconomical design. This will be demonstrated on the silo structure (height $h = 56$ m and diameter $d = 25$ m), which was already mentioned in section 5.2.2.

Figure 5.31 shows the distribution of the bending moments and normal forces in circumferential direction for a single force of $F = 5 \text{ m} \times 5 \text{ m} \times 100 \text{ kN/m}^2 = 2500 \text{ kN}$. A comparison of this result with that of a distributed uniform load over an area of 5×5 m shows, that the internal forces are higher but on the safe side (see Table 5.4). The greatest bending moment in circumferential direction, m_x , under a concentrated load is three times higher than if a distributed load was applied.

It should be noted, that the maximum values will greatly increase with the number of elements in the loaded area.

Restricted Page

This page is unavailable for viewing ([why?](#)). You may continue browsing to view unrestricted pages, or visit the [About this Book](#) page.

Finite element design of concrete structures

- [14] Busjaeger, D. and Quast, U.: Programmgesteuerte Berechnung beliebiger Massivbauquerschnitte unter zweiachsiger Biegung mit Längskraft. Deutscher Ausschuss für Stahlbeton. Heft 415. Berlin 1990.

Restricted Page

This page is unavailable for viewing ([why?](#)). You may continue browsing to view unrestricted pages, or visit the [About this Book](#) page.

- [33] Bergan, P. G.: *Computational Challenges for the Finite Element Method in Offshore Engineering*. Tagung Finite Elemente in der Baupraxis, Darmstadt, 1998.
- [34] Schlaich, J. and Schäfer, K.: *Konstruieren im Stahlbetonbau. Betonkalender 1998, Teil II*. Berlin, 1998.
- [35] Peabody, D.: Continuous frame analysis of flat slabs. *J. Boston Society of Civ. Eng.*, January, 1948.

Restricted Page

This page is unavailable for viewing ([why?](#)). You may continue browsing to view unrestricted pages, or visit the [About this Book](#) page.

Index

Page numbers in italics refer to diagrams or illustrations.

- Bangkok (Thailand)
 - Don Muang Tollway 91
 - Expressway System 20, 20
- Baumann model, spatial structure
 - dimensioning 231–234, 231, 232, 233, 235
- beams
 - see also* concrete joist floors; deep beams; foundation beams; reinforced beams; T-beams
 - beam intersections 30
 - bending moment distributions 32–34, 32, 33
 - characteristic length 43–44
 - column intersections 30
 - loading analysis 15
 - shear walls 58, 60, 60
 - halving joints 30, 32, 32
 - bending moments 35–36, 36
 - strut-and-tie models 36
 - openings in 30, 32, 32
 - stress distribution 34–36, 34
 - strut-and-tie models 37
 - restrained, bending moments 36, 38, 38
 - torsional moments 70, 71
 - variable depth, inclined haunches 25–30, 26, 27, 28, 29
- bending moments
 - beams
 - distributions 32–34, 32, 33
 - restrained 36, 38, 38
 - circumferential, silos 255, 256
 - column supports 130, 130
 - column head 131, 132
 - Finite Element mesh 135, 135
 - distribution, high-rise buildings 74, 76, 77
 - footings, distribution 207–208, 207, 208
 - foundation beams 40–44, 41, 42, 43
 - concentrated loads 44
 - hollow box girder bridges 21–25, 22, 23, 24
 - top slab 88, 89
 - inclined bored pile foundations 56–58, 57
 - Kirchoff plate theory
 - equation 151, 158–159
 - singularities 216
 - uses 236
 - portal frame bridges 18–19, 19
 - residential building slabs 154, 155
 - shell structures 271–272, 272
- slabs
 - Baumann model 231–234, 231, 232, 233, 235
 - cantilever 227–228, 227
 - circular 224, 224
 - columns 197–198, 197
 - discontinuous line support 178, 179
 - edge supported 205

- bending moments, slabs (*continued*)
 - Eurocode 2 (EC2) model 234, 235
 - Finite Element Method 236–237, 236, 240, 241, 242, 243
 - flat 189–191
 - one-way 162, 163, 165–166, 165, 166, 167–168, 169, 171–173
 - partially lifting 175, 176
 - with partition walls 181, 182
 - Pieper–Martens model 237, 240, 243
 - pin supports 191–194, 192, 193
 - skewed 213, 214
 - Stiglat model 229–230, 230, 235
 - at support points 161–162, 161
- strip foundations 210–211, 211
- T-beam bridges 92, 93, 94
- T-beams
 - distribution 261–262, 262
 - total 265
- Bernoulli hypothesis 14, 35, 113
- bored pile foundations
 - bedding modulus 48, 48
 - bridge columns 49, 49, 50
 - forces carried 47–48, 48
 - horizontal deformation 55, 55
 - inclined, bending moments 56–58, 57
 - manual analysis 51, 52
 - rigs 51
 - truss system 51–52, 52, 53
 - vertical spring stiffness 52–53, 54
- box girder bridges *see* hollow box girder bridges
- bracing systems
 - high-rise buildings 67, 67, 74
 - bending moment distribution 74, 76, 77
 - coupling of nodes 71–74, 71, 72, 73
 - design software 67
 - fictitious bar method 65–66, 66, 68–69
 - modelling 74, 75
 - structural deformation 78–80, 79
 - torsional moments 76–77, 76, 77
- bridges
 - see also* hollow box girder bridges; portal frame bridges; T-beam bridges
 - bored pile foundations 49, 49, 50
 - columns, loadings 49, 51
- building materials, modulus of elasticity 180
- calculators, first programmable 3
- cantilever slabs
 - bending moments 227–228, 227
 - inadequate modelling 226–228
- characteristic length, calculation of 43–44
- column supports
 - bending moments 130, 130
 - column head 131, 132
 - Finite Element mesh 135, 135
 - bending stiffness 127–128, 128
 - deep beams, stiff connections 132, 134
 - deformations, time-dependant 160
 - modelling
 - with beam elements 131–132, 132, 133–134, 135–136, 135
 - equivalent spring stiffness 127–130, 128
 - normal stiffness 127, 128
 - rotational stiffness 128, 129
- composite shell structures 270, 270
- concentrated loads, singularities 218–220, 220, 221, 222
- concrete
 - cracked members
 - considerations 4
 - torsional stiffness 70
 - cracking considerations 4
 - materials behaviour 3, 112, 113
 - nonlinear behaviour 44–45, 45
 - steel, stress-strain relationship 113, 113
- concrete floor joists
 - dimensioning 183, 184
 - models 181–183, 183
- Condeep-type platforms 4
 - see also* Sleipner A platform
- cracked members
 - considerations 4
 - torsional stiffness 70

- Czerny tables, slabs, shear forces
236–237, 236
- deep beams
column supports
beam element modelling 131–132,
132, 133–134, 135–136,
135
spring equivalent modelling
127–130, 128, 129, 130
corner plates, stress distribution
135–136, 136
definition 117, 118
degrees of freedom 131, 133
horizontal restraint 136–137, 137
internal forces, linear-elastic
calculations 118–119, 118
membrane force distribution 136–137,
137
multi-span
loading forces 124–125, 125
support settlement 126–127, 126,
127
reinforcement
horizontal distribution 137,
138–139, 138, 139, 140
vertical distribution 138, 139,
143–144
single-span
membrane forces 122, 123–124,
123
node deformations 120
reinforcement requirements 120,
140–144, 141, 142
stress resultants 119–124, 119, 120,
122, 123
strut-and-tie models 144–145,
145
tensile forces 124, 126
singularities 147, 148, 149
and slender beams 118
stress/stain distribution
cracked members 143, 143
uncracked members 143, 143
strut-and-tie models 144–146, 145,
146, 147
two-span, strut-and-tie models
145–146, 146, 147
- discontinuity regions 14
truss systems 30, 31
discretization
definition 6
modelling errors in 12–13
displacements, T-beam bridges 92, 93,
94
double T-beam bridges 95
beams
locations 97, 97, 98
numbers 99–100
stiffness 100–1102, 101, 102
design 95
girder calculations 95, 96, 97
inclined haunches 101, 102
loads
deflection 102, 102
deformation 99, 99, 105
longitudinal girders, bending moments
106–107, 107
member forces
three-dimensional truss systems
102, 103, 105
two-dimensional truss systems 102,
104, 105
moment distributions 105, 106
numerical models 96
torsional moments 97, 99
transverse beams 107, 107
- effective slab widths, high-rise buildings
65, 65
elastic structure analysis, shell models
23–24
elastic support
foundations
modelling 39, 39
settlement forces 45–47, 46, 47
- fictional bar method, high-rise building
bracing 65–66, 66, 68–69
- Finite Element analysis
errors, Sleipner A platform 246–249,
247, 248
shell structures, silos 252, 253, 254
- Finite Element design
introduction 6–8, 6, 7, 8
principles of 1–2

Finite Element design (*continued*)

- software
 - availability 1, 2
 - uncritical use of 4–5
- T-beams 268, 268
- Finite Element Method
 - bending moments, rectangular slabs 236–237, 236, 240, 241, 242, 243
 - shell structures, mesh generation 244
 - slab analysis 152, 152, 157, 236–237, 236
- Finite Element nodal loading, and real loading 9–11, 10, 11
- flat slabs 184, 185
 - see also* foundation slabs
 - bending moments 189–191
 - bedding modulus variations 200
 - columns 197–198, 197
 - deflections 193, 193
 - hinge coupling of nodes 201
 - nodes restrained 196–197, 196
 - pin supports 191–194, 192, 193
 - circular 184, 186
 - coupling of nodes
 - hinge 198–199
 - rigid 198–199
 - equivalent frame models 188, 188, 189, 190
 - moment distribution 189
 - nodes restrained 194, 195, 196–197
 - pin supports
 - all nodes 194
 - single nodes 191–194, 192, 193
 - plane plate models 185–186, 187
 - span moments 191
- footings
 - bending moment distribution 207–208, 207, 208
 - definitions 206
 - uses 206–207
- foundation beams
 - bending moments 40–44, 41, 42, 43
 - concentrated loads 44
 - concrete, nonlinear behaviour 44–45, 45
 - elastic bedded 38–40, 39
 - settlement forces 45–47, 46, 47
 - shear forces 42, 42
- foundation slabs
 - circular
 - membrane forces 209–210, 209
 - strut-and-tie models 210, 210
 - definitions 206
- footings
 - bending moment distribution 207–208, 207, 208
 - definitions 206
 - uses 206–207
- internal forces, determination 206
- strip foundations
 - bending moment distribution 210–211, 211
 - definition 206
 - membrane force 212
 - modelling 210, 211
 - tensile force 211, 212
- foundations
 - see also* pile foundations
 - portal frame bridges 17–18, 18
 - soil deformation 40–41, 40, 41
- frame models, straight truss elements 58
- frame structures, rigid regions 15
- haunches
 - inclined
 - double T-beam bridges 101, 102
 - internal forces 26–29, 27, 28
 - nodal tension 26, 26
- Heidelberg (Germany), Theodor-Heuss Bridge 108
- high-rise buildings
 - see also* shear walls
 - bracing systems 67, 67, 74
 - bending moment distribution 74, 76, 77
 - coupling of nodes 71–74, 71, 72, 73
 - design software 67
 - fictitious bar method 65–66, 66, 68–69
 - modelling 74, 75
 - structural deformation 78–80, 79
 - torsional moments 76–77, 76, 77
 - slab widths, effective 65, 65

- stability
 - support forces 81–83
 - sway systems 80
- stability parameters 80, 84, 85
- hollow box girder bridges
 - bending moments
 - distribution 21–25, 22, 23, 24
 - top slab 88, 89
 - decks, equivalent slab model 221
 - distortions 86–87, 87, 88
 - load cases 86, 87
 - longitudinal design 85, 86
 - reinforcement
 - frame corners 21, 25, 25
 - layout 21
 - shear forces, top slab 89
 - shell models 87
 - torsional moments 85–86
 - transverse design 20–21, 20
 - truss model 21, 21
- inclined haunches
 - double T-beam bridges 101, 102
 - internal forces 26–29, 27, 28
 - nodal tension 26, 26
- industrial buildings, T-beam girders
 - 25–26, 26
- Kirchoff plate theory
 - equation 151, 158–159
 - singularities 216
 - uses 236
- materials parameters
 - constraints 3
 - modulus of elasticity 180
 - Poisson's ratio 157–160, 158
- modelling errors
 - discretization 12–13
 - Finite Element nodal loading, and real loading 9–11, 10, 11
 - nonlinear materials 9
 - reinforcement determination 11–12
- modulus of elasticity, building materials 180
- nodal displacements, and nodal reactions
 - 6–7, 6, 7
- nonlinear behaviour, concrete
 - foundation beams 44–45, 45
- numerical analysis
 - problems
 - modelling errors 9–13, 10, 11
 - program errors 9
- openings, singularities, re-entrant corners 217–218, 217
- patch loadings, silos 250–252, 253
- Pieper–Martens model, rectangular slabs 237, 240, 240
- pile foundations
 - bored
 - bedding modulus 48, 48
 - bridge columns 49, 49, 50
 - forces carried 47–48, 48
 - horizontal deformation 55, 55
 - inclined 56–58, 57
 - manual analysis 51, 52
 - rigs 51
 - soil stiffness modulus 48–49
 - truss system 51–52, 52, 53
 - vertical spring stiffness 52–53, 54
 - caps, horizontal restraints 55–56, 56
 - uses 47
- plates, nodal forces 10–11, 11
- Poisson's ratio 157–160, 158
- portal frame bridges 17
 - bending moments 18–19, 19
 - foundations 17–18, 18
 - loadings 15–17, 16
- re-entrant corners, singularities 218, 218
- real loading, and Finite Element nodal loading 9–11, 10, 11
- rectangular slabs
 - bending moments 236–237, 236
 - shear forces 236–237, 236
- reinforced beams
 - see also* deep beams
 - actions/resistance 112–113, 113
 - dimensioning 114–115
 - parameters 112
 - shear/torsion design 115–116, 116
 - strain distributions 113, 114
 - stress-strain relationship 113, 113

- reinforced beams (*continued*)
 - tension stiffening effect 114, 114
- reinforcement
 - deep beams
 - horizontal distribution 137, 138–139, 138, 139, 140
 - vertical distribution 138, 139
 - determination, by modelling 11–12
 - hollow box girder bridges 21
 - frame corners 21, 25, 25
 - internal arrangements 4
 - slabs 160
- Reissner/Midlin plate theory 236–237
- residential buildings
 - slabs 153, 153, 156–157
 - bending moments 154, 155
 - deflections 154
 - shear forces 155
- shear forces
 - foundation beams 42, 42
 - hollow box girder bridges, top slab 89
 - rectangular slabs 236–237, 236
 - slabs
 - Czerny tables 236–237, 236
 - discontinuous line support 178, 179
 - one-way 171, 174
 - partially lifting 175, 176
 - residential buildings 155
 - skewed 213, 214, 215
 - T-beam bridges 92, 93
- shear walls
 - beam/column junctions 58, 60, 60
 - definition 117, 118
 - finite element stresses 117, 117
 - high-rise buildings 58, 59, 60, 61, 62
 - large openings
 - deformation 62–65, 62, 64
 - modelling 60, 60, 61, 62
 - singularities 147, 148, 149
 - as truss systems 58, 59, 60, 60
- shell models
 - see also* Sleipner A Platform
 - elastic structure analysis 23–24
 - truss model verification 77, 78
- shell structures
 - composite 270, 270
 - definition 244
- mesh generation
 - coarseness 249
 - Finite Element Method 244
- nodal degrees of freedom 244, 245
- silos
 - bending moments 255, 256
 - Finite Element analysis 252, 253, 254
 - internal forces 254–255
 - patch loadings 250–252, 253
 - singularities, internal forces 271–272, 272
- Sleipner A platform 5, 246
 - collapse 4, 245
 - erroneous Finite Element analysis 246–249, 247, 248
 - tensile force distribution 249, 250
 - tricells 246, 247
- T-beams
 - additional beam elements 258, 259, 263, 264, 266
 - bending moment distribution 261–262, 262
 - eccentric beam elements 258, 259, 263, 264, 266–267, 267
 - internal forces 260, 260
 - knife-edge supports 256–257, 258
 - shell elements 257, 257, 258, 259
 - shell models 261–262, 261
 - support region forces 263
 - uses 255–256
- silos 223, 252
 - circular slabs
 - bending moments 224, 224
 - boundary nodes 224–225
 - circumferential bending moments 255, 256
 - Finite Element analysis 252, 253, 254
 - internal forces 254–255
 - patch loadings 250–252, 253
- singularities
 - concentrated loads 218–220, 220, 221, 222
 - deep beams 147, 148, 149
 - Kirchoff plate elements 216
 - linear-elastic calculations 215, 215

- openings, re-entrant corners 217–218, 217
- re-entrant corners 218, 218
- shear walls 147, 148, 149
- shell structures, internal forces 271–272, 272
- skewed slabs 213, 213
 - bending moments 213, 214
 - shear forces 213, 214, 215
- slabs
 - see also foundation slabs
 - analysis
 - Finite Element Method 152, 152, 157
 - strip method 151–152
 - bending moments
 - Baumann model 231–234, 231, 232, 233, 235
 - Eurocode 2 (EC2) model 234, 235
 - Finite Element Method 236–237, 236
 - Pieper–Martens model 237, 240, 240, 243
 - Stiglat model 229–230, 230, 235
 - bending stiffness 160
 - cantilever
 - bending moments 227–228, 227
 - inadequate modelling 226–228
 - circular
 - bending moments 224, 224
 - boundary nodes 224–225
 - element sizes 225–226, 226
 - Finite Element meshes 224, 224, 225
 - concrete floor joists
 - dimensioning 183, 184
 - models 181–183, 183
 - definition 150, 150
 - degrees of freedom, 4-node plate element 153
 - discontinuous line support
 - bending moments 178, 179
 - models 177–178, 177, 178
 - opening regions 180
 - outer wall support forces 180
 - shear forces 178, 179
 - discretization
 - element mesh generation 222
 - restraint node location 222–225, 224
 - edge supported
 - bedding moduli 203, 204, 205
 - bending moments 205
 - column connections 202, 204, 205, 205
 - effective widths, high-rise buildings 65, 65
 - flat 184, 185
 - bending moments 189–194, 192, 193, 194, 199–202, 200, 201
 - circular 184, 186
 - column bending moment 197–198, 197
 - equivalent frame models 188, 188, 189, 190
 - hinge coupling of nodes 198–199
 - moment distribution 189
 - nodes restrained 194, 195, 196–197
 - plane plate models 185–186, 187
 - rigid coupling of nodes 198–199
 - span moments 191
 - internal forces 150, 151, 151
 - Kirchoff equation 151, 158–159
 - materials parameters, Poisson's ratio 157–160, 158
 - one-way 162, 162
 - bending moments 162, 163, 165, 165, 166, 167–168, 169, 171–173
 - line support models 164
 - modelling 162–164, 164
 - shear forces 171, 174
 - stress distribution 169–170, 170
 - partially lifting
 - bending moments 175, 176
 - deflections 175, 176–177
 - shear forces 175, 176
 - partition walls, bending moments 181, 182
 - point loads, moment distribution 218–219, 220
 - rectangular
 - bending moments 236–237, 236
 - shear forces 236–237, 236
 - reinforcement 160, 229–235, 235

- slabs (*continued*)
 - residential buildings 153, 153, 156–157
 - bending moments 154, 155
 - deflections 154
 - shear forces 155
- shear forces, Czerny tables 236–237, 236
- singularities
 - corners 217–218, 217
 - linear-elastic calculations 215, 215
 - openings 217–218, 217, 218
- skewed 213, 213
 - bending moments 213, 214
 - internal forces 214–215
 - shear forces 213, 214, 215
- stiff, bending displacement 72–73, 73
- supports
 - bending moments at 161–162, 161
 - conditions 160–161
 - time-dependant deformations 160
- Sleipner A platform 5
 - collapse 4, 245–247
 - Finite Element analysis, errors 246–249, 247, 248
 - tensile force distribution 249, 250
 - tricells 246, 247
- slender beams, and deep beams 118
- software
 - Finite Element design
 - availability 1, 2
 - uncritical use of 4–5
 - high-rise building design 67
 - program errors 9
- soil deformation, foundations 40–41, 40, 41
- soils, stiffness modulus 48–49
- spatial shell structures, simplification by simple beams 14
- spatial structures
 - dimensioning
 - Baumann model 231–234, 231, 232, 233
 - cracking 228, 229
 - internal forces 228
 - simplifications 228–229
 - Stiglat model 229, 230
 - stability
 - high-rise buildings
 - support forces 81–83
 - sway systems 80
 - stability parameters, high-rise buildings 80, 84, 85
 - steel
 - concrete, stress-strain relationship 113–114, 113, 114
 - reinforcing, materials behaviour 112
 - Stiglat model, spatial structure dimensioning 229, 230, 235
 - stress distribution
 - beams with openings 34–36, 34
 - one-way slabs 169–170, 170
 - strip foundations
 - bending moment distribution 210–211, 211
 - definition 206
 - membrane force 212
 - modelling 210, 211
 - tensile force 211, 212
 - structural deformation, high-rise buildings 78–80, 79
 - structural modelling, usefulness 5
 - strut-and-tie models, deep beams 144–146, 145, 146, 147
 - support settlement, multi-span deep beams 126–127, 126, 127
 - sway systems, high-rise buildings 80
 - Sydney (Australia), Opera House 89
- T-beam bridges
 - see also* double T-beam bridges
 - bending moments 92, 93, 94
 - design 89
 - displacements 92, 93, 94
 - eccentric loads, torsional moments 103, 104, 108–109, 108
 - longitudinal girders
 - eccentric line load forces 110–111
 - placement 109, 109, 112
 - rectangular solid slab, vertical load displacements 89–92, 91
 - shear forces 92, 93
 - torsional stiffness 92–94, 94

- T-beams
 - additional beam elements 258, 259, 263, 264, 266
 - bending moments
 - distribution 261–262, 262
 - total 265
 - eccentric beam elements 258, 259, 263, 264
 - coupled 259, 263, 265, 266–267, 267
 - Finite Element design 268, 268
 - internal forces 260, 260
 - knife-edge supports 256–257, 258
 - shell elements 257, 258
 - web/flange junctions 257, 257
 - shell models 261–262, 261
 - shell structures, uses 255–256
 - structure 268, 268
 - support region, membrane forces 263
 - tensile stresses, anchorage points 267–268, 269, 270
- tensile force, strip foundations 211, 212
- torsional moments
 - beams 70, 71
 - bracing systems, high-rise buildings 76–77, 76, 77
 - double T-beam bridges 97, 99
 - hollow box girder bridges 85–86
 - T-beam bridges, eccentric loads 103, 104, 108–109, 108
- torsional stiffness, T-beam bridges 92–94, 94
- tricells, Sleipner A platform 246, 247
- truss model verification, shell models 77, 78
- truss systems
 - bored pile foundations 51–52, 52, 53
 - discontinuity regions 30, 31
 - equivalent cross-sections 69–70
 - high-rise buildings, shear walls 58, 59, 60, 61, 62
 - portal frame bridges 17
 - bending moments 18–19, 19
 - foundations 17–18, 18
 - loadings 15–17, 16
 - uses of 14
- Zuse, Konrad 3

Finite element design of concrete structures

G.A. Rombach

Over the last few years numerical calculations based on the finite element design method have become a standard tool for the design of many structures. Today, it seems it's only a question of computer capacity, the size of the element mesh, and the modelling of the non-linear material behaviour that is required in order to analyse an arbitrary complex reinforced structure, with almost unlimited accuracy.

In *Finite element design of concrete structures* the author addresses this 'blind belief' in computer results by offering a useful critique that 'important details are overlooked due to the flood of information' from the output of computer calculations. Indeed, errors in the numerical model may lead in extreme cases to structural failures such as the collapse of the so-called Sleipner platform has demonstrated.

Finite element design of concrete structures highlights that complex numerical calculations should not be used to compensate for any lack of practical knowledge of the behaviour of a structure. An engineer should be able to simplify any real structure into a well defined, known, understandable and designable equivalent structural system.

The problems of finite element calculations are illustrated, not just by theoretical systems but also by relating them to real structures, many of which, the author actually worked on. *Finite element design of concrete structures* is an invaluable book for both practising structural engineers and students who are using software for designing concrete structures. This book will help those who develop software for structural design to understand the difference between theory and the daily problems of designing reinforced concrete structures.

Prof. Dr.-Ing. Günter A. Rombach, graduated as a civil engineer from the University of Karlsruhe, Germany, where he also obtained his doctorate in the field of numerical simulations of granular flow. In 1990 he joined a large construction company where he worked as design and project manager for various projects, mainly bridges, both in Europe and further afield. Since 1996 he has been a professor in the field of design of concrete structures at the University Hamburg-Harburg. In 2003 he became a Certified Checking Engineer in Germany.

ISBN 07277-3274-9



9 780727 32743



Thomas Telford

www.thomastelford.com/books